City Research Online

City, University of London Institutional Repository

CITY UNIVERSITY

INFLUENCE OF TEMPERING AND NORMALISING ON THE STRUCTURE AND PROPERTIES OF LOW ALLOY AND PLAIN CARBON-MANGANESE STEELS

H. A. MEHRABI

Thesis submitted for the Degree of Doctor of philosophy

in the faculty of Engineering

Department of Mechanical Engineering

The city University (U.K.)

June 1993.

TO MY PARENTS

Contents

3

5   INFLUENCE OF LOWER TEMPERING TEMPERATURE ON THE IMPACT AND TENSILE PROPERTIES OF QUENCHED C-Mn-Al STEELS   164

6   THE INFLUENCE OF NORMALISING AT 900 °C AND 1050 °C ON THE IMPACT AND STRENGTH OF V AND V FREE FLANGES   225

List of Tables

List of Figures

10

11

14

15

16

LIST OF SYMBOLS AND ABBREVIATIONS

c	crack length
σ	applied stress
U_e	elastic energy
E	Young's modulus
U_s	surface energy
G	elastic strain energy
K	Stress intensity factor
k_c	critical stress intensity factor
G_c	critical release rate of strain energy
G_{1c}	critical value of strain energy release rate
ν	Poisson's ratio
k_{1c}	critical value of stress intensity
d_p	Packet width
C_0	carbide diameter
A	solid solution strengthening coefficient
b	Burgers vector of the dislocations
B	precipitation strengthening coefficient
B_{50}	temperature at which 50% bainite is formed
C_V	Charpy shelf energy value
d_L	mean linear intercept of the bainite ferrite grain size
D	prior austenitic grain size of carbide particle diameter
D_P	pearlite dilution factor
f	volume fraction of precipitate

f_{MA}	volume fraction of the MA constituent
f_P	mass fraction of pearlite
f_α	mass fraction of ferrite
k_y	dislocation locking term
M_s	martensite start temperature
n	work hardening exponent
σ_d	dislocation strengthening
σ_f	flow stress
σ_{fr}	fracture stress
σ_i	friction stress
σ_{MA}	strengthening due to MA constituent
σ_p	precipitation strengthening
σ_{Pe}	yield stress of pearlite
σ_s	solid solution strengthening
σ_{ss}	sub-structure or sub-grain size strengthening
σ_t	crystallographic texture strengthening
σ_y	yield stress
σ_{alpha}	yield stress of ferrite
t_b	Grain boundary carbide thickness
t_c	Thickness of carbides in the matrix
p	pearlite colony size
P	texture parameter
S	pearlite interlaminar spacing
S_{opt}	optimum pearlite interlamellar spacing
t	pearlite lamellae thickness or the thickness of grain boundary carbides
T	ductile-brittle transition temperature

x	mean planar intercept diameter of precipitate particles
δ	volume fraction of delta ferrite
ϵ	strain value
ϵ_t	true thickness strain
ϵ_u	maximum uniform strain
ϵ_w	true width strain
ϵ_T	fracture true strain
ρ	dislocation density
λ	carbide spacing or size of MA particles
μ	shear modulus
$d\sigma/d\epsilon$	work hardening rate
σ_b	strengthening by low angle lath boundaries
COD	crack opening displacement
HV_{10}	Vickers hardness
MA	martensite-austenite constituent
IQ	Ice-water quenched
IQ-900	Ice-water quenched from 900°C
IQ-900-300	Ice-water quenched from 900°C and tempered at 300°C for 1 hour
IQ-900-600	Ice-water quenched from 900°C and tempered at 600°C for 1 hour
IQ-950	Ice-water quenched from 950°C
IQ-950-600	Ice-water quenched from 950°C and tempered at 600°C for 1 hour
IQ-950-650	Ice-water quenched from 950°C and tempered at 650°C for 1 hour
IQ-950-700	Ice-water quenched from 950°C and tempered at 700°C for 1 hour
IQ-1250-300	Ice-water quenched from 1250°C and tempered at 300°C for 1 hour
IQ-1250-600	Ice-water quenched from 1250°C and tempered at 600°C for 1 hour
OQ	Oil quenched

OQ-900   Oil quenched from 900°C

OQ-900-300   Oil quenched from 900°C and tempered at 300°C for 1 hour

OQ-900-600   Oil quenched from 900°C and tempered at 600°C for 1 hour

OQ-950   Oil quenched from 950°C

OQ-950-600   Oil quenched from 950°C and tempered at 600°C for 1 hour

OQ-950-650   Oil quenched from 950°C and tempered at 650°C for 1 hour

OQ-950-700   Oil quenched from 950°C and tempered at 700°C for 1 hour

OQ-1250-300 Oil quenched from 1250°C and tempered at 300°C for 1 hour

OQ-1250-600 Oil quenched from 1250°C and tempered at 600°C for 1 hour

AQ   As quenched

CAL   Calculated

ACKNOWLEDGEMENTS

DECLARATION

I grant powers of discretion to the university Librarian to allow this thesis to be copied in whole or in part without further reference to me. This permission covers only single copies made for study purposes, subject to normal conditions of acknowledgement.

ABSTRACT

The influence of tempering on the impact and tensile properties of various types of microstructures has been examined. The following heat treatments were investigated during the course of this project.

- The structure property relationships for two quenched and tempered C-Mn-Al steel flanges made to ASTM A350 LF2 specification have been determined. Samples heated to temperatures in the range 900 - 1250°C to produce a wide range in γ grain size and quenched in oil or iced water followed by tempering at 300, 600, 650 and 700°C to produce a variety of commercially obtainable micro-structures. Impact transition curves as well as the tensile strength and the Vickers hardness values were obtained. Increasing the cooling rate and quenching temperature increased the hardness and strength.

  The microstructural parameters have been determined and related to the Vickers hardness, the yield stress, and impact behaviour. The results obtained have been analysed and it has been found that γ grain size is the major structural parameter controlling the mechanical properties of these quenched and tempered flanges.

  Tempering improved the impact behaviour of quenched steels while the strength and hardness fell. The fall in strength and hardness was found in part to be related to a reduction in dislocation density. However spheroidization of carbides and a reduction in the k_y value after tempering are also possible reasons for the further fall in strength. The improvement in impact behaviour, however, is associated with the fall in strength and coarsening of the grain boundary carbides.

- A V free and a V containing steel flange have been examined and the impact and tensile behaviour determined after normalising at 900°C and austenitising at 1050°C . After normalising, both steels had fine grain sizes and passed the ASTM A350 LF2 specification. Austenitising at 1050°C coarsened the grain size and produced a large amount of precipitation hardening in the V steel. However, because of its low S level and higher shelf energy the V steel met the impact requirement, while the V free steel in which there was no precipitation hardening failed the specification.

26

Chapter 1

INTRODUCTION

During the last fifty years vast strides have been made in the advance of metallurgy. As a result, a wide range of materials are now available for the engineer. Among them are alloys which have high strength and resistance to fatigue and have proved useful in saving weight in aeroplanes and automobiles, alloys which have strength at elevated temperatures and are invaluable for chemical plant and for boilers working at high temperatures and pressures, and finally, a number of metals which a few years ago were little more than laboratory curiosities.

The use of such new alloys, however, often presents problems in processing, heat-treatment and machining. If the full advantages are to be obtained it is essential that the engineer be equipped with the fullest possible information as to the characteristics of the materials he is using.

Too frequently the engineer is only concerned with the mechanical properties of the metals he uses, but composition, casting, shaping and heat-treatment have a tremendous effect on the ultimate behaviour of the new alloys. Consequently, some knowledge of metallurgical theory and practice is becoming more essential to the modern engineer, and this involves such

things as microscopic examination of metals and the interpretation of the structures revealed. There exists a close relationship between structure and properties of metals.

Our understanding of structure/property relationships is still, however, far from complete and the present work has been designed both to extend our understanding and to make use of knowlege already obtained to try to improve the impact behaviour of steels. The following topics have been chosen for examination:

1) The influence of high tempering temperatures on the tensile and impact behaviour of quenched C-Mn-Al steels.

2) The influence of lower tempering temperature and prior austenite grain size on the tensile and impact behaviour of quenched C-Mn-Al steels.

3) The influence of a Vanadium addition on the tensile and impact properties of normalized C-Mn steels.

All these topics involve the tensile and impact behaviour of low alloy and plain carbon steels and their relation with the microstructures obtained during various heat-treatment, and the thesis has therefore been entitled 'THE INFLUENCE OF TEMPERING AND NORMALISING ON THE STRUCTURE AND PROPERTIES OF LOW ALLOY AND PLAIN CARBON-MANGANESE STEELS'.

Chapter 2

LITERATURE SURVEY

2.1   Introduction

Most groups of alloys can exhibit failure by cracking in circumstances where
the apparent applied stress is well below that at which failure would nor-
mally be expected as identified from traditional tensile tests. Steels are no
exception to this, and probably exhibit a wider variety of failure mechanisms
than any other category of material. While ultimate failure under excessive
stress must occur and can be reasonably predicted by appropriate mechan-
ical tests, premature failure is always dangerous, involving a considerable
element of unpredictability. However, a detailed knowledge of structure and
of the distribution of impurities in steels is gradually leading to a much better
understanding of the different fracture mechanisms.

2.1.1   Cleavage Fracture in Steel

Cleavage fracture is familiar in many minerals and inorganic crystalline solids
as a crack propagation mode frequently associated with very little plastic

deformation and occurring in a crystallographic fashion along planes of low indices, i.e. high atomic density. At low temperatures zinc cleaves along the basal plane, while bcc iron cleaves along 100 planes, as do other bcc metals. This behaviour would appear to be an intrinsic characteristic of iron but it has been shown that iron, highly purified by zone refining and containing minimal concentrations of carbon, oxygen and nitrogen, is very ductile even at extremely low temperatures. For example, at 4.2 K reductions in area in tensile tests of up to 90% have been observed with iron specimens of the highest available purity. As the carbon and nitrogen content of the iron is increased, the transition from ductile to brittle cleavage behaviour takes place at increasing temperatures, until in some steels this can occur at ambient and above-ambient temperatures. Clearly, the significant variables in such a transition are of great basic and practical importance. The propagation of a cleavage crack in steel requires much less energy than that associated with the growth of a ductile crack. This is easily shown by carrying out impact tests in a pendulum apparatus over a range of temperature. The energy absorbed by the specimen from the pendulum when plotted as a function of temperature usually exhibits a sharp change in slope Fig 2.1, as the mode of fracture changes from ductile to brittle. These resulting impact transition curves are a simple way of defining the effect of metallurgical variables, eg. heat treatment, on the fracture behaviour of a steel from which a fairly precise transition temperature, T_c, can be readily obtained for a particular heat treatment. However, it should be emphasized that T_c is not an absolute value and it is likely to change appreciably as the mode of testing is altered. It nevertheless provides a simple way of comparing the effects of metallurgical variables on the fracture behaviour.
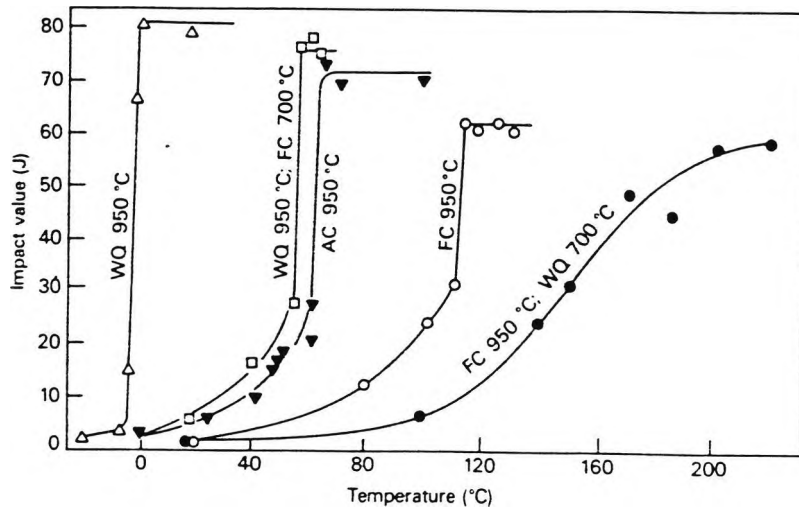
Figure 2.1: Effect of heat treatments on the impact transition temperature of a pure iron-0.12C alloy (after Allen et al., JISI, 1953, 174, 108)

2.1.2   Factors Influencing The Onset Of Cleavage Fracture

There are several factors, some interrelated, which play an important part in the initiation of cleavage fracture[1]:

- The temperature dependence of the yield stress

- The development of a sharp yield point

- Nucleation of cracks at twins

- Nucleation of cracks at carbide particles

- Grain size

- Non metallic inclusions (impurities)

- Surface geometric discontinuities

All body-centered cubic metals including ferritic iron show a marked temperature dependence of the yield stress, even when the interstitial impurity content is very low, i.e. the stress necessary to move dislocations, the Peierls Nabarro stress, is strongly temperature dependent[1]. This means that as the temperature is lowered the first dislocations to move will do so more rapidly, as the velocity is proportional to the stress, and so the chances of forming a crack nucleus, e.g. by dislocation coalescence, will increase. The interstitial atoms, carbon and nitrogen, will cause the steel to exhibit a sharp yield point either by the catastrophic break-away of dislocations from their interstitial atom atmospheres (Cottrel-Bilby theory), or by the rapid movement of freshly generated dislocations[1] (Gilman- Johnson theory). In either case, the conditions are suitable for the localized rapid movement of dislocations

as a result of high stresses which provides a favourable situation for the nucleation of cracks by dislocation coalescence. The flow stress of iron increases rapidly with decreasing temperature to a point where the critical stress for deformation twinning is reached, so that this becomes a significant deformation mechanism. It has been shown that cracks are preferentially nucleated at various twin configurations , e.g. at twin intersections and at points where twins contact grain boundaries, so that, under the same conditions, crack propagation is more likely in twinned iron. It should also be noted that the temperature dependence of the flow stress makes plastic deformation more difficult at the tip of a moving crack, so less plastic blunting of the crack tip will take place at low temperatures, thus aiding propagation.

So far, the crack nucleation mechanisms which can take place in single phase material, e.g. relatively pure iron have been discussed, but in the presence of a second phase such as cementite it becomes easier to nucleate cracks. Plastic deformation can crack grain boundary cementite particles or cementite lamellae in pearlite so as to produce micro-cracks which, in certain circumstances, propagate to cause catastrophic cleavage failure. Other work[2] supports the view that this microstructural parameter is extremely important in determining the fracture characteristics of a steel. Brittle inclusions such as alumina particles or various silicates found in steels and MnS can also be a source of crack nuclei[1].

Grain size is a particularly important variable for, as the ferrite grain size is reduced, the transition temperature T is lowered, despite the fact that the yield strength increases[3]. This is, therefore, an important strengthening mechanism which actually improves the ductility of the steel. It has been shown by Petch[4] that T is linearly related to $\ln d^{-1/2}$, and an appropriate

relationship of this type can be derived from a dislocation model involving the formation of crack nuclei at dislocation pile-ups at grain boundaries. The smaller the grain size, the smaller the number of dislocations piling-up where a slip band arrives at a boundary. This situation will lead to fewer crack nuclei regardless of whether they are formed by dislocation coalescence or by dislocation pile-ups causing carbides to crack or by twinning interactions[1].

2.1.3 Brittle Fracture

The starting point of all theories on brittle fracture derives from the work of Griffith[5], who considered the condition needed for the propagation of a pre-existing crack, of length 2c, in a brittle solid such as glass. When the applied stress σ is high enough, the crack will propagate and release elastic energy. This energy Ue in the case of thin plates (plane stress) is:

$$U_e = -\frac{\pi c^2 \sigma^2}{E} \quad per\ unit\ plate\ thickness \tag{2.1}$$

Where E = Young's modulus. The term is negative because this energy is released. However as the crack creates two new surfaces, each with energy = 2cγ there is a positive surface energy term U_s:

$$U_s = 4c\gamma \quad where \quad \gamma = \quad surface\ energy\ per\ unit\ area \tag{2.2}$$

Griffith showed that the crack would propagate if the increase in surface energy, U_s, was less than the decrease in elastic energy U_e. The equilibrium position is defined as that in which the change in energy with crack length

is zero:

$$\frac{d_U}{d_c} = \frac{d(U_e + U_s)}{d_c} = 0 \qquad (2.3)$$

This is the elastic strain energy release rate, usually referred to as G.

$$(-\frac{2\pi c \sigma^2}{E} + 4\gamma) = 0 \qquad (2.4)$$

and

$$\sigma_{fr} = (\frac{2\gamma E}{\pi c})^{1/2} \qquad (2.5)$$

where σ_{fr} is the fracture stress, which is defined as that just above which energy is released and the crack propagates. This equation shows that the stress σ is inversely related to the crack length, so that as the crack propagates the stress needed drops and the crack thus grows rapidly. Orowan[6] pointed out that in many crystalline solids, plastic deformation will occur both during nucleation of the crack, and then at the root of the crack during propagation. This root deformation blunts the crack and, in practice, means that more energy is needed to continue the crack propagation. Thus the Griffith equation is modified to include a plastic work term γ_p:

$$\sigma_{fr} = (\frac{E(2\gamma + \gamma_p)}{\pi c})^{1/2} \qquad (2.6)$$

It has been found that $\gamma_p \gg \gamma$, hence the condition for the crack spreading in a crystalline solid such as iron is

$$\sigma_{fr} = (\frac{E\gamma_p}{\pi c})^{1/2} \qquad (2.7)$$

35

The local stress field at the crack tip is usually characterized by a parameter K, the stress intensity factor, which reaches a critical value K_c when propagation takes place. This critical value is given by

$$K_c = \sigma_{fr}\sqrt{\pi c} \qquad (2.8)$$

In plane stress conditions

$$K_c = \sqrt{(EG_c)} \qquad (2.9)$$

Where G_c = the critical release rate of strain energy. In plane strain conditions, the critical value of strain energy release rate is $G_{1c} = \gamma_p$ where

$$\sigma_{fr} = \left(\frac{EG_{1c}}{\pi(1-\nu^2)c}\right)^{1/2} \qquad (2.10)$$

where ν = poisson's ratio The critical value of stress intensity , K_{1c} , is then related to G_{1c}:

$$K_{1c} = \left(\frac{EG_{1c}}{(1-\nu^2)}\right)^{1/2} \qquad (2.11)$$

The fracture toughness of a steel is often expressed as a K_{1c} value obtained from tests on notched specimens which are precracked by fatigue, and are stressed to fracture in bending or tension. Nucleation of a cleavage crack occurs when a critical value of the effective shear stress is reached, corresponding to a critical grouping, ideally a pile up, of dislocations which can create a crack nucleus, e.g. by fracturing a carbide particle[1]. In contrast, propagation of a crack depends on the magnitude of the local tensile stress which must reach a critical level σ_{fr}. Simple models of slip-nucleated fracture

36

assume either interaction of dislocations or cracks formed in grain boundary carbides. However, it has been realized[1] that both these structural features must be taken into account in deriving an expression for the critical fracture stress σ_{fr}. This critical stress does not appear to be temperature dependent. At low temperatures the yield stress is higher, so the crack propagates when the plastic zone ahead of the crack is small, where as at the higher temperatures, the yield stress being smaller, a larger plastic zone is required to achieve the critical local tensile stress σ_{fr}.

This tensile stress σ_{fr} has been determined for a wide variety of low carbon steels, and has been shown to vary roughly linearly with d, Fig 2.2[1]. The scatter probably arises from differences in test temperature and carbide dimensions. This is conclusive evidence for the role of finer grain sizes in increasing the resistance to crack propagation. Regarding grain boundary carbide thickness size, effective crack nuclei will occur in particles above a certain critical size so that, if the size distribution of carbide particles in a particular steel is known, it should be possible to predict its critical fracture stress. Therefore, in low carbon steels in which the structure is essentially ferrite grains containing carbide particles, the particle size distribution of carbides together with grain size are the most important factor[1]. In contrast, in bainitic and martensitic steels the austenite grains transform to lath structures where the lath width is usually between 0.2 and 2 μm[1]. The laths occur in bundles or packets with low angle boundaries between the laths. Larger misorientations occur across packet boundaries. In such structures, the packet width is the main microstructural feature controlling cleavage crack propagation[1].

The critical local fracture stress σ_{fr} has been related to the following

37
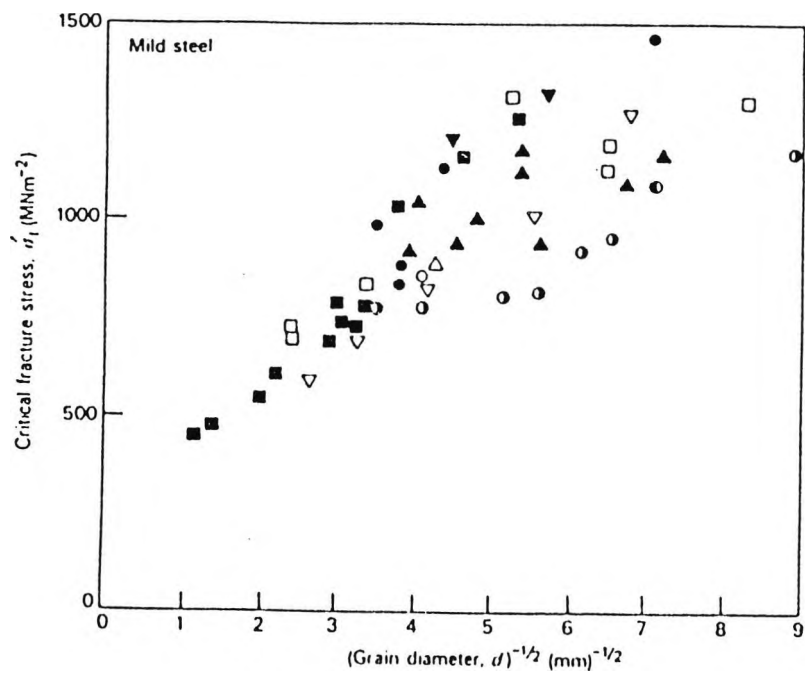
Figure 2.2: Dependence of local fracture stress σ_{fr} on the grain size of mild steel. Date from many sources (Knott)

types of structure, as follows.

For ferritic steels with spheroidal carbide particles[1]:

$$\sigma_{fr} = \left(\frac{\pi E \gamma_p}{2C_0}\right)^{1/2} \qquad (2.12)$$

Where C_0 = carbides diameter. For bainitic and martensitic steels with packets of laths[1]:

$$\sigma_{fr} = \left(\frac{4E\gamma_p}{(1-\nu^2)d_p}\right)^{1/2} . \qquad (2.13)$$

Where d_p = packet width and ν = poisson's ratio.

2.1.4 Ductile Fracture

The higher temperature side of the ductile/brittle transition is associated with a much tougher mode of failure, which absorbs much more energy in the impact test. While the failure mode is often referred to as ductile fracture, it could be described as rupture, a slow separation process which, although transgranular, is not markedly crystallographic in nature, although the deformation processes leading to fracture are on slip planes.

It is now well-established that ductile failure is initiated by the nucleation of voids at second phase particles. In steels these particles are either carbides, sulphide or silicate inclusions. The voids form either by cracking of the particles, or by decohesion at the particle/matrix interfaces, so it is clear that the volume fractions, distribution and morphology of both carbides and of inclusions are important in determining the ductile behaviour, not only in the simple tensile test, but in complex working operations. Therefore, significant variables, which determine ductility of steel, are to be found in

39

the steel-making process, where the nature and distribution of inclusions is partly determined, and in subsequent solidification and working processes. Likewise, the carbide distribution will depend on composition and on steel-making practice, and particulary on the final heat treatment involving the transformation from austenite, which largely determines the carbide size, shape and distribution.

The formation of voids begins very early in a tensile test, as a result of high stresses imposed by dislocation arrays on individual hard particles. Depending on the strength of the particle/matrix bond, the voids occur at varying strains, but for inclusions in steels the bonding is usually weak so voids are observed at low plastic strains. These elongate under the influence of the tensile stress but, additionally, a lateral stress is needed for them to grow sideways and link up with adjacent voids forming micronecks.

2.2   Structure-Property Relationships in Steels

One of the most significant developments in ferrous physical metallurgy over the past few years has been the methodology by which the microstructure has been related quantitatively to the mechanical properties. This approach to understanding what controls the properties of steels has been based on many years of research into the individual mechanisms which influence the strength, ductility and toughness and many other properties. Three typical cases can be cited, namely the effect of the matrix grain size on the yield strength of ferrite[3,4] and the fracture transition temperature of ferrite[9], the effect of pearlite inter lamellar spacing on its strength[10] and solid solution strengthening in ferrite[11]. The most common properties which have been quantitatively related to microstructure are the yield stress, σ_y, the flow

stress σ_f, the fracture stress, σ_{fr}, work hardening rates, $d\sigma/d\epsilon$ at specific strain values, ϵ, the maximum uniform strain, ϵ_u, the fracture true strain, ϵ_T, the ductile-brittle transition temperature, T, and the charpy shelf energy value, C_v. The extent of the data available varies considerably for different properties and microstructures, and although much use has been made of empirical multiple linear regression equations, the functions of the various parameters used are based on fairly sound physical metallurgical principles. Many published equations for the yield stress. σ_y, are of the type

$$\sigma_y = \sigma_i + \sigma_s + \sigma_p + \sigma_d + \sigma_{ss} + \sigma_t + k_y d^{-1/2} \qquad (2.14)$$

where σ_i is the friction stress opposing dislocation motion, σ_s is solid solution strengthening, σ_p is precipitation strengthening, σ_d is 'forest' dislocation strengthening, σ_{ss} is sub-structure or sub-grain size strengthening , σ_t is a crystallographic texture strengthening parameters, k_y is a constant related to the difficulty of unlocking dislocations, or of activating dislocation sources, sometimes called the dislocation locking term, and d is the matrix grain diameter (or a linear function of it). Often many of the strengthening terms are omitted so that σ_i includes various strengthening effects.

The first scientific analysis of the relationship between grain size and the strength, carried out on ARMCO iron by Hall and Petch[3,4], led to the Hall-Petch relationship between the yield stress σ_y and the grain diameter d,

$$\sigma_y = \sigma_i + k_y d^{-1/2} \qquad (2.15)$$

where σ_i is called friction stress. But according to Gladman and Pickering[12] equation (2.15) implies that all the strengthening mechanisms are additive,

which is a simplifying assumption. They[12] have also pointed out that whilst the function $d^{-1/2}$ has a respectable pedigree and fits a large body of data, equally statistically significant results can often be obtained with an exponent between 0.25 and 1.0, which may simply reflect the uncertainty of the phenomenological model on which the Hall-Petch equation is based.

In the present chapter, quantitative relationships will be shown relating the microstructural parameters, including solid solution effects to the following mechanical properties:

- yield stress or 0.2 % proof stress (σ_y)

- ductile-brittle transition temperature (T)

- upper charpy shelf energy value (C_v)

These relationships will be discussed with respect to the following microstructures and types of steels:

- ferrite-pearlite structures containing up to 20 vol.% pearlite

- ferrite-pearlite structures containing more than 20 vol.% pearlite up to fully pearlitic structures such as occur in medium-high carbon steels for rods, bars and rails.

- acicular ferrite and bainite, in constructional steels

- martensite, which is the basis of the quenched and tempered engineering steels

- tempered ferrite-pearlite

- tempered martensite or bainite

Unless otherwise stated, all temperatures are given in ^0C, stresses in Mpa, the impact energy absorbed on fracturing a standard charpy specimen in J and lengths in mm.

2.3   Ferrite-Pearlite Microstructures

Several extensive reviews have been published on the structure-property relationships for this type of microstructure[12,13].

2.3.1   The Yield Stress (σ_y)

For ferrite-pearlite steels in which ferrite predominates in the structure, Petch[4] has argued that, as the lower yield point represents the stress required to propagate a Luders-band front through the ferrite, σ_y should be independent of pearlite content. In accord with this argument, Petch found that increasing the carbon content from 0.04% to 0.16% produced no significant change either in σ_i or k_y.

Two major investigations by Gladman et al[14] and Pickering and Gladman[15] on structure property relationship of ferrite-pearlite steels (up to 20% pearlite) have also failed to establish an influence of pearlite on yield stress. However some equations show an effect of pearlite[16]. The pearlite may be indicating the carbon content and its effect in lowering the transformation temperature and decreasing the grain size, but there is also a suggestion[17] that pearlite may affect k_y, by as much as 11%. A typical regression equation[18] is:

$$\sigma_y = 88 + 37(wt.\%Mn) + 83(wt.\%Si) + 2918(wt.\%N_{free}) + 15.1d^{-1/2}(2.16)$$

The friction stress, σ_i, of 88 MPa in Eq.(2-16) relates to air cooled specimens

43

Element	A in MPa per wt.% alloy
Mn	37
Si	83
Ni	33
Cr	−30
P	680
Cu	38
Mo	11
Sn	120
C and N	5000

Table 2.1: Effects of various elements on the solid solution strengthening coefficient for ferrite[15]

in which there may be some carbon in solution or as finely precipitated carbides, but for furnace cooled material where there is no carbon in solution and where any carbides are coarse and overaged, then σ_i is reduced to 62 MPa. Values of k_y vary from 14 MPa mm$^{-1/2}$[19] to 23 MPa mm$^{-1/2}$[9] but the usual values quoted lie in the range 15-18 MPa mm$^{-1/2}$. Solid solution strengthening is often related to the square root of the atom concentration, but for low concentrations there is an approximately linear dependence of solution strengtening on the wt.% of the alloying element, i.e. $\sigma_s = A$ (wt.% alloy). The effects of a number of alloying elements on the coefficient A are shown in Table 2.1, and the value of A tends to increase with increasing difference in atom size between the solvent and solute[15].

A significant effect on the yield stress is obtained from sub-grains produced by recovery processes, such as result from controlled rolling in the ferrite range[20]. In the absence of "forest" dislocations, the subgrains re-

44
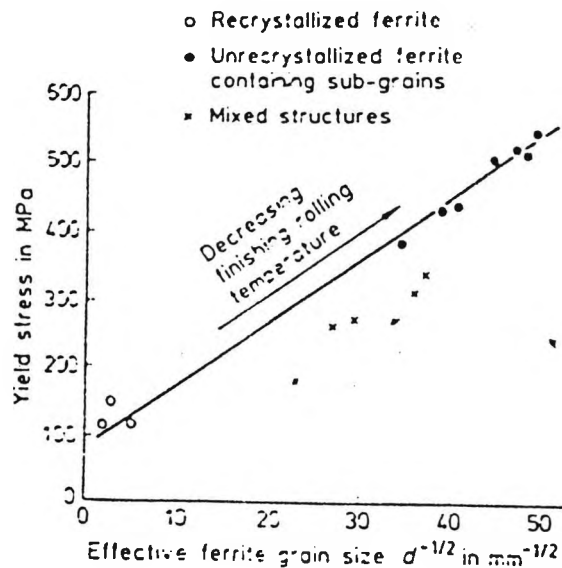
Figure 2.3: The effect of the 'effective' ferrite grain size on the yield stress of controlled rolled steel[21].

place the dislocation strengthening contribution. Subgrain strengthening is also described by a Hall-Petch type of relationship, using the sub-grain diameter. In some cases mixed recovered and recrystallized grains are observed, and because all boundaries act as obstacles to dislocation movement the yield stress can be described by a type of law of mixtures. This gives rise to an "effective" grain size which can approximately be used to describe the yield stress[21], Fig 2.3, the partially recrystallized structures showing the greatest deviation. According to Morrison and Mintz[22] rolling below the Ar_1 temperature in the ferrite range, apart from producing recovered sub-grains, also produces a crystallographic texture which causes a small increase in yield stress of 30 MPa, and the contributions of both texture and sub-grains are shown in Fig 2.4[22] as a function of rolling finishing temperature. The contributions of the ferrite grain size and various solid solution strengthening elements to the yield stress of a normalised 0.2 wt.% C steel are shown in Fig 2.5[23].

45
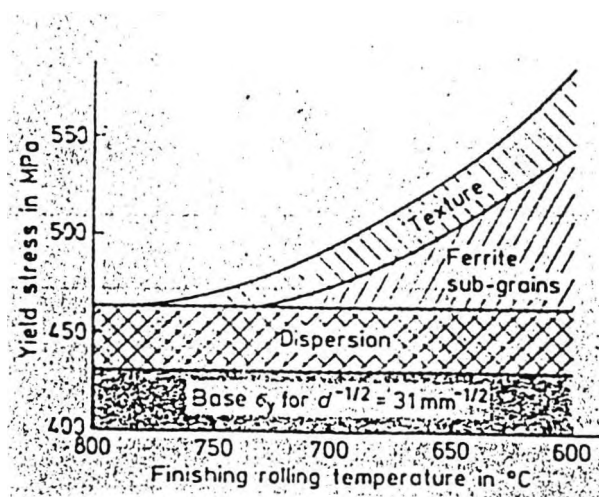
Figure 2.4: The effect of controlled rolling finishing temperature on the contributions of various strengthening mechanisms to the yield stress of ferrite[22].
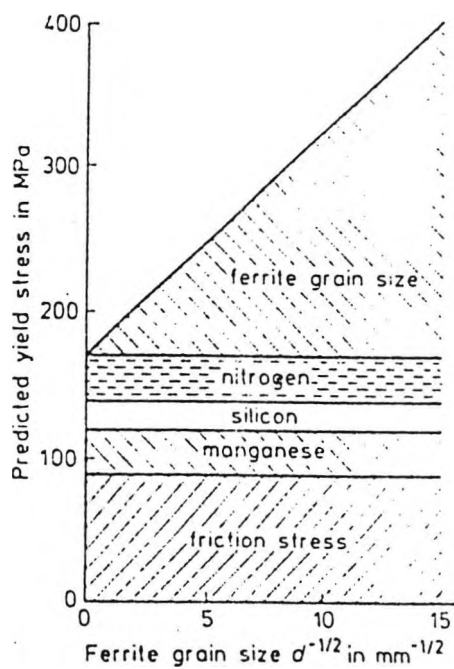
Figure 2.5: The effect of ferrite grain size on the yield stress of normalized steel containing 0.20 wt.%C, 1.0 wt.% Mn, 0.20 wt.%si, 0.010wt.%N[23].
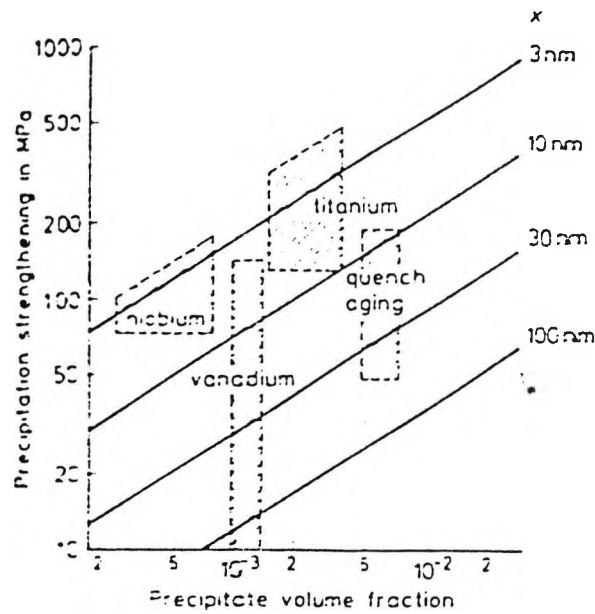
Figure 2.6: Dispersion strengthening as predicted by a modified Ashby-Orowan model compared with the observed strengthening by quench aging and by microalloy carbonitrides[25].

Precipitation strengthening effects have been described by the Ashby-Orowan model[24]:

$$\sigma_p = 5.9 f^{1/2} . \ln(\frac{x}{2.5 . 10^{-4}}) \qquad (2.17)$$

where f is the volume fraction of precipitates and x is the mean planar intercept diameter of the precipitate particles.

According to Gladman et al.,[25] Eq. (2-17) gives good predictability for the precipitation strengthening by quench aged carbides and by precipitated carbonitrides in Nb, V and Ti microalloyed steels Fig 2.6[25]. The above equation is difficult to manipulate, but a simplified approach has been to use the relationship $\sigma_P = B$ (wt.% alloy), some results being shown by Morrison[13] in Table 2.2. The reason for the variation in the intensity of precipitation strengthening is that some precipitates may form in the austenite where they exert no strengthening but decrease the maximum available effect

47

Precipitate	B in MPa per wt.% alloy		Alloy range (wt.%)
	Maximum	Average	
VC	1000	500	0 − 0.15
VN	3000	1500	0 − 0.06
Nb(CN)	3000	1500	0 − 0.05
TiC	3000	1500	0.03 − 0.18

Table 2.2: Effects of microalloy carbide/nitride precipitate on precipitation strengthening in high strength low alloy steels[13].

in the ferrite[26]. Also precipitation strengthening decreases with increasing austenite transformation temperature (2 MPa/^{0}C) and also with a slower cooling rate i.e. overaging occurs[26]. The precipitation strengthening, σ_p, is clearly dependent upon the volume fraction of precipitate, f, which depends on the solubility of the precipitating phase as a function of temperature. For many of the carbo-nitrides of elements such as Nb, V and Ti, these solubility relationships are well known[27] and it is possible to calculate the volume fraction of precipitate which should be formed at any given temperature. An important factor which is now appreciated is that the maximum σ_p occurs at stoichiometric metal : carbon/nitrogen ratios[28], because at the stoichiometric ratio the temperature dependance of the solubility of the microalloy carbon-nitride is a maximum.

Decreasing the transformation temperature or rolling at low temperatures introduces ' dislocations into the ferrite, which result in an increase in strength. This can be related to the dislocation density, ρ, using equation

48

2.18[29]:

$$\sigma_d = \alpha\mu b\rho^{1/2} \tag{2.18}$$

where μ is the shear modulus, b is the Burgers vector of the dislocations and α is a constant.

In general the effect of transformation temperature in the polygonal ferrite range gives only a modest increase in yield stress of 60 MPa as the transformation temperature decreases from 800 $^\circ$C to 600 $^\circ$C, but if the dislocations form sub-grains the yield stress is related to the sub-grain diameter by an equation of the Hall-Petch type and can give an increase in $d^{-1/2}$ ($mm^{-1/2}$)[30].

Very little work has been done on the influence of grain boundary carbide thickness on σ_y. Pickering[31] found no influence of grain boundary carbides on yield strength. However Mintz[32] has shown that the grain boundary carbide thickness t_c does seem to be related to the fall in σ_y on tempering or slow cooling from the normalising temperature, as illustrated in Fig 2.7[32]. Such a relationship can also be inferred from the work of Cochrane[33] who examined the stress relieving of C-Mn steels. The best equation for the curve in Fig 2.7.

$$\sigma_y = 70(t_c - 0.2)^{2/3} \tag{2.19}$$

where σ_y is in Mn/mm^2 and t_c is in μm.

49
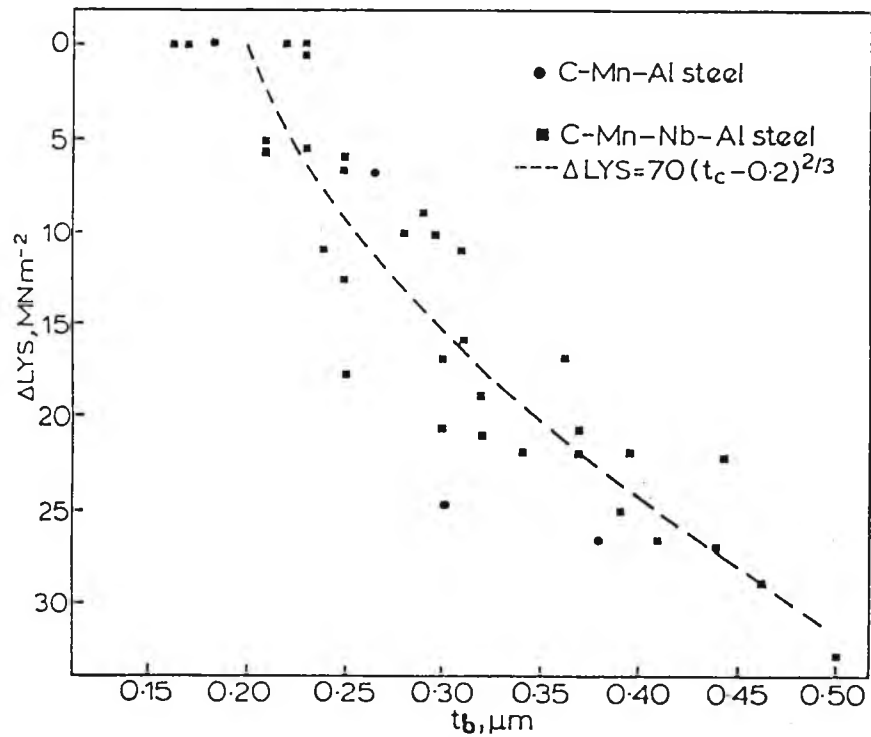
Figure 2.7: Influence of GBC thickness on fall in LYS[32]

2.3.2 Toughness

Due to their general ductility, the toughness of the polygonal ferrite-pearlite structures is usually characterised by the ductile-brittle transition temperature, T, measured by the Charpy impact test, and the Charpy shelf energy value, C_v, although some fracture toughness work has also been done using crack opening displacement and other measurements.

2.3.3 The Ductile-Brittle Transition Temperature

Many equations have been used to describe the fracture transition temperature, one being used by Pickering[34]:

$$T(^0C) = -19 + 44(wt.\%Si) + 700(wt.\%N_{free})^{1/2} +$$

$$2.2(\%pearlite) - 11.5d^{-1/2} \qquad (2.20)$$

wt.-% C

0.11

0.23

0.31

0.4?
0.4?
0.5?
0.5?

0.60

Impact energy in J

200

150

100

50

0

-150 -100 -50 0 50 100 150 200

Test temperature in °C
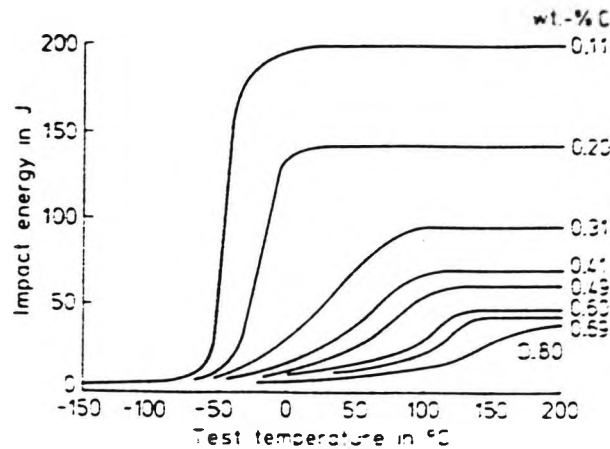
Figure 2.8: The effect of testing temperature on the impact energy for normalized steels containing various carbon contents, showing the effect of carbon content on the ductile-brittle transition temperature and shelf energy value[35].

Factors affecting the validity of this type of equation, and the constants, have been discussed by Gladman and Pickering[12]. Clearly grain refinement and a decrease in the pearlite content will increase the toughness by lowering T. Eq. (2-20) does not show an effect of Mn, the effect of which is implied in the grain size and pearlite terms. As various grain refining methods may be used, e.g. second phase particles in microalloyed steels, solute additions or an increased cooling rate to depress the $\gamma - \alpha$ transformation temperature, the effect of the method used may be critical and influence T by an additional strengthening mechanism or an impurity scavenging effect[26]. These additional factors may be incorporated in the constant in Eq. (2-20), from which it can be seen that carbon as pearlite is very detrimental, Fig.2-8, and increases T by the cracking of the cementite lamellae[35]. However, as will be shown later, the pearlite colony size and cementite lamella thickness ' are also important parameters. A problem arises when subgrains occur within

51

the ferrite, because it is not clear whether such sub-grains affect $T^{[26]}$. In general low angle sub-grain boundaries do not greatly hinder the propagation of a cleavage crack[26]. On the other hand dislocation strengthening by forest dislocations increases T by 0.2/0.6°C per MPa increase in σ_d [13,35]. Most values are around the bottom of this range, i.e. 0.2°C per MPa. Should the forest dislocations begin to form subgrains by a recovery process, their detrimental effect may be removed and no beneficial effect of the sub-boundaries introduced. As the development of the subgrains becomes more perfect with more complete recovery, the boundaries show higher angles of misorientation and then may commence to produce a beneficial effect by decreasing T. These effects, however, require to be quantified[26].

Precipitation strengthening, σ_P, invariably increases T, a resonable average value being 0.2/0.5°C per MPa increase in σ_P[26]. An increase in the friction stress due to solid solution strengthening would be expected to increase T. With the exception of manganese, which decreases the grain boundary carbide thickness, and nickel, which possibly increases the abililty for cross slip, both of which decrease T, all other solid solution strengtheners increase it[26]. Irvine et al[36]., suggest aluminium is a special case, however, as in small quantities it decreases T by removing nitrogen from solution but larger additions of aluminium cause T to increase by solid solution strengthening. Mintz et al[37]., also suggests that aluminium acts as grain refiner which decreases T. It has recently been suggested by Pickering[34] that for solid solution strengthening elements except nickel, manganese and aluminium, their effect on T should be proportional to their influence on σ_s. Some effects of various elements are shown in Table 2-3.

Attempts have been made by Morrison[13] to relate T to the crystallo-

Element	Change in T ('C) per MPa increase in σ_s
Ni	−0.9
Mn	−0.3
Cu	+0.4
Mo	÷0.5
Si	÷0.5
C	÷0.7 *
N	÷2.0 *
P	+3.5

For interstitially dissolved C or N.

Table 2.3: Typical effects of various elements in solid solution in ferrite on the change in ductile- brittle transition temperature[26].

graphic texture of the ferrite, because steels controlled rolled in the ferrite region give a [100] < 011 > texture. A texture parameter has been defined by Bramfit and Marder[30]:

$$P = [(1_{111})_{RP}.(1_{110})_{TP}] - 1 \qquad (2.21)$$

where $(I_{111})_{RP}$ is the relative intensity of 111 in the rolling plane and $(I_{110})_{TP}$ is the relative intensity of 110 in the transverse plane.

Changes in the value of T in the longitudinal direction, but not in the transverse direction, have been related to this texture parameter[30], and an equation of the following type has been developed:

$$T(^0C) = 75 - 13.0d^{-1/2} + 6.3P \qquad (2.22)$$

Mintz and Morrison[38] have, however, shown that the empirical texture relationship developed by Bramfitt and Marder is fortuitous and that the
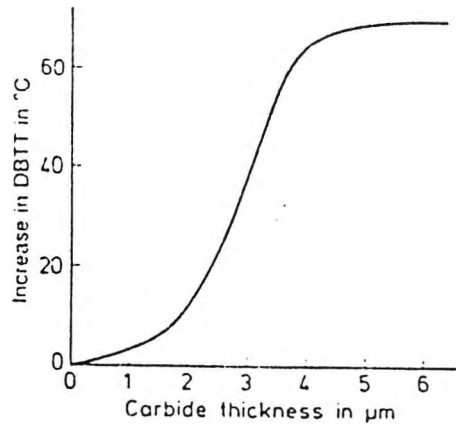
Figure 2.9: The effect of carbide thickness on the ductile-brittle transition temperature (DBTT)[33].

change in impact behaviour is due to the production of fissures on the fracture surface which are unrelated to texture development.

It has already been shown that pearlite increases T, Fig 2-8 and Eq. (2-20), but Cochrane[33] argues that carbide filaments occuring along ferrite grain boundaries have a particularly detrimental effect when they are thicker than about 2μm, Fig 2-9[33]. It has been shown by McMahon and Cohen[39], that such carbides crack under stress and initiate a cleavage crack. Gladman[21] suggests that manganese supresses the formation of these grain boundary carbides, as also does an increased cooling rate. It has also been suggested by Almond[40], that embrittlement can be more pronounced and produced by thinner carbides when the ferrite grain size is decreased. By studying microalloyed steels, Mintz et al[41] have incorporated a factor for carbide thickness (t_c), together with one for σ_p, into the following equation[41]:

$$T(^0C) = 46 + 0.45\sigma_p + 131t_c^{1/2} - 12.7d^{-1/2} \qquad (2.23)$$

54

It can be seen that the coefficient for σ_p is in the range given earlier.

In view of the effects discussed for large carbides, it might be expected that non-metallic inclusions would increase T. The evidence however is inconclusive [13]. It seems that increasing the S content to 0.05 wt.% initially slightly increases T[42], possibly due to facilitated crack initiation. A further increase in S, however, decreases T appreciably, more markedly so in longitudinal than in transverse tests[42]. In longitudinal tests, elongated MnS inclusions are effective obstacles to crack propagation, and in effect the steel behaves as a composite. The elongated MnS particles may also decrease the secondary principal stresses by causing delamination[42], which also occurs in composites of a crack dividing type. This delamination decreases the stresses parallel to the notch root, thereby decreasing the principal flow stress and making plastic deformation preferable to cleavage, so that T decreases. It seems fairly well established that T for transverse tests is 20/40 ^{0}C higher than for longitudinal tests, possibly due to structural fibering by elongated inclusions[42]. By eliminating elongated inclusions and eliminating their crack stopping or dividing effects, inclusion shape control has been observed by Gladman[42] to increase T by as much as 50 ^{0}C. However, most structural applications require good through the thickness impact properties and inclusion shape control is therefore of prime importance.

2.3.4   The Shelf Energy Value

It is well known[35], and indeed clear from Fig 2.8, that increasing the carbon content and therefore the pearlite content decreases the upper shelf energy, C_v. Gladman and Pickering[12] suggest that as there is also a linear relationship between the true strain, ϵ_T and Log C_v, the influence of various

factors on C_v may be inferred from their known effects on ϵ_T. It may be concluded[43] that carbide spheroidisation would increase C_v. Little quantitatively is known about the effect of ferrite grain size on C_v, but as true strain $,\epsilon_T$ increases slightly with decreasing grain size it might be assumed that grain refinement would also increase C_v. In fact the opposite trend seems to be shown by Bucher et al. [44] in the following equation for the transverse C_v, although the effect is quite small:

$$C_v(J) = 112 - 2.8d^{-1/2} - 0.18\sigma_p - 832(wt.\%S) -$$

$$43(wt.\%Al) - 0.76(\%pearlite) + 107(wt.\%Zr) \qquad (2.24)$$

In Eq (2.24), the marked effect of S (MnS inclusions) in reducing the shelf energy is clearly shown. It has been suggested[12] that it would not be expected that S and pearlite would have linear effects, and as shown later they do not. The linear effects indicated in Eq. (2.24) are a result of the rather small range of the variables studied. The positive effect of Zr on C_v is related to its inclusion shape controlling properties, and as such it would be expected to increase the transverse C_v[12]. Little data on the effect of solid solution strengthening on C_v seems to be available, but the effect might be expected to be relatively small[26]. Eq.(2.24) shows that increasing precipitation strengthening decreases C_v by about 2 J per 10 MPa increase in σ_p, but other work by Mintz et al[45] indicate a rather higher value of 3 J per 10 MPa increase in σ_p. Further Mintz et al[45] believe that dislocation strengthening decreases C_v by some 3.5 J per 10 MPa increase in σ_d. An effect of the crystallographic texture has been observed by Bramfitt and Marder[30], on the longitudinal C_v, and the effect of the texture parameter, (see Eq.

56
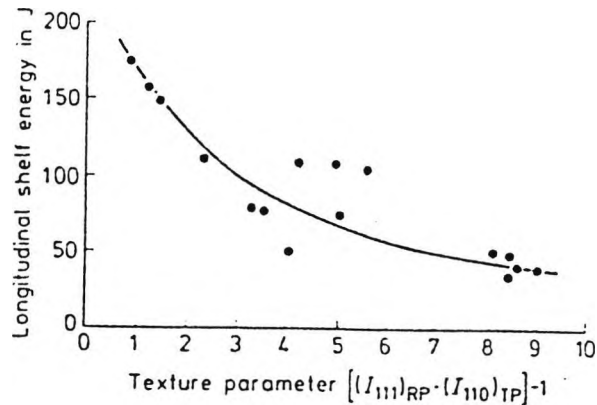
Figure 2.10: The relationship between the longitudinal shelf energy and the texture parameter[30].

(2.21)) is shown in Fig.2.10. This has been suggested to the due to dislocation strengthening, the texture parameter in Eq. (2.21) appearing to indicate the ready activation of the slip systems operative during rolling ferrite below the Ar_1 temperature.

Much information[42] is available on the effect of non-metallic inclusions on C_v, and as might be expected the effect is similar to that on true strain, ϵ_T, increasing inclusion volume fraction causing an exponential decrease in C_v, Fig. 2.11. This type of relationship is shown for both sulfide and oxide inclusions, and again the well known anisotropic effect is observed, Fig. 2.11, due to elongated inclusion particles. This anisotropy of C_v is largely eliminated by the technology of inclusion shape control[46], see Fig. 2.12. Inclusion shape control produces inclusions which do not deform and elongate during hot rolling, and this effect is clearly shown by some of the few fracture toughness data available. The crack opening displacement (COD) markedly increases as the inclusion length decreases, Fig. 2.13 by Baker and
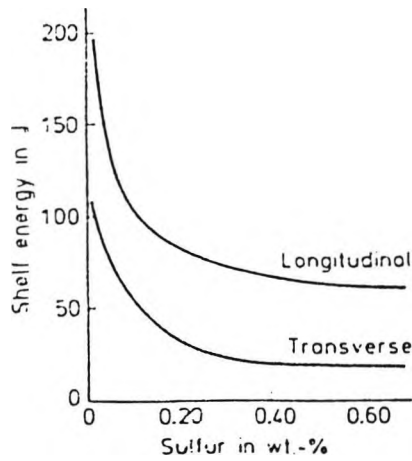
Figure 2.11: The effect of sulfur content on the shelf energy, showing the anisotropy of shelf energy due to elongated inclusions. The sulfur content is proportional to the volume fraction of MnS inclusions[42].
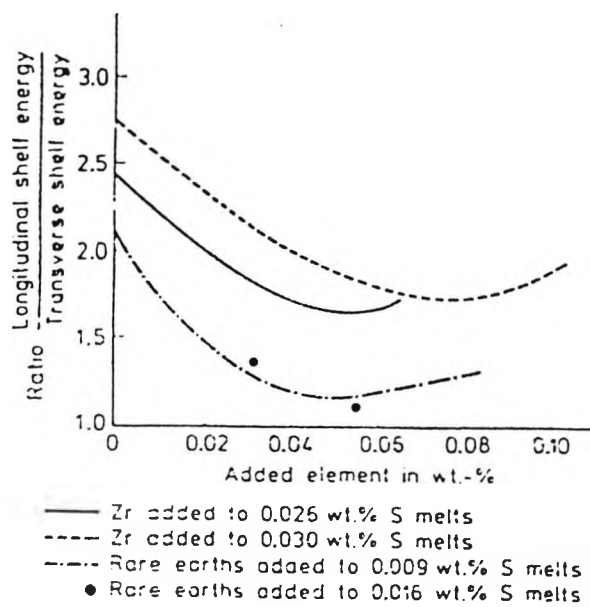
Figure 2.12: The elimination of the anisotropy of shelf energy by inclusion shape control additions[46].

58
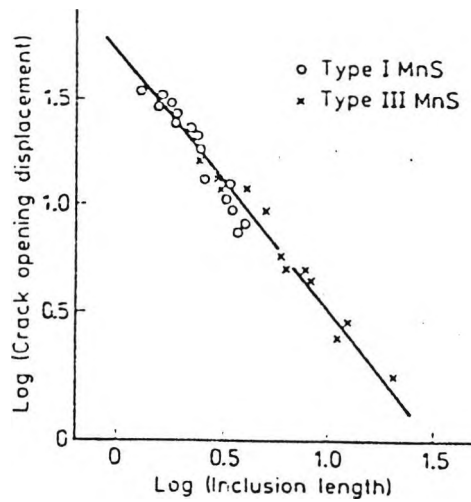
Figure 2.13: The relationship between the inclusion length and the fracture toughness measured by the crack opening displacement[47].

Charles[47]. These results have been interpreted by Gladman[42] to indicate a significant effect of inclusion size on C_v or COD, and there is a growing body of evidence that with smaller inclusions or the less separation between them the toughness in a ductile fracture process, i.e. the COD, decreases, Fig. 2.14[48]. Inclusion size effects have been discussed by Baker[49] who suggests that C_v decreases down to an inclusion size of 5 μm for a given volume fraction. Smaller inclusions than this appear to be much less detrimental, but it has been pointed out by Gladman[42] that small inclusions are relatively non-deforming which is likely to outweigh any inherent effect of small particle sizes on C_v, i.e. small inclusions do not elongate.
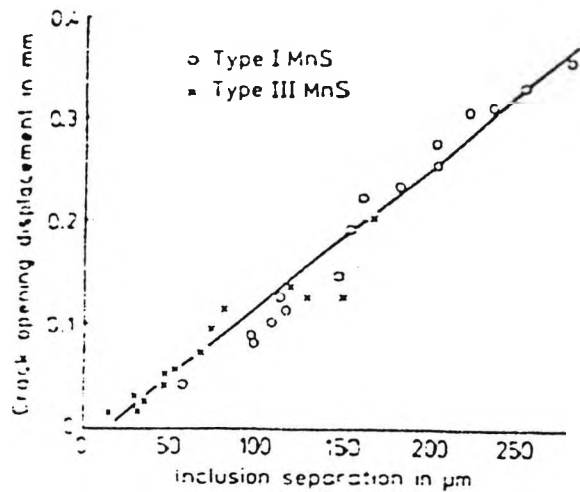
Figure 2.14: The relationship between the separation between inclusions and the fracture toughness measured by the crack opening displacement[48].

2.4 Higher Carbon Ferrite-Pearlite and Fully Pearlitic Microstructures

As the pearlite content increases up to 100%, the pearlite itself begins to play an increasing role in controlling both the strength and toughness. Gladman[50] have established relationships between microstructural parameters and strength and toughness. However, because the steels comprising these structures are used for rails, tyres, wheels, axles, reinforcing bars, forgings, wire and drill rods, the work has not been extended to ductility.

2.4.1 The Yield Stress

For steels with large amounts of pearlite the yield stress has been found to be best described by a modified law of mixtures for the ferrite and pearlite constituents and which allows the strength to vary linearly with the pearlite

content, Fig, 2.15[50]:

$$\sigma_y = (f_\alpha)^n \sigma_\alpha + (1 - (f_\alpha)^n) \sigma_{pe} \qquad (2.25)$$

where f_α is the mass fraction of ferrite, and σ_α and σ_{pe} are the yield stresses of the ferrite and pearlite respectively. The index, n, allows for the non-linear variation of σ_y with increasing pearlite content, and it is observed that a value of n = 1/3 gives least residual error. Several authors believe that σ_α obeys a normal Petch type relationship with the ferrite grain size, where as σ_{pe} has been shown to be related by a Petch type relationship to the pearlite interlamellar spacing, S[51,52]. A typical equation for the yield stress of the pearlite is:

$$\sigma_{pe} = \sigma_i + KS^{-1/2} \qquad (2.26)$$

where σ_i is an apparent friction stress, K is a constant and S is the pearlite interlamellar spacing (mm). It has also been reported[51,53] that σ_{pe} is related to S^{-1} rather than to $S^{-1/2}$ and indeed S^{-1} may have some advantages over $S^{-1/2}$. According to Pickering[26] the pearlite colony size, p(mm), and the pearlite cementite lamellae thickness, t(mm), do not influence σ_{pe}, but do affect the ductile-brittle transition temperature as will be shown later. In ferrite-pearlite structures containing pearlite contents of 20% to 100%, the following equation was obtained by Gladman[50]:

$$\sigma_y = (f_\alpha)^{1/3}[35 + 58(wt.\%Mn) + 17.4d^{-1/2}] +$$
$$(1 - (f_\alpha)^{1/3})[178 + 3.8S^{-1/2}]$$

61
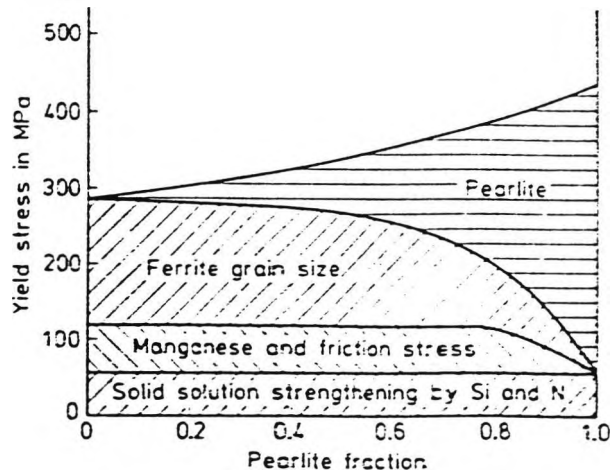
Figure 2.15: The effect of the pearlite fraction on the yield stress of normalized carbon-manganese steels, showing the effect of the various strengthening mechanisms[50].

$$+63(wt.\%Si) + 425(wt.\%N_{free})^{1/2} \qquad (2.27)$$

where d is the mean linear ferrite grain size intercept and S is the pearlite interlamellar spacing.

Solid solution strengthening by other solutes was very similar to that discussed for the lower carbon steels[15]. Whittaker[54] has also reported that precipitation strengthening by microalloy carbonitrides occurs in the pearlitic ferrite and may well be described by Eq.(2.17).

For a fully pearlitic structure, Eq. (2.27) reduces to:

$$\sigma_{pe} = 178 + 3.8S^{-1/2} + 63(wt.\%Si) + 425(wt.\%N_{free})^{1/2} \qquad (2.28)$$

The effects of other strengthening mechanisms would require to be added. Another equation has been proposed by Krauss[55] and Hyzak[56] for the yield stress of pearlite which incorporates effects due to the pearlite colony size (p)

62

and the prior austenite grain size (D):

$$\sigma_{pe} = 52.3 + 2.18S^{-1/2} - 0.40p^{-1/2} - 2.88D^{-1/2} \qquad (2.29)$$

Pickering[26] argues that this equation must be viewed with some suspicion as it is difficult to understand why p and D influence σ_{pe} when they are on a very much coarser scale than S, and also why σ_{pe} should 'decrease' with finer pearlite colony and prior austenite grain size.

According to Gladman[50], Eq. (2.27) shows that the yield stress of a ferrite-pearlite steel depends on the ferrite grain size, which contributes less as the volume fraction of pearlite increases, and that as the composition approaches the eutectoid composition the pearlite contributes ever more to the yield stress, and this contribution is very dependent on S.

2.4.2 Toughness

An examination of Fig. 2.8 immediately reveals that increasing the carbon content of a steel, and therefore the pearlite content, increases the ductile-brittle transition temperature and markedly lowers the shelf energy. But the effects are by no means simple, involving some rather complex microstructural parameters.

2.4.3 The Ductile-Brittle Transition Temperature

The transition temperature T, has been shown by Gladman[50] to be dependent on the proportions of ferrite and pearlite, the pearlite colony size, p, interlamellar spacing, S, and the thickness of the cementite lamellae, t_c, as well as the ferrite grain size:

$$T(^0C) = f_\alpha[-46 - 11.5d^{-1/2}] + (1 - f_\alpha)[-335 + 5.6S^{-1/2}$$

$$-13.3p^{-1/2} + (3.48x10^6)t_c] + 49(wt.\%Si) + 762(wt.\%N_{free})^{1/2} \quad (2.30)$$

where f_α is the volume fraction of pro-eutectoid ferrite. Again further factors involving the effects of solid solution, precipitation and dislocation strengthening on T must be used as appropriate. It can also be seen that the detailed morphology of the pearlite has a pronounced effect on T. Just as a refined ferrite grain size is beneficial to T, so is a small pearlite colony size because cleavage cracks are often observed to stop and change direction at pearlite colony boundaries. These effects have been further confirmed[55,56] by the following equation, which also incorporates a term for the prior austenite grain size, D. This equation is for a fully pearlitic structure.

$$T(^0C) = 218 - 0.83p^{-1/2} - 2.98D^{-1/2} \quad (2.31)$$

Also for a fully pearlitic structure, Eq (2.30) reduces to:

$$T(^0C) = -335 + 5.6S^{-1/2} - 13.3p^{-1/2} + (3.48 \ x \ 10^6)t_c \quad (2.32)$$

again with appropriate terms for other strengthening effects.

Decreasing S increases T by virtue of the increased strength, but the simultaneous decrease in t, will decrease T because the thin cementite lamellae deform rather than crack. Either effect may predominate, but they may also be self-cancelling so that no effect of S is observed on T. The effects are further complicated by changes in the pearlite colony size, p, which may ac-
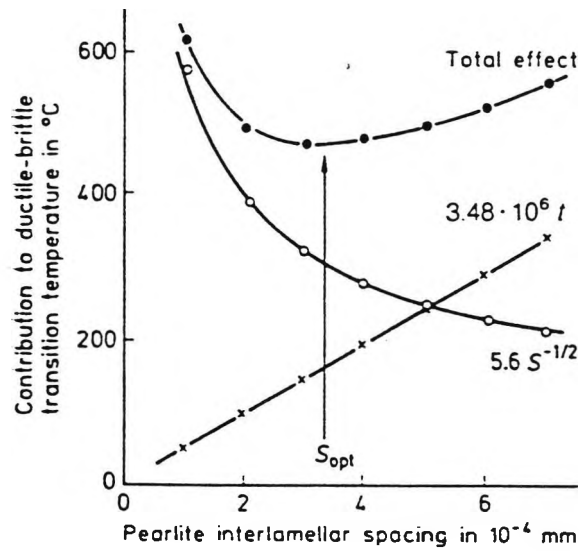
Figure 2.16: The contributions of the pearlite interlamellar spacing (S) and the carbide lamella thickness (t) to the ductile-brittle transition temperature, showing the occurrence of an optimum value of the inter lamellar spacing[58].

company changes in S due to the effect of transformation temperature. Both p and S decrease as the transformation temperature decreases[57,58] and generally for a given austenite grain size, p decreases as S decreases. However, Garbarz et al[59] suggests that austenite grain size has little effect on p or S for a given transformation temperature. Pickering[58] suggests that, because S and t_c have opposite effects on the ductile-brittle transition temperature, it is clear that there will be an optimum interlamellar spacing which will give the lowest value of T, as shown in Fig. 2.16. But since a small value of t_c will lower the transition temperature for a given interlamellar spacing, it is equally clear that a 'dilute' pearlite containing less than the equilibrium carbon content will be advantageous, because this will give a smaller carbide lamellae thickness.

Pickering[58] has shown that a low carbon dilute pearlite in a hypoeutectoid steel is conducive to producing a low ductile-brittle transition tem-

perature, and increasing the pearlite fraction at a given carbon content, either by alloying or increasing the cooling rate to lower the transformation temperature, will be beneficial. In a structure comprising both ferrite and pearlite, the precise effects will however depend on the balancing those of the ferrite and the pearlite, as shown in Eq. (2.30), especially if the ferrite is fine grained and therefore has a low ductile-brittle transition temperature. Pickering[58], suggests that replacing coarse grained ferrite by dilute pearlite of a fine colony size would be beneficial, especially if a lower transformation temperature had just decreased S to its optimum. Any further decrease in S by a further depression of the transformation temperature might then be detrimental to toughness, although the strength would be greater. Pickering[58] notes however, that a depression of the transformation temperature can be useful in achieving a fine ferrite grain and pearlite colony size. Some of these interactions between the amounts of ferrite and pearlite, and ferrite grain size and pearlite colony size, are shown in Fig. 2.17, and can lead to structures in which the value of T is independent of both ferrite and pearlite morphology[26]. A recent interesting effect relating to the pearlite colony size has been reported by Garbarz[57] and Pickering[58]. According to several authors[56,60] in general, pearlite colonies occur in orientationally related groups within a pearlite nodule and fracture is controlled by the pearlite nodule unit which in turn is related to the prior austenite grain size, D. This may be the reason why D occurs in Eq. (2.31).

2.4.4 The Shelf Energy Value

Over a limited range of pearlite fraction, the upper shelf energy, C_v, is given by Eq. (2.24), which clearly shows the decrease in C_v, as the pearlite content
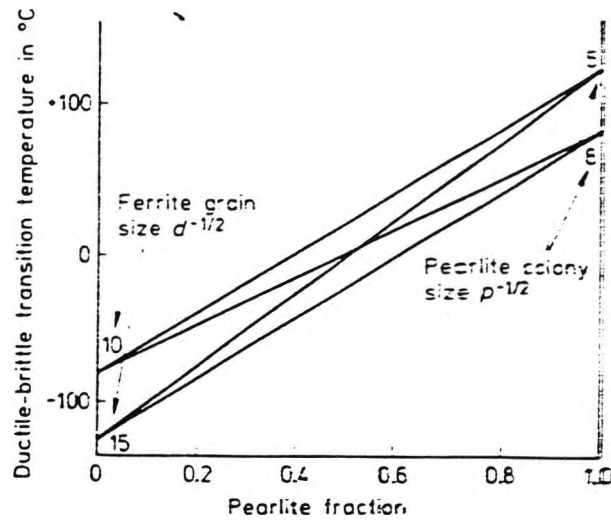
Figure 2.17: The interaction between the pearlite fraction, the pearlite colony size (p) and the ferrite grain size (d) on the ductile-brittle transition temperature of normalized ferrite-pearlite micrstructures[26].

increases[35].

Over a wide range of pearlite contents, the effect has been shown[58] not to be linear, C_v decreases exponentially with increasing pearlite fraction, Fig. 2.18. The effect parallels that of pearlite on true strain, ϵ_T, Fig. 2.19.

There is no systematic data on the effect of pearlite morphology on C_v. Pickering[58] suggests that this is probably because in other than recently developed ultra-fine grained high carbon steels, the ductile-brittle transition temperature for pearlite is 100-150 °C, Fig. 2.8, so the brittle cleavage rather than ductile fracture occur during testing near ambient temperature. However, it has been noted[26] that because there is a good relationship between C_v and ϵ_T, the effects of certain features of the pearlite morphology might be inferred, especially as C_v is often related to the area under the stress-strain curve. Thus decreasing S would be expected to increase C_v by increasing the general strength level and increasing the area under the stress strain curve
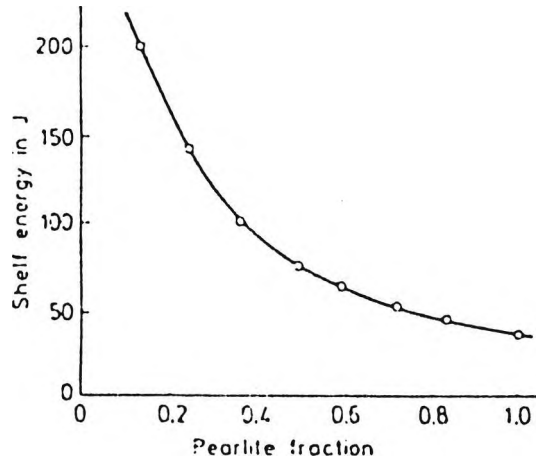
Figure 2.18: The effect of the pearlite volume fraction on the shelf energy in normalized ferrite- pearlite microstructures[58].
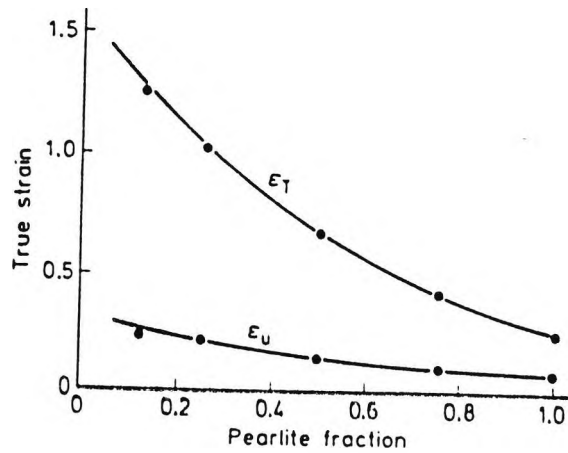
Figure 2.19: The effect of the pearlite fraction on the uniform true strain (ϵ_u) and the true strain at fracture (ϵ_T) in normalized ferrite-pearlite microstructures[58].
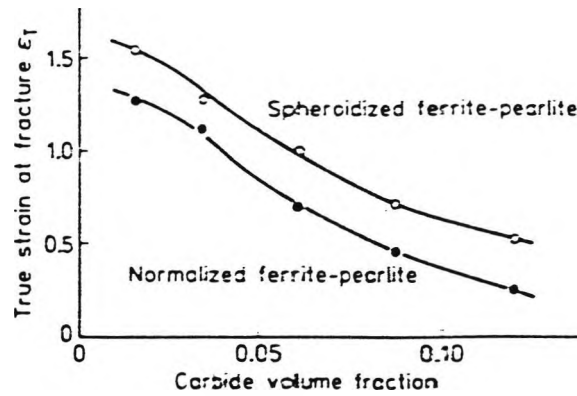
Figure 2.20: The effect of the volume fraction of carbides on the true strain at fracture for normalised and spheroidized ferrite-pearlite microstructures. The normalized microstructure contained lamellar pearlite[58].

despite a decrease in overall ductility. Decreasing S will also decrease t, so that the carbide lamellae will bend rather than crack, thus delaying void nucleation, and it might be anticipitated that S will therefore influence the ease of void coalescence. However, Pickering[58] note that often some cleavage fracture occurs together with ductile fracture because, as shown in Fig. 2.8, the transition temperature range is very wide. Thus a decrease in pearlite colony size might be beneficial. Certainly there is evidence[59] that when the pearlite comprises unrelated individual colonies, the C_v value may be increased appreciably. Additionally, Pickering[58] suggests that spheroidizing the pearlite would undoubtedly increase C_v, Fig. 2.20. The effects however are complex and require further elucidation.

69

2.5   Acicular Ferrite and Bainitic Microstructures

Bainitic and acicular ferrite have been shown to have many common morphological similarities, and indeed acicular ferrite may often be considered to be a form of very low carbon upper bainite[61]. These structures form the basis of the bainitic structural steels, used in larger section sizes for pressure vessels, pipework and power generation, and they are common structures found in weld metals and heat affected zones. Many measurements of their properties have been made, but much less success has been achieved in terms of quantitatively relating the microstructures to the properties than is the case for ferrite-pearlite structures. Because the structure is complex and difficult to characterize quantitatively, there are many factors influencing impact behaviour and these have been listed[26] as follows:

- 'packets' of lath-like ferrite grains of low misorientation between laths within a 'packet'. 'Packet' and prior austenite grain boundaries are high angle boundaries[61].

- a variable dislocation density, and dislocation arrays between ferrite laths.

- large carbides at ferrite lath, 'packet' and prior austenite boundaries, and carbides within the ferrite laths in lower bainite.

- alloy enriched ferrite islands, or high carbon bainite, martensite or even retained austenite between the ferrite laths, i.e. the martensite-austenite (MA) constituent.

70

- solid solution of both interstitial carbon, nitrogen and substitutional solutes.

To describe the individual effects of all these features on the mechanical properties is a formidable problem, and particularly to isolate the effect of grain size.

2.5.1 The Yield Stress

Due to the continuous yielding of these structures, σ_y usually refers to the 0.2% proof stress. The major strengthening mechanisms are due to grain size, dislocations, carbide dispersion and solid solution. It is well known[62] that the tensile strength increases linearly with decreasing transformation temperature, Fig. 2.21, and because the proof stress : tensile strength ratio is about 0.7 for these steels according to Pickering[63] the proof stress or σ_y will increase with decreasing transformation temperature. This is because all the above strengthening mechanisms increase with decreasing transformation temperature. But Steven and Haynes[64] believe that, the transformation temperature is related linearly to the steel composition so a linear equation of the following type can be used to describe σ_y approximately:

$$\sigma_y = 170 + 1300(wt.\%C) + 160(wt.\%Mn) + 160(wt.\%Cr) + 130(wt.\%Mo) +$$
$$88(wt.\%Ni) + 63(wt.\%W) + 45(wt.\%Cu) + 270(wt.\%V)$$

$$(2.33)$$

Many years ago it was observed[65] that the proof stress increased more or less linearly with $d^{-1/2}$, where d was the mean linear intercept of the bainitic fer-

71
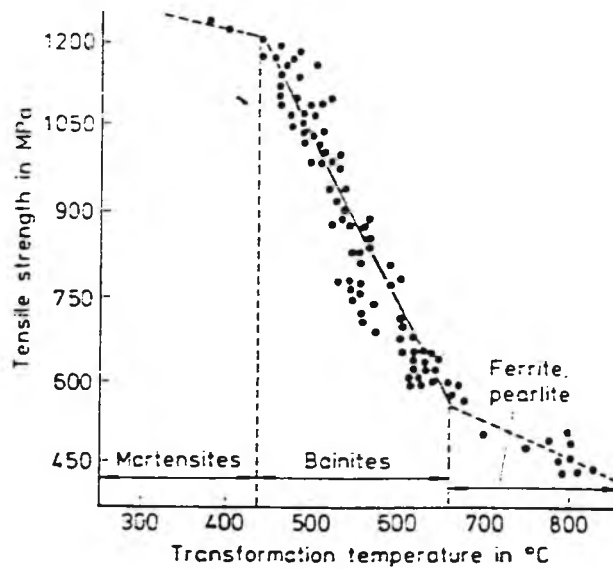
Figure 2.21: The relationship between the transformation temperature and the tensile strength in low carbon bainitic microstructures containing 0.05-0.15 wt.% C[62].

rite grain size, and also increased with increasing density of carbide particles. It was confirmed by Gladman[25], that in low carbon bainite the contribution to σ_y from the bainitic ferrite grain size could be described by a Petch analysis, and a small amount of dispersion strengthening was observed due to Fe_3C carbides. Several workers[25,65] concluded that the bainitic ferrite grain size contributed less than 50% of σ_y. In an attempt to produce a predictive equation for the proof stress of bainite, the individual effects of the bainitic ferrite grain size, d, and the number of carbide particles per unit planar section of the structure, n , were used,

$$\sigma_y = -191 + 17.2d^{-1/2} + 14.9n^{1/4} \qquad (2.34)$$

It has been observed[26] that the coefficient of $d^{-1/2}$ is very similar to k_y for polygonal ferrite structures. Also it has been noted[26] that the empirical nature of Eq.(2.34) is shown by the negative constant which indicates

72
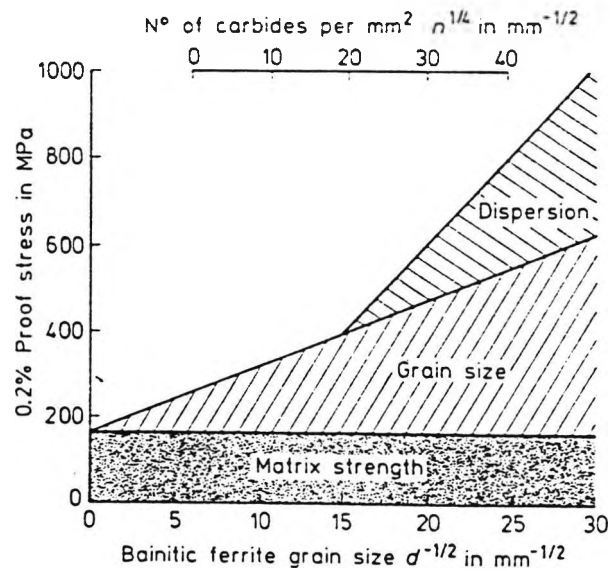
Figure 2.22: The contributions of the bainitic ferrite grain size and the carbide dispertion strengthening to the 0.2% proof stress of low carbon bainitic microstructures containing 0.05-0.15 wt.% C[25].

a threshold carbide distribution below which carbides do not contribute to the strength. Thus in upper bainite the carbides at the bainitic ferrite lath boundaries do not add to the strengthening, as their spacing is equal to or greater than the bainitic ferrite lath size. In lower bainite however, the carbides do contribute to the strength, as they occur within the ferrite laths[61]. It has been suggested[26] that, it is probable that in Eq. (2.34), n could be replaced by a σ_p term of the type given by Eq.(2.17), which has been shown to describe carbide dispersion strengthening reasonably effectively. The data used to drive Eq.(2.34) are shown in Fig. 2.22 which indicates that carbide strengthening only becomes significant at the finer bainitic ferrite lath sizes. i.e. at the lower transformation temperatures at which lower bainite is formed and contains carbides within the ferrite laths. Confirmation of this type of analysis has been obtained on the acicular ferrite structures[67] in the 4% Mn 'Fama' type steels, whilst the concept has also been successfully

applied to recent work on tempered martensite (see section 2.7.2). Bush and Kelly[68] have also suggested that the dislocation strengthening, which can be appreciable in bainite because of its shear transformation temperature, and can be described by:

$$\sigma_d = 1.2 \cdot 10^{-3}(\rho)^{1/2} \tag{2.35}$$

where ρ is the dislocation density in lines cm^{-2}.

Virtually no information has been presented for the solid solution strengthening effects in bainite, although it has been suggested[26] that values similar to those given in table 2.1 might be appropriate. An assessment has however been made[68] of the effect of the MA constituents, which is usually found in bainites formed during continuous cooling. The contribution to σ_y from the MA constituent, σ_{MA}, has been reported to be:

$$\sigma_{MA} = 360 + 900 f_{MA} \tag{2.36}$$

where f_{MA} is the volume fraction of the MA constituent.

It has been noted[26] that using the bainitic ferrite lath width in a Hall-Petch equation gives much too high a strength contribution, but using the prior austenite grain size seems to give more reasonable values. It is possible however that the bainitic ferrite 'packet' dimensions may produce a more reasonable estimate.

In view of the similarity of the coefficients of $d^{-1/2}$ for the bainitic and the polygonal ferrite structures, Gladman[21] and Whiteman[69] have developed an equation which indicates a precipitation strengthening term, σ_p, and a dislocation strengthening term, σ_d, to describe the yield strength σ_y, of low

carbon bainite/acicular ferrite. Omitting solid solution strengthening terms, the equation developed was:

$$\sigma_y = 88 + 15.1 d_L^{-1/2} + \sigma_d + \sigma_p \qquad (2.37)$$

where d_L is the mean linear intercept of the bainitic ferrite grain size (mm), σ_d is the dislocation strengthening term described by Eq. (2.18) and σ_p is the precipitation strengthening term described by Eq. (2.17) or by Onel and Nutting[66]:

$$\sigma_p = \frac{0.015}{\lambda} \cdot \ln \frac{D}{2|b|} \qquad (2.38)$$

where λ is the carbide spacing (μm), D is the carbide particle diameter (A) and b is the Burgers vector of the slip dislocations. It has been suggested[69] that for the very low carbon acicular ferrite steels the grain size coefficient in Eq. (2.37) should be increased from 15.1 MPa mm$^{-1/2}$ to about 17 MPa mm$^{-1/2}$, which would bring it closer to that in Eq. (2.34), and which would presumably incorporate the contributions from dislocations in lath and sub-grain boundaries.

2.5.2 Toughness

Very little work has been done on the value of the Charpy shelf energy, C_v, in bainitic and acicular ferrite structures, but there is clear evidence that increasing the carbon content decreases C_v and it can also be inferred that increasing both σ_d and σ_p decrease C_v[70]. Consequently attention will be concentrated on factors influencing the ductile-brittle transition temperature.
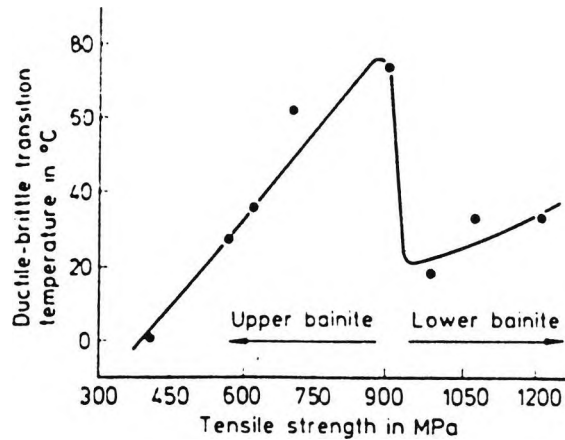
Figure 2.23: The relationship between the ductile-brittle transition temperature and the tensile strength for low carbon bainitic microstructures containing 0.05-0.15 wt.% C[65].

2.5.3 The Ductile-Brittle Transition Temperature

The transition temperature, T, has been shown by Pickering[65] to increase with increasing strength for both upper and lower bainite and it is observed that upper bainite has a higher transition temperature than lower bainite, as shown in Fig. 2.23. According to Pickering[65] this latter observation is largely due to:

- the easy initiation of cleavage cracking in upper bainite due to the cracking of the large inter-lath carbides, and the inability of the low angle bainitic ferrite lath boundaries to impede cleavage crack propagation

- the fine carbides within the lath of lower bainite, which impede cleavage crack propagation.

Of particular importance in controlling the transition temperature is the spacing of the high angle 'packet' or prior austenite grain boundaries,

76
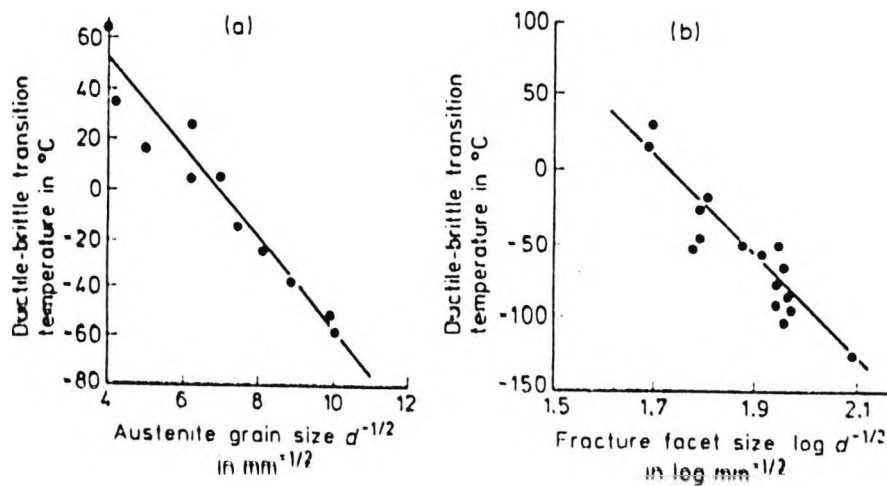
Figure 2.24: The dependence of the ductile-brittle transition temperature on the prior austenite grain size or the fracture facet size in: (a) bainitic microstructures, (b) martensitic bainitic microstructures[70].

which act as effective barriers to cleavage crack propagation. An early observation[70] on the impact properties of bainite was the increase in T with increasing prior austenite grain size. The data reported can be interpreted to show a linear dependence of T on $D^{-1/2}$, where D is the mean linear intercept of austenite grain size, Fig 2.24(a). It has also been shown[34,71] that there is a linear relationship between T and log $d^{-1/2}$, where d is now the unit cleavage crack path or the cleavage facet size, Fig 2.24(b), both of which are synonymous with the bainitic ferrite and or martensite 'packet' size. Confirmation of this analysis has been obtained for acicular ferrite structures[67]. An analysis of the factors affecting T for bainitic structures[21] has been based on Eq. (2.20) for ferrite-pearlite structures, but modified to omit the effect of pearlite and to include a precipitation strengthening term, σ_p, and terms describing strengthening by low angle lath boundaries, σ_b, and by random forest dislocations, σ_d.

77

The equation used, omitting solid solution effects, was:

$$T(^0C) = -19 + 0.26(\sigma_p + \sigma_b + \sigma_d) - 11.5d^{-1/2} \qquad (2.39)$$

The term, d, is the mean intercept of high angle boundaries, i.e. 'packet' or prior austenite grain boundaries. This equation assumes that σ_p, σ_b and σ_d all have the same embrittling effect, for which there is evidence[13,35] and accepts that low angle ferrite lath boundaries do not impede cleavage crack propagation. σ_d can be described by Eq. (2.18) but σ_b, which is strengthening due to low angle boundaries, is more difficult to evaluate as it is only part of the 15.1 $d_L^{-1/2}$ term in Eq.(2.37). High angle boundaries increase the strength and decrease the T by acting to impede crack propagation, the effect being -0.7 ^{0}C per MPa increase in σ_y[13,21]. On the other hand low angle boundaries increase σ_y and by so doing raise T because they do not act as barriers to cleavage crack propagation[35]. The value of σ_b can be obtained from the difference in yield strength between structures containing high angle boundaries of grain size, d, and those with a bainitic ferrite lath size of d_L :

$$\sigma_b = 15.1(d_L^{-1/2} - d^{-1/2}) \qquad (2.40)$$

Using this approach it has been shown[35] that the predicted yield stress versus ductile-brittle transition temperature relationship agrees well with the experimental values over a wide range of σ_y, Fig. 2.25, but in some low carbon bainitic steels there are anomalously high values of T that are due to an embrittlement effect caused by coarse carbides at the bainitic ferrite lath boundaries[35]. Gladman[21] suggests that these coarse carbides affect T in a manner previously described for filamental grain boundary carbides

Ductile-brittle transition temperature corrected for composition in °C

50
0
-50
-100

$d^{-1/2} = 7 mm^{-1/2}$
$d^{-1/2} = 8 mm^{-1/2}$
$d^{-1/2} = 9 mm^{-1/2}$

200   400   600   800

Yield stress corrected for composition in MPa

• Steels without large carbides
× Steels with large carbides
d = High angle grain size, i.e. bainitic ferrite packet size
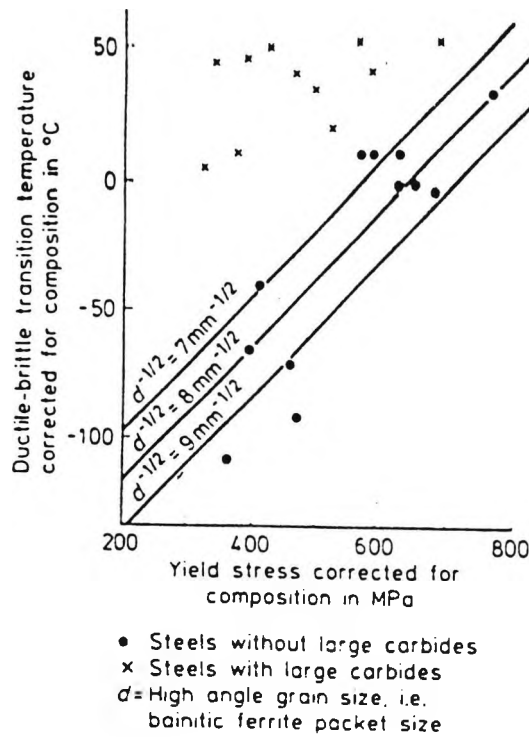
Figure 2.25: The relationship between the yield stress and the ductile-brittle transition temperature for bainitic microstructures containing 0.05-0.15 wt.% C[35].

by Eq.(2.23)[41]. It has been suggested[26] that similar embrittlement may be anticipated from regions of high carbon bainite or martensite between bainitic ferrite laths, i.e. the MA constituent, but these effects have not been quantified.

Plautt and Whiteman[69] have confirmed the validity of Eq. (2.39) to acicular ferrite structures but it has been noted[26] that, it seems the use of the prior austenite grain size instead of the acicular ferrite 'packet' size gives more reliable predictions.

2.5.4   The Effects of Non-Metallic Inclusions

Upper bainite and acicular ferrite often occur in weld metals and the heat affected zones of low carbon low alloy steels, the acicular ferrite being particularly beneficial to toughness[72]. Pro-eutectoid polygonal ferrite has often been found to nucleate at MnS inclusions[72], which may be due to Mn de-

pletion around the MnS or due to the MnS/matrix interface acting as a heterogeneous nucleation site. Indeed this type of ferrite nucleation has been utilised in 0.05 wt.% S steels to produce more ferrite of a finer grain size and thus high toughness in microalloyed steel automotive components[73]. A mechanism for enhancing intragranular ferrite nucleation in medium C-V steels has been suggested by Ochi et al[74]., to involve the initial precipitation of VN on MnS particles followed by VC precipitation on the VN, then ferrite nucleation on the VC.

There is also evidence[75] that oxidic inclusions of the silicate or spinel types can act as nuclei for the lower transformation temperature products, acicular ferrite and bainite. Recent work[76] has shown that the desirable acicular ferrite transformation is controlled by oxide inclusions. The mechanisms involved are not fully understood and have been commented upon by Pickering[72].

2.6 Martensitic Microstructures

Much work has been done on the mechanisms contributing to the strength of martensite, but quantitative and predictive equations have not been well developed. Even less quantitative data is available on the toughness parameters. In the case of both strength and toughness, the complexity of the microstructure renders quantitative characterization difficult, and the many mechanisms contributing to the strength makes their individual identification a problem. The inherent brittleness of untempered martensite, and the very real danger of the higher carbon steels containing quench cracks, also make the validity of some measured properties rather doubtful. It has been noted[26] that the strengthening mechanisms which occur in martensite are:

80

- (i) carbon and/or nitrogen in solid solution.

- (ii) the fine martensite plate or lath size.

- (iii) the high dislocation density in low carbon lath martensite.

- (iv) the restriction of dislocation movement by twin boundaries in high carbon lenticular martensite.

- (v) The precipitation of carbides, especially in tempered and auto-tempered structures, and the clustering of carbon atoms.

- (vi) the interaction between interstitially dissolved carbon and nitrogen and dislocations.

Leslie et al[77] suggests many of these features interact, or are mutually influenced by, for example, carbon and the various mechanisms may not be simply additive. The effect of carbon and/ or nitrogen on the hardness of martensite is shown by Pickering[78] in Fig. 2.26. Solid solution hardening by carbon and/or nitrogen is reported[78] to be linearly related to a power function of the concentration:

$$\sigma_y = \sigma_0 + k(wt.\%C)^n \qquad (2.41)$$

where σ_0, k and n are constants.

n can vary between 0.33 and 1.00, and various equations have been proposed to describe the yield or proof stress, σ_y, a typical one proposed by Cohen[79], being:

$$\sigma_y = 290 + 1800(wt.\%C)^{1/2} \qquad (2.42)$$

81
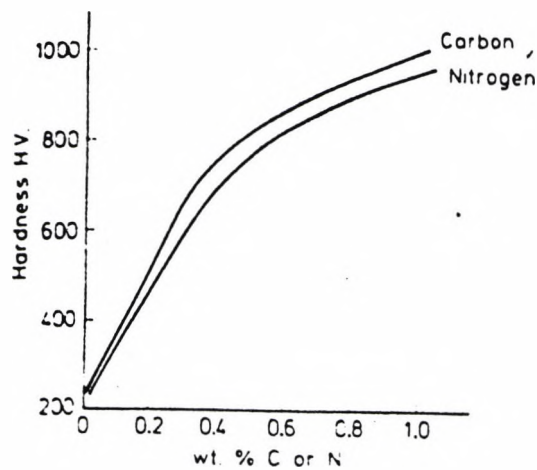
Figure 2.26: The effect of carbon or nitrogen on the hardness of quenched fully martensitic microstructures[78].

According to Irvine et al[80]., alloy martensites are often somewhat harder at a given carbon content, not so much due to solid solution strengthening by the alloying elements but rather due to the fact that the M_s is depressed and less auto-tempering occurs. It has been suggested by Kelly and Nutting[81] that carbon as carbide precipitated in martensite may be twice as effective as that in solid solution and any precipitated carbide will detract from both solid solution strengthening and strengthening from clusters or dislocation atmospheres. These effects have been discussed by Pickering[35]. Precipitation, or the rearrangement and clustering of carbon atoms, occurs in martensite at temperatures above -60 $^{\circ}$C[83], the strengthening effects increasing with increasing carbon content[80]. It is difficult to differentiate between clustering, precipitation, dislocation atmosphere and solid solution strengthening effects. Extracted data by Pickering[26] from the literature give some guide to the efficacy of the different strengthening mechanisms in contributing to the yield (0.2% proof) stress in a 0.4 wt.% C steel of σ_y 2200 MPa and this

Strengthening mechanism	Strength contribution (MPa)		
	Kelly and Nutting (1965)	Smith and Hehcman (1971)	Williams and Thompson (1981)
Boundaries	−	450 − 600	620
Dislocations	150 − 300	−	270
Solid solution	350	−	400
Clustering, precipitation, etc.	750	−	1000

Table 2.4: Some estimates of the contributions of the different strengthening mechanisms to the 0.2 % proof stress of 0.4 wt.% martensite[26].

is given in Table 2.4.

2.6.1 The Yield (0.2% Proof) Stress

The major strengthening is due to carbon in its various forms and to dislocations, and there is evidence that the grain size contribution only accounts for some 25-30% of the 0.2% proof stress[84]. Variations in the prior austenite grain size have been shown to produce significant changes in the strength of both 'as quenched' and tempered low alloy martensites[85]. It is probable however that the prior austenite grain size only controls the martensite crystal grain size or the martensite 'packet' size. In fact it has been shown by Swarr and Krauss[86], that the martensite packet size is related to the prior austenite grain size and moreover that the yield stress is related to the martensite 'packet' size by a Petch type relationship. An interesting features suggested by Roberts[87], is that the coefficient for the 'packet' size is much greater for carbon martensite than that for carbon-free martensite. This strong de-

83

pendency of the yield stress on 'packet' size has been attributed to carbon segregation at the 'packet' boundaries and prior austenite grain boundaries, but tempering reduces the dependency of σ_y on the 'packet' size due to the formation of carbides[86]. Another analysis[69] of the yield (0.2% proof) stress of low carbon lath martensite has used a modified form of Eq.(2.16) omitting substitutional solid solution strengthening which contributes a very small amount to martensite strength:

$$\sigma_y = 88 + 28d^{-1/2} + \sigma_d + \sigma_b \qquad (2.43)$$

where d is the mean linear intercept of the martensite 'packet' size, σ_d is the forest dislocation strengthening, Eq. (2.18), and σ_b is a balancing term to take account of the strengthening by martensite lath boundaries, given by Eq. (2.40). The effect of the martensite 'packet' size on the 0.2% proof stress is shown in Fig. 2.27. Pickering[90] believes that there seems no reason why the σ_b term should not entirely replace the martensite 'packet' size strengthening term, especially as the analysis showed that in some cases the martensite 'packet' boundaries did not contribute to the strength. It should be noted that the coefficient of $d^{-1/2}$ is greater than the k_y value for the polygonal ferrite, in agreement with the previous work by Roberts[87].

2.6.2 Toughness

The hardness and inherent brittleness of martensite, together with the possibility of quench cracking causing premature failure, makes accurate determination of the ductile-brittle transition temperature, T, difficult. Pickering[90] also notes that the shelf energy, C_v, can only be determined at testing tem-
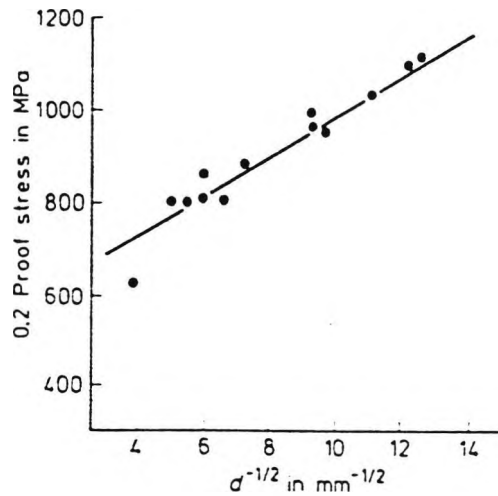
Figure 2.27: The effect of the martensite 'packet' size (d) on the 0.2% proof stress of low carbon martensitic microstructures[69].

peratures at which some decomposition by tempering takes place, and the same problem can render the determination of the transition temperature uncertain. Despite these difficulties, an analysis of the transition temperature for the low carbon martensites has been used Eq.(2.39) with good agreement between observed and calculated values, provided the austenite grain size was used as a measure of d. As shown in Fig. 2.24b, however there is a clear relationship between T and the martensite fracture facet size, i.e. the 'packet' size[71]. As has already been mentioned there is a relationship between the prior austenite grain size and the martensite 'packet' size. Consequently it is not surprising that it has often been shown[71,88] that the martensite 'packet' size controls T. Surprisingly, it has also been suggested by Naylor and Krahe[89] that the martensite lath width in low carbon steels controls the transition temperature and it has been suggested that some difficulty may be experienced in identifying the lath boundaries[26]. There is very little quantitative data available on the effect of grain dimensions on C_v

in martensitic structures.

2.7 Tempered Microstructures

2.7.1 Tempered Ferrite-Pearlite Microstructures

According to Mintz et al[32]., tempering ferrite/pearlite steels can lead to fall in strength and increase in T. Mintz suggests that the substantial fall in σ_y is only in part due to spheroidization whereas the marked fall in UTS is probably due solely to spheroidization. In the main, T increases with extensive tempering because the increase in T from the thickening of the grain boundary carbides outweighs the decrease in T from the loss in strength. Increasing the pearlite volume fraction by raising the C level causes the T to increase due to the greater volume fraction of the harder carbide phase. It is possible that an increase in grain boundary carbide density might reduce the sensitivity of the T to the carbide thickness. For fully pearlitic steels, tempering produces a large fall in σ_y, which dominates the fracture process and leads to a marked decrease in T[32].

2.7.2 Tempered Bainite and Tempered Martensite Microstructures

Pickering[90] suggests that in the case of tempered bainite or martensite the problems of the quantitative characterization of the microstructure are acute, particularly as the dislocation density will vary with tempering temperature and there is usually a multi-model size distribution of carbide particles, which can occur at four different positions, namely within laths, and at lath, 'packet'

and prior austenite grain boundaries. In addition, in medium-high carbon steel tempered at low temperatures, and in steels containing strong carbide forming elements such as Mo and V which are tempered at secondary hardening temperatures, fine dispersions of $\epsilon(Fe_{2.4}C)$, $\nu(Fe_2C)$ and alloy carbides (VC, Mo_2C etc.) will be formed in the matrix and the coherency of these carbides with the matrix will vary with tempering temperature and time. Little or no work on the quantitative relationships between these complex microstructures and their properties has been reported.

2.7.3 The Yield Stress

Work of Onel and Nutting[66] on heavily tempered plain carbon martensites has thrown considerable light on these microstructures. The results can also probably be equally well applied to heavily tempered bainites. It has been shown possible by Pickering[90] to distinguish between microstructures in which the carbides are exclusively at the ferrite grain boundaries, and those in which carbides also occur within the tempered ferrite grains. In the former the carbides contribute no strengthening and the yield stress is predominantly controlled by the tempered ferrite grain size, d:

$$\sigma_y = 108 + 18.2d^{-1/2} \tag{2.44}$$

Both σ_i and k_y are rather higher than for polygonal ferrite, probably as suggested[26] due to a contribution from residual dislocations to σ_i, which will also increase k_y. On the other hand structures containing carbides within the grains showed an additional strengthening effect, σ_p:
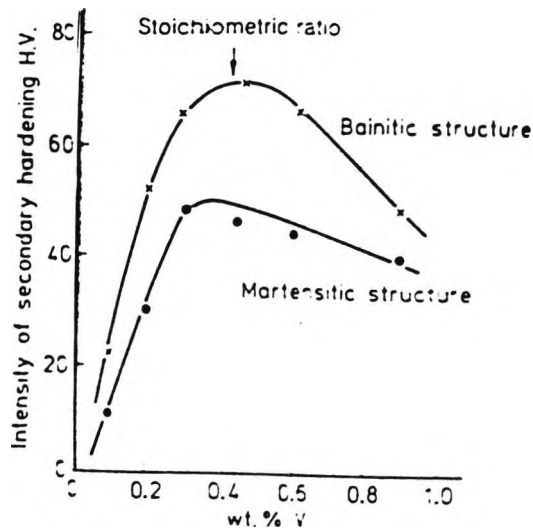
Figure 2.28: The effect of vanadium on the intensity of the secondary hardening in tempered 0.1 wt.% C steels comprising prior bainitic or martensitic microstructures, showing the maximum effect at the stoichiometric ratio[90].

$$\sigma_y = 77 + 23.9d^{-1/2} + \sigma_p \qquad (2.45)$$

where σ_p is described by Eq.(2.38). The very high coefficient of $d^{-1/2}$ may well indicate a non-additive interaction between the two strengthening effects. Similar analysis have also been used to describe the flow stress of the different microstructures at the given strain. Pickering[90] argues that the similarity of this approach to that used to describe the properties of low carbon bainite, see Eq.(2.37), should be noted, and there is no reason why relationships of the type shown in Eq. (2.45) could not be used for the yield stress of tempered bainite. An interesting feature of secondary hardening alloy steels is that the yield (0.2% proof) stress is maximum at steel compositions for which the metal: carbon ratio (wt.%) is in the stoichiometric ratio for the precipitating alloy carbide. This occurs for both prior martensite and prior
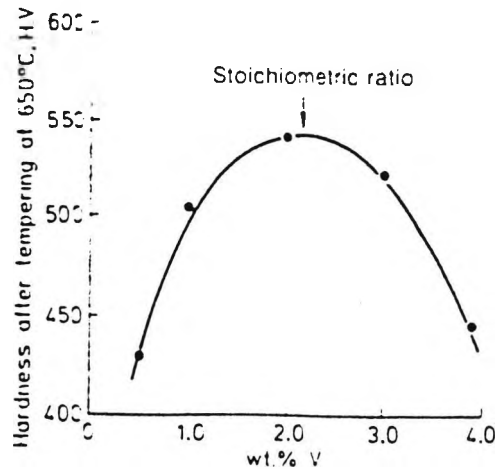
Figure 2.29: The effect of vanadium on the overaged hardness of 0.6 wt.% C martensitic microstructures tempered for 1 hour at 650 ^{o}C, showing the maximum effect at the stoichiometric ratio[90].

bainite microstructures, as shown for the hardness in Fig. 2.28, and the effect persists even for heavily overaged microstructures, Fig. 2.29. According to Wadsworth[91] the reason for this effect is that at stoichiometric ratio, the temperature dependence of the solubility is a maximum so that there is an increasing volume fraction of the alloy carbides to give increased precipitation strengthening according to Eqs. (2.17) or (2.38), see Fig. 2.30.

2.7.4 Toughness

The various types of embrittlement phenomena which can occur during the tempering of martensite and bainite make it difficult to quantify the effect of grain size on both the ductile-brittle transition temperature and the upper shelf energy value. Pickering[65] notes that whilst systematic data is not available, there is evidence that the transition temperature, T, of tempered martensite and bainite increases with increasing carbon content. The effect

89
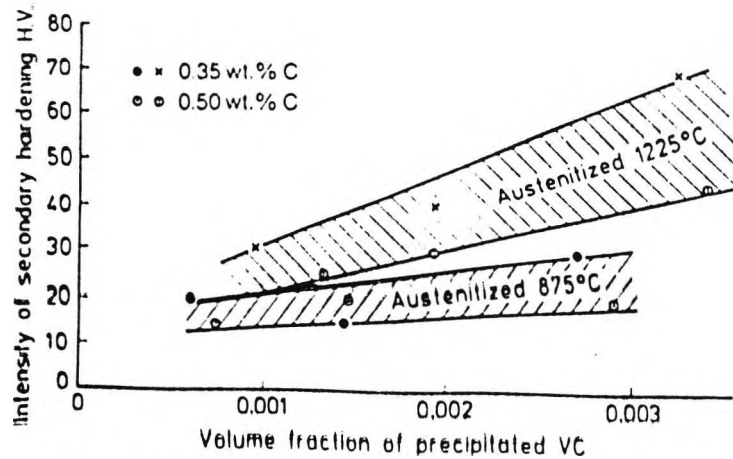
Figure 2.30: The dependence of the intensity of secondary hardening on the volume fraction of VC precipitated during tempering 0.35-0.50 wt.% C martensitic microstructures[90].

of tempering on the transition temperature of tempered bainites has been shown[67,70] generally to decrease T due to the decrease in both σ_p and σ_d, Fig. 2.31. The effect is virtually linear, T decreasing by 0.2/0.3 ^{0}C for each MPa decrease in the yield or proof stress[34]. This has also been confirmed by Little et al[92] for tempered martensite, the decrease in T being 0.2/0.5 ^{0}C per MPa decrease in σ_y. At higher tempering temperatures, towards the A_1 temperature, the recrystallization and grain growth of the ferrite matrix results in an increase in T, despite a decrease in σ_y. This is also shown in Fig. 2.31, the increase in T with decreasing σ_y being precisely that which would be expected from ferrite grain coarsening according to Eq. (2.20). As in bainite and martensite, there is evidence[92] that an increase in the prior austenite grain size of tempered martensite increases T. An increase in $d^{-1/2}$ of 1 mm$^{-1/2}$ results in an increase in the value of T by 23 ^{0}C. This is about twice the value obtained for the polygonal ferrite grain size which according

90
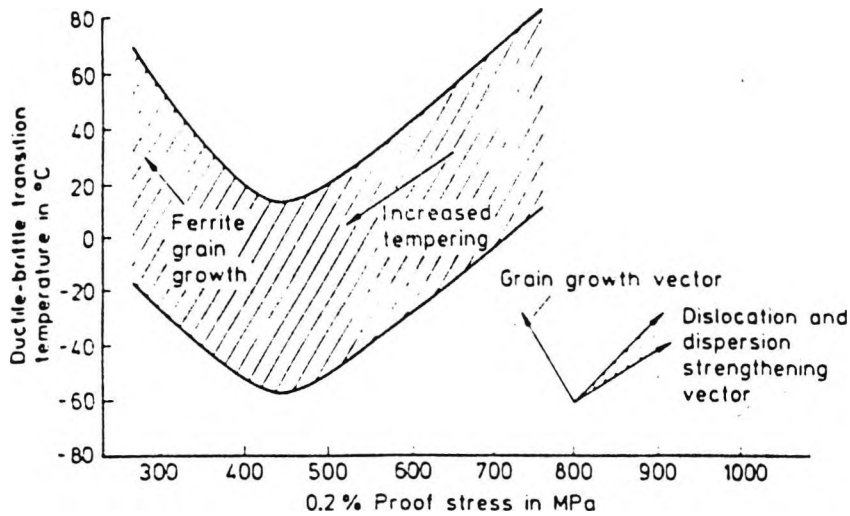
Figure 2.31: The effect of tempering on the relationship between the 0.2% proof stress and the ductile-brittle transition temperature for low carbon bainitic microstructures, showing the effect of different strengthening mechanisms[34].

to Pickering[65] may reflect residual dislocations and solute elements, but it is identical with the value obtained by other workers[71] on martensitic structures, although in that case a martensite 'packet' size was used. Pickering[65] also notes that, these rather fragmentary observations suggest that providing no anomalous embrittlement occurs during tempering, an analysis based on Eq.(2.20) could be used to relate the microstructure to the transition temperature in tempered martensite. However, modifications would be required to take into account the effect of precipitation and dislocation strengthening, and to omit the pearlite term, as in Eq.(2.39), together with the fracture facet or martensite 'packet' size. It might also be necessary to take into consideration the thickness of the carbide particles, as indicated in Eq. (2.23).

Some information is available[55] on the effect of various types of embrittlement on the toughness of tempered martensite, but quantitative relationships are not known. This is not surprising because of the toughness
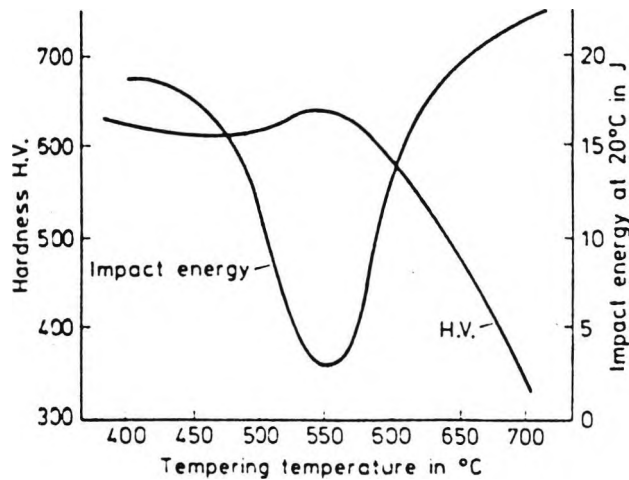
Figure 2.32: Embrittlement caused by secondary hardening during the tempering of a 0.4 wt.% C, 5 wt.% Cr-Mo-V steel[93].

minima which occur under certain conditions, as shown for the embittlement occurring during secondary hardening, Fig. 2.32 and this is also shown by a minimum K_{1c} value, Fig. 2.33. Similar effects are shown[55,90] for tempered martensite embrittlement, reversible temper embrittlement and upper nose embrittlement and are dependent on the tempering time. Krauss[55] notes that the embrittlement is always associated with an increase in T, but also the brittle fracture mechanism often changes from cleavage to various types of intergranular cracking, which again makes quantitative analysis difficult.

Some data[90] on the effect of microstructure on the fracture toughness parameter, K_{1c}, indicates that decreasing the strength by carbide coarsening and a decrease in dislocation density cause more or less the same increase in K_{1c}. However, it has been stated[26] general relationships between the microstructure and K_{1c} are rarely attempted probably because K_{1c} is not a unique material property but varies with both testing temperature and fracture mode. Increasing carbon content does decrease K_{1c}, as expected[94].
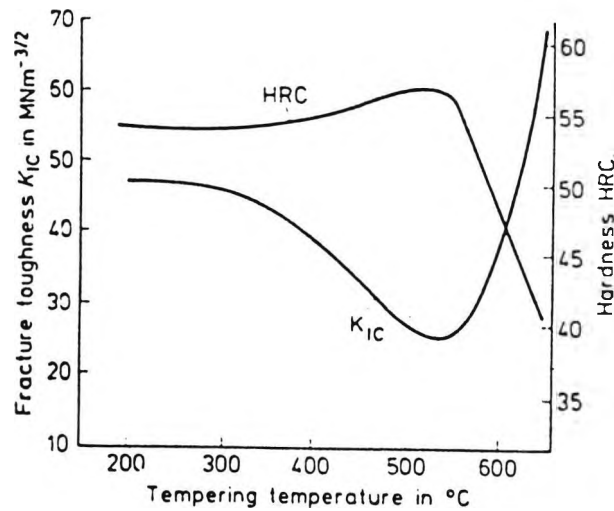
Figure 2.33: The effect of secondary hardening embrittlement on the fracture toughness parameter (K_{1C}) during the tempering of a 0.4 wt% C, 5 wt.% Cr-Mo-V steel[93].

Much of the fracture toughness data[72] is related to the effect of non-metallic inclusions, which have a pronounced effect on the ductile fracture mode K_{1c} value. Table 2.5 indicates that increased S content and volume fraction of MnS in a high strength steel decreases the K_{1c} value for a quenched and tempered microstructure. Other work[96] has also shown that the basic features of the inclusion distribution which control ductility and C_v values also control K_{1c} in high strength steels when fracture occurs by the ductile mechanism, Fig. 2.34, and that K_{1c} shows an isotropy in just the same way as does C_v. The interesting feature noted by Pickering[72] is that there is little anisotropy at low inclusion volume fractions because the grain size was coarser which gave cleavage rather than ductile fractures. Thus it may be concluded that the inclusions have relatively little effect on K_{1c} for cleavage fracture, and indeed the cleavage fracture energy in the Charpy test does not

93
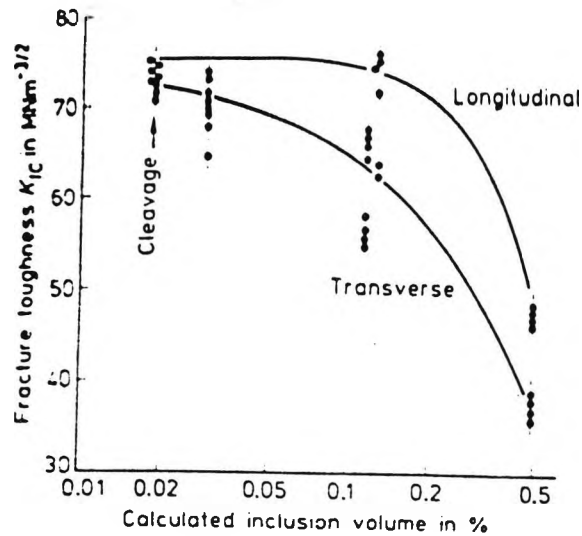
Figure 2.34: The effect of the non-metallic inclusion content on the fracture toughness parameter (K_{1C}) for a quenched and tempered high strength steel, showing the anisotropy of toughness[96].

seem to be greatly influenced by inclusions.

According to Pickering[72], very little data is available on the effect of microstructure, particularly grain size in tempered martensite or bainite, on the value of C_v. There is very limited evidence[92] to show that prior austenite grain size has no marked effect. It has also been reported[92] that C_v decreases exponentially with increasing strength in tempered martensite as would be expected, because this probably reflects the decrease in dispersion strengthening, σ_p, rather than any effect of grain size.

Wt.% S	Volume fraction, MnS	K_{IC} in MNm$^{-3/2}$
0.008	4.3×10^{-4}	72
0.016	8.6×10^{-4}	62
0.025	1.3×10^{-3}	56
0.049	2.6×10^{-3}	47

Table 2.5: Effect of wt.% S and volume fraction of MnS on the K_{1c} value for a quenched and tempered medium carbon steel[95].

Chapter 3

EXPERIMENTAL PROCEDURE

3.1   Introduction

Much progress has been made in relating the quantitative parameters which describe the microstructure of steel to the mechanical properties. The most commonly used measurements to describe the microstructures are (i) the proportion of volume fraction of phases (ii) the assesssment of grain size (iii) the determination of particle size distribution.

Charpy and tensile tests are most frequent experiments used to give an indication of mechanical property of materials. The chief engineering use of the charpy test is in selecting materials which are resistant to brittle fracture by means of transition temperature curves. The design philosophy using transition temperature curves centres about the determination of a temperature above which brittle fracture will not occur at elastic stress levels. Obviously, the lower this transition temperature, the greater the fracture toughness of

the material. The principal advantage of a charpy V-notch impact test is that is a relatively simple test that utilizes a relatively cheap, small test specimen. Tests can be carried out over a range of sub-ambient temperatures and simulates severe brittle fracture conditions. Thus a combination of tensile and impact data should provide enough information for designers to enable them to select the appropriate material.

3.2   Impact Test

Various types of notch impact tests are used to determine the tendency of a material to behave in a brittle manner. This type of test will detect differences between materials which are not observable in a tension test. Two classes of specimens have been standardized for notch testing. The charpy test is most commonly used in the United States, while the Izod specimen was favoured in Great Britain. Nowadays, the more recent charpy test seems to be internationally used for most impact tests thus the charpy test was chosen for the purpose of this research.

The charpy specimen has a square cross-section (10 x 10 mm) and contains a 45^0 V-notch, 2 mm deep, with a 0.25 mm root radius, Fig 3.1. The specimen is supported as a beam in a horizontal position and is loaded behind the notch by the impact of a heavy swinging pendulum, Fig 3.2. The specimen is forced to bend and fracture at a high strain rate of the order of 10^3 s^{-1}. The principal measurement from the impact test is the energy absorbed in fracturing the specimen. The notch bar impact test is most meaningful when conducted over a range of temperatures so that the temperature at which the ductile-to-brittle transition takes place can be determined.

An Avery-Dension, Izod, Charpy Impact machine, No. 6703/A/31045,

was used at all times calibrated to B.S.131, part 4 having a striking velocity of 5 m/s at 300 J capacity. All the charpy V-notch samples were machined and checked to B.S.131 part 2[97]. These were taken in mid-thickness radially to the flange face, Fig 3.3. The notch was cut in the through thickness direction.

3.3   Cooling Equipment

In order to obtain a ductile-brittle transition curve for each heat treatment various cooling baths were used to achieve different test temperatures. According to B.S.131, part 2[97] in all cases the period of immersion of the test piece and the holder in the bath at the required temperature must not be less than 10 minutes and the test piece must be broken within 5 seconds from the time of removal from the bath. A holder/ carrier was designed Fig 3.4 to reduce the fracture time to less than 5 seconds.

The following cooling media were used for the various temperatures.

- 20 $^{\circ}$C to 80 $^{\circ}$C. Samples were placed in a stainless steel beaker having at least 100 mm of water after which the container was immersed in a larger water bath. This was heated to required temperature ensuring a constant distribution of heat using a magnetic stirrer. A 0 $^{\circ}$-200 $^{\circ}$C mercury thermometer manufactured to B.S.1704 was used to record the temperature.

- 0 $^{\circ}$C. An ice/water mixture in a well lagged beaker was chosen for this temperature. A 35 to -140 $^{\circ}$C alcohol thermometer manufactured to B.S.1704 was used to measure all sub-ambient temperatures.

- 20 to -140 $^{\circ}$C. An Amsler Tv742 cooling chamber containing liquid ni-

trogen which circulates around an isopentane chamber was employed. The samples were placed in the isopentane chamber which has a stirring device keeping the temperature constant at all times. The liquid nitrogen is circulated around the isopentane chamber with the aid of a pump which was controlled by means of a cut-off switch. The switch was set such to stop the flow of nitrogen around the isopentane chamber when the desired temperature was achieved. The above-mentioned alcohol glass thermometer was used to measure the temperature in the isopentane chamber.

The manufacturers have stated that with this device the temperature gradient within the cooling chamber is negligible and that a ten minute interval was sufficient for even cooling of specimens.

3.4   Tensile Test

As already mentioned the tensile behaviour of steel has been found much more amenable to interpretation in terms of structure/property relationships than impact behaviour. Since Hall-Petch [3,4] a considerable amount of work has been done in correlating lower yield strength (LYS) to the micro-structure of materials. In the present excercise tensile testing was carried out on a Lloyds tensile testing machine (floor model W30K) calibrated prior to testing. The samples were cut in a direction perpendicular to the flange face Fig 3.3. The gauge length and the guage diameter of the samples were 18 mm and 4.5 mm respectively. Samples were strained generally at an average strain rate of 1.7×10^{-3} s^{-1}. In this way stress-strain graphs could be obtained for each sample. This strain rate is within the maximum strain rate specified by

B.S.18, part 2[98] of 0.0025/s.

All the tests were carried out at room temperature at a cross head speed of 1.8 mm/min (equivalent to a strain rate of 1.7 x 10^{-3} s^{-1}).

3.5   Hardness Test

A Vickers-Armstrong (NO.254222) pyramidal diamond hardness machine[99] was used to obtain hardness values. Initially the hardness machine was checked against standard samples supplied by the manufacturer. Hardness impressions were made on the charpy samples, an average of at least five impressions being taken per sample. A 10 Kg load was used and the zero reading was checked after every five readings.

3.6   Micro-Structural Measurements

The following micro-structural measurements were made in order to correlate the micro-structure to the tensile and impact properties. Ferrite grain size (d), percentage of pearlite (%Pe), percentage of martensite (%M) or Bainite (%B) and grain boundary carbide thickness (t_c).

3.6.1   Mechanical Polishing and Etching

The broken charpy samples were cut to a smaller size (10 x 10 x 10 mm) so that micro-structural observation could be carried out both optically and using the SEM (the latter holder was too small to accommodate the full length of a broken charpy). The face opposite to the notch was examined. This was initially ground with coarse and fine grinders. The samples were

then polished with Struers, six, one and quarter micron diamond polishing wheels.

The final etching treatments used for the various measurements is as follow:

- 2% nital solution (2% nitric acid in alcohol) for measurement of ferrite grain size.

- 5% picral solution (5% picric acid in alcohol) for measurement of percentage of pearlite.

- Mixture of 70% picral and 30% nital solution for measurement of grain boundary carbide thickness and density.

- Mixture of 50% picral and 50% nital solution for measurement of percentage of martensite.

- Boiling picric acid (40 ml) with 10 drops of concentrated HCL and a few drops of teepol, for the measurement of the γ grain size.

3.6.2 Ferrite Grain Size

The mean linear intercept method was used to measure the ferrite grain size. This was done by securing a micrometer stage onto a Vickers optical microscope (NO.M124790) fitted with a cross wire. The micrometer moved the stage and 1000 ferrite grains were intercepted on each sample in order to obtain an average grain size, (relative error[100] of 2.5%).

3.6.3 Volume Fraction of Pearlite and Bainite

The volume fraction of pearlite was measured by point counting at least eight hundred counts being made (relative error[100] of 2.5%). A Swift point counter model F.415 C (NO.4992) attached to the Vickers optical microscope was employed.

3.6.4 Grain Boundary Carbide Thickness

The grain boundary carbide thickness was measured using the method of Mintz et al[101] on a Jeol JSM T100 Scanning electron microscope working at 25 KV. Measurements were made with 0^0 tilt. For each specimen the thickness of one hundred grain boundary carbides was measured. In order to achieve consistent results, the rules listed below were followed when measuring carbide thickness.

- Measurement was taken at the thickest part of the carbide, perpendicular to the grain boundary direction.

- Isolated grain boundary carbides and carbides at the tail of pearlite colonies were measured.

- Carbides at triple grain boundary intersections were measured across the thickest limb.

- Where a number of carbides occured in close proximity, only the largest two were measured.

Measurement was simply achieved using a short length of transparent ruler held against the cathode ray screen. From the measured results, the mean value was calculated for the complete set of one hundred values.

3.6.5   Volume Fraction of Martensite

The Stigmator mode on SEM T100 was used to create a grid on the screen. The stage was moved at regular intervals (0.05 mm steps) using the micrometer attached and at each interval the number of martensite regions intercepted by the cross was counted. A total of 400 counts was carried out on each sample and the percentage of martensite calculated. Magnification was kept constant at all times (5000x).

3.7   Transmission Electron Microscopy

The application of the electron microscope in metallography depends first and foremost on the considerably higher resolving power that can be obtained in the electron microscope in comparison with the optical microscope. While the resolving power for the optical microscope is about 300 nm the resolving power for the transmission electron microscope is 1000 times better, namely of the order of 0.3 nm. Transmission electron microscopy of thin metal foils provides information, among other things of the deformation in the interior of the metal sample. The thin film is detached from the metal and shows a true picture of all the surface irregularities when examined in the electron microscope. TEM work was carried out using a Philips CM 20 electron microscope at 200 KV, in the Department of Materials at Oxford university.

3.7.1   Thin Foil Preparation

It is a primary objective in the preparation of TEM specimens to prepare and mount successfully in the microscope a thin specimen from which it will be possible to deduce accurately the structure and composition of a larger

sample of the material. There are several possible approaches to achieving this objective, of which thining a small piece of the material by electro polishing is one of the most common. The thinning of bulk materials to electron transparency was carried out in two stages: the initial preparation and the final thinning stages.

- The initial preparation stage:

  The initial preparation of TEM specimens was carried out in 3 steps. The first step was to machine a bar with 3 mm diameter and 25 mm in length from a half charpy (already heat treated under the required conditions and tested). The next step was to cut a slice with 0.5 mm thickness from the bar using a microslice. Having cut the slice the next step was to polish both surfaces of the disc on conventional metallographic papers (fine grade) until the thickness of the disc was reduced to about 0.1 mm.

- Final thinning:

  Finally, the thinned discs were thinned further to electron-transparent thickness using a tenupol unit. The electrolyte used consisted of 10% perchloric acid in a 50 : 50 mixture of absolute alcohol and 2-butoxyethanol. The polishing conditions used were as follows:

  cell current :   0.15

  Electrolyte temperature : 5^0C

  Jet speed :   2.5

3.8   Heat Treatment

Flanges were heat treated to the desired temperature in a muffle furnace fitted with a microprocessor based 3-term controller (Isoheat type 810). In all conditions, to check cooling and heating rates a chormel alumel[108,109] thermocouple connected to a potentiometer was placed at the centre of each block. All sample blocks had a hole drilled from one side to the centre so that a chromel alumel thermocouple could be inserted for temperature measurement. The furnace was set at the required temperature and when this was attained, the blocks with attached thermocouples were placed in the furnace. After heat treatment, a cooling curve was obtained for each condition and the gradient between 800 and 400 ^{0}C, Fig 3.5, was taken as the average cooling rate.
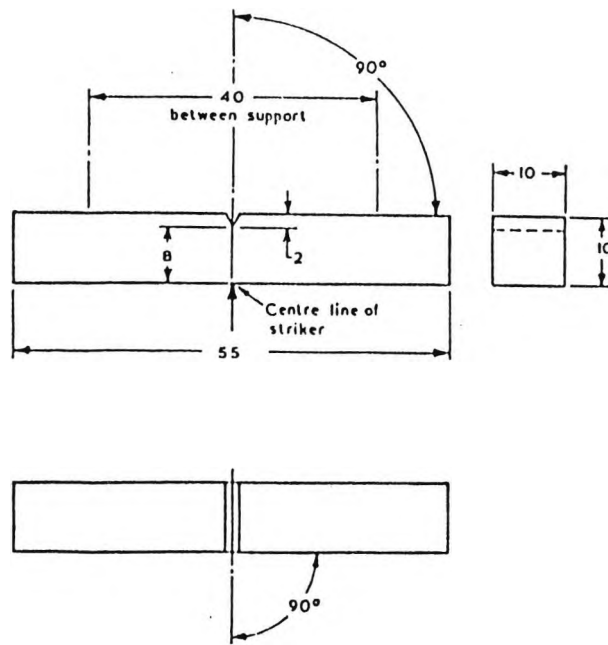
Figure 3.1: Standard test piece[97]
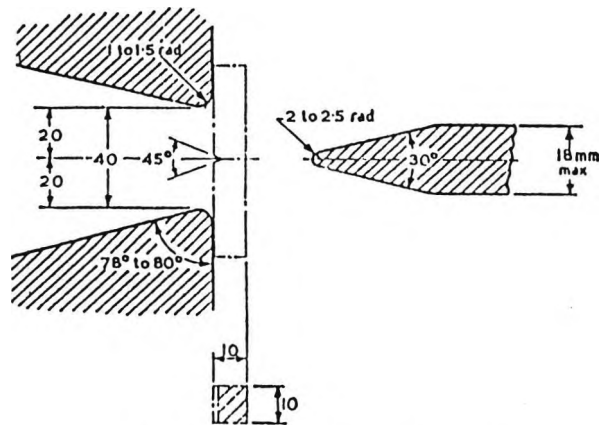
All dimensions are in millimetres unless otherwise stated

Figure 3.2: Charpy V-notch impact test[97]

106
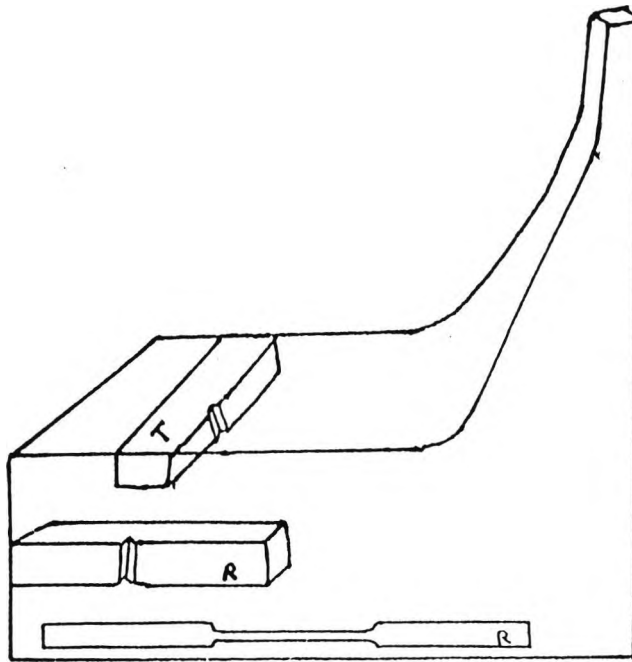
Figure 3.3: Position of charpy and tensile samples cut out of flanges
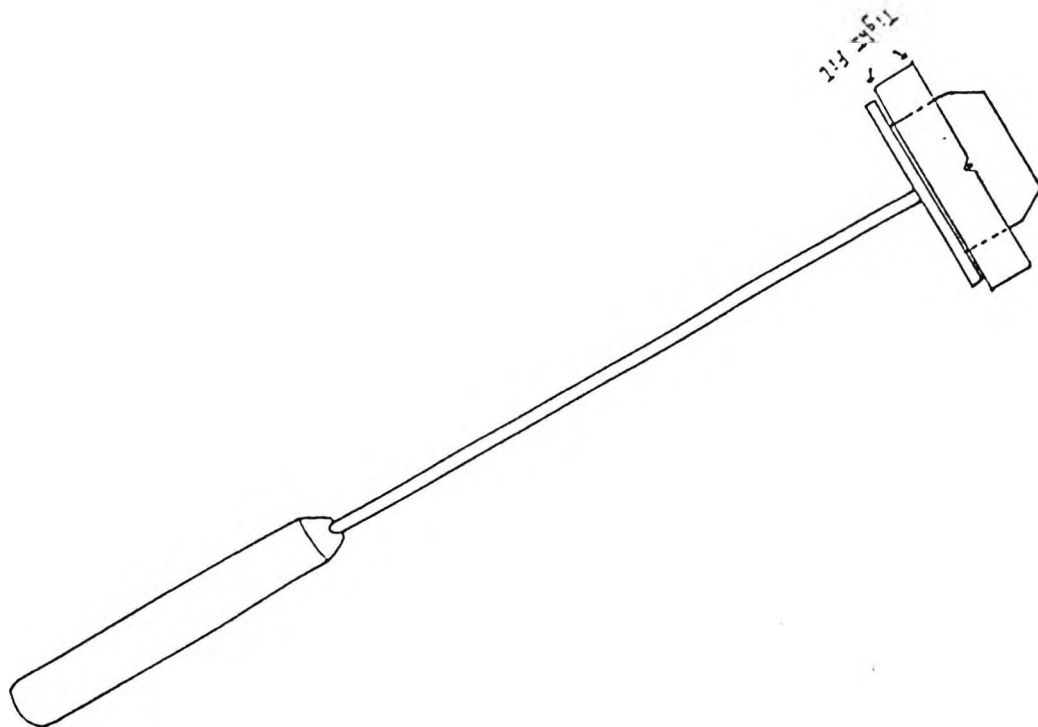
Figure 3.4: Diagram of specimen holder
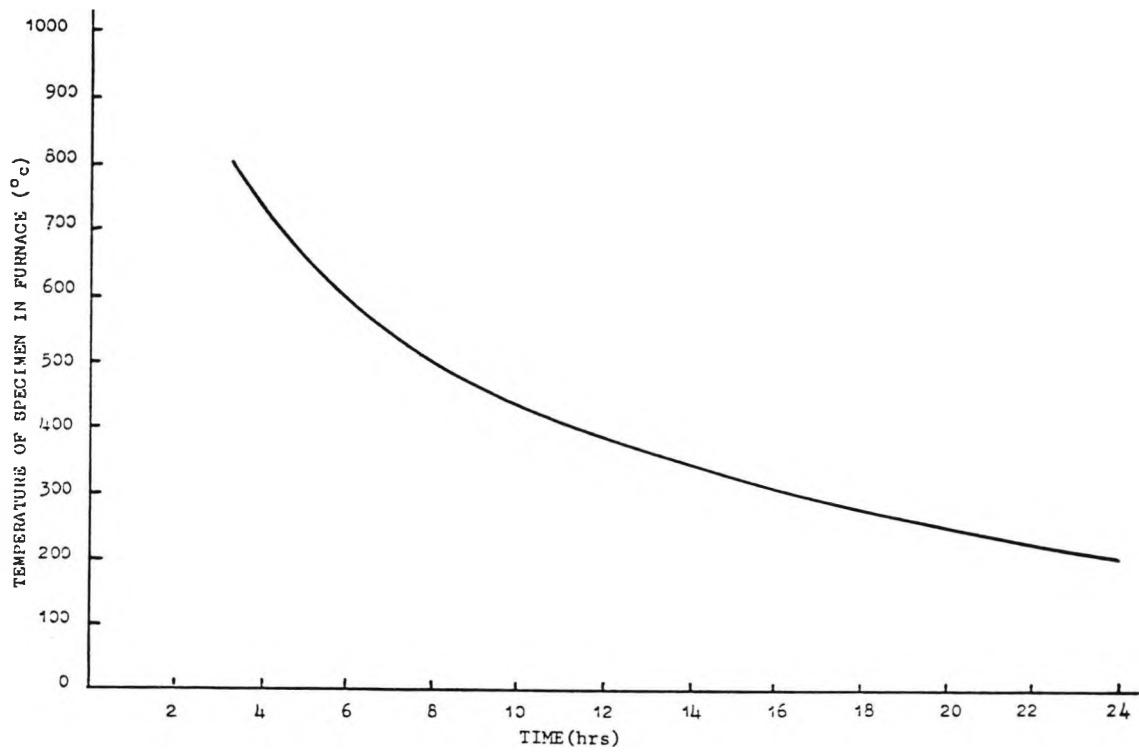
Figure 3.5:   Cooling curve for "Isoheat" furnace, used for the tempering treatments[97]

108

Chapter 4

THE INFLUENCE OF TEMPERING ON THE IMPACT AND TENSILE PROPERTIES OF QUENCHED C-Mn-Al STEELS

4.1 Introduction

Structure/property relationships in quenched and tempered steels are difficult to derive because of the complexity of the resulting microstructures. Some progress has been made in determining these relationships for fully martensitic or bainitic steels, but there is little information available for quenched and tempered steels having lower hardenability in which the microstructure can vary from fine grained ferrite-pearlite to ferrite-upper bainite mixtures through to fully bainitic. These low hardenability steels are often used commercially in the quenched and tempered condition for structural applications. One important application is for flanges where the steel may contain little in the way of alloying additions, as can be seen from the specification requirement for flanges for low temperature service made to the ASTM A350 LF2 specification Table 4.1. This specification allows flanges to be supplied in the normalised, normalised and tempered, and quenched and tempered conditions. Generally there is no problem in meeting the strength requirement but the minimum impact energy requirement of 20 J at -46 ^{0}C has presented difficulties [17,18].

Previous work by Mintz et al[37] was carried out on quenched and tempered C-Mn and C-Mn-Al steels, quenched from a range of austenitizing temperature to produce a wide variation in austenite grain size and a variety of micro-structures from ferrite/pearlite through to lower bainite. Impact behaviour was found to be mainly dependent on the austenite grain size. However, only one tempering temperature at 600 ^{0}C was examined in that exercise and it is considered necessary to examine the influence of tempering in more detail to obtain a fuller understanding of their structure/property relationships.

110

In this chapter, the effect of tempering at three different temperatures (600, 650 and 700 $^{\circ}$C) on the impact and tensile behaviour of C-Mn-Al steel flanges has been examined and the changes in properties related to the micro-structural changes have been observed. The steel used was identical to that examined by Kolahi-aval[8].

4.2 Experimental

The composition of the flange examined is given in Table 4.2. The steel was a C-Mn-Al steel. Blocks of 80*70*45 mm (the last measurement being the thickness of the flange face) were cut from this flange so that standard charpy v-notch impact samples could be taken from radial positions in the face of the flange.

Samples were heated at 950 $^{\circ}$C for 1 hour. After austenitizing the samples were oil-quenched or ice-water quenched (average cooling rates in the temperature range 800-400 $^{\circ}$C were 600 and 1200 K/min, respectively) so that a variation in microstructure could be produced typical of that observed in commercially heat treated flanges. The following conditions were examined:

- 1) As quenched from 950 $^{\circ}$C.

- 2) As quenched from 950 $^{\circ}$C and tempered at 600 $^{\circ}$C for 1 hour.

111

- 3) As quenched from 950 $^{\circ}$C and tempered at 650 $^{\circ}$C for 1 hour.

- 4) As quenched from 950 $^{\circ}$C and tempered at 700 $^{\circ}$C for 1 hour.

A total of eight heat treatments were carried out, four for the cooling rate of 600 K/min and four for the cooling rate of 1200 K/min. After tempering, the blocks were air cooled to room temperature.

Standard charpy v-notch samples were machined for each heat treated condition from these blocks with the notch perpendicular to the flange face. The charpies were located at positions between one quarter depth and midthickness from the flange surfaces. Samples were impact tested at different temperatures to obtain a charpy transition curve for each condition. Duplicate tensile tests were carried out on a Hounsfield tensometer at a cross-head speed of 1.6 mm/min. The gauge length and the gauge diameter of the tensile samples were 18 mm and 4.5 mm respectively. Vickers Hardness measurements (five per sample) using a 10 kg load were made on a charpy sample from each heat-treated condition and the average taken as the hardness value.

Samples were then prepared for microstructural examination and the amount of ferrite was estimated by point counting. A minimum of 500 counts were made per sample. The austenite grain size before tempering was obtained by heating small samples to the austenitizing temperature at 950°C for 1 hour and rapidly quenching into ice/brine to produce martensitic structures.

The austenite and ferrite grain sizes were measured using the linear intercept method and a total of 500 intercepts being measured. The Scanning Electron Microscope (SEM) and Transmission electron microscopy (TEM) were used to identify the microstructural features and to obtain the carbide morphology and distribution and grain boundary carbide thickness with 0^{0}

tilt.

4.3   Test Results

4.3.1   Impact Test Result

The charpy impact transition curves for the steel flanges quenched in ice-water from 950 $^{\circ}$C and tempered at temperatures of 600, 650 and 700 $^{\circ}$C are shown in Fig 4.1. Tempering can be seen to have a marked effect on impact properties. For example for the ice-water quenched samples (IQ), tempering at 600 $^{\circ}$C (IQ-600) has produced an improvement in impact energy of about 100 J at 0 $^{\circ}$C and an improvement of 75 J at -46 $^{\circ}$C Fig 4.1. It can also be seen that increasing the tempering temperature from 600 $^{\circ}$C to 700 $^{\circ}$C has little significant effect on impact properties.

Similar behaviour was noted when oil quenching (OQ) was used; temper-

ing improved the impact behaviour Fig 4.2. At 0 $^\circ$C, tempering caused an average improvement of about 40 J and at -46 $^\circ$C, the impact energy was improved by about 30 J. Again there was little influence on the impact behaviour of oil quenched steel flanges, when the tempering temperature was raised from 600 $^\circ$C to 700 $^\circ$C. At 700°C there were some indication that the shape of the transition curve was changing to give a more abrupt transition.

In the as quenched state, oil quenching gave better impact properties than ice/water quenching. However, after tempering, there was little difference in impact behaviour, Figs 4.3, 4.4.

4.3.2   Tensile and Hardness Results

For the ice-water quenched samples in the as quenched condition no yielding was observed in stress- strain curve so therefore yield stress was specified in terms of a 0.2 % proof stress, Fig 4.5. As would be expected, tempering at 600 $^\circ$C caused a marked reduction in strength and hardness for the ice-water quenched flanges, the yield stress being reduced by almost 240 MN mm^{-2} and hardness by 164 Hv_{10} Tables 4.3 and 4.4. Tempering produced yield point in the stress-strain curve of the ice-water quenched samples, Fig 4.6. Increasing the tempering temperature (i.e. to 650 $^\circ$C and 700 $^\circ$C), reduced the strength and hardness even further, Tables 4.3 and 4.4, Figs 4.7 and 4.8 respectively.

The stress/strain curves for the oil quenched flanges, in the as quenched and as quenched and tempered at 600°C conditions are given in Fig 4.9 and 4.10 respectively.

The reduction in strength and hardness after tempering at 600 $^\circ$C was of the order of 90 MN mm^{-2} and 32 Hv10 respectively Tables 4.3 and 4.4. Increasing the tempering temperature to 700 $^\circ$C, produced, as for

114

the ice-water quenched samples, only a further small reduction in strength and hardness, Tables 4.3 and 4.4, Figs 4.7 and 4.8 respectively.

Oil quenched flanges invariably gave lower strengths and hardness than ice-water quenched flanges given equivalent heat-treatments.

4.4   Metallography

The microstructural measurement are given in table 4.5 and 4.6. The austenite grain size was 26 μm. Two types of microstructures were found in these heat treated flanges; ferrite-degenerate pearlite and almost fully bainitic/martensitic structures, Figs 4.11 and 4.12 respectively.

4.4.1   Ferrite / Degenerate Pearlite Microstructures

Quenching in oil from 950 ^{o}C resulted in a ferrite-degenerate pearlite structure (64% ferrite, 36% degenerate pearlite) Fig 4.11 and 4.13. After tempering at 600 ^{o}C the carbides inside the pearlite colonies started to break up and partially spheroidise Fig 4.14. In all cases the carbides observed at the grain boundaries were coarser than within the interior of the colonies. Tempering at 650 ^{o}C continued the process of spheroidisation and a coarsening of the spheroidised carbides was apparent Fig 4.15. At 700°C the carbides were even coarser and it was obvious that many of the fine carbides had redissolved and the interparticle spacing had increased Fig 4.16 and Table 4.6.

4.4.2 Bainitic Microstructures

Quenching in ice-water from 950 °C resulted in an apparently martensite/bainite structures with only a small amount of ferrite (18% ferrite and 82% mixture of bainite and martensite), Fig 4.12. In the as quenched condition, SEM micrographs showed lines of carbides across the structure Fig 4.17. The very high strength and hardness of this structure suggests that the bainite was mainly lower rather than upper-bainite. Tempering at 600°C for one hour can be seen to break up these long carbides into very fine spherical particles Fig 4.18. At the higher tempering temperature of 650°C the carbides coarsened. However many rod shaped carbides were still present, Fig 4.19. Tempering for one hour at 700°C caused almost complete spheroidisation and an increase in the interparticle spacing, Fig 4.20. At a tempering temperature of 700°C, little difference was observed between the carbide thickness for oil and ice-water quenched samples, Table 4.6.

4.5 Discussion

The charpy transition curves from the work of Kolahi-aval[8] (denoted J in the curves) in which the same steel as used in present exercise was examined in the ice-water and oil quenched from 950°C and tempered for 1 hour at 600°C conditions are given in Fig 4.21 and 4.22 respectively. It can be seen that the agreement between the present and previous work is reasonable.

Kolahi-aval[8] established from his work a regression equation to account for the impact behaviour of steels with low hardenability. The equation derived was:

$$impact \quad enegy \ /J \ at \ -46^{o}C = 82 + 18.6d^{-1/2} - 0.8H + 0.05CR \quad (4.1)$$

Where d is the austenite grain size in mm, H is the hardness in HV_{10}, CR is the cooling rate K/min.

and a similar equation can be derived from his work to calculate the impact energy at 0 °C test temperature.

$$impact \quad energy \ /J \ at \ 0^{o}C = 119 + 18.6d^{-1/2} - 0.8H + 0.05 \ CR \quad (4.2)$$

The values calculated from these equations and the observed values of the impact behaviour at -46°C are given in table 4.7. It can be seen that there is in general a good agreement between calculated and experimental results. Thus for these steels the impact behaviour is dictated by the γ grain size although it is probably the bainitic colony size which actually controls fracture. The finer the grain size, the higher the impact energy. The effect of γ grain size will be discussed in more detail in chapter 5.

Another factor influencing impact behaviour is known to be the hardness. The hardness influences fracture because this is related to the dislocation density as well as the carbide distribution and the amount of polygonal ferrite present. Increasing hardness generally results in lower impact energy values. In the present exercise, prior austenite grain size which controls fracture, remained the same for all conditions and did not change during tempering treatment.

117

4.5.1 Influence of Cooling Rate on Hardness and Fracture

The present observations indicate that ice/water quenching results in a higher hardness level and strength as compared with oil quenching.

One possible explanation to account for the increase in hardness on ice/water quenching is that increasing the cooling rate will lower the transformation temperature favouring the more bainitic/martensitic structures. Hence a significant part of the hardness decrease on oil quenching can be related to an increase in the amount of polygonal ferrite. Although in the present exercise the individual contributions to hardness have not been seperated, it is well accepted that an increase in hardness will give rise to a deterioration in impact behaviour unless there is some other micro-structural change such as the production of a finer grain size which will offset the deleterious influence of this increase in hardness.

Oil quenched and tempered steels gave lower hardness value than ice/water quenched and tempered steels yet the impact behaviour was similar, Figs 4.4 and Table 4.4. Finer carbides at the interlath boundaries were obtained at the higher quench rate (compare Figs 4.14 and 4.18). The carbides found at the slower quench rates at the low angle interlath boundaries would be expected to provide excellent paths for crack propagation as well as produce easy initiation of cleavage cracking[37]. Therefore, it would appear that the detrimental effect on impact behaviour on having a higher hardness on ice/water quenching is balanced by the improved carbide distribution produced at the faster quench rate.

4.5.2 Tempering at 600, 650 and 700°C

The results from the present work are interesting as they suggest that tempering at 600°C has a marked effect on impact behaviour and strength. Increasing the tempering temperature from 600 to 700°C reduces the strength and hardness with no further improvement in the impact behaviour. However, the increase in tempering temperature produced further coarsening of the carbides by spheroidisation accompanied by an increase in interparticle spacing Figs 4.23 and 4.24.

The microstructures produced at the two cooling rates are very different. In the case of oil quenching, the structure is mainly ferrite, whereas on ice-water quenching it is essentially bainitic. Therefore to explain the changes in properties related to microstructural changes, each cooling rate is discussed seperately.

4.5.3 Steels Quenched in Oil

In this case, the as quenched micro-structure was mainly ferrite with 35% of second phase consisting of bainite or probably degenerate pearlite and small islands of martensite. Because of the slower cooling some tempering of carbides will also have occurred during the quench. As a consequence tempering produced little change in strength and impact behaviour as compared with the ice-water quenching, and this relative insensitivity is due to two reasons:

- Ferrite is the dominant phase

- Tempering has little influence on the ferrite grain size which probably controls the strength and impact behaviour as in ferrite/pearlite steels.

119

4.5.3.1 Influence of tempering on strength and hardness

The oil quenched and tempered structures are indeed similar to the tempered ferrite-pearlite structures. Yield points were obtained in these oil quenched steels indicating that the ferrite was playing an important role in influencing yielding behaviour. It is therefore interesting to explore whether a similar explanation as has been used to explain the effect of tempering on yield and tensile strength of ferrite/pearlite steels can be used for oil quenched flanges. However, it is important to note that high dislocation densities may be obtained during oil quenching as shown in Fig 4.25, due to the lower transformation temperature as compared with structures obtained during normalising. The fall in LYS, UTS and hardness can therefore be in part related to a reduction in dislocation density after tempering. This part can be estimated by using an empirical equation obtained for steels having no precipitates or cold worked dislocations present.

$$\text{LYS} \quad \text{MN mm}^{-2} = 105 + 43.1 \ \%\text{Mn} + 83 \ \%\text{Si} + 15.4\text{d}^{-1/2} + 1540\%\text{N} \ ^{[43]}$$

$$(4.3)$$

This gives a value of 355 MNm^2. Thus the large drop in yield strength from 459 MNm^{-2} to 369 MNm^{-2} which occurs on tempering at 600 °C is most likely associated with the removal of dislocations.

It has been shown[26] that the yield stress of a ferrite-pearlite steel depends on the ferrite grain size, which contributes less as the volume fraction of pearlite increases, and that as the composition approaches the eutectoid composition the pearlite contributes ever more to the yield stress.

Raising the tempering temperature from 600 to 700 °C results in a further fall in LYS of 24 MNm^{-2}. Although some coarsening of the ferrite grain size

occurs during tempering it is small $(0.5 \text{ mm}^{-1/2})$ and would only be expected to contribute a small amount to this decrease in the LYS, (8 MNm^{-2})

Cochrane[33] has suggested that as pearlite can increase the yield strength of steels, then tempering because it spheroidises the carbides may be responsible for the fall in LYS. Cochrane[33] also found a good relationship between the interparticle spacing in pearlite (which is related to the degree of spheroidization) and the fall in yield strength after tempering.

Present work, appears at first sight to follow work of Cochrane[33] who suggests that the LYS decreases with the degree of spheroidization and increase in interparticle spacing, Figs 4.26 and 4.27. However, Mintz and Kolahi-aval have suggested that the changes in interparticle spacing are too small to influence the strength.

Previous work by Mintz et al[32] has also shown that the activation energy for the process producing the fall in yield strength in the early stages of tempering is much lower than might be expected from a spheroidization process in which the activation energy has been shown to be that for the self diffusion of iron. The activation energy was found to be that for the growth of carbides at the boundaries. On the basis of these observations and the similar kinetics of growth of carbides to that governing the fall in yield strength, it was postulated that the fall in yield strength at tempering may be due to a lowering of the k_y value of the steel where k_y is from the Hall-Petch relation. It was suggested[32] that on transformation boundaries become supersaturated with C giving a high k_y value and that tempering causes the carbon to precipitate out on existing carbides reducing the k_y value.

Summarising, it would seem that for the oil quenched samples the fall in yield strength that occurs on tempering, are in the first part mainly due to a fall in the dislocation density and that tempering causes spheroidization of the carbides and possibly a reduction of carbon in solution at the grain boundaries reduces the k_y value[32].

4.5.3.2 Influence of tempering on the impact behaviour

The main part of the present exercise was to establish the effect of tempering on the impact properties of quenched flanges. For ferrite/pearlite steels, it is not clear whether all the fall in strength on tempering corresponds to reduction in σ_0 or k_y in the Petch relationship $\sigma_y = \sigma_0 + k_y\ d^{-1/2}$ where σ_y = yield stress, σ_0 = the friction stress which opposes dislocation motion and k_y is taken as a constant relating to the difficulty in spreading yield from grain to grain. However, a reduction in the value of either σ_0 or k_y will give rise to a decrease in ITT, and for the purpose of the present work to simplify interpretation changes in yield strength will be taken as changes in σ_0.

Previous work[43] on ferrite/pearlite steels has established the following equations relating structure to the ITT.

$$54\ \text{J}\quad \text{ITT,}\ ^\circ\text{C} = 192\ t_b{}^{1/2} - 10.1 d^{-1/2} + 0.5\ \delta\ \text{y - constant} \qquad (4.4)$$

and

$$27\ \text{J}\quad \text{ITT,}\ ^\circ\text{C} = 173\ t_b{}^{1/2} - 8.3 d^{-1/2} + 0.37\ \delta\ \text{y - constant} \qquad (4.5)$$

where t_b is the grain boundary carbide thickness and d is the grain diameter μm and δy is taken as being,

$$\delta\text{y} = \text{LYS}_{ACT} - \text{LYS}_{CALC}$$

122

where LYS can be calculated from equation 4.3[43]:

The constant in the equation has been shown by Mintz[43] to be related to the shelf energy. The original regression equations were based on steels which had average shelf energies of 120 J. The present steel has a much higher shelf energy, on average about 170 J due to the finer dispersion of the carbides that are produced on quenching and this will result in a lower negative value for the constants. Assuming that the brittle shelf is low generally between 5 to 10 J, independent of the ductile shelf energy then some estimate of the revised constants to account for the higher shelf energy can be made as follow:

Taking the brittle shelf energy in all cases as zero for simplicity, all impact energies in the present exercise are scaled down by a factor of 110/170. The new curve obtained Fig 4.28, is then compared with the actual curve and the shift in transition noted for impact energies of 54 J and 27 J. These then are added onto the original constants, $-23^{\circ}C$ for 54 J and $-42^{\circ}C$ for 27 J. Hence the new constants should be -43 and -62 respectively. Although the changes in impact behaviour are accounted for by these equations, Table 4.8, the observed impact values are significantly lower (about $40^{\circ}C$ lower) even with the adjusted constant. Forged material has however been shown to give improved impact behaviour over plate properties although the reason for this is not clear.

The regression equations 4.4 and 4.5 show that the thickness of grain boundary carbides is an important factor in determining the impact properties. Increasing the tempering temperature from 600 to $700^{\circ}C$ produced little significant change in impact behaviour even though the carbide thickness coarsened. However, offsetting this coarsening which would cause a

deterioration in impact behaviour, is the fall in LYS which would improve the impact behaviour. This is in accordance with previous work by Mintz[7] on normalised and tempered ferrite/pearlite steels which suggests that the changes in impact behaviour on tempering depends on the balance between the beneficial effect of reducing strength and the detrimental influence of coarsening the grain boundary carbides. Thus summarising, it seems reasonable to conclude that for oil quenched steels the changes in impact behaviour and strength that occur on tempering in the range 600 to 700°C are very similar to those obtained in normalised steels having ferrite/pearlite structures and have the same origins.

4.5.4   Steels Quenched in Ice-Water

The explanation in previous section can not be used to explain the changes in behaviour that occur on tempering the ice-water quenched samples. Here the substructure is essentially bainite/martensite and the carbides are uniformly dispersed in the ferrite matrix. To explain the changes occurring in impact and tensile strength related to the microstructural changes during tempering, it is useful to discuss the stucture property relationships of bainitic structures.

It has been shown by Pickering[65] that there is a clearly defined relationship in which the tensile strength increases linearly with increasing value of reciprocal of the square root of bainitic ferrite grain size. A similar effect was found by Siriwardene[105]. In a bainitic structure there will always be a variable bainitic ferrite grain size because the bainitic ferrite nucleated later in the progress of transformation, will invariably show a smaller grain size. Nevertheless, it is clear that the bainitic ferrite grain size is one of the factors which controls the strength[65], and it is interesting to note that the low angle

124

boundaries are apparently capable of exerting, a strengthening effect.

With decreasing transformation temperature, the carbides in the bainitic structures for a given carbon content in the steel, tend to become smaller and to increase in number. It is shown by Pickering[65] that there is a clearly defined effect for an increasing amount of dispersion strengthening with decreasing transformation temperature. Dispersion strengthening by the bainitic carbides therefore also plays a part in the strength of bainite.

Another factor influencing strength, with decreasing transformation temperature is a greater expansion during the bainitic transformation, and this must lead to a higher level of internal stress especially as there will be less tendency for the thermal relief of such internal stresses at the lower transformation temperatures. The internal stresses may well contribute to the strength of the structure, but this effect is probably of secondary importance compared with other strengthening mechanisms[65].

However, the greater dislocation density, the greater is the strength, due to larger stresses being required to force a slip dislocation through the structure. It has been shown[65] that all bainites even those formed in low carbon steels at high temperature, contain a higher dislocation density than polygonal ferrite, due to the strain associated with the shear transformation. These not only cause dislocations to be generated in the bainitic ferrite, but also in the adjacent austenite. The dislocation density of the bainitic ferrite increases with decreasing transformation temperature, presumably due to the greater strains accompanying the transformation, and because there is less chance of dislocations being annealed out. Consequently, this increased dislocation density can also contribute to the higher strength of bainite with decreasing transformation temperature.

4.5.4.1 Influence of tempering on strength and hardness

The hardness and tensile strength of the ice-water quenched samples decreases during tempering; the rate of change being significantly larger than with oil quenched samples. As is to be expected, it is the highest strength steels which undergo the largest changes in strength during tempering[68]. It can be seen from the results and previous work[104] that the strength at any stage of tempering correlates well with the coarsening of the matrix carbides and increase in interparticle spacing Figs 4.29 and 4.30. These results could be taken to imply that the strength depends mainly on carbide dispersion strengthening, but the particle size and distribution and dislocation density are not independent parameters.

Most dispersions lead to strenghening, but often they can have adverse effects on ductility and toughness. In the as ice-water quenched condition, fine dispersions, ideally small spheres of carbides randomly dispersed in matrix may be the reason for high strength of the bainite. However, tempering at 600 ^{0}C results in coarsening of these fine carbides by breaking and spheroidizing them and the increased inter-particle spacing may be the reason for the fall in strength by providing passages for dislocations to manouver through the dispersed carbides. Increasing tempering temperature to 650 ^{0}C and 700 ^{0}C produced further coarsening and spheroidizing together with an increase in interparticle spacing Figs 4.29, 4.30 and therefore a further drop in strength was observed.

An attempt was made to relate the yield stress to the interparticle spacing as suggested by Onel and Nutting[66]. In their work there was considerable scatter in their experimental results but a least squares analysis gave the line of best fit as:

$$\sigma_y = 204 + 2.26 \text{ x } 10^{-2} \ 1/\lambda \ \ln{(d/2b)} \qquad (4.6)$$

where σ_y is in MNm^{-2}, b is the burgers vector taken as 2.48 A[111], d the average measured particle diameter in μm and λ the particle spacing in μm (in this case taken as between the centers). Data in the present exercise was used to calculate σy using the equation (4.6). The calculated values and observed data seem to be in a reasonable agreement except for the steel tempered at 600°C, Table 4.9.

It should be noted that for tempering temperatures of 650 and 700 °C the yield stresses for the ice/water quenched samples were only 35 Mpa higher than the oil quenched samples. This increase may reflect the dispersion strengthening of the carbide particles in the ferrite matrix. However, at 600 °C the difference between the yield stress for the ice/water quenched and oil quenched samples was 160 Mpa. This suggests that the dislocation densities were still probably high in the ice/water quenched condition and tempered at 600 °C Fig 4.31 a,b and only at temperatures of 650 and 700 were they completely removed.

4.5.4.2 Influence of tempering on the impact behaviour

The effect of tempering on transition temperature of tempered bainite has been shown[34] generally to decrease the impact transition temperatures, due to the decrease in strength. The effect is virtually linear, ITT decreasing by 0.2/0.3 °C for each MPa decrease in the yield or proof stress [34]. A shift of about 70°C to the left of the impact transition curve Fig 4.1 with a fall of 240 MN/mm^2 in strength is within this range.

In the present instance the structure is a mixture of martensite/bainite and the change in strength and transition temperature on tempering is prob-

127

ably more related to the tempering off of the martensite.

Raising the tempering temperature from 600 to 650 and 700°C produced a further very marked fall in strength with little change in impact behaviour. The fall in strength may be related to removal of dislocations but it is surprising that this was not accompanied by a marked improvement in impact behaviour.

4.6   Commercial Implications

There is no doubt that of the two quenching conditions examined, ice/water quenching is the most beneficial, giving after tempering the highest strength and the best impact behaviour. However as far as meeting the ASTM A350 LF2 impact specification is concerned, oil quenching will in most instances meet the specification comfortably.

Of greatest interest is the observation that tempering is not required in oil quenched flanges. Previous work [37] had indicated that for steel having an austenite grain size greater than 40 μm, there are problems in guaranteeing the ASTM A350 LF2 impact requirement. Hence to be sure of meeting specification an Al addition was recommended to obtain grain sizes smaller than 40 μm. In the present instance in which an aluminium steel was examined the grain size was 26 μm. There should be no problems in meeting the impact specification on Al grain refined steels provided the austenitising temperature is in the range 900 to 950 °C.

However, with the oil quenched condition, tempering at highest tempering temperature 700 °C should be avoided as the brittle shelf is too close to -46 °C to give a comfortable safety margin.

4.7   Conclusions

- 1) Ice/water quenching of plain C-Mn-Al flanges (45 mm thick) from 950 ^{0}C results in bainite/martensite structures, with a small amount of ferrite.

- 2) In contrast, oil quenching of plain C-Mn-Al steel flanges from 950 ^{0}C results in structure consisted of mainly ferrite and a mixture of pearlite/bainite and small amount of martensite.

- 3) Tempering at 600 ^{0}C has a marked effect in improving the impact properties of ice-water quenched flanges.

- 4) In contrast, for oil quenched flanges tempering at 600 ^{0}C caused a much smaller improvement in impact behaviour as auto-tempering had already taken place during the quench.

- 5) As expected, tempering at 600 ^{0}C resulted in a reduction in both strength and hardness of the oil and ice-water quenched flanges.

- 6) Increasing the tempering temperature in the range 600 ^{0}C to 700 ^{0}C further reduced the strength and hardness of both oil and ice-water quenched flanges. Little change in impact behaviour was in general noted, for both oil and ice-water quenched flanges. However tempering at 700 ^{0}C produced the largest strength decrease and worst impact behaviour. In the case of oil-quenched flanges, tempering at 700 ^{0}C produced an ITT curve in which the brittle shelf was very close to the specification temperature of -46 ^{0}C.

- 7) Tempering caused the carbides to spheroidise and the degree of

129

spheroidisation and interparticle spacing increased with tempering temperature in the range 600 to 700 °C.

- 8) Falls in strength are most likely to be associated with the spheroidisation process and the change in dislocation density.

- 9) The general insensitivity of impact behaviour to increasing tempering temperature in the oil quenched condition is probably due to the coarsening of carbides being matched by the beneficial influence of a reduction in strength.

- 10) In the case of ice-water quenching the structure was essentially bainitic and the large changes in strength with no change in impact behaviour could not be interpreted in these term.

- 11) The ice-water quenched flanges after tempering gave the best combination of strength and impact behaviour. However, oil quenching without tempering produced adequate enough properties to meet the ASTM A350 LF2 specification comfortably and this needs to be examined more closely.

- 12) An improvement in impact behaviour is associated with a fall in strength in both conditions, Fig 4.32.

Chemical requirements, wt-%

C	0.30 (max)
Si	0.15 - 0.30
Mn	1.5 (max)
P	0.035 (max)
S	0.040 (max)

Mechanical property requirements

Tensile strength, Mn m^{-2}	483 - 655
Min. yield strength, Mn m^{-2}	248
Min. elongation in 50 mm, %	22
Min. reduction of area, %	30
Min. charpy v-notch energy, J	20*

* Requirement for standard size 10 x 10 mm specimens at -45.6 ^{o}C for average of three specimens, no individual value being less than 16 J.

Table 4.1 CHEMICAL AND MECHANICAL PROPERTY REQUIREMENT OF ASTM A350 LF2 SPECIFICATION

C	Mn	Si	S	P	Cr	Mo	Al	Cu	Ni	N
0.21	0.96	0.3	0.012	0.013	0.18	0.033	0.038	0.07	0.09	0.0055

Table 4.2 THE COMPOSITION OF THE STEEL Wt%

QUENCH TEMP ^{0}C	QUENCH MEDIA	TEMPERING TEMP ^{0}C	LYS MN m^{-2}	UTS MN m^{-2}	%EL	%RA
950	IQ	—	770**	770	31	55
950	IQ	600	530	628	48	62
950	IQ	650	394	542	57	68
950	IQ	700	388	530	70	72
950	OQ	—	459	591	40	62
950	OQ	600	369	554	54	70
950	OQ	650	357	525	55	72
950	OQ	700	345	510	58	74

TABLE 4.3 TENSILE TEST RESULTS

** = 0.2% proof stress

IQ = Ice-Water Quench

OQ = Oil Quench

QUENCH TEMP °C	QUENCH MEDIA	TEMPERING TEMP °C	AVERAGE HARDNESS HV_{10}	IMPACT ENERGY J	
				0 °C	-46 °C
950	IQ	—	374	34	15
950	IQ	600	210	171	99
950	IQ	650	193	183	126
950	IQ	700	181	161	114
950	OQ	—	199	107	61
950	OQ	600	167	193	115
950	OQ	650	159	158	72
950	OQ	700	153	140	112

Fig 4.4 HARDNESS TEST RESULTS

*IQ = Ice-Water Quench

OQ = Oil Quench

Average hardness = Average taken from all the charpies tested at various test

temperature

QUENCH TEMP °C	QUENCH MEDIA	TEMPERING TEMP °C	AUSTENITE GRAIN SIZE μm	FERRITE GRAIN SIZE μm	%F	%P	%B
950	IQ	—	26	—	18	—	82
950	IQ	600	26	—	20	—	80
950	IQ	650	26	—	20	—	80
950	IQ	700	26	—	23	—	77
950	OQ	—	26	7	64	36	—
950	OQ	600	26	7	65	35	—
950	OQ	650	26	7	65	35	—
950	OQ	700	26	7	64	36	—

TABLE 4.5 MICROSTRUCTURAL MEASUREMENTS

* F = Ferrite * P = Pearlite * B = Bainite

IQ = Ice-Water Quench

OQ = Oil Quench

QUENCH TEMP ^{0}C	QUENCH MEDIA	TEMPERING TEMP ^{0}C	t_c μm	S μm	GBT μm
950	IQ	—	0.17	—	—
950	IQ	600	0.19	0.6	—
950	IQ	650	0.22	0.7	—
950	IQ	700	0.31	0.9	—
950	OQ	—	0.18	—	0.27
950	OQ	600	0.23	0.7	0.36
950	OQ	650	0.29	0.8	0.40
950	OQ	700	0.30	0.9	0.47

TABLE 4.6 CARBIDE THICKNESS MEASUREMENT

* IQ = Ice-Water Quench

OQ = Oil quench

t_c = Average Carbide Thickness

S = Inter particle spacing

GBT = Grain Boundary Carbide Thickness

QUENCH TEMP °C	QUENCH MEDIA	TEMPERING TEMP °C	IMPACT ENERGY at -46°C/J		IMPACT ENERGY at 0°C/J	
			OB	PRED	OB	PRED
950	IQ	—	15	0	34	0
950	IQ	600	99	89	171	126
950	IQ	650	126	103	183	140
950	IQ	700	114	112	161	150
950	OQ	—	61	68	107	105
950	OQ	600	115	94	193	131
950	OQ	650	95	100	158	137
950	OQ	700	112	105	140	142

TABLE 4.7 PREDICTED AND OBSERVED IMPACT ENERGY VALUES AT

-46 and 0 °C.

IMPACT   ENERGY   / J at -46 °C = 82 + 18.6d$^{-1/2}$ - 0.8 H + 0.05 CR[37]

IMPACT   ENERGY / J at 0 °C = 119 + 18.6 d$^{-1/2}$ - 0.8 H + 0.05 CR[37]

QUENCH TEMP °C	QUENCH MEDIA	TEMPERING TEMP °C	54 J ITT		27 J ITT	
			PRED °C	OB °C	PRED °C	OB °C
950	OQ	—	0	-43	-20	-84
950	OQ	600	-26	-66	-35	-84
950	OQ	650	-24	-64	-33	-88
950	OQ	700	-21	-58	-29	-72

TABLE 4.8 PREDICTED AND OBSERVED, 54 J ITT AND 27 J ITT.

IMPACT ENERGY / at 54 J $= 192\ t_b{}^{1/2}$ - 10.1 $d^{-1/2}$ + 0.5δy - constant[43]

IMPACT ENERGY / at 27 J $= 173\ t_b{}^{1/2}$ - 8.3 $d^{-1/2}$ + 0.37 δy -constant[43]

QUENCHE TEMP °C	QUENCH MEDIA	TEMPERING TEMP °C	YIELD STRENGTH	
			OB MN mm^{-2}	PRED
950	IQ	600	530	428
950	IQ	650	394	400
950	IQ	700	388	368

TABLE 4.9 PREDICTED AND OBSERVED YIELD STRENGTH.

PREDICTED VALUES WERE OBTAINED USING ONEL AND

NUTTING[66] EQUATION.

$$* \; \sigma_y = 204 + 2.26 \times 10^{-2} \; 1/\lambda \; \ln \; (d/2b)^{[66]}$$

TEMPERING
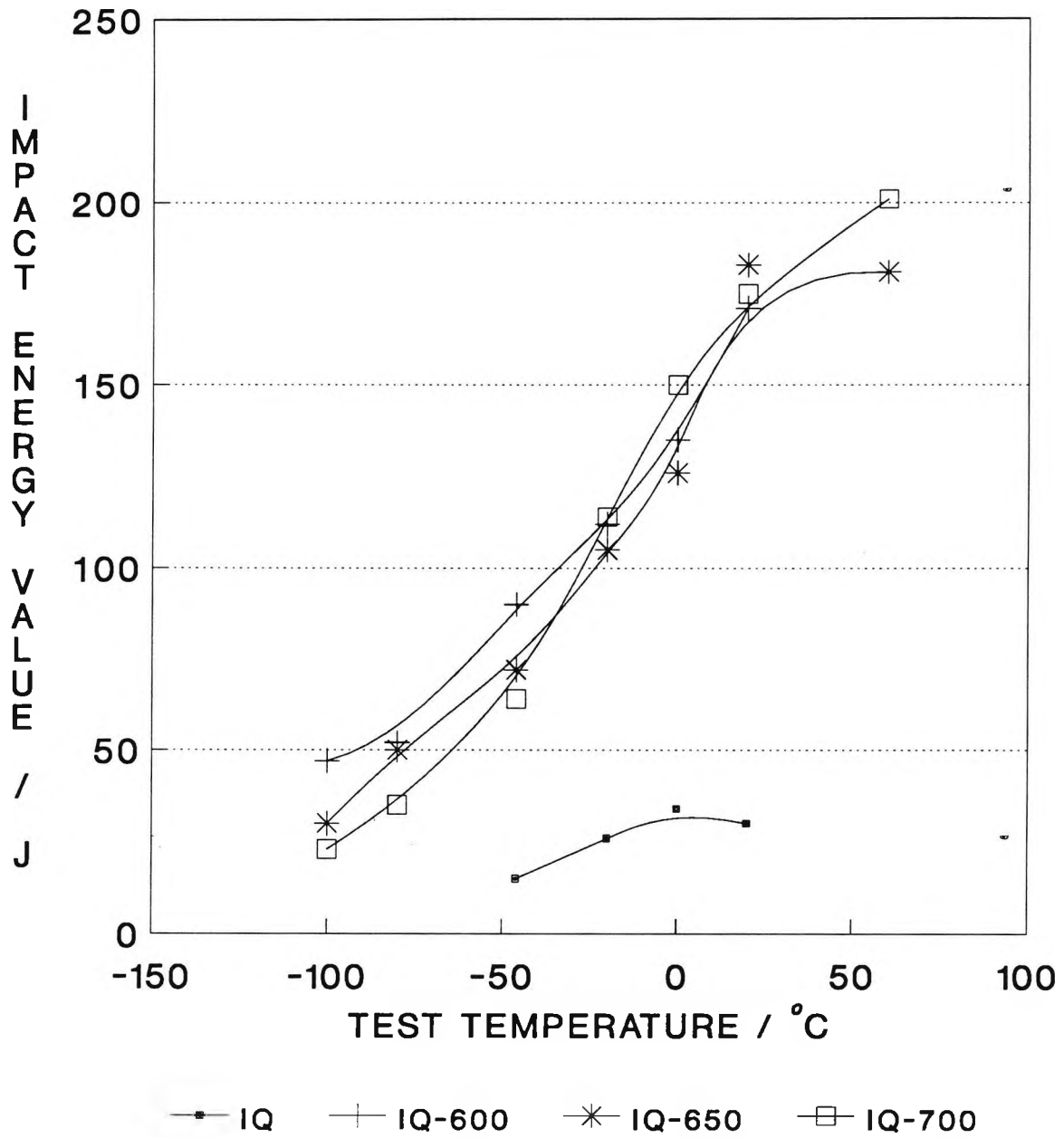
Fig 4.1 Impact transition curves for samples ice-water quenched from 950 °C
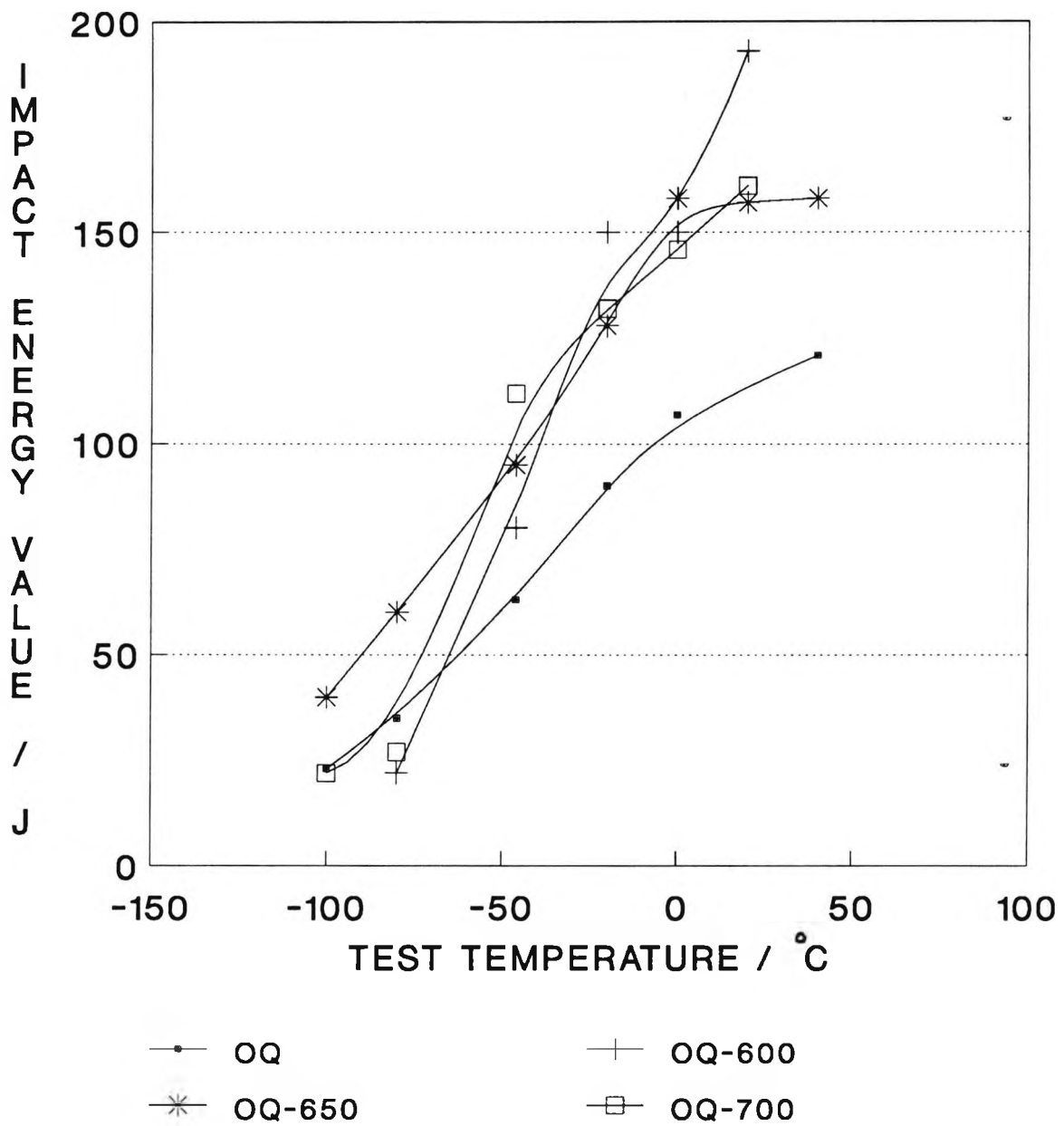
TEMPERING

4.2 Impact transition curves for samples
oil quenched from 950 °C

140
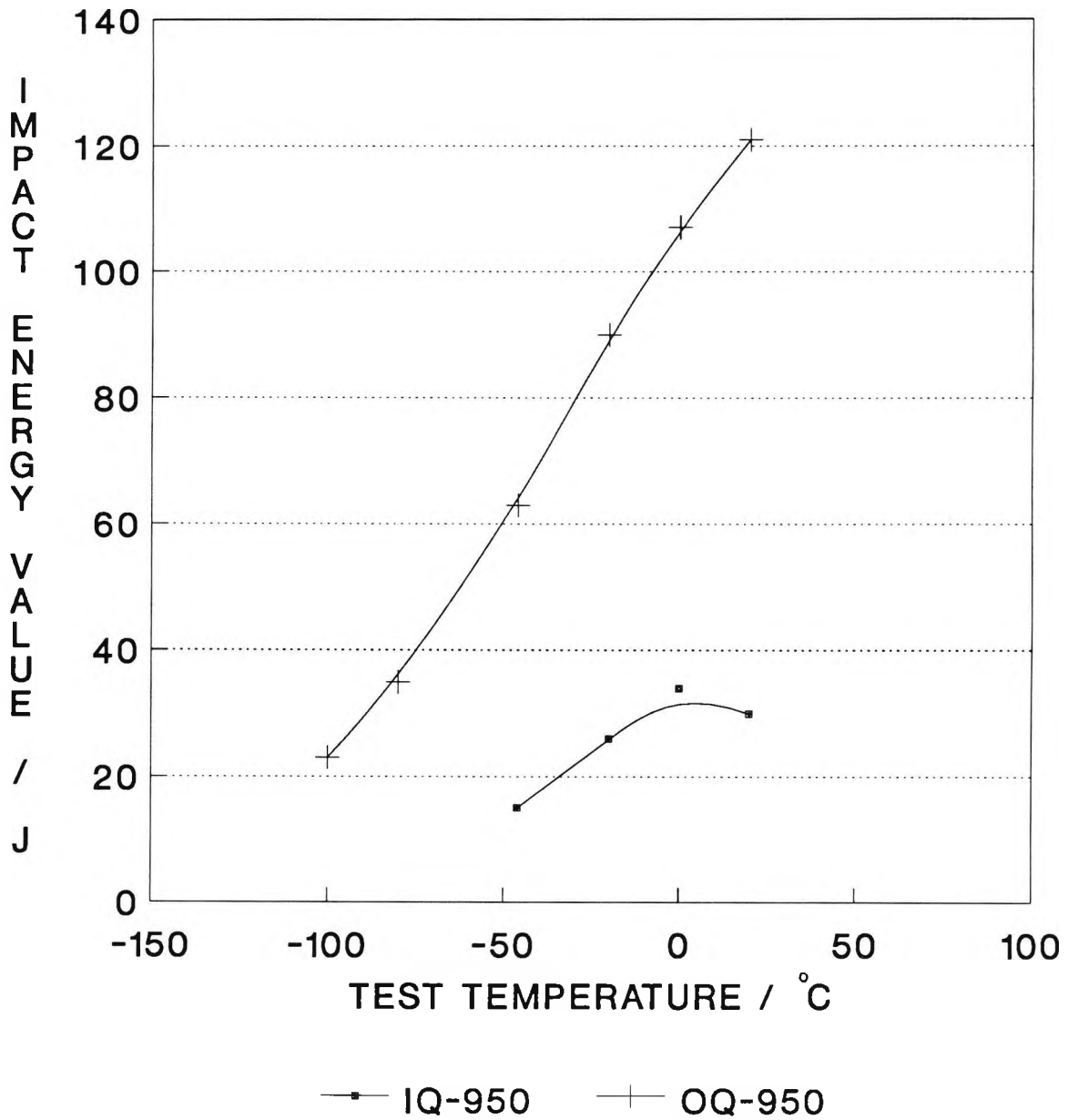
TEMPERING

Fig 4.3 Impact transition curves for
samples ice-water or oil quenched
from 950 °C.

TEMPERING
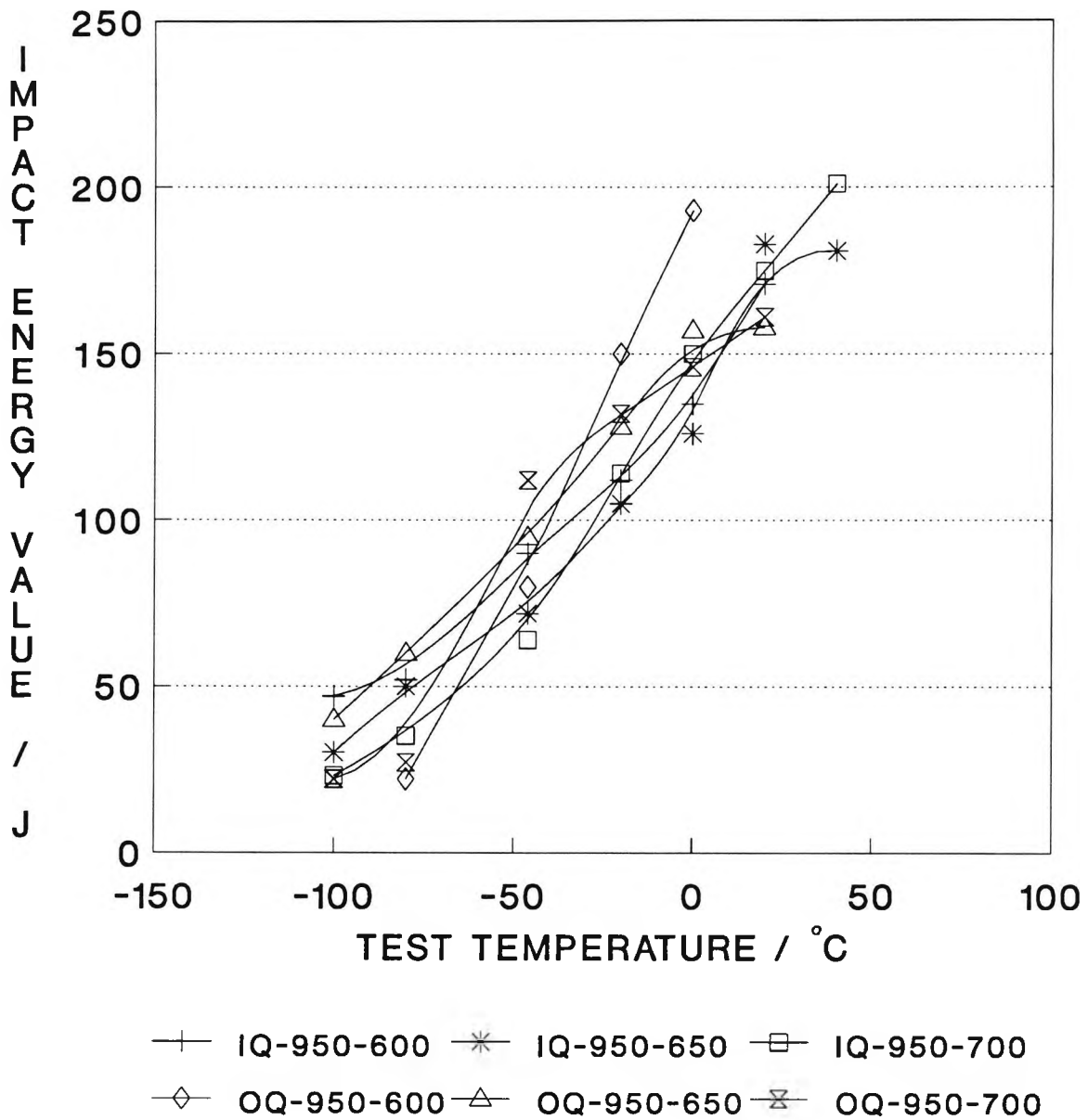
Fig 4.4 Impact transition curves for
samples ice-water or oil quenched
from 950 °C and tempered.
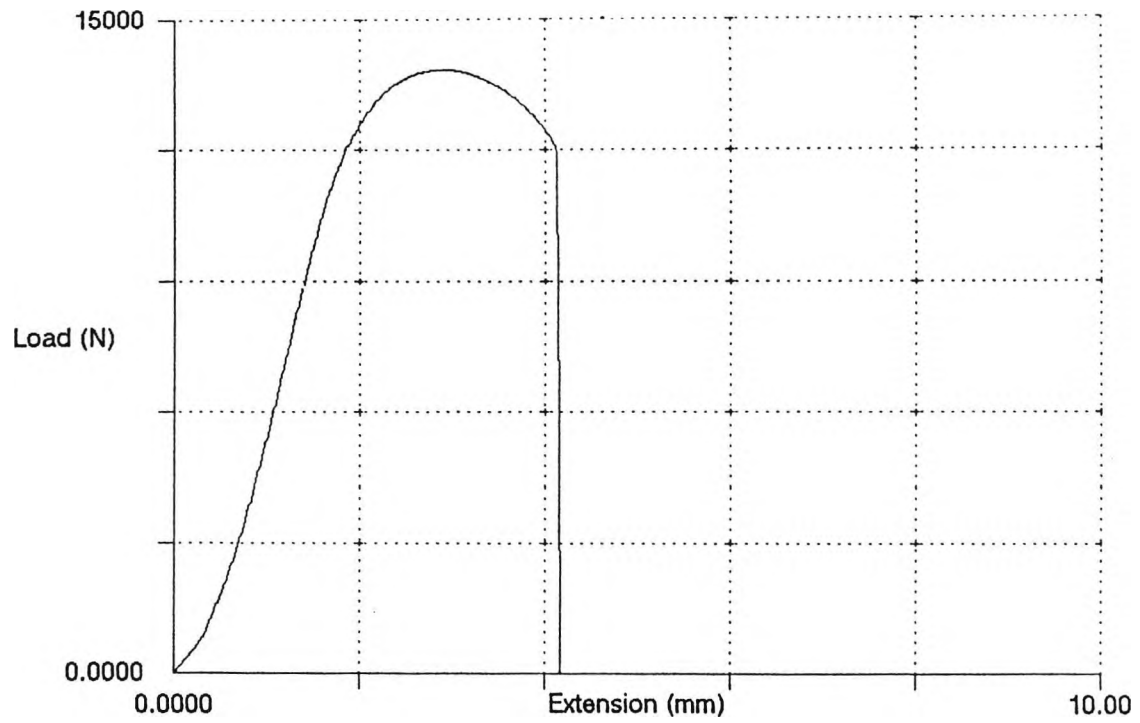
Figure 4.5: Stress-strain curve for sample ice-water quenched from 950°C.
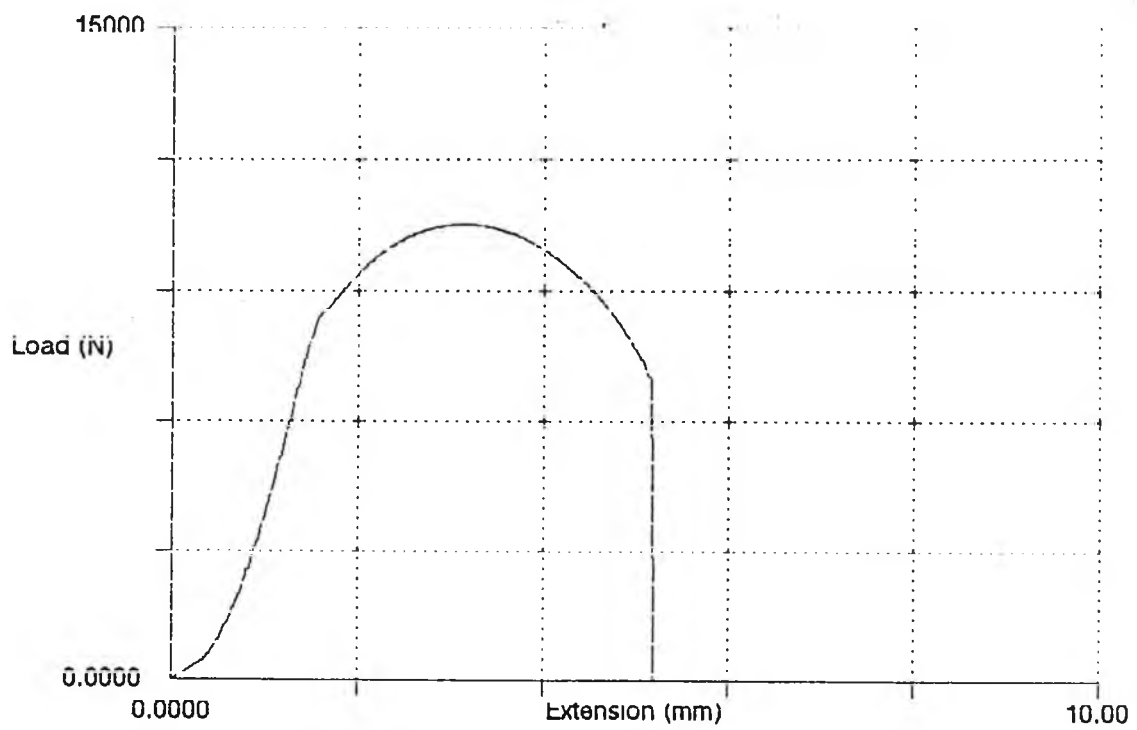
Figure 4.6: Stress-strain curve for sample ice-water quenched and tempered at 600°C.

143
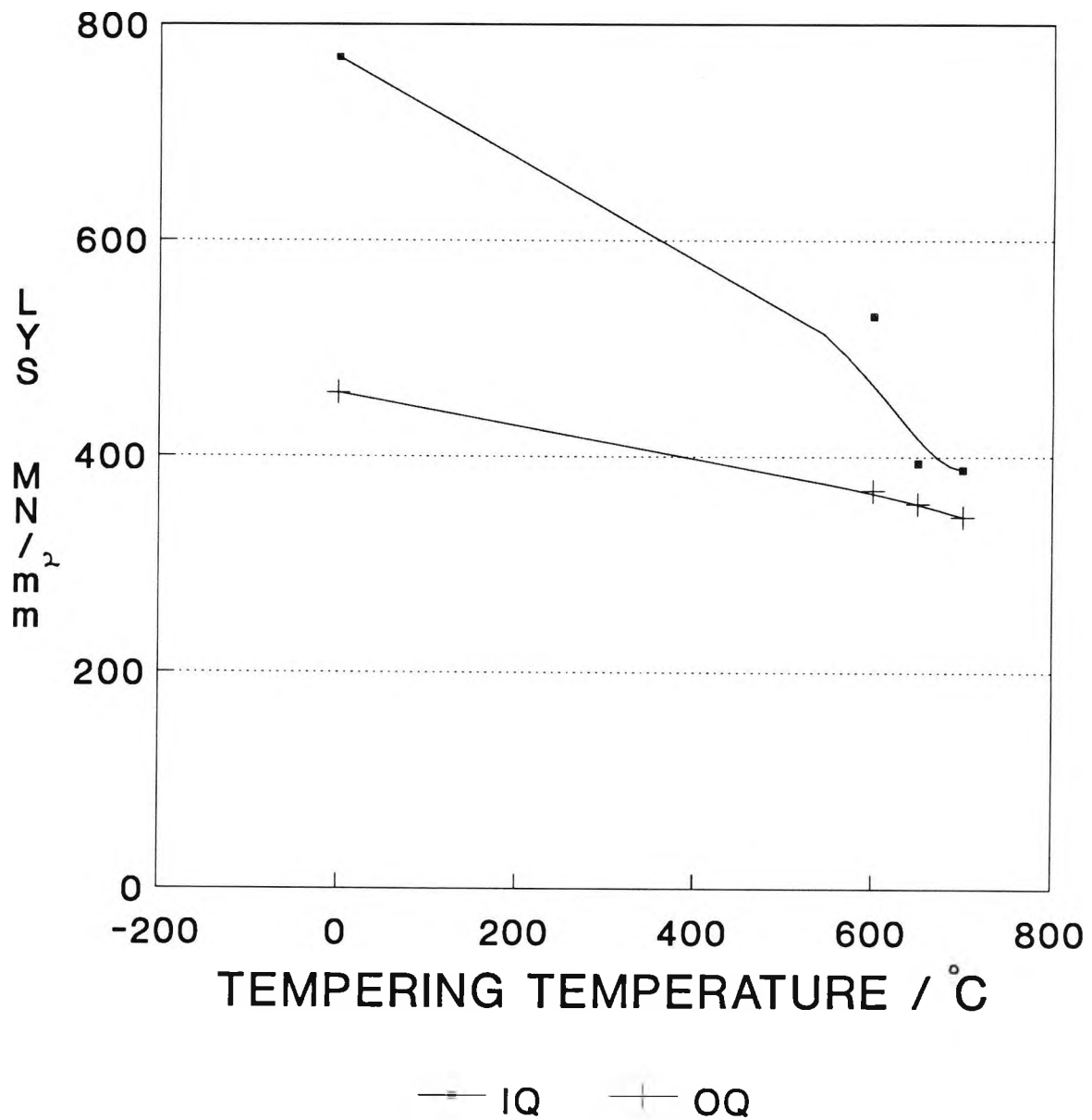
TEMPERING

Fig 4.7 Effect of tempering on LYS of
samples ice-water or oil quenched
from 950 °C
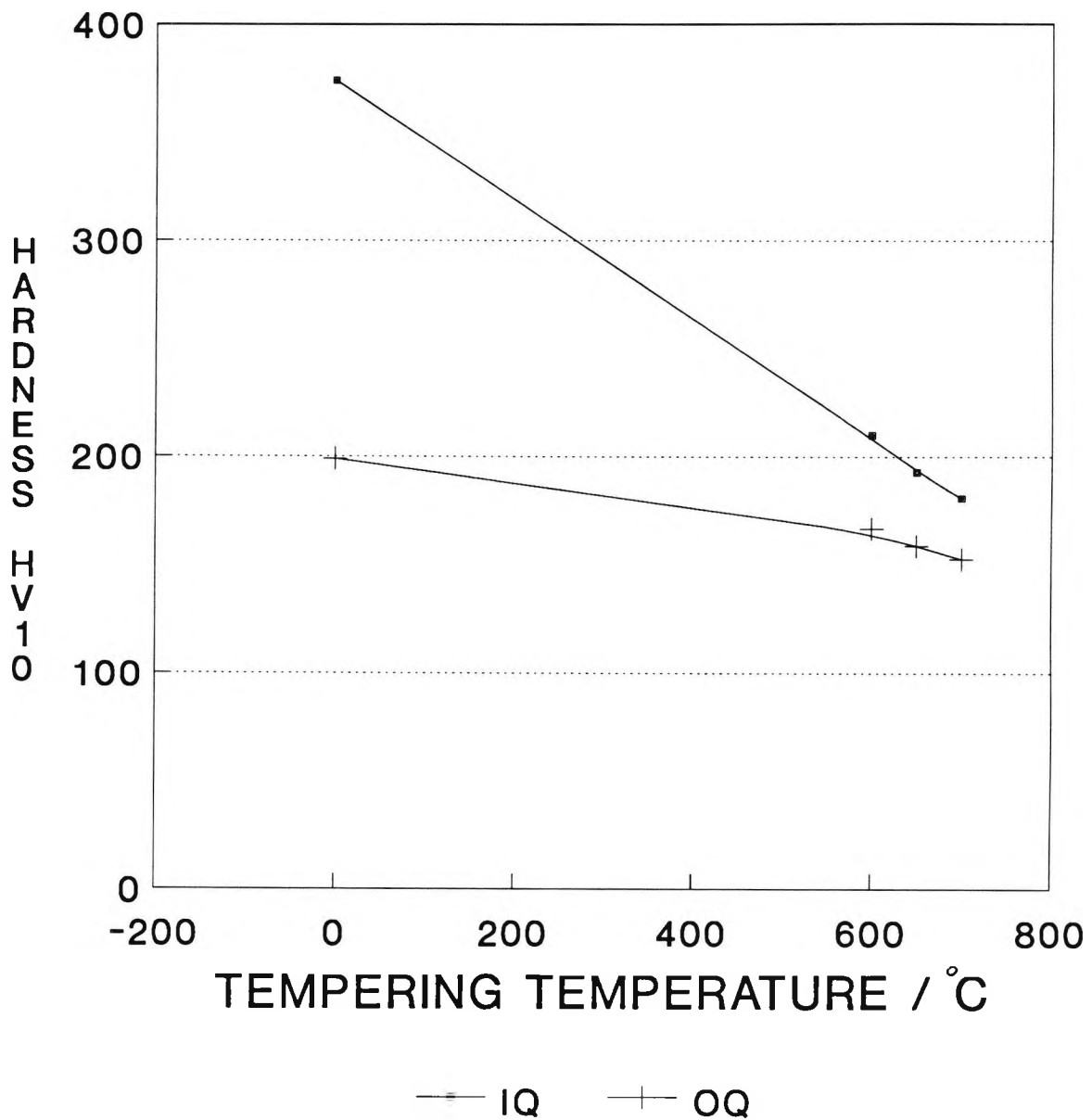
TEMPERING

Fig 4.8 Effect of tempering on hardness
of samples ice-water or oil quenched
from 950 °C (0 ▪ AQ)
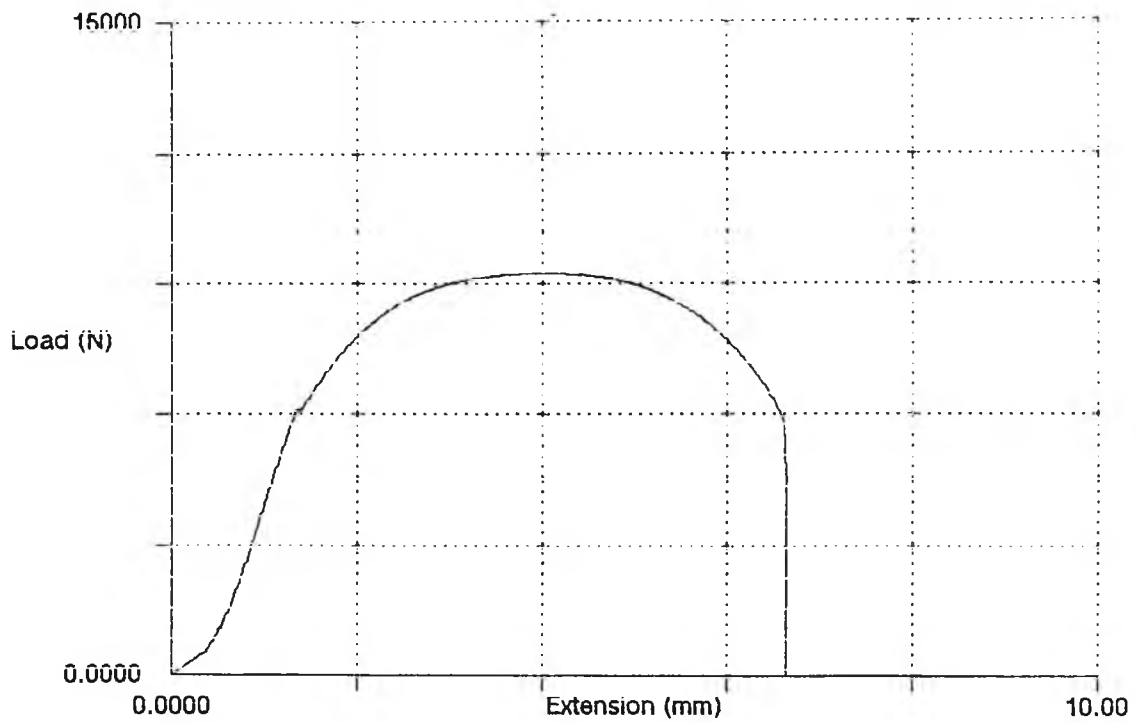
Figure 4.9: Stress-strain curve for sample oil quenched from 950°C.
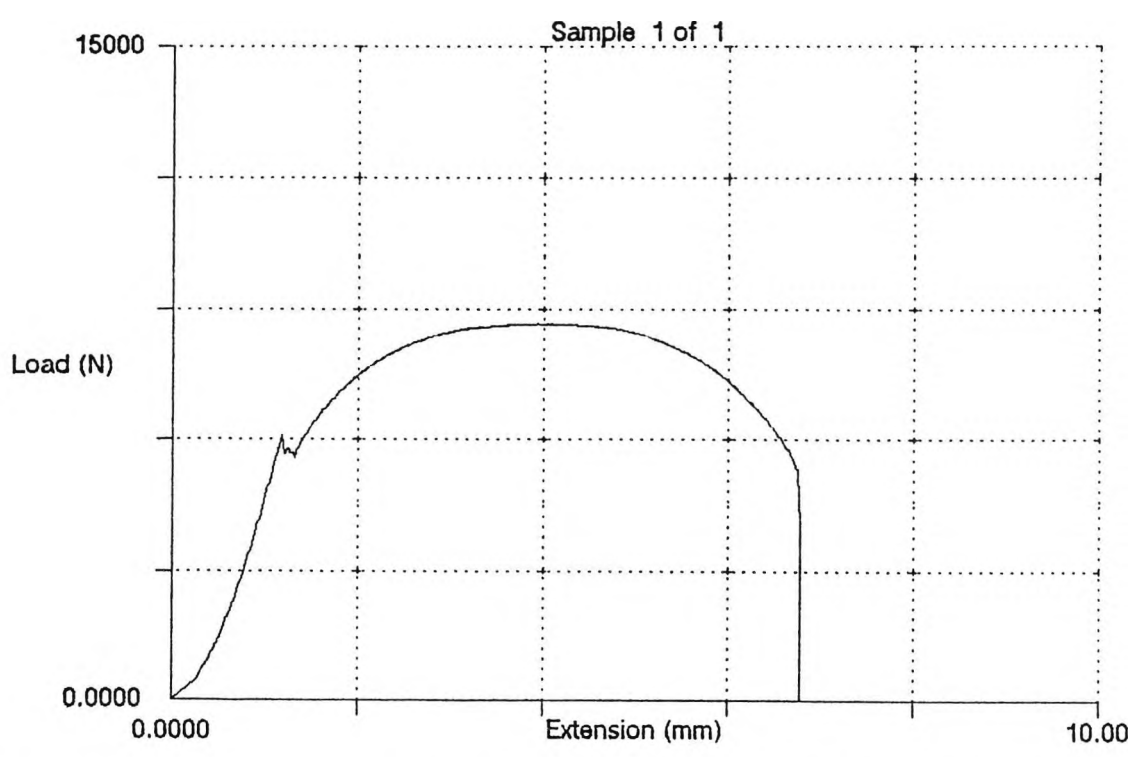
Figure 4.10: Stress-strain curve for sample oil quenched and tempered at 600°C.

146
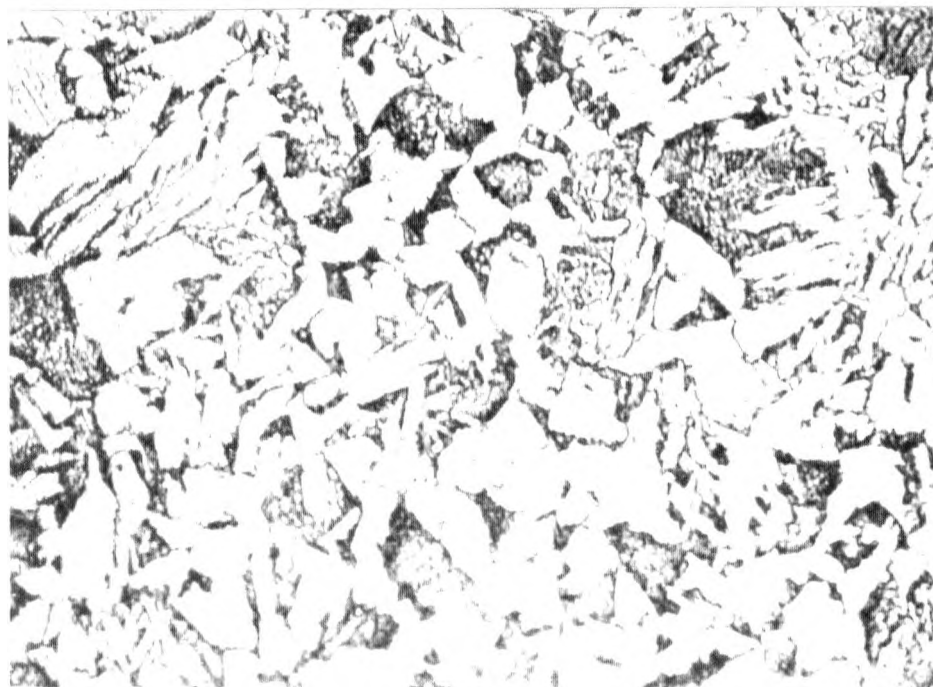
Fig 4.11 Microstructure of steel flanges oil quenched from 950 °C. (optical)
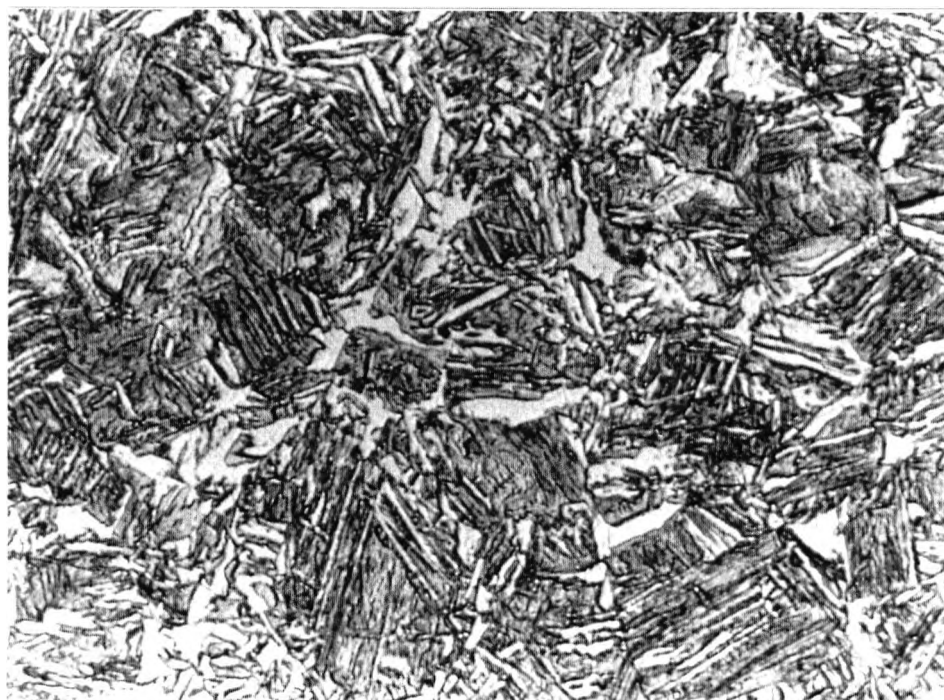
Fig 4.12 Microstructure of steel flanges ice-water quenched from 950 °C.

(Optical)

4.6 μm

Figure 4.13: Degenerate pearlite micro-structure produced when oil quenched from 950°C after holding for 1 hour. (SEM)

2.3 μm
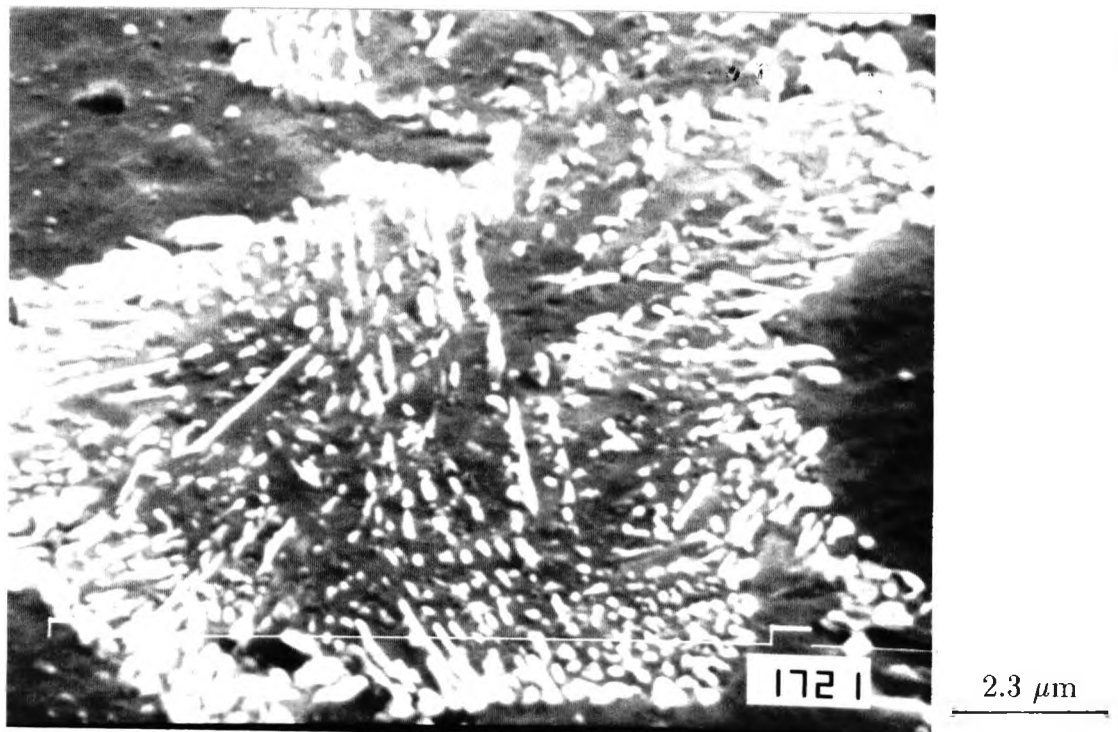
Figure 4.14: Partial spheroidisation of carbides when tempered at 600°C for 1 hour. Steel was oil quenched from 950°C. (SEM)
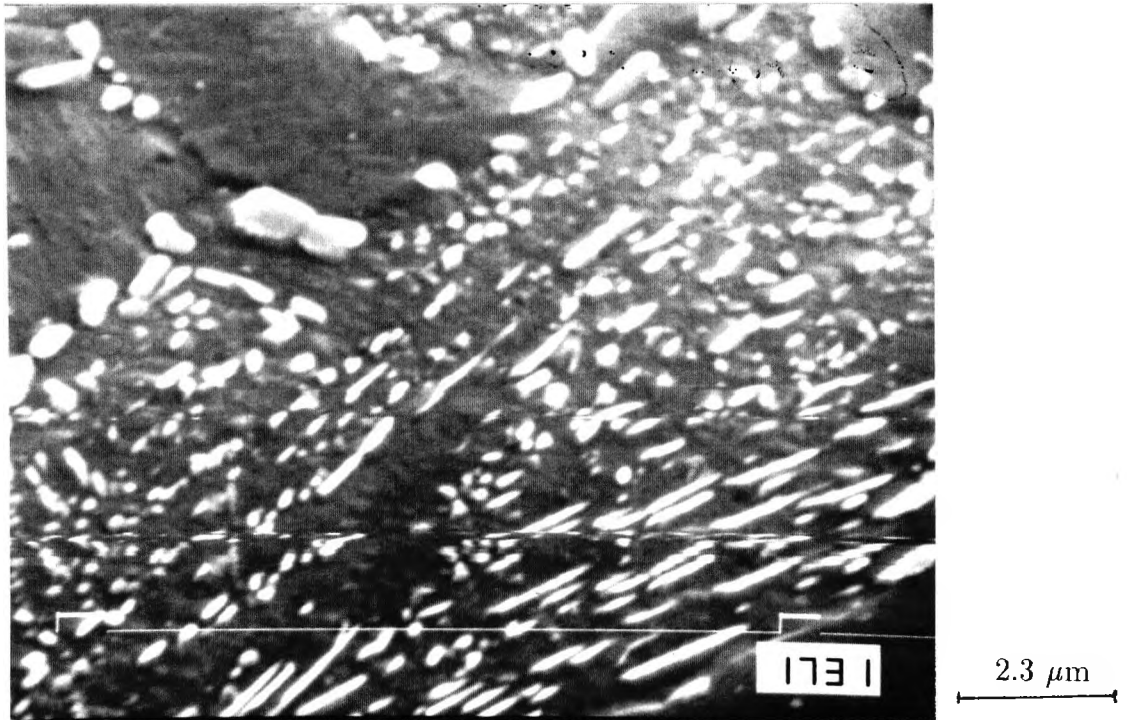
Figure 4.15: Partial spheroidization when tempered at 650°C for 1 hour. Steel was oil quenched from 950°C after holding for 1 hour. (SEM)
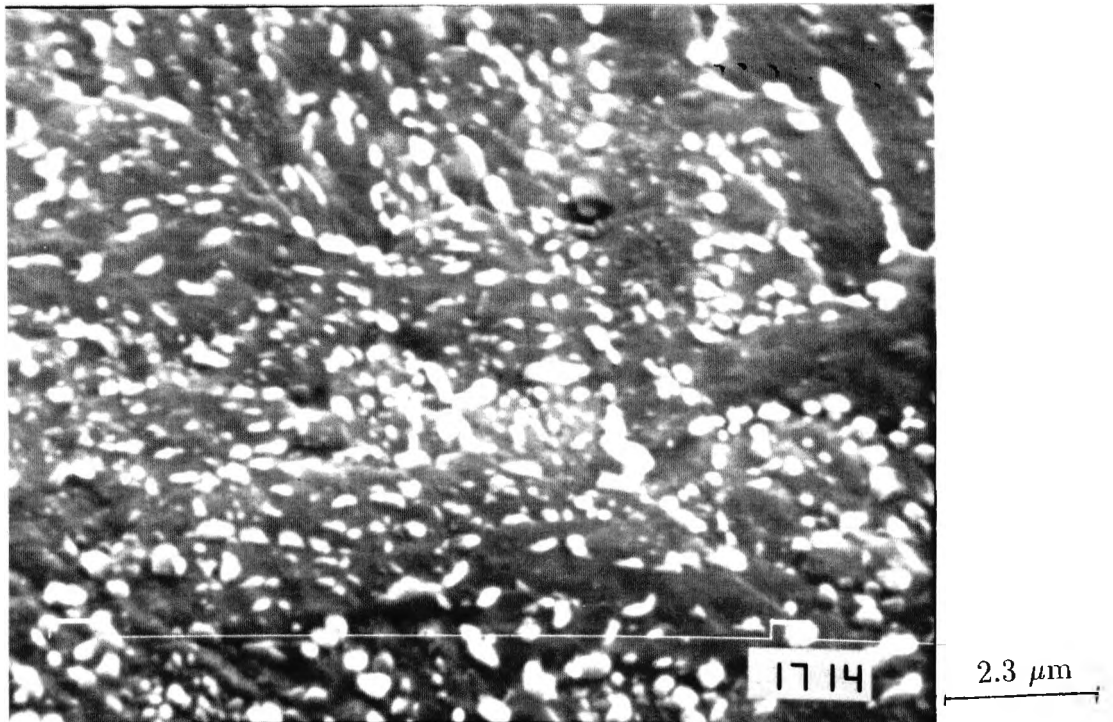
Figure 4.16: Almost complete spheroidization when tempered at 700°C for 1 hour. Steel was oil quenched from 950°C for 1 hour. (SEM)
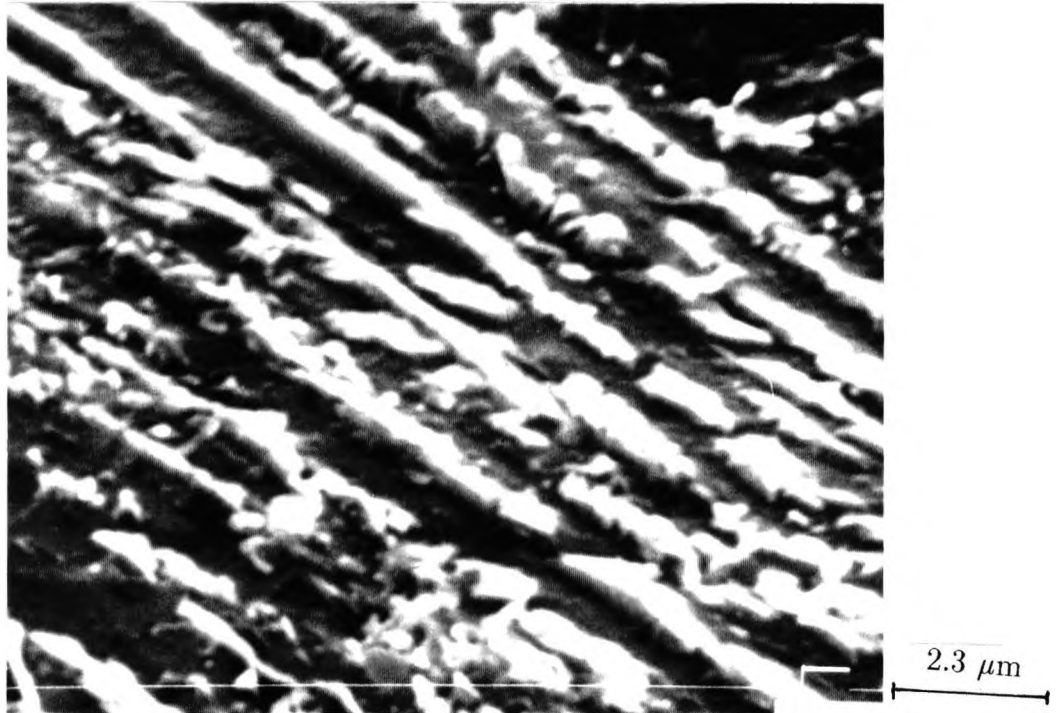
Figure 4.17: Microstructure of steel flanges ice-water quenched from 950°C. (SEM)
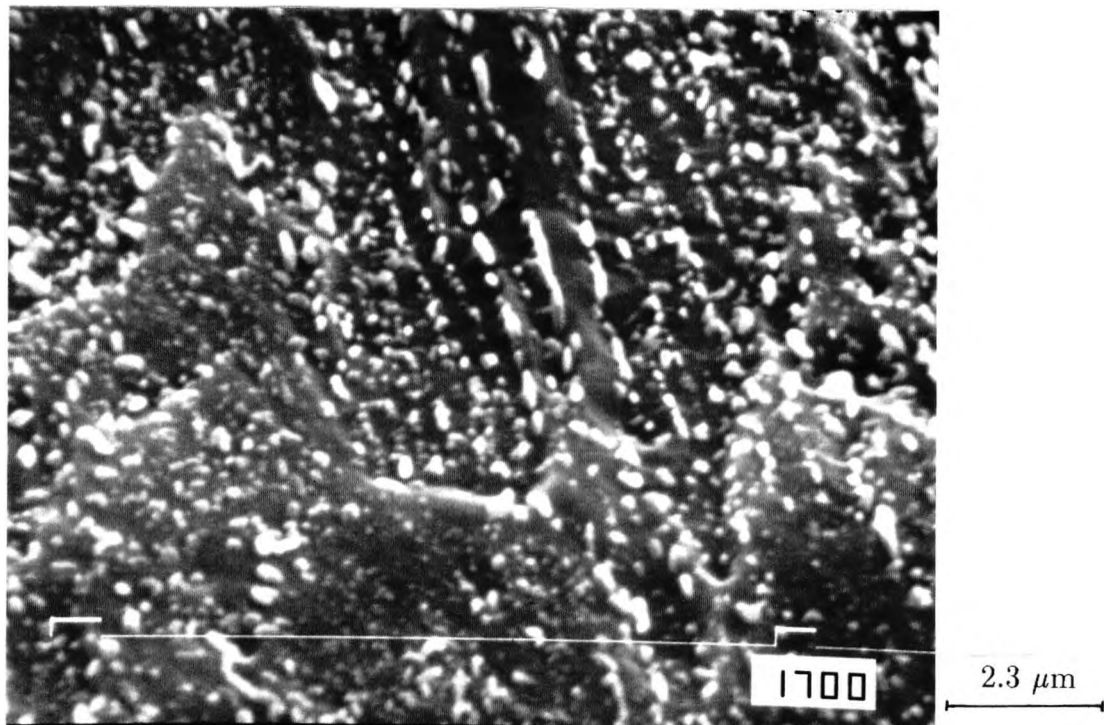
Figure 4.18: Microstructure of steel flanges ice-water quenched from 950°C after holding for 1 hour and tempered at 600°C for 1 hour. (SEM)
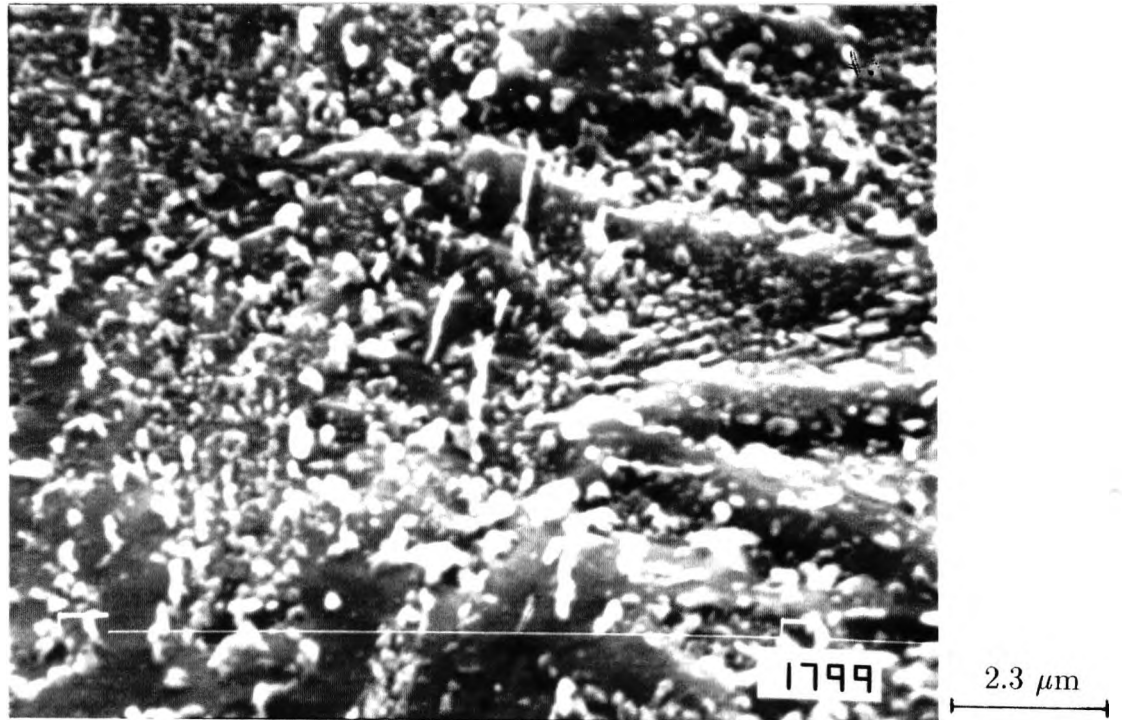
Figure 4.19: Microstructure of steel flanges ice-water quenched from 950°C after holding for 1 hour and tempered at 650°C for 1 hour. (SEM)
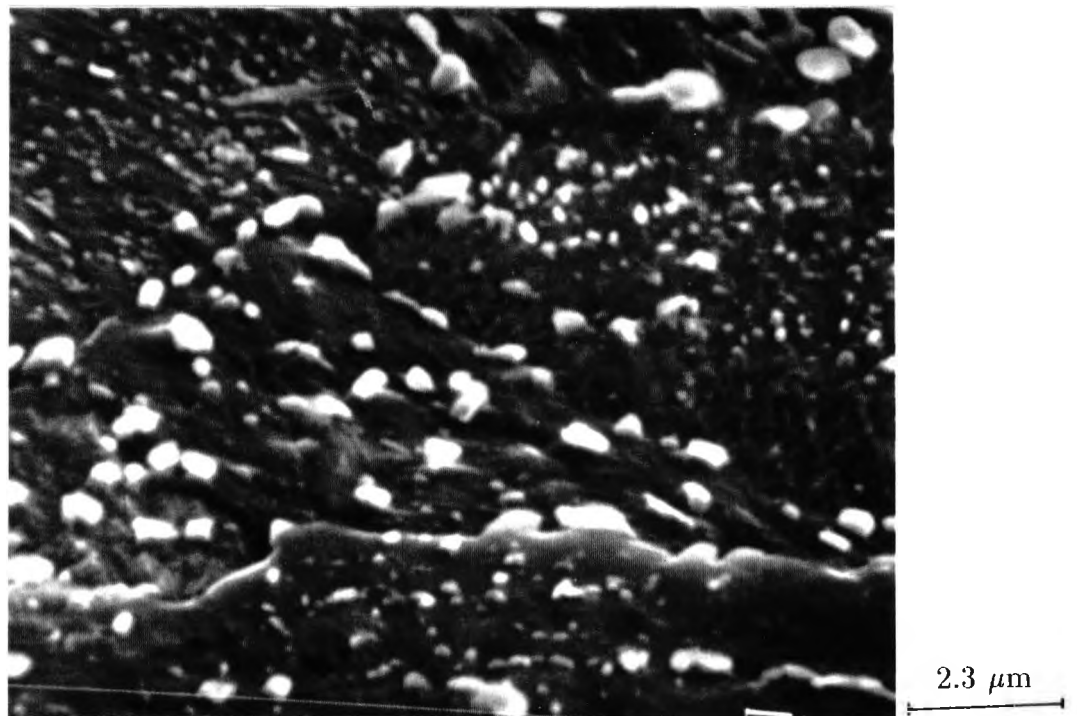
Figure 4.20: microstructure of steel flanges ice-water quenched from 950° C after holding for 1 hour and tempered at 700° C for 1 hour. (SEM)

TEMPERING
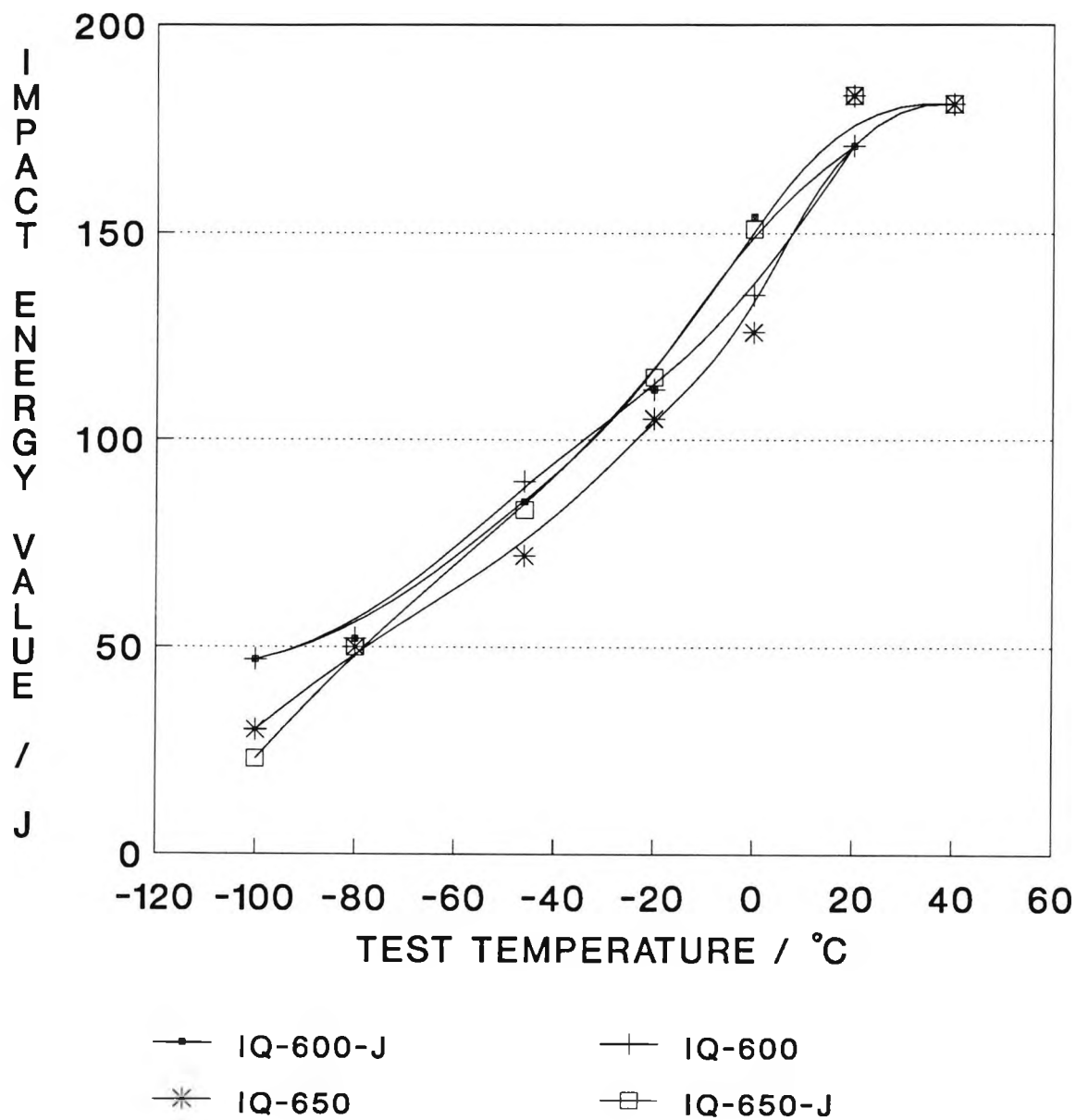
Figure 4.21: Impact transition curves for samples ice-water quenched from 950° C as compared with previous work[8]. Previous work by Kolahi-aval is denoted by letter J.

TEMPERING
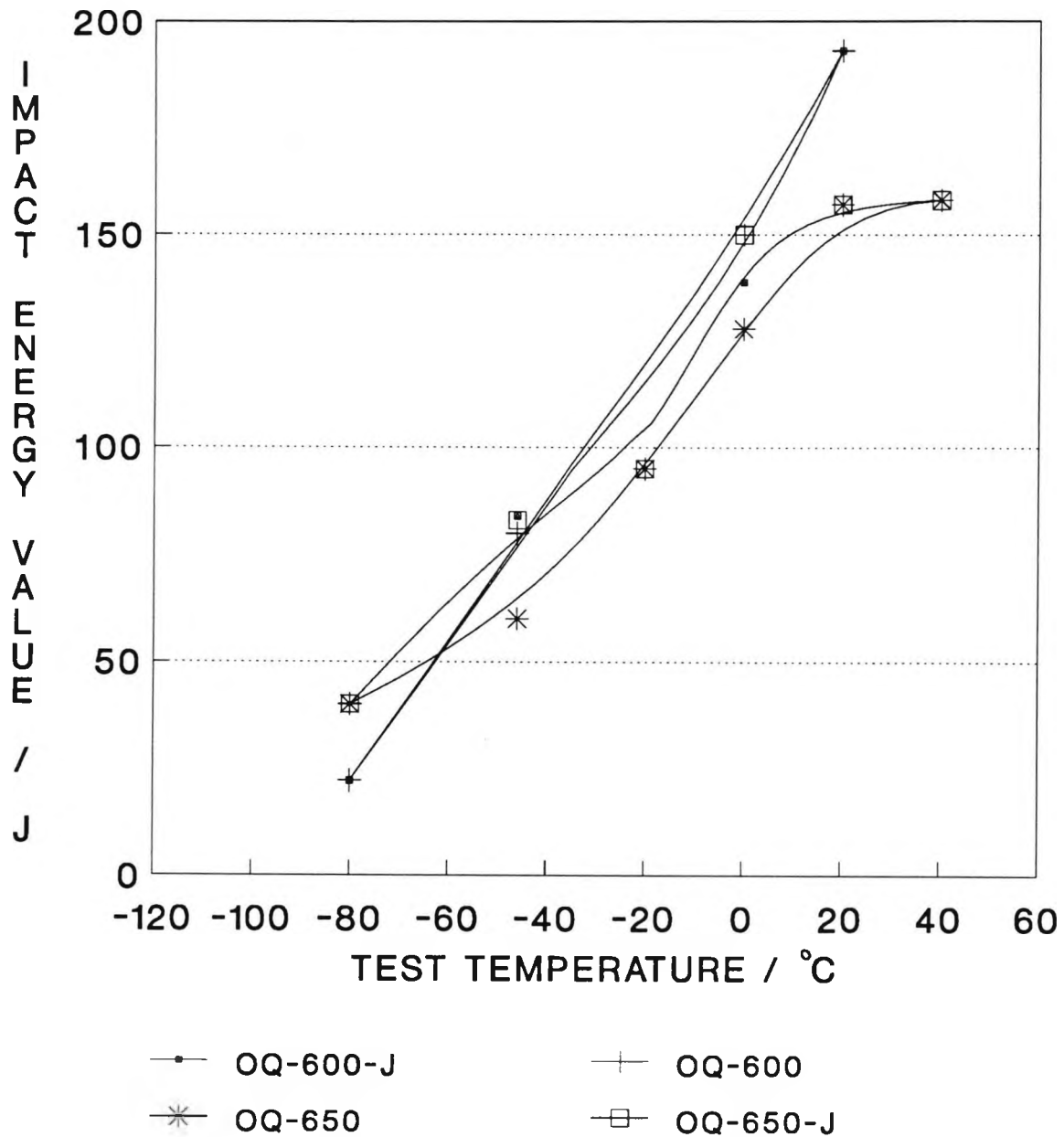
Figure 4.22: Impact transition curves for samples oil quenched from 950° C. Comparison of present work with that of Kolahi-aval[8] refferred to as J in the figure.

153
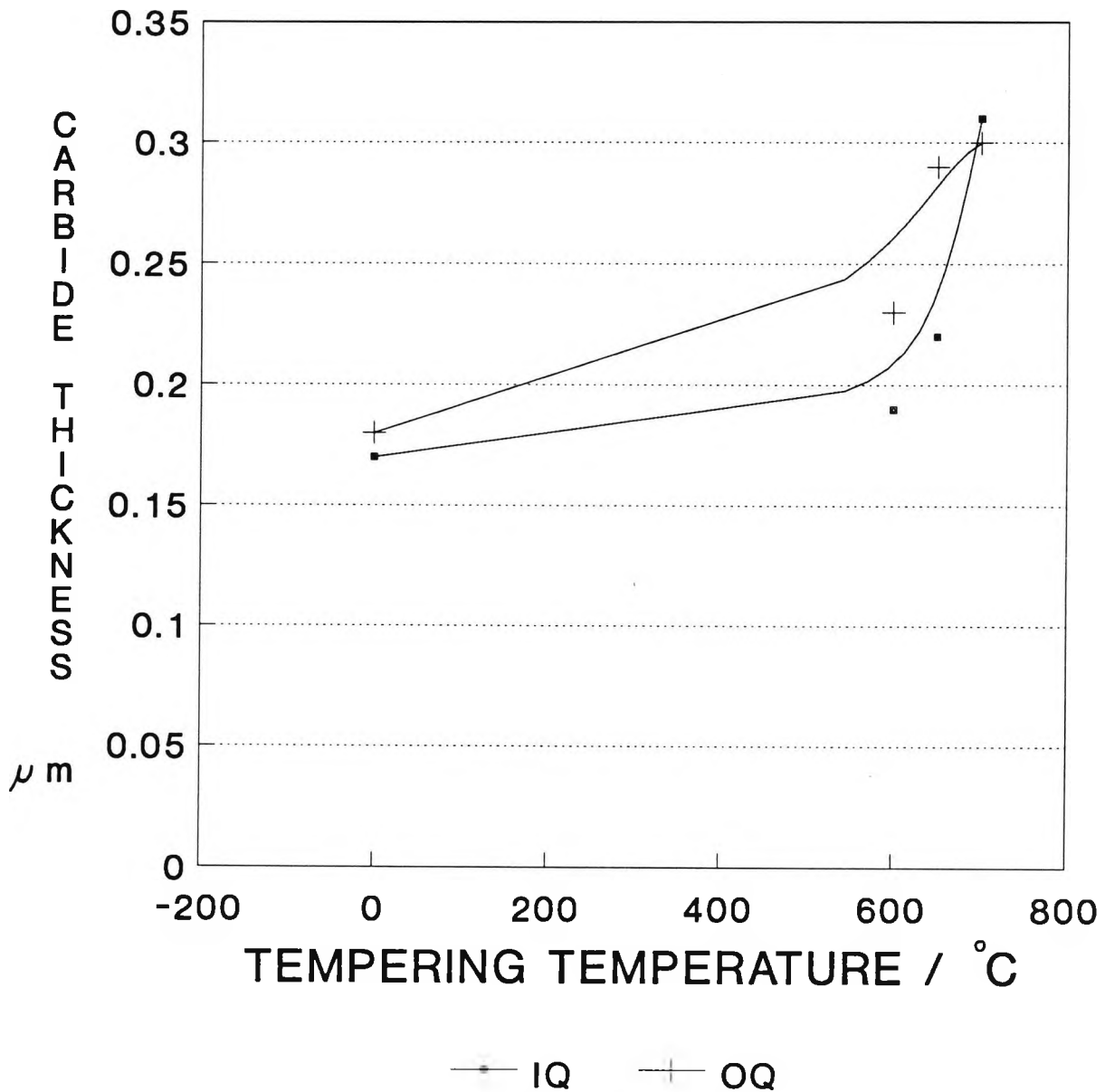
TEMPERING

FIG 4.23 Variation of carbide thickness with tempering temperature for both ice-water and oil quenched samples (0 ▪ AQ).

TEMPERING
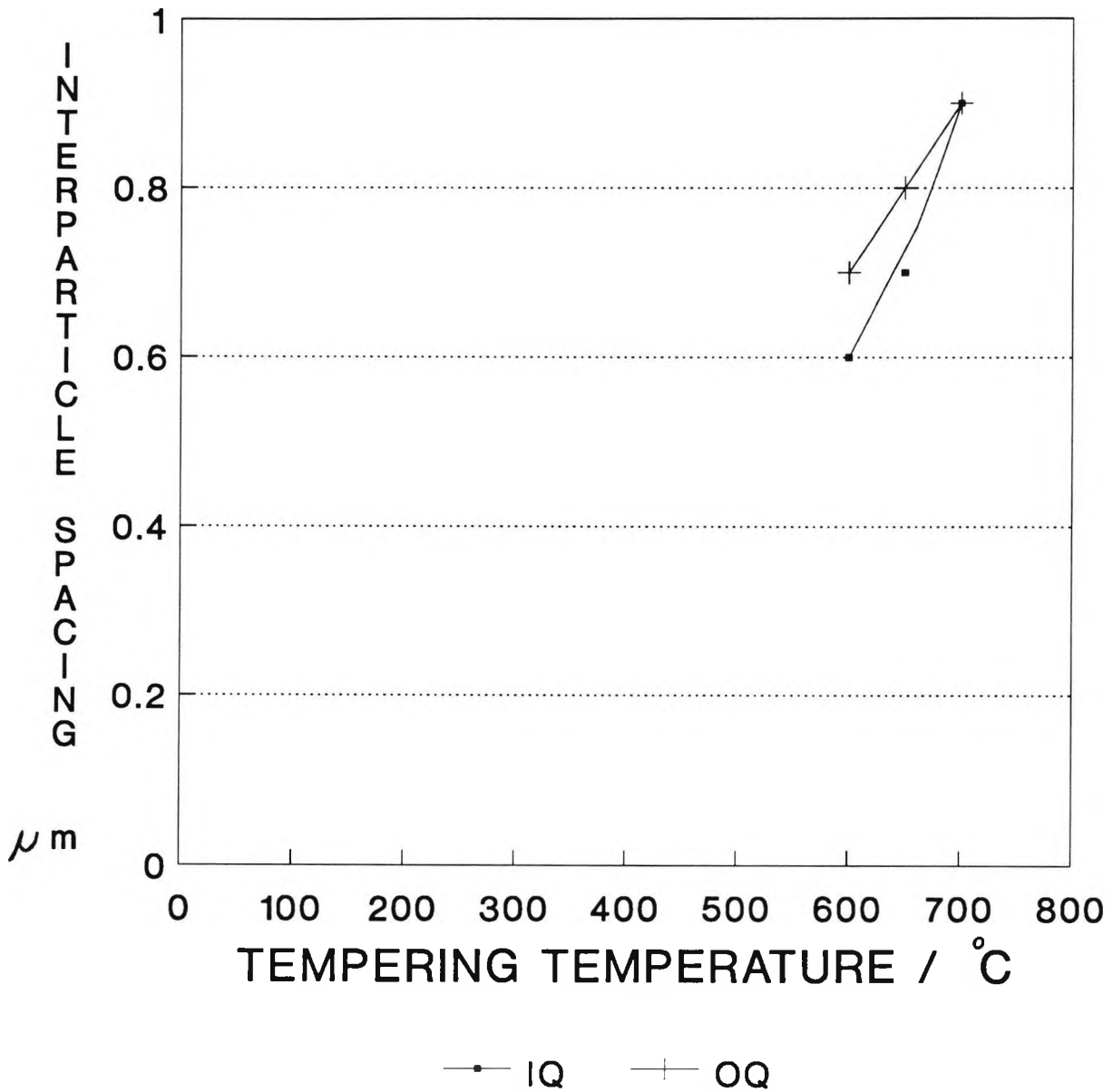
FIG 4.24 Variation of interparticle
spacing with tempering temperature
for both ice-water and oil quenching

155
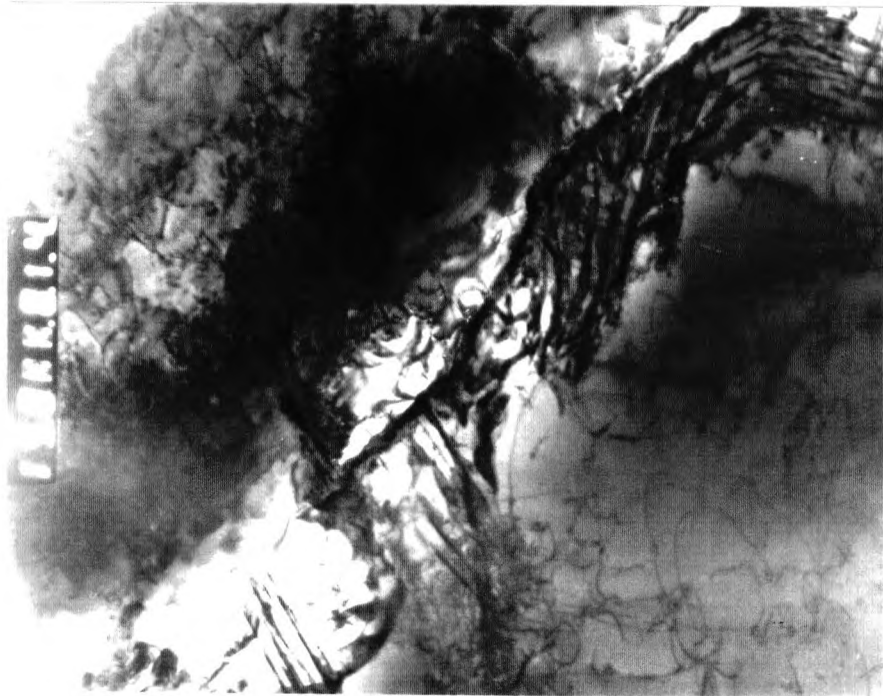
MAG 21000 X

MAG 38000 X

Figure 4.25: TEM observation of oil quenched samples.
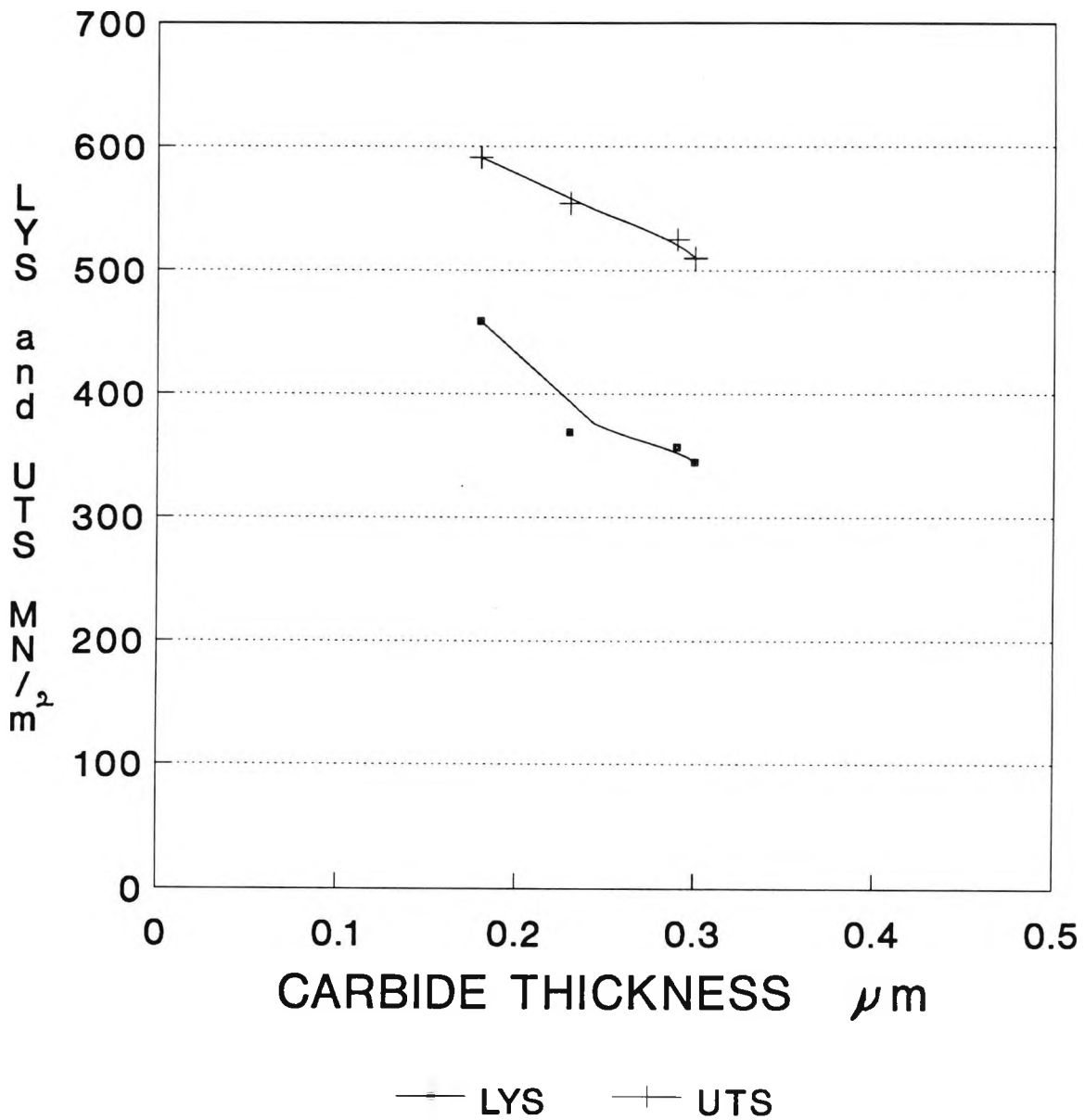
TEMPERING

FIG 4.26 Variation of LYS and UTS
with carbide thickness for oil
quenched samples
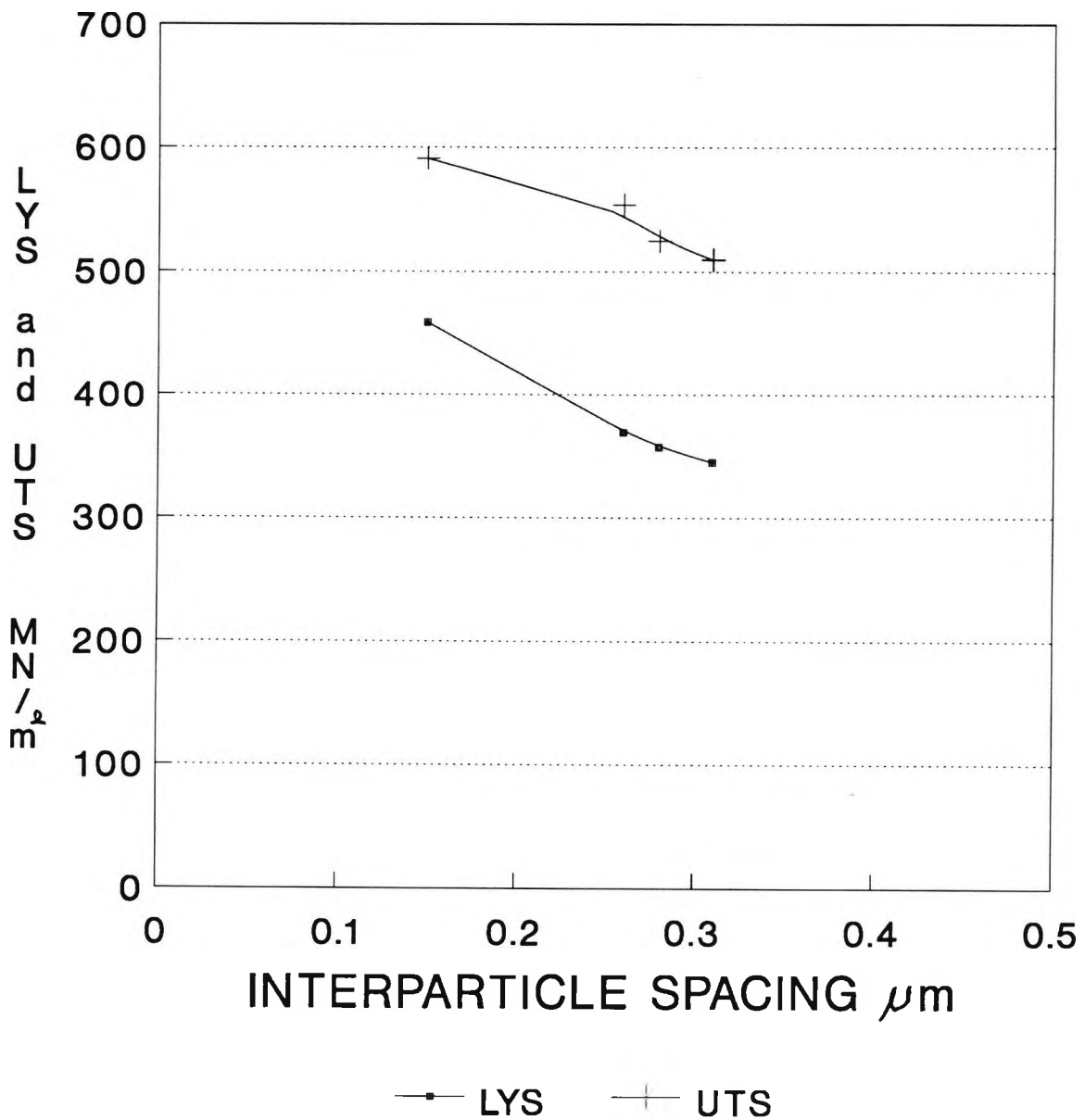
TEMPERING

FIG 4.27 Variation of LYS ana UTS with
interparticle spacing for oil quenched
samples
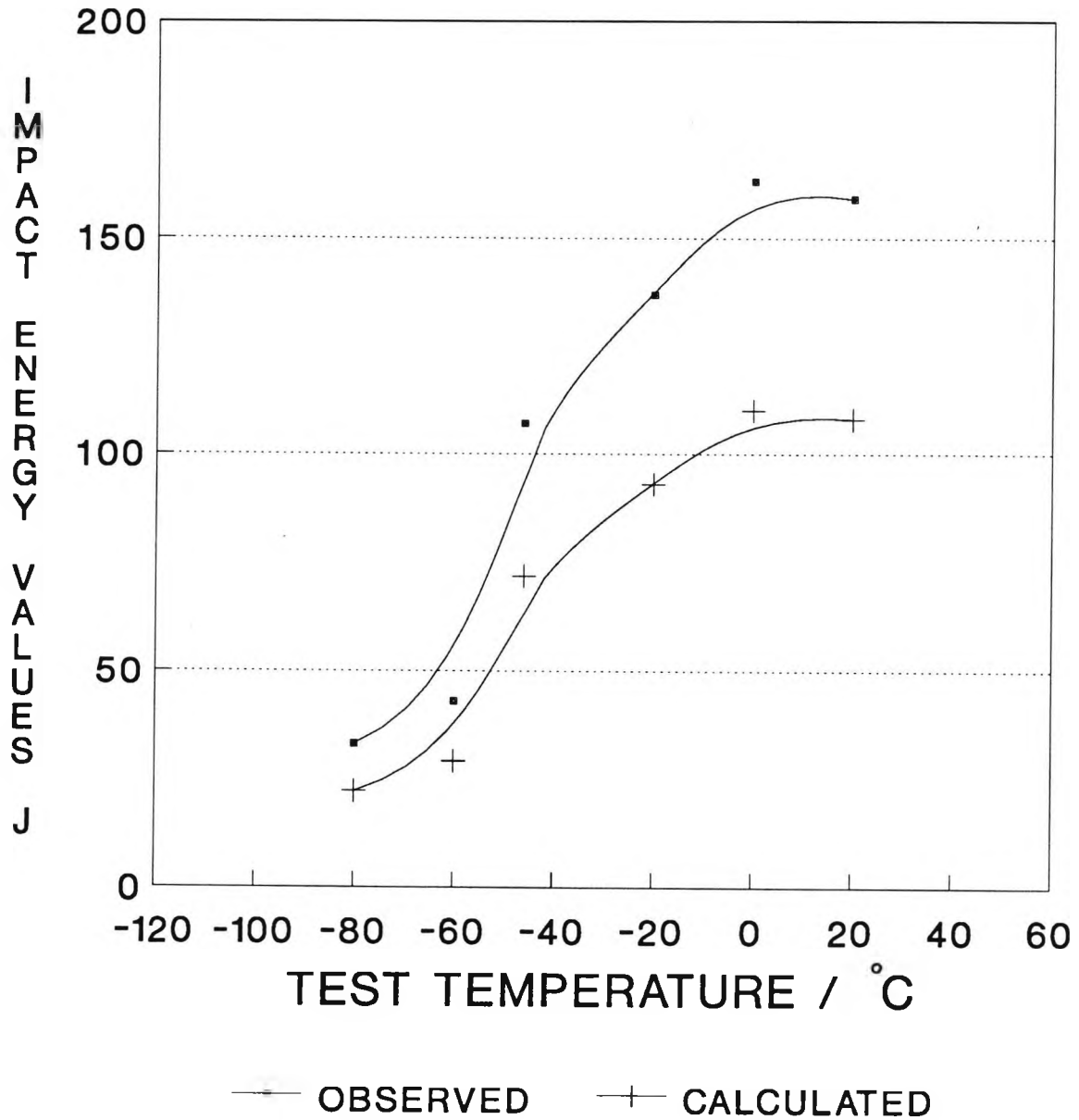
TEMPERING

Figure 4.28: Upper curves is the average impact energy for the tempered flanges after oil quenching. The lower curve represents the calculated from the upper curve assuming a lower shelf energy.

159
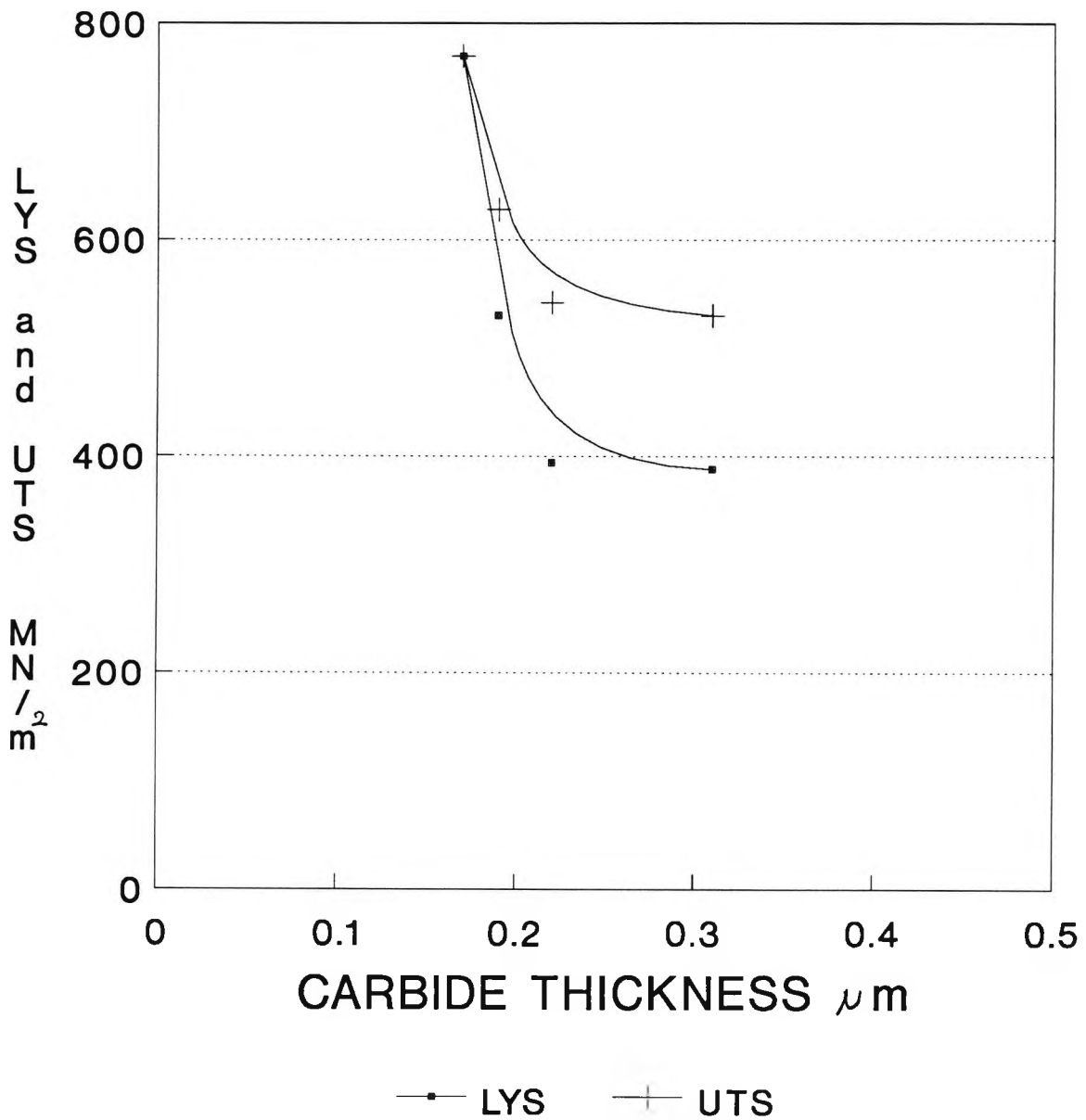
TEMPERING

FIG 4.29 Variation of LYS and UTS with
carbide thickness for ice-water quenched
samples on tempering

160
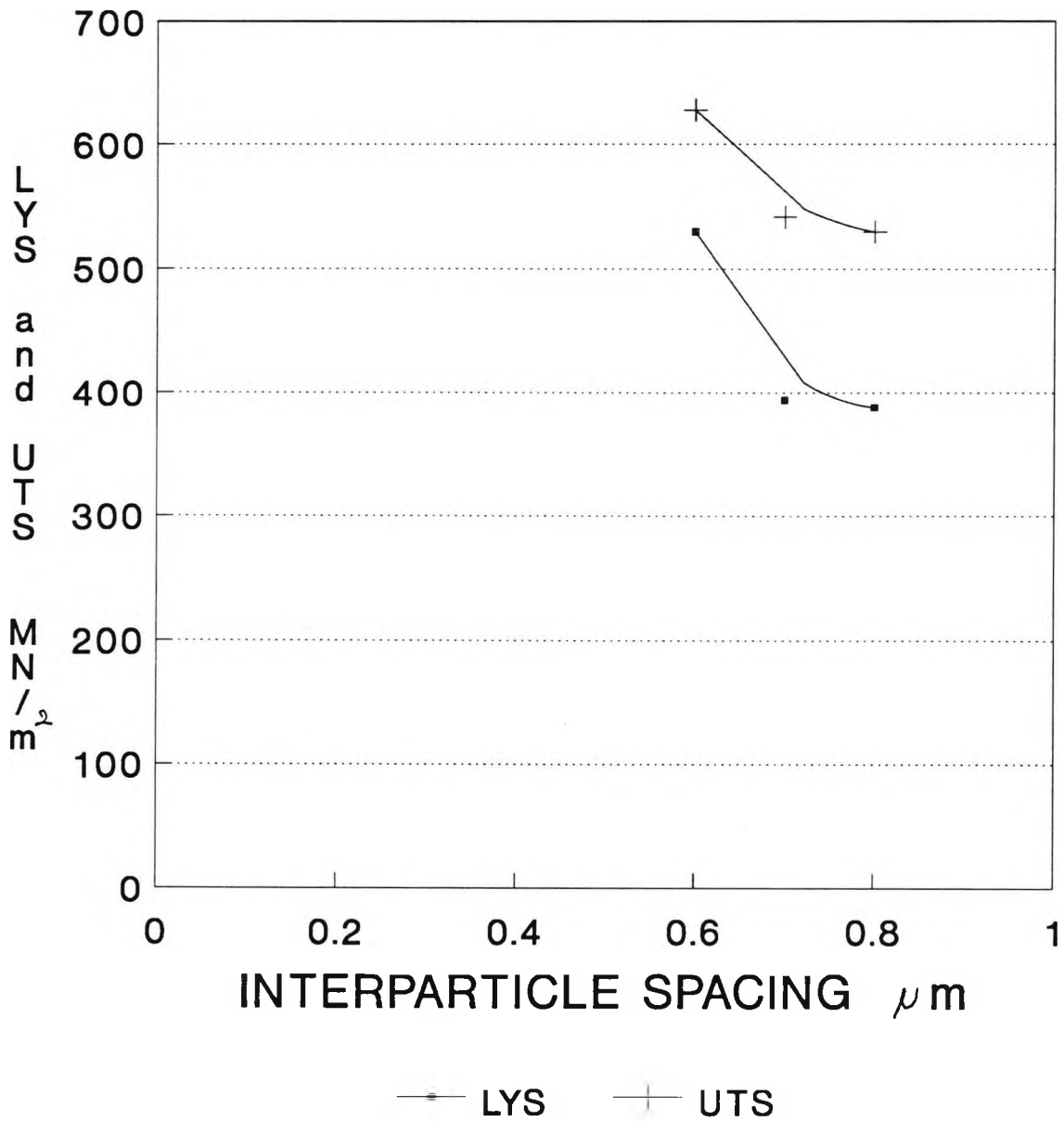
TEMPERING

FIG 4.30 Variation of LYS and UTS with
interparticle spacing for ice-water
quenched samples during tempering

161
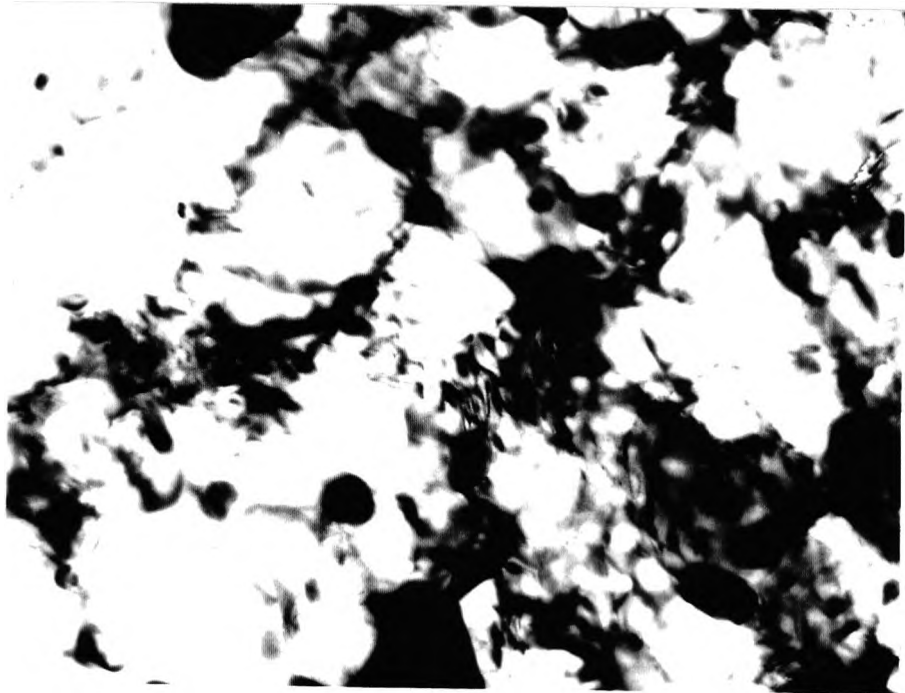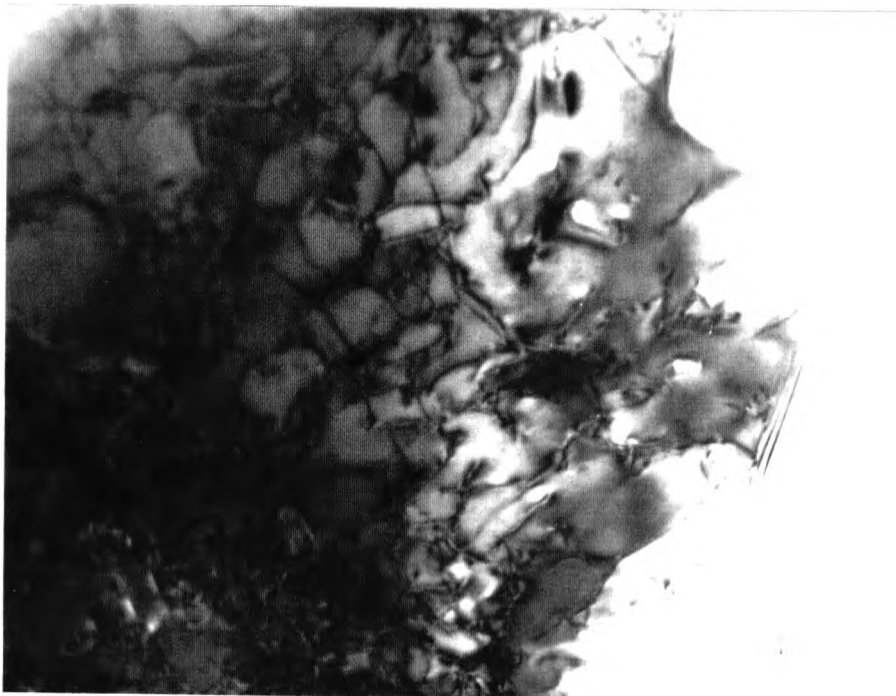
MAG 38000 X

MAG 38000 X

Figure 4.31: TEM observation of ice-water quenched samples after tempering at 600° C.

TEMPERING
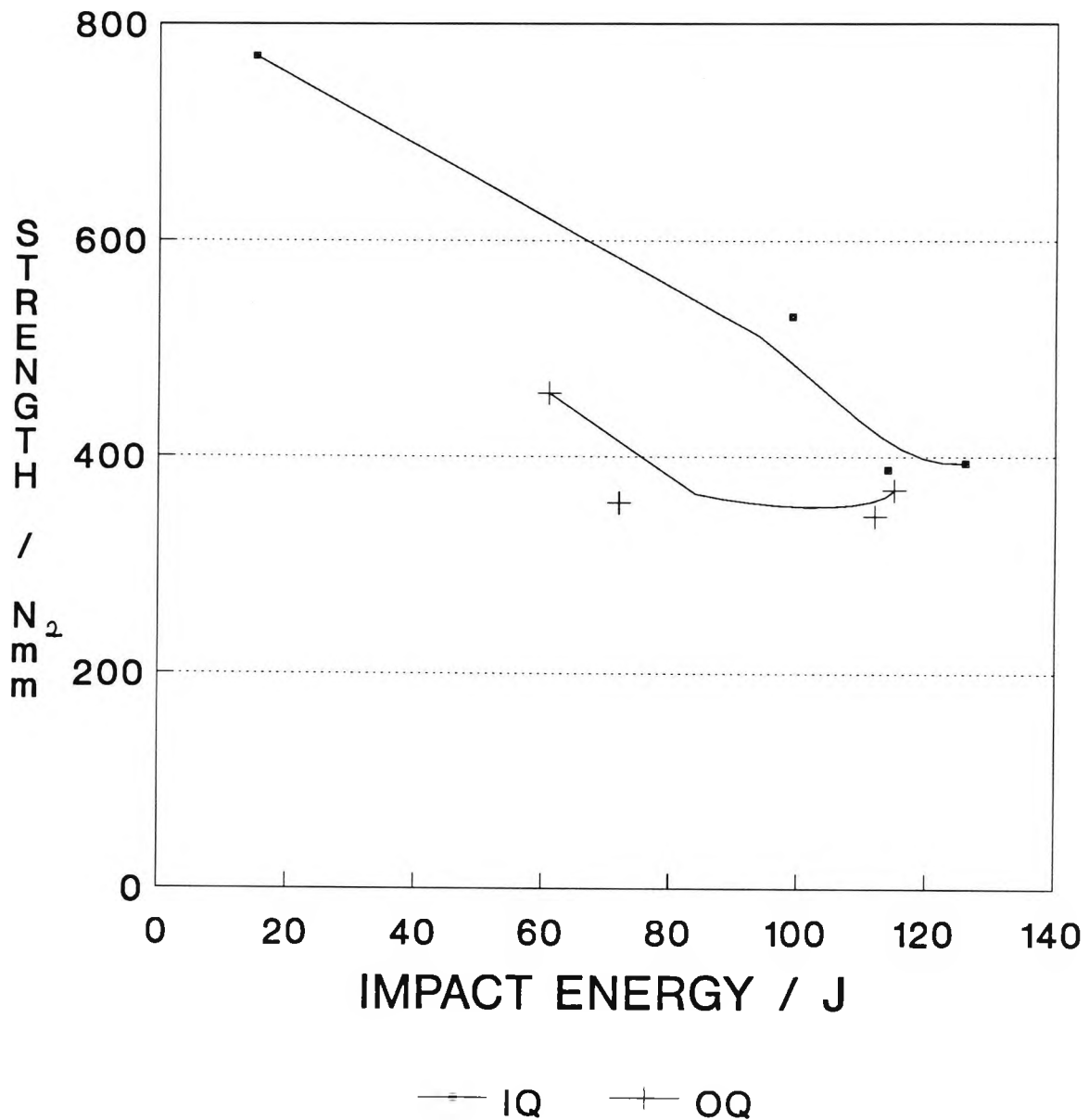
FIG 4.32 Variation of impact energy
at -46°C with changes in strength
on tempering

Chapter 5

INFLUENCE OF LOWER TEMPERING TEMPERATURE ON THE IMPACT AND TENSILE PROPERTIES OF QUENCHED C-Mn-Al STEELS

5.1 Introduction

Generally, the interplay of hardness and toughness is of major concern in the heat treatment and application of quench and tempered steels. However, the changes in other mechanical properties with increasing tempering temperature are also tabulated for common grades of carbon and alloy steels and are quite important for the selection of steels and design of heat treatments for some applications. There are two tempering temperature ranges that produce significant improvements in toughness from that of the as quenched state [55]. Tempering in the range of 150 to 200 ^{0}C produces a modest increase in toughness that is adequate for applications that require high strength and fatigue resistance (medium-carbon steels). Tempering above 425 ^{0}C is the other important tempering temperature range. Toughness improves significantly after tempering in this range, but as noted before (chapter 4 and previous work by Kolahi-aval[8]) hardness and strength also decrease significantly. Tempering above 425 ^{0}C is used where high toughness is of major concern and strength and hardness are important but of secondary concern.

The toughness may actually decrease if steels are tempered in the range of 260 to 370 ^{0}C[55]. This decrease in toughness is refered to as tempered embrittlement.

In chapter 4 it was noted that an increase in tempering temperature , from 600, to 700 ^{0}C showed an insignificant improvement in toughness even though strength and hardness decreased. Tempering at 600 ^{0}C produced an optimum toughness together with strength and hardness.

In this chapter the influence of a significantly lower tempering temperature of 300 ^{0}C is examined for C-Mn-Al steel flanges made to the ASTM A350 LF2 specification. The influence of a coarser γ grain size on the impact

behaviour is also examined.

5.2 Experimental

The composition of the flange examined is given in table (5.1). This flange contained Al as a grain refining micro-alloying addition with slightly higher C and S content and lower Mn level than steel examined in chapter 4.

Blocks of 80*60*40 mm (the latter measurement being the thickness of the flange face) were cut from these flanges so that standard charpy V-notch impact samples could be taken from radial positions and tensile samples were taken tangentially to the face of the flange, (see chapter 3 Fig 3.3). The austenite grain size was varied by heating for 1 hour at temperatures of 900 and 1250 ^oC. Temperature was monitored by inserting thermocouples into the centre of the blocks. After austenitising the samples were either oil-quenched or ice-water quenched (average cooling rates in the temperature range 800 to 400 ^oC were 600 and 1200 K/min respectively) so that a variation in microstructure could be produced typical to that observed in commercially heat-treated flanges. After quenching some of the blocks were tempered at 600 and 300 ^oC for 1 hour followed by air cooling.

The following conditions were examined:

- 1) As quenched from 900 ^oC

- 2) As quenched from 900 ^oC and tempered at 300 ^oC for 1 hour

- 3) As quenched from 900 ^oC and tempered at 600 ^oC for 1 hour

- 4) As quenched from 1250 ^oC and tempered at 300 ^oC for 1 hour

- 5) As quenched from 1250 ^oC and tempered at 600 ^oC for 1 hour

166

A total of 10 heat treatments were carried out, five for each quenching conditions. (oil and ice-water)

Standard charpy V-notch samples were machined for each heat treated condition from these blocks with the notch perpendicular to the flange face. The charpies were located at positions between one quarter depth and mid-thickness from the flange surfaces.

Samples were impact tested at different temperatures to obtain a charpy transition curve for each condition. Tensile tests were carried out on a Hounsfield tensometer at a cross-head speed of 1.6 mm /min. The gauge length of the tensile samples was 18 mm with diameter of 4.5 mm. Vickers hardness measurements (five per sample) using a 10 Kg load were made on a charpy sample from each heat-treated condition and the average taken as the hardness value.

Samples were then prepared for microstructural examination, and the amount of ferrite was estimated by point counting. A minimum of 500 counts were made per sample. The austenite grain size was obtained before tempering as in chapter 4. The austenite and ferrite grain sizes were measured using the linear intercept method, a total of 500 intercepts being measured.

The scanning Electron Microscopic (SEM) and Transmission Electron Microscope (TEM) were used to help identify the microstructural features and to obtain the carbide morphology and distribution. Grain boundary carbide thickness measurement were taken at 0° tilt using the SEM.

5.3   Results

In the present investigation the micro-structures were predominantly ferrite-pearlite and ferrite-bainite for flanges oil or ice-water quenched from 900 ^{o}C

respectively Figs 5.1 and 5.2. Fully martensitic and a mixture of bainite and martensite and some ferrite were obtained when ice-water and oil quenched from austenitising temperature of 1250 ^{0}C, Figs 5.3 and 5.4 respectively.

5.3.1 Ferrite-Degenerate Pearlite Microstructures

Oil quenching from 900 ^{0}C has resulted in the transformation of austenite into ferrite and degenerate pearlite, (55% ferrite and 45% mixture of pearlite,bainite and some martensite) Fig 5.1. The mechanical properties of this steel in its various oil quenched and tempered conditions are given in tables 5.2 and 5.3. The impact behaviour of the oil quenched flanges in the as quenched condition (27 J at -46 ^{0}C) satisfied the ASTM A350 specification requirement of 20 J at -46 ^{0}C. Tempering at 300 ^{0}C for 1 hour did not effect impact behaviour significantly whereas tempering at 600 ^{0}C improved the impact behaviour slightly Fig 5.5. For example, at a test temperature of 0 ^{0}C, a 36 J improvement was observed. The load elongation curves are given in Figs 5.6, 5.7 and 5.8, and show that yield points are present for all the conditions indicating that ferrite is controlling strength. The yield point, UTS and hardness dropped on tempering at 300^{0}C and a further reduction in both strength and hardness was observed after tempering at 600 ^{0}C, Figs 5.6, 5.7, 5.8 and 5.9.

Comparing Figs 5.10, 5.11, 5.12 not much change in microstructure occurred on tempering the as quenched flanges when tempered at 300 ^{0}C whereas after tempering at 600 ^{0}C, the lines of carbides start to break and partially spheroidise.

5.3.2 Ferrite-Bainite Microstructures

Ice-water quenching from 900 °C resulted in the formation of a complex structure namely ferrite-bainite with a small amount of martensite, Fig 5.2 with very poor ductility and toughness and a high strength and hardness. The austenite grain size for this austenitising temperature was 25 μm. For the as quenched condition the impact behaviour of these flanges did not meet the ASTM A350 LF2 specification requirement at -46°C but after tempering at 300 and 600 °C an improvement in impact behaviour was observed with a reduction in strength and hardness Figs 5.13, 5.14, 5.15, 5.16 and tables 5.2 and 5.3. Comparing the two tempering temperatures, it can be deduced that tempering at 600 °C was more effective than at 300 °C in improving the impact behaviour. SEM observation was used to justify this view, Figs 5.18 and 5.19 show the variation of carbides after tempering at both temperatures and these can be compared with the as quenched condition, Fig 5.17. After tempering at 300 °C, there was no significant change in carbide morphology, whereas at 600 °C it seemed the lines of carbides started to break up and partially spheroidise.

5.3.3 Fully Martensitic Microstructures

Fully martensitic structures were obtained when ice-water quenched from 1250 °C, Fig 5.3, with a coarse γ grain size, of 209 μm.

Figs 5.20, 5.21 show the effect of tempering on martensite at 300 and at 600 °C on the microstructure respectively. It is evident that the martensite is still largely intact after this low tempering treatment at 300°C. Impact properties are therefore poor. However, increasing the tempering temperature to 600 °C, causes a significant change in carbide size, morphology and

distribution which could be the reason for an improvement in the impact behaviour Fig 5.22 and a sharp reduction in strength and hardness (Figs 5.23 and 5.24 tables 5.2 and 5.3).

After tempering at 600 $^\circ$C, according to SEM observation Fig 5.21, the carbides in the matrix break into smaller pieces and start to spheroidise. Compared with the lower tempering temperature of 300 $^\circ$C, tempering at 600 $^\circ$C caused an improvement in impact energy of 40 J at 0 $^\circ$C. Tempering at 300°C did not satisfy the specification requirement of 20 J at -46 $^\circ$C.

5.3.4 Ferrite + Martensite Microstructures

Oil quenching from the austenitising temperature of 1250 $^\circ$C resulted in the formation of an 85% mixture of martensite/bainite and 15% ferrite Fig 5.4.

SEM observation of Fig 5.25 suggests that at 300°C plate like carbides are formed in the martensite matrix. An increase in tempering temperature to 600 $^\circ$C resulted in the spheroidising of these carbides, Fig 5.26 and an improvement in impact behaviour at test temperatures above 0 $^\circ$C (improvement of about 40 J at 20 $^\circ$C).i.e. below 0°C there was little difference in the brittle region of the impact transition curve Fig 5.27. Raising the tempering temperature to 600 $^\circ$C resulted in a significant decrease in both strength and hardness Figs 5.28 and 5.29 and tables 5.2 and 5.3.

5.4 Discussion

As expected prior austenite grain size had a large influence on the impact properties, strength and hardness. Quenching from an austenitising temperature of 1250 $^\circ$C produced a coarse γ grain size (209 μm), and therefore worse

impact behaviour compared with quenching from 900 °C, when the grain size was fine (25 μm) Figs 5.30 and 5.31. This applied to both the oil and ice water-quenched conditions.

Previous work by Mintz et al[37] on quenched and tempered steels suggests that, in martensite- bainite structures the most important microstructural parameter controlling fracture has been shown to be the colony or packet size which is related to the austenite grain size. The strong relationship between the γ grain size and impact behaviour has also been noted by Naylor and Krahe[88] in fully upper bainitic structures. However, they[88] suggest the actual microstructural unit controlling fracture is the bainitic colony size, which is related to the γ grain size.

Gladman et al[21], suggest that the lath width, although influencing strength, is believed generally to have little influence on impact behaviour. This is because the fracture path is not affected significantly by the small change in orientation on crossing a lath boundary, whereas a large amount of energy is required to cross the high angle boundaries associated with the colony or austenite grain boundaries[37]. The facet size in the present work is always less than the γ grain size, indicating that the high angle boundaries were also having some effect in resisting cleavage fracture. The facet size controls the distance between obstacles for crack propagation, i.e. the more high angle boundaries the better the impact behaviour[37].

Another factor influencing the impact behaviour is the hardness[37] which will be related to the dislocation density, carbide distribution (possibly lath width), and the amount of polygonal ferrite in the structure. It has been shown[65] that the lower the transformation temperature at which the upper bainite forms, the higher the dislocation density. Generally increasing the

171

hardness will cause a deterioration in impact behaviour[37].

Mintz et al[37] also suggest that, the carbide distribution is another factor which may influence fracture by the ease of nucleation of cracks and their subsequent propagation. However Pickering[65] has observed that the carbides at the ferrite lath boundaries in upper bainitic structures do not exert much influence on crack propagation, whereas a more dispersed finer form breaks up the fracture path. In the present exercise it was noticeable that increasing the γ grain size also increased hardness, Fig 5.32. This would be expected since increasing the grain size lowers the transformation temperature at which bainite forms giving higher dislocation densities. As a consequence of this, the impact energy also decreased with an increase in hardness, Fig 5.33.

5.4.1 Influence of Cooling Rate on Hardenability and Fracture

It can be seen from Fig 5.34 and Table 5.3 that ice/water quenching results in higher hardness and lower impact values after oil quenching from the same austenitising temperature of 900°C.

Previous work[37] suggests that the increase in hardness on ice/water quenching arises because increasing the cooling rate will lower the transformation temperature favouring the more bainitic structure rather than the polygonal ferrite structures obtained on oil quenching.

Increasing cooling rate has little influence on the effective γ grain size which controls fracture, i.e. facet size, but was observed to produce shorter carbides at the interlath boundaries and a finer interlath spacing with more carbides within the laths and/or bainitic ferrite subgrains[37]. Oil quenching tended to produce long continuous plates of carbides at the interlath bound-

172

aries, characteristic of upper bainite, whereas ice/water quenching produced much shorter carbides with less alignment, more characteristic of lower bainite Figs 5.10 and 5.17 respectively. The long carbides at the low angle interlath boundaries would be expected[37] to provide excellent paths for crack propagation as well as produce easy initiation of cleavage cracking. Therefore, it would appear that the detrimental effect on impact behaviour on having a higher hardness on ice/water quenching is balanced by the improved carbide distribution produced at the faster quench rate.

Mintz et al[37] derived a regression equation for the quenched and tempered flanges as follow:

$$\text{Impact energy, J at -46°C} = 82 + 18.6d^{-1/2} - 0.8\,H + 0.05\,CR$$

$$(5.1)$$

where d is austenite grain size in millimeters, H is hardness HV_{10} and CR is cooling rate in $kmin^{-1}$. The correlation coefficient R for this equation is 0.9 and the 95% confidence limit $+ 32\,J^{[37]}$.

However, it should be noted that this equation only applies to a very narrow compositional range of the ASTM 350 LF2 specification. Calculated impact energy values at -46°C using the above equation, are not in agreement with the experimental results obtained in the present exercise, Table 5.5, for the more normal austenitising temperature range of 900 to 950°C. Predicted values were much higher than the observed impact values.

It is important to note that the equation 5.1 was derived for steel with lower carbon content and higher Mn level and a much lower sulphur content (Tables 4.2 and 5.1). For ferrite/pearlite steels the marked effect of S (MnS inclusions) in reducing the shelf energy was shown by Bucher et al[44]. Examination of the sulphide distribution in this steel indicated that not only

173

was the volume fraction higher than for the steel in chapter 4 but stringers of sulphide and silicates were present Fig 5.35. In chapter 4, the shelf energies for the tempered at 600°C conditions were 170J, for the lower S steel. In the previous exercise[43] for the higher S steel the shelf energy was 120 J. As in chapter 4 it is possible to make some allowance for the effect of the lower shelf energy on the impact energy criteria by proportionating along the curve.

The two sets of data are shown in Fig 5.36 for the low and high S steels both for oil quenched and ice-water quenched conditions. Adjusting for the differences in shelf energy as in chapter 4, and normalising the data of the higher S steel, it can be seen that agreement is now reasonably close. Thus the fall in shelf energy due to a higher volume fraction of sulphides could well account for the overall increase in impact transition temperatures.

5.4.2   Tempering at 300 and 600 °C

Most of the discussion so far has concentrated on the as quenched steels and the effect of γ grain size on the mechanical properties. Previous work[70] on quenched and tempered steels indicates that the impact properties should improve by increasing the tempering temperature at the expense of hardness and strength. However, it is not possible to confirm whether the improvement is purely due to the fall in strength and hardness or due to changes in microstructure.

In the present exercise, four different types of structures were obtained on quenching. To simplify, the effect of tempering, each microstructure is discussed seperately.

5.4.3   Steels Quenched in Oil from 900°C

Quenching in oil resulted in the formation of 55% ferrite and 45% of second phase consisting of mainly pearlite and small amount of bainite and martensite.

As yield points were observed in the stress/strain curves for the oil quenched from 900°C condition, the ferrite is the dominant phase in controlling the properties. However, previous work[25] on ferrite/pearlite steels indicates that the mechanical properties of these structures can be influenced by an increase in the amount of the second phase present i.e pearlite.

Austenite and ferrite grain size which are said to be the factors controlling the properties remained unchanged during tempering process.

5.4.3.1   Infuence of tempering on LYS

For ferrite/pearlite steels, Cochrane[33] suggested that as pearlite increases the yield strength of steels, then tempering because it spheroidises the carbides may be responsible for this fall.

The work of Cochrane on ferrite/pearlite steels and the work in previous exercise (chapter 4) also suggests that there is a good relationship between the interparticle spacing in the pearlite (which is related to the degree of spheroidisation) and the fall in yield strength after tempering.

However, no such relationship appears to be followed for the early stages of tempering in the present work. Little change in microstructure is noticeable after 1 hour at 300 °C Fig 5.11 yet a yield strength drop of 51 Nmm^{-2} has occurred, table 5.2.

Certainly there is a marked change in structure on tempering for 1 hour at 600 °C Fig 5.12, and this corresponds to a further fall in yield strength of 46

N mm^{-2}. As stated in the previous exercise (chapter 4), the high dislocation densities obtained during oil quenching are due to the lowering of the transformation temperature. These high dislocation densities are not observed in normalised steels in which the ferrite/pearlite structures are obtained. The fall in LYS and UTS can therefore be in part related to a reduction in dislocation density after tempering at 300 °C. The further fall in the yield strength on raising the tempering temperature to 600°C could be related to the further reduction in dislocation densities and partial spheroidisation of carbides and possibly a reduction of carbon in solution at the grain boundaries which reduces the k_y value[43].

5.4.3.2   Influence of tempering on impact behaviour

Equations, established by Mintz[43] on ferrite/pearlite steels, relating structure to the ITT, have been used in the present exercise to calculate the impact transition temperatures at 54 J and 27 J.

The constants in these equations have been shown by Mintz[43] to be related to the upper shelf energy. The original equations were based on steels which had shelf energy of 120 J. The present steel shows a shelf energy in the same range of 130 J. The calculated and observed values shown in Table 5.7 are in reasonable agreement.

As in previous work on ferrite/pearlite steels, it would appear that the thickness of the grain boundary carbides together with the fall in strength on tempering are important parameters in determining the impact properties, Fig 5.37.

Comparing the impact transition curve for the as quenched and tempered at 600 °C in this exercise with oil quenched and tempered at 600°C steel in the

previous chapter (4) Fig 5.38 it can be seen that there is a marked difference in the impact transition curves for these two steels. The γ grain size which is generally believed to be the most important parameter controlling the impact behaviour, however, only differs by 1 μm.

The increased level of the volume fraction of second phase (degenerate pearlite), probably due to the higher carbon content, in the present work, could be one factor accounting for the deterioration of the impact behaviour of this steel. The effect of carbon content on the impact properties, is summarized in the literature Fig 2.28, which shows that the lower carbon steels have somewhat better impact properties. However, here the difference in carbon content is not very great and certainly not sufficient to justify the large difference in the impact behaviour of these two steels.

As already observed the difference is most likely due to the higher volume fraction of MnS inclusions and the presence of coarse stringers of silicates and sulphides as noted in Fig 5.35.

5.4.4 Steels Quenched in Ice-Water from 900 ^{0}C

The steel microstructure obtained on quenching from 900 ^{0}C, was untempered bainite with 37% ferrite. The tensile strength of these structures was in order of 794 Mn/mm^2, and a very poor impact energy of about 16 J at -46°C was obtained. The strength level and hardness combined with the poor impact properties, suggest that bainite is the dominant phase in controlling the properties.

The factors affecting the impact properties of low carbon bainitic steels have been investigated[70]. It has been shown[70] that the structure and strength of a bainitic steel have a pronounced effect on the impact prop-

177

erties.

The individual effects of the major strengthening mechanisms and their effect on impact behaviour was described in the literature and chapter 4. However here in this section the effect of lowering the tempering temperature from 600°C to 300°C on the tensile strength and impact behaviour and how this influences the microstructural changes are investigated.

As mentioned previously[62], the major strengthening mechanisms are due to grain size, dislocations, carbide dispersion and solid solution hardening.

In this work a shift of about 10 °C to the left of the transition curve Fig 5.13, and a fall in both yield and hardness on tempering the ice-water quenched structure at 300°C, may well be accounted for by a small change in dislocation density. There are, however, still a large number of dislocations present after tempering at 300°C, Fig 5.39.

The break up and coarsening of the carbides at the interlath boundaries is associated with an increase in the interparticle spacing and combined with the removal of dislocations may account for the fall in strength on tempering at 600°C.

According to Materkowski and Krauss[112], the same microstructural changes which improve the toughness, however also decrease the hardness and strength. It has also been shown[70] that, the effect of tempering on the transition temperature of bainitic structures is generally to decrease T, due to a decrease in both σ_p and σ_d. This is in accordance with previous work[34] and observation in this exercise, which shows the impact behaviour improves with a fall in the tensile strength and hardness, Fig 5.40.

Irvine and Pickering[70] found that the tensile and impact strength of bainites depend mainly on the bainitic grain size. According to these authors,

the width of the ferrite plates decreased with bainite formation temperature but their length was always determined by the dimensions of the prior austenite grain. In addition, the carbides precipitated mainly between the ferrite plates of the bainite. Both factors account for the brittleness observed in the intermediate bainites. Finally, for very low formation temperatures, carbides precipitated inside the ferrite plates because the carbon diffusion was very much restricted. As a result the carbides were very finely dispersed in the ferrite so the strength increased without a prohibitive sacrifice of ductility. Indeed, the carbides and dislocations tangles at the grain boundaries presented so many obstacles obliging the cleavage cracks to deviate from one cleavage point to another.

Again comparing the impact transition curve for the as ice-water quenched and tempered at 600 °C condition in this exercise with the steel ice-water quenched and tempered at 600 °C in chapter 4, Fig 5.41, the shift to the right of the impact transition curve could be related to the higher volume fraction of silicates and sulphides present in this exercise.

5.4.5   Steels Quenched in Ice-Water from 1250^0C

Rapid quenching of austenite from 1250 °C in ice-water resulted in the formation of fully martensitic structure. The martensite reaction is readily recognized by its appearance in the optical microscope. Each grain of austenite transforms by the sudden formation of thin plates or laths of martensite of striking crystallographic character.

Essentially, martensite is a highly supersaturated solid solution of carbon in iron which, during tempering, rejects carbon in the form of finely divided carbide phases. The end result of tempering is a fine dispersion of carbides in

179

an α iron matrix which often bear little structural similarity to the original as quenched martensite[113].

According to Krauss[55], at low tempering temperatures the lath and plate boundaries and the morphologies of the as quenched martensite crystals remain unchanged. However, at the higher tempering stage the martensite boundary structure coarsens and eventually approaches an equiaxed grain morphology. Early in this process all supersaturation of carbon quenched into the martensite has been relieved by cementite formation and the matrix phase is b.c.c ferrite. Nevertheless the b.c.c matrix, because of its origin from martensite, is referred to as tempered martensite[55].

Figs 5.42 and 5.43 show the dispersion of carbides through out the martensite laths when tempered at 300°C. The coarsening of the cementite particles is apparent.

Caron and Krauss suggest[113], that the coarsening of the matrix structure is a result of recovery mechanisms which cause the elimination of low-angle interlath boundaries and a reduction of the high dislocation density of as quenched lath martensites. They also suggest[113] that the high angle boundaries within lath martensite packets remain, and eventually readjust themselves into equiaxed arrays as the pinning effect of the fine carbide dispersion is reduced by the coarsening of the carbides.

Here, tempering, causes an increase in interparticle spacing and the cementite particles undergo a coarsening process and essentially lose their crystallographic morphology, becoming partially spheroidized. The coarsening commences at 300°C, while spheroidization takes place increasingly up to 600 °C. The spheroidization of the carbides (Fe_3c) rods is encouraged by the resulting decrease in surface energy. The particles which preferentially

180

grow and spheroidize are located mainly at the interlath boundaries and prior austenite boundaries, although some rod shaped particles remain in the matrix.

According to Krauss[55] there is considerable rearrangement of the dislocations within the laths and at those lath boundaries which are essentially low angle boundaries at higher tempering temperature. Rearrangement of the dislocations may be influenced by an increase in interparticle spacing and coarsening of the carbides. This leads to a marked reduction in the dislocation density which reduces the hardness and strength and causes an improvement in the impact properties. Fig 5.44 shows how an increase in impact energy is accompanied by a fall in strength on tempering.

5.4.6   Steels Quenched in Oil from 1250^0C

Quenching austenite from 1250^0C in oil resulted in the formation of structures consisting of a mixture of martensite/bainite 85% and ferrite 15%, with ferrite forming at the grain boundaries.

The various instabilities in the martensitic microstructure provide the thermodynamic driving forces for phase transformations and microstructural changes. Thus when quenched steels are heated, in a tempering treatment martensitic microstructures are converted to new microstructures with different mechanical properties.

The most important function of tempering is to improve the toughness or fracture resistanse of quenched steels. All of the microstructural changes produced during tempering are dependent on diffusion. Therefore, at low tempering temperature, where diffusion is limited, the microstructural changes occur on a very fine scale and strength level reached depend also on the

detailed structure of the martensite.

In addition to the changes in carbide type, morphology and dispersion which develop throughout tempering at 600 °C profound changes in the microstructure of the matrix martensite also develop. Throughout tempering at low temperature, the lath and plate boundaries and the morphology of the as quenched martensite remain unchanged. However, at higer tempering temperature the martensite boundary structure coarsens and eventually approaches an equiaxed grain morphology.

On tempering from 300 to 600 °C both strength and hardness decreased in accordance with SEM observations showing coarsening of carbides and an increase in interparticle spacing, with increase in tempering temperature Fig 5.25 and 5.26.

It is difficult to comment on mechanical properties related to the microstructral changes obtained during tempering of the oil quenched samples. It can be argued that because of the higher transformation temperature due to slower cooling rate (as compared with ice-water quenched), auto-tempering may take place during quench. Inother words, by self tempering, a cementite dispersion during the quench takes place which reduces the effect of further tempering on the strength. However, improvement in the impact properties at 600°C could be related to the coarsening of carbides and the fall in strength at that temperature, Fig 5.45.

5.5   Conclusions

- 1) Oil quenching from 900 °C resulted in ferrite/pearlite structures.

- 2) Oil quenching from 1250 °C resulted in structures consisting of 85%

martensite and 15% ferrite.

- 3) Ice-water quenching from 900 $^\circ$C resulted in ferrite/upper bainite structures.

- 4) Ice-water quenching from 1250 $^\circ$C resulted in fully martensitic structures.

- 5) Quenching from austenitizing temperature of 1250 $^\circ$C produced a very coarse γ grain size whereas quenching from 900 $^\circ$C produced finer grains.

- 6) Flanges with coarser austenite grain size showed worse impact behaviour compared with flanges with finer grain size.

- 7) Tempering at 600 $^\circ$C improved the impact behaviour of all quenched flanges significantly, and reduced strength and hardness, but tempering at 300 $^\circ$C did not influence the impact properties of the flanges significantly, eventhough a fall in strength and hardness was observed.

- 8) SEM observation provides evidence of fine carbide precipitation due to tempering at 300 $^\circ$C and an increase in carbides size and particle spacing with increase in tempering temperature to 600 $^\circ$C. Lines of long carbides start to break and partially spheroidise which could be the reason for the fall in strength.

- 9) Overall the ice-water quenching from 900 $^\circ$C, showed the best combination of strength and impact behaviour after tempering at 600 $^\circ$C. However, oil quenching from 900 $^\circ$C without any tempering produced adequate enough properties to meet the ASTM A350 LF2 specification comfortably.

183

- 10) An improvement in impact behaviour seems to be associated with a fall in strength in all conditions, Fig 5.46.

C	Mn	Si	P	S	Cr	Mo	Ni	Al	Cu	N
0.24	0.82	0.24	0.015	0.02	0.08	0.016	0.08	0.039	0.18	0.0072

TABLE 5.1 THE COMPOSITION OF STEEL %Wt

Austenitizing Temp/^{0}C For 1 hour	Quench Media	Tempering Temp/^{0}C For 1 hour	0.2% proof stress MN/mm^2	LYS MN/mm^2	UTS MN/mm^2	EL %	RA %
900	IQ	—	794	—	794	45	55
900	IQ	300	754	—	754	42	45
900	IQ	600	—	408	597	45	62
900	OQ	—	—	484	637	40	40
900	OQ	300	—	433	594	65	60
900	OQ	600	—	388	566	45	62
1250	IQ	300	1021	—	1021	15	5
1250	IQ	600	—	791	739	42	55
1250	OQ	300	680	—	680	52	50
1250	OQ	600	—	489	663	60	50

TABLE 5.2 TENSILE TEST RESULTS

Austenitizing Temp/^{0}C For one hour	Quench Media	Tempering Temp/$^{\circ}$C For one hour	Hardness HV_{10}
900	IQ	—	244
900	IQ	300	222
900	IQ	600	207
900	OQ	—	209
900	OQ	300	195
900	OQ	600	180
1250	IQ	300	358
1250	IQ	600	255
1250	OQ	300	251
1250	OQ	600	217

TABLE 5.3 HARDNESS TEST RESULTS

Austenitizing Temp/°C For one hour	Quench Media	Tempering Temp/°C For one hour	F Grain size μm	%F	%M	%p	%B	γ Grain size μm
900	IQ	—	4.5	37	—	—	63	25
900	IQ	300	4.5	37	—	—	63	25
900	IQ	600	5.0	38	—	—	62	25
900	OQ	—	6.5	55	—	45	—	25
900	OQ	300	6.5	56	—	44	—	25
900	OQ	600	6.5	56	—	44	—	25
1250	IQ	300	—	2	98	—	—	209
1250	IQ	600	—	2	98	—	—	209
1250	OQ	300	—	15	85	—	—	209
1250	OQ	600	—	15	85	—	—	209

TABLE 5.4 MICROSTRUCTURAL MEASUREMENTS

*F = Ferrite

P = Pearlite

B = Bainite

M = Martensite

IQ = Ice-Water Quench

OQ = Oil Quench

Austenitizing Temp /°C For one hour	Quench Media	Tempering Temp /°C For one hour	Impact energy At -46°C PRED OB	
900	IQ	—	64	16
900	IQ	300	82	17
900	IQ	600	92	41
900	OQ	—	62	30
900	OQ	300	73	28
900	OQ	600	85	40
1250	IQ	300	0	9
1250	IQ	600	0	28
1250	OQ	300	0	16
1250	OQ	600	0	28

TABLE 5.5 OBSERVED AND PREDICTED IMPACT ENERGY VALUES

$$\text{IMPACT ENERGY AT -46}^\circ\text{C} = 82 + 18.6 \ d^{-1/2} - 0.8 \ H + .05 \ CR$$

Quench Temp °C	Quench Media	Tempering Temp °C	GBt μm
900	OQ	—	0.24
900	OQ	300	0.25
900	OQ	600	0.3

Fig 5.6 Grain boundary carbide thickness measurements

Quench Temp °C	Quench Media	Tempering Temp °C	54 J ITT PRED OB °C	27 J ITT PRED OB °C
900	OQ	—	-19 -18	-35 -50
900	OQ	300	-40 -18	-55 -60
900	OQ	600	-58 -40	-63 -80

Fig 5.7 Observed and calculated impact transition temperature at 54 and 27 J.

$$54 \text{ J} = 192 \ t_b^{1/2} - 10.1 \ d^{-1/2} + 0.5 \ \delta y - 23 \text{ [43]}$$

$$27 \text{ J} = 173 \ t_b^{1/2} - 8.3 \ d^{-1/2} + 0.37 \ \delta y - 42 \text{ [43]}$$

189
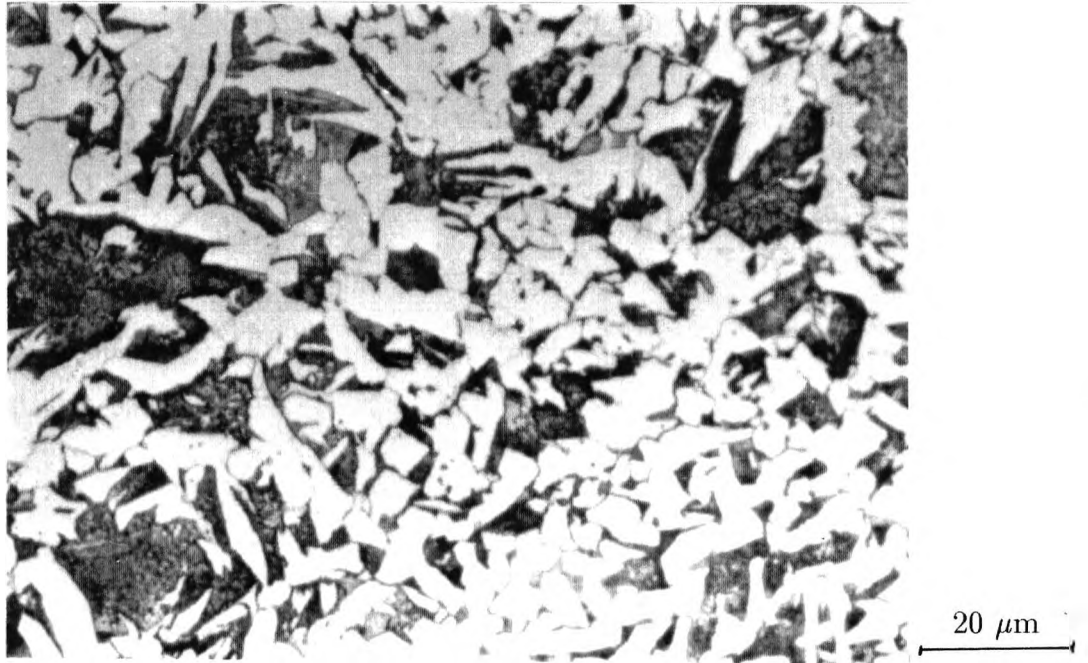
Figure 5.1: Microstructure of steel flanges oil quenched from 900^oC after holding for 1 hour. (optical)
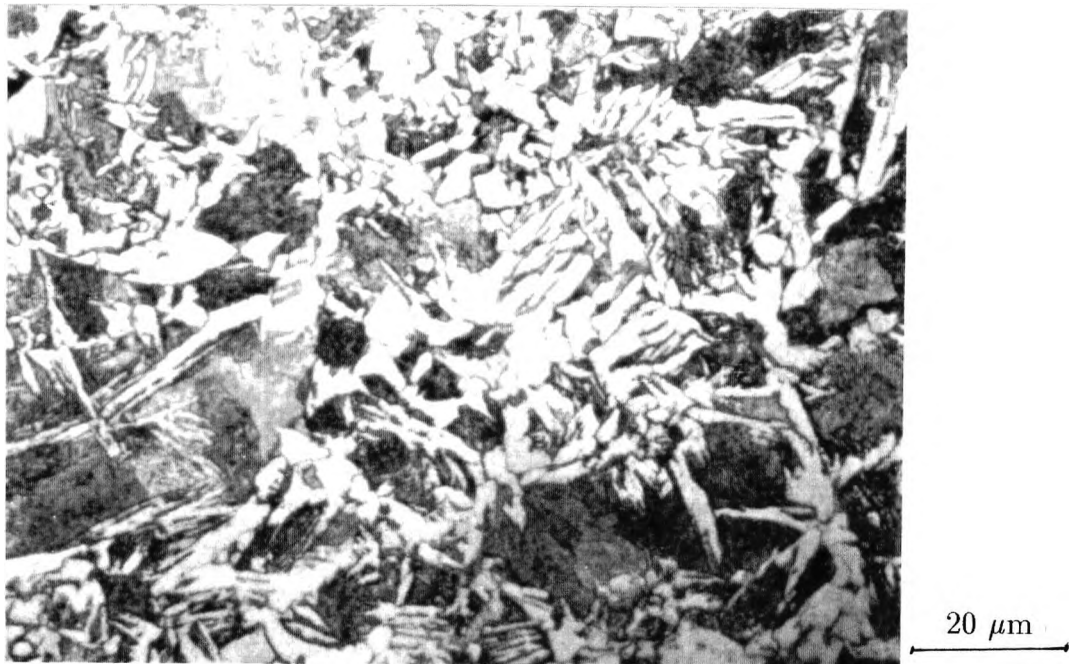
Figure 5.2: Microstructure of steel flanges ice-water quenched from 900^oC after holding for 1 hour. (optical)

190
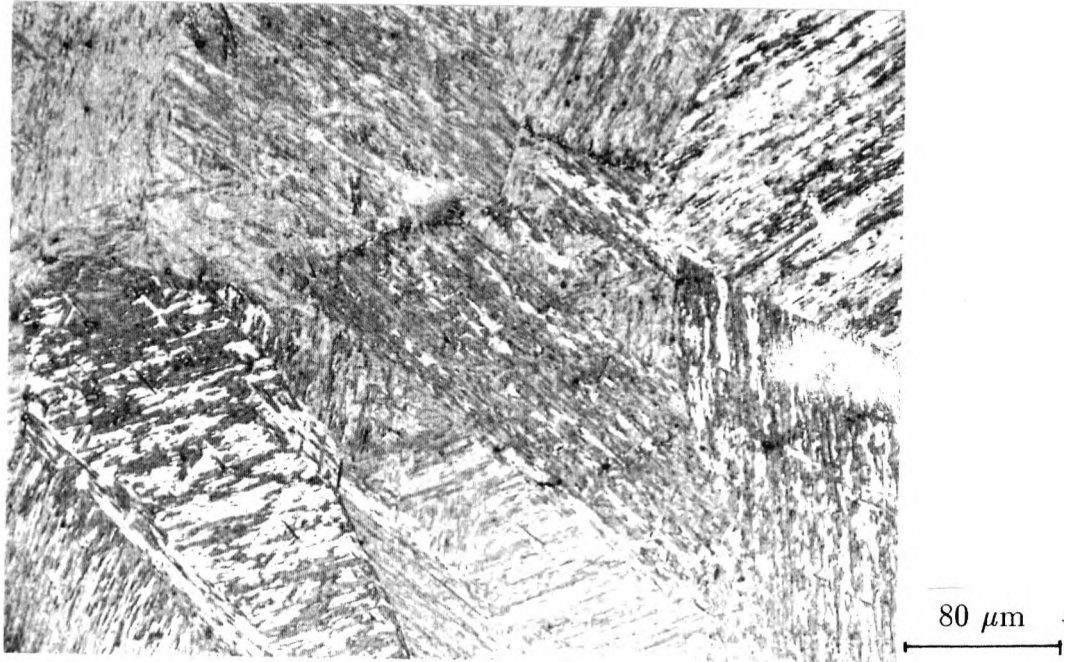
Figure 5.3: Microstructure of steel flanges ice-water quenched from 1250°C after holding for 1 hour. (optical)
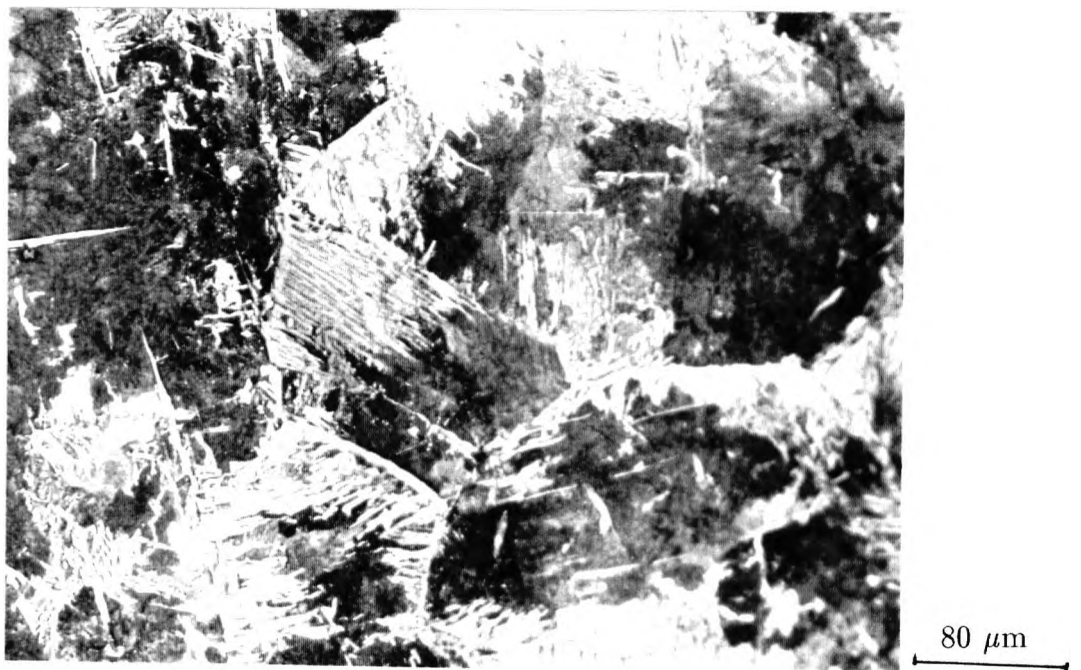
Figure 5.4: Microstructure of steel flanges oil quenched from 1250°C after holding for 1 hour. (optical)

TEMPERING
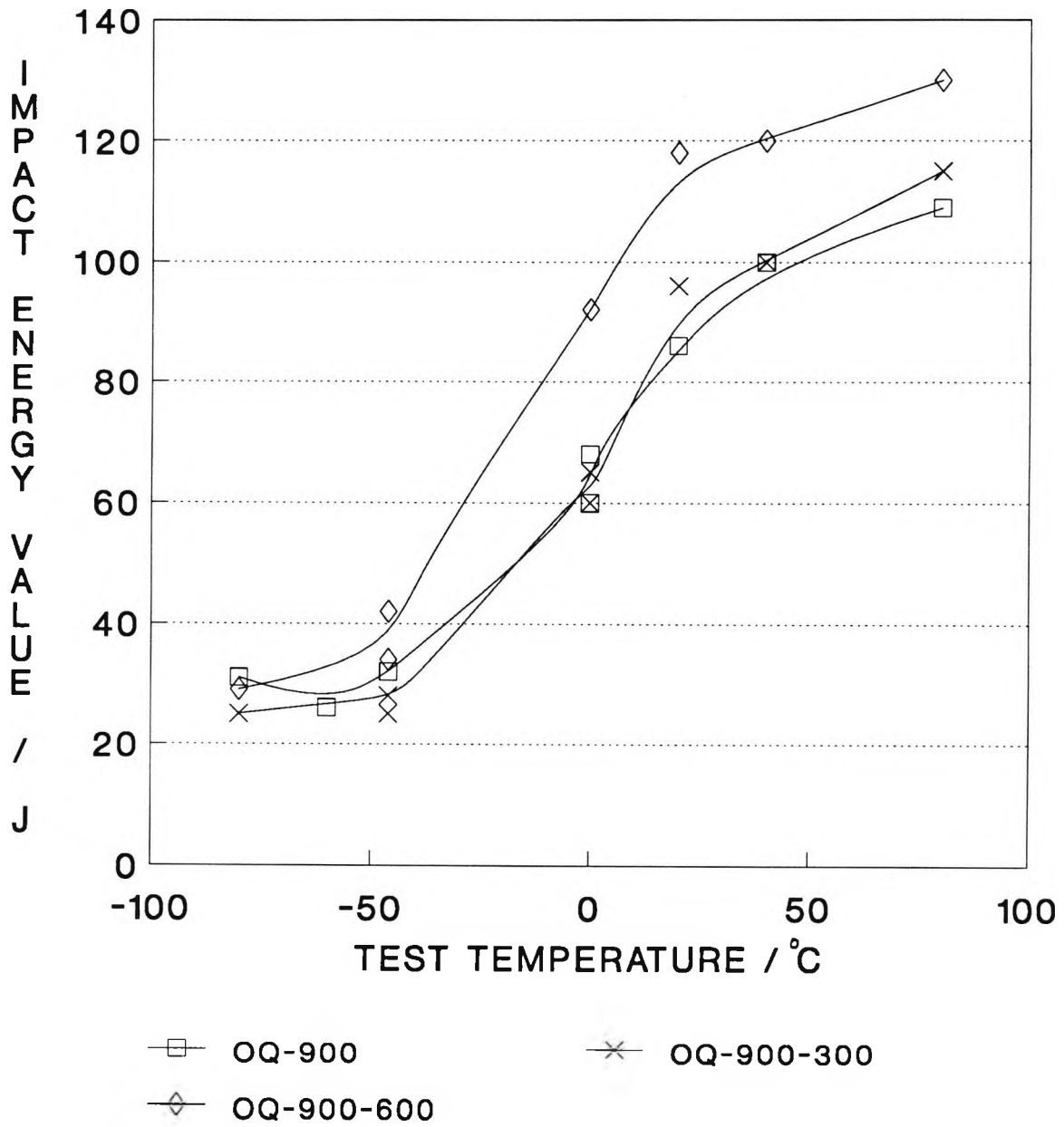
Fig 5.5 IMPACT TRANSITION CURVES FOR
OIL QUENCHED SAMPLES FROM 900 °C.
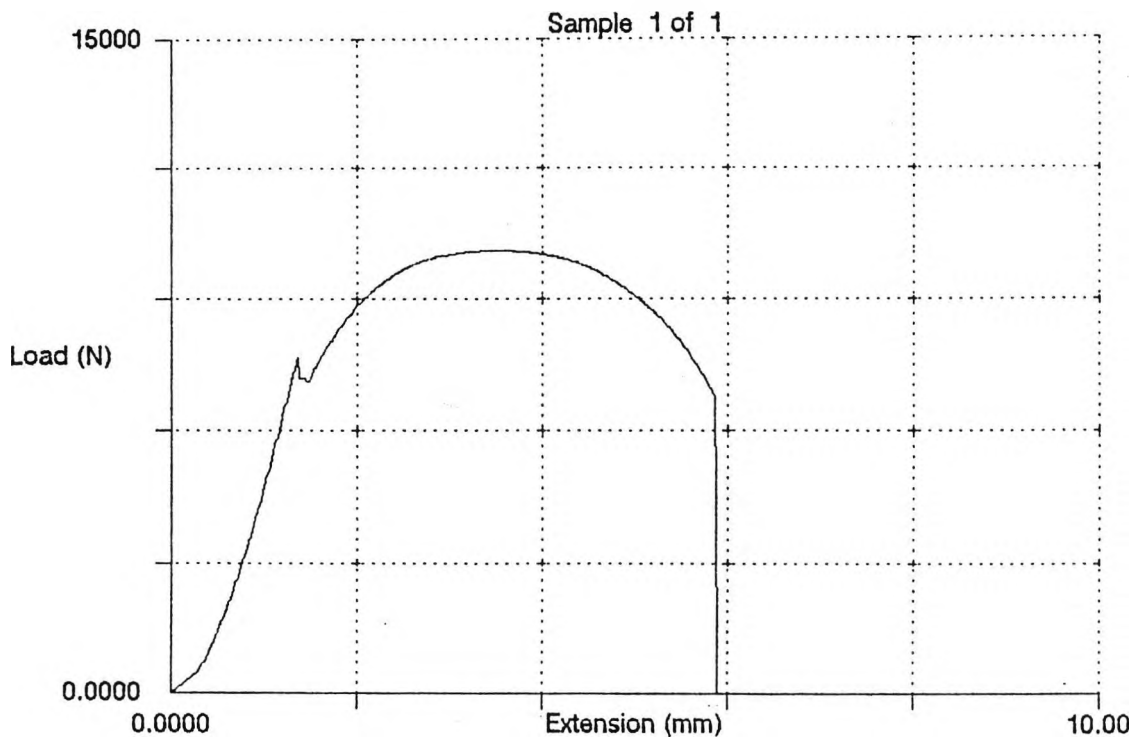
Figure 5.6: Stress/strain curve for the flanges oil quenched from 900°C.
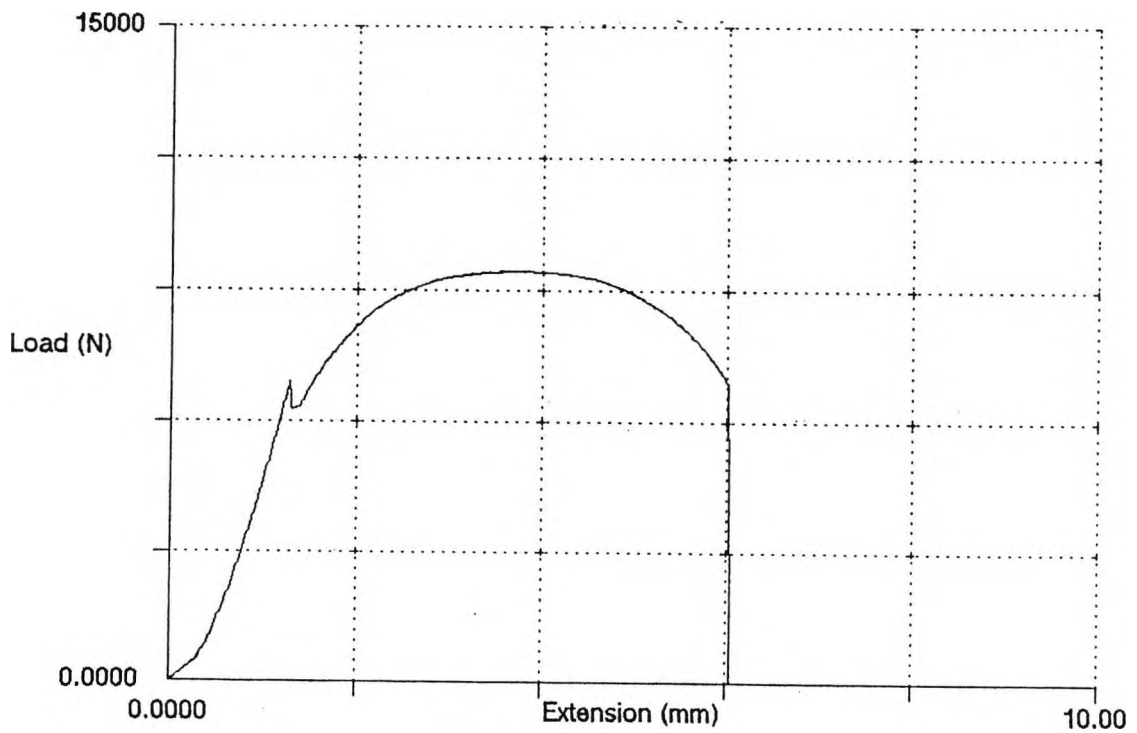
Figure 5.7: Stress/strain curve for the flange oil quenched and tempered at 300°C.

193
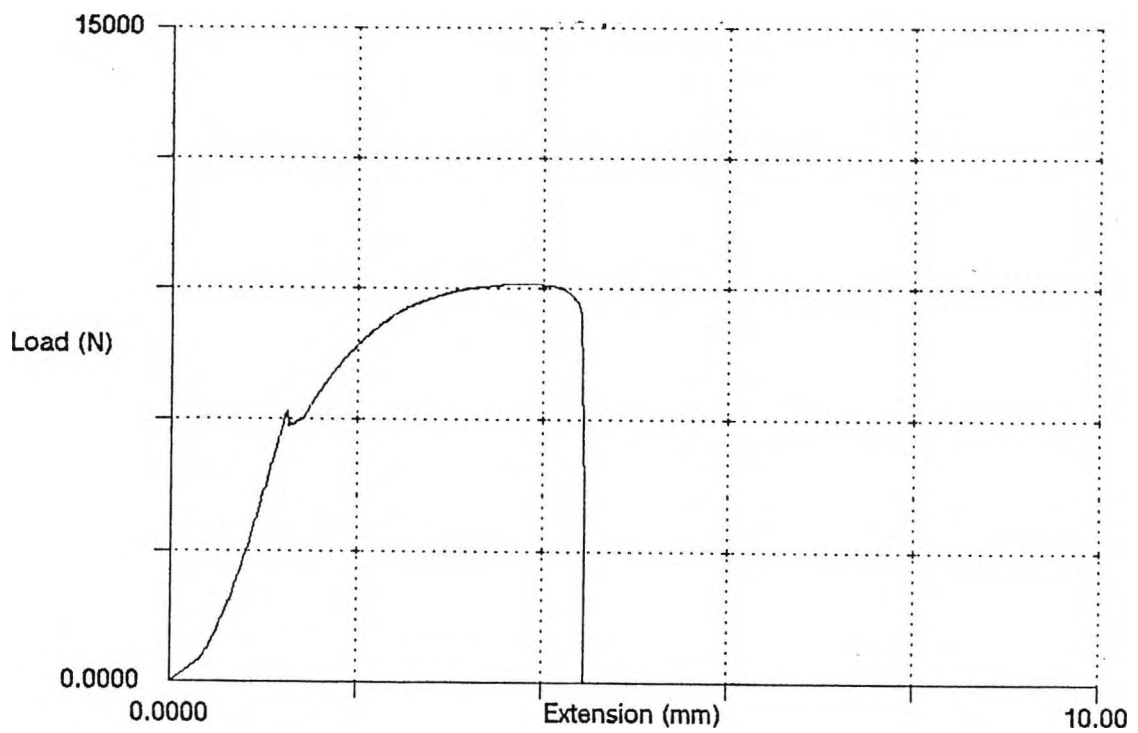
Figure 5.8: Stress/strain curve for the flange oil quenched and tempered at 600°C.

194
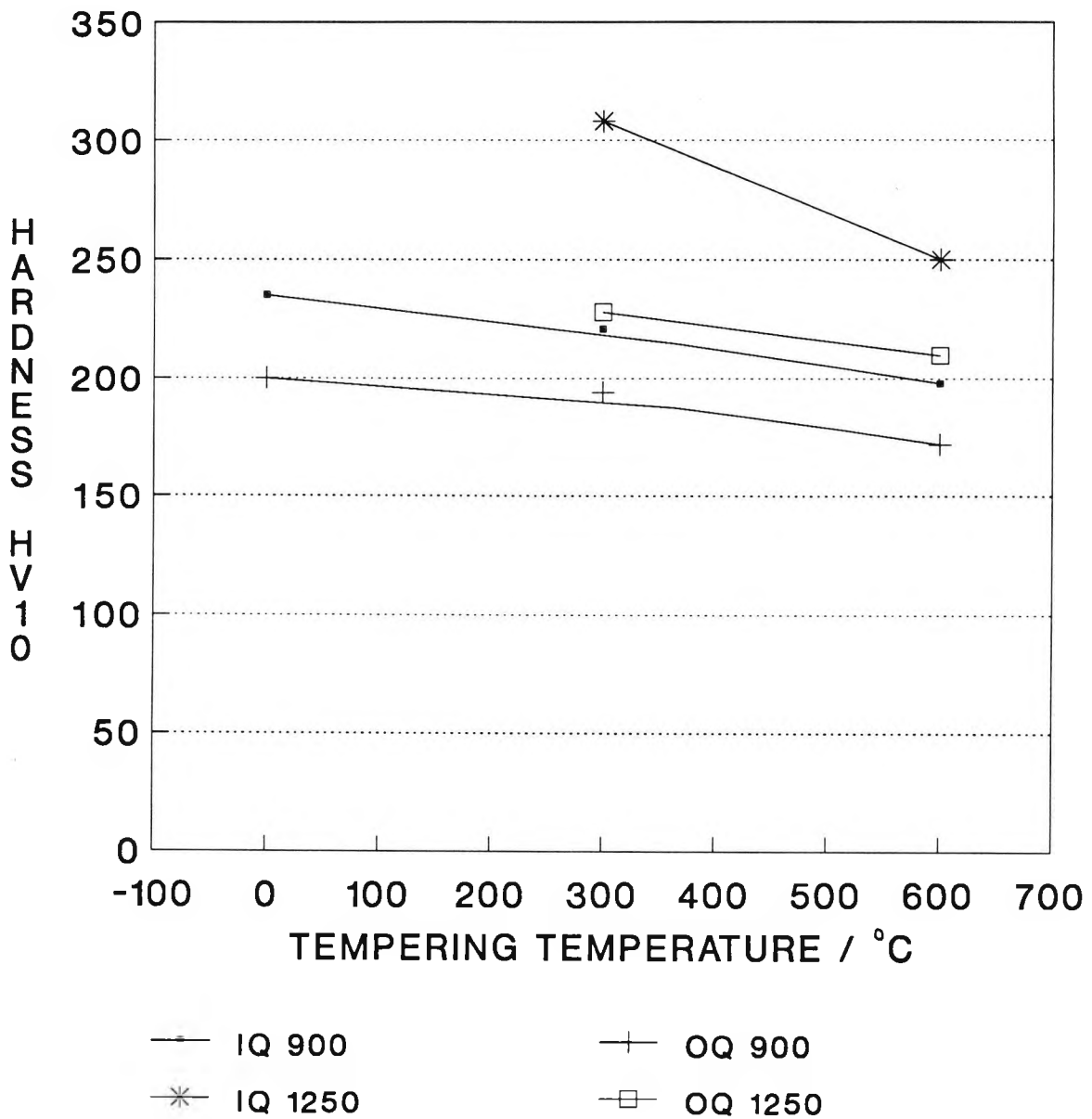
TEMPERING

Fig 5.9 Effect of tempering on hardness
for samples ice-water or oil quenched
from 900 and 1250 $^{\circ}$C. (0 ▪ As quenched)
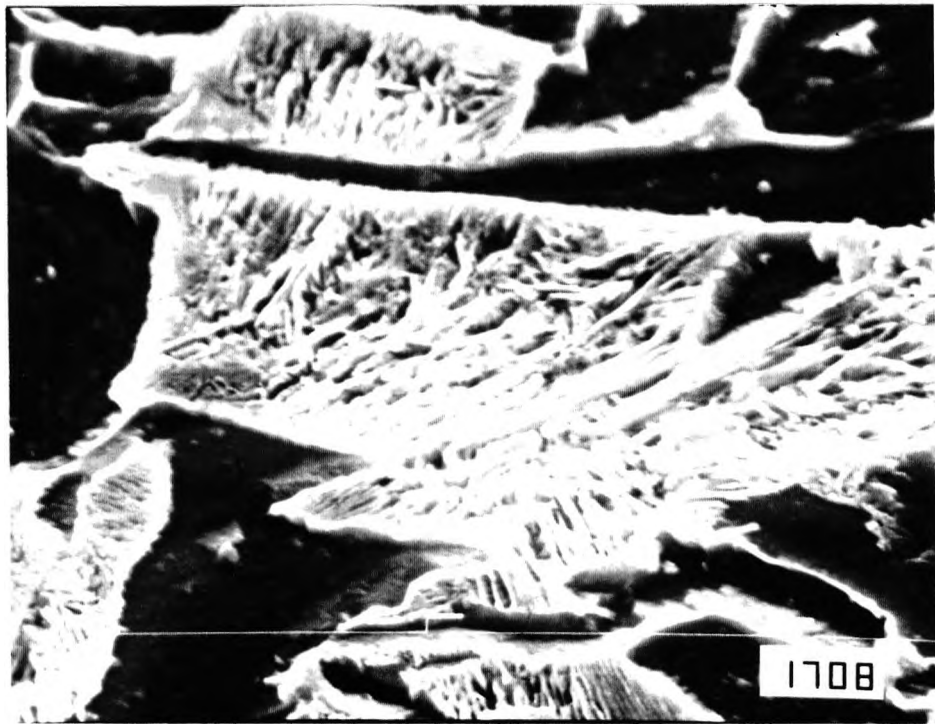
Ferrite/carbide structure
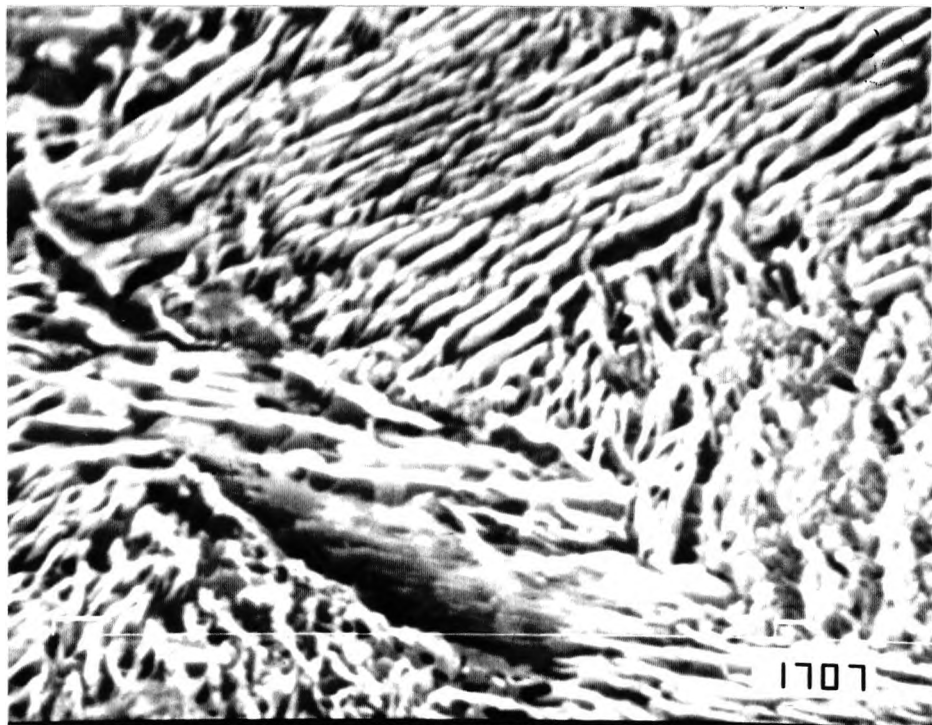
Enlarged view of carbide in second phase region

Figure 5.10: Microstructure of oil quenched flanges, as quenched condition. (SEM)

4.6 μm
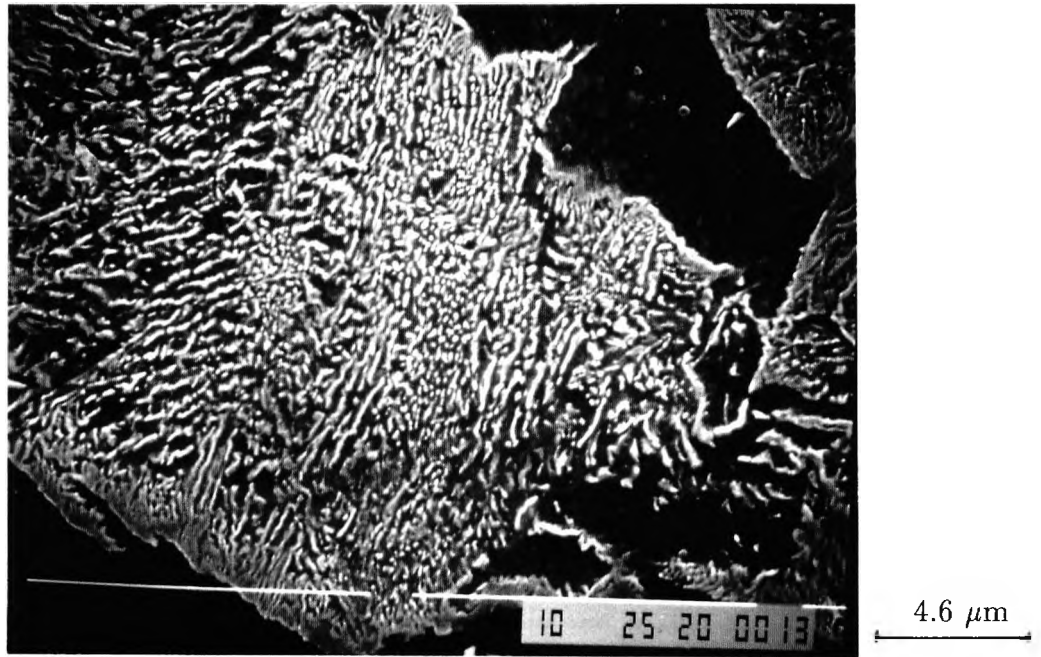
Figure 5.11: Microstructure of oil quenched flanges when tempered at 300°C. (SEM)

4.6 μm
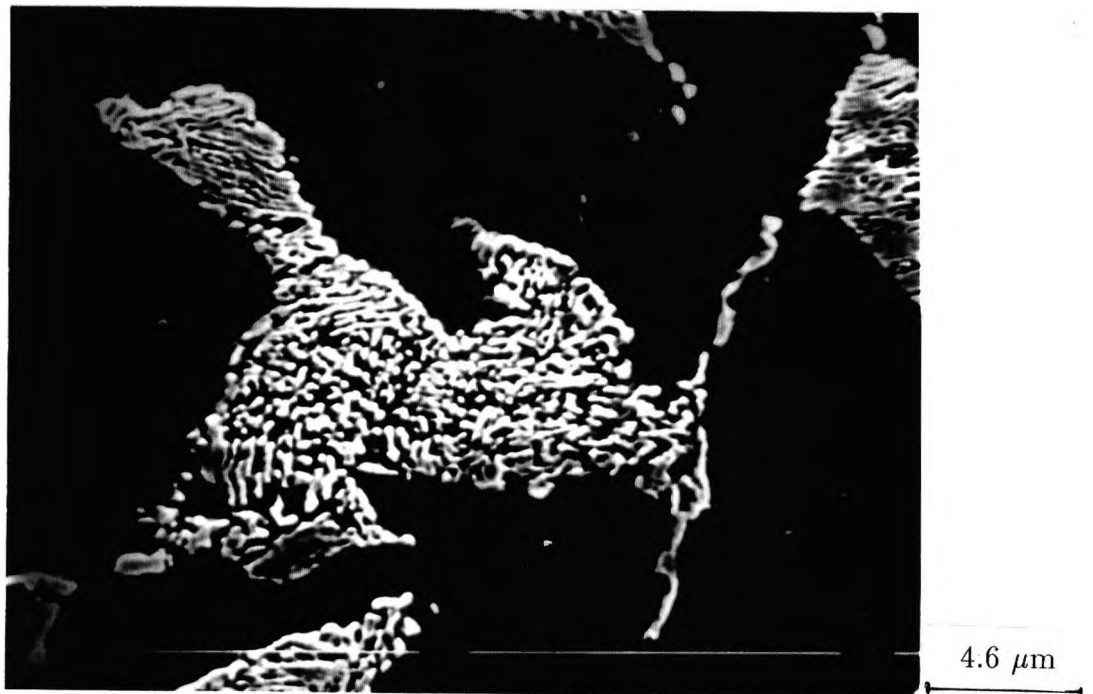
Figure 5.12: Microstructure of oil quenched flanges when tempered at 600°C. (SEM)

197

TEMPERING

Fig 5.13 Impact transition curves
for samples ice-water quenched
from 900 °C
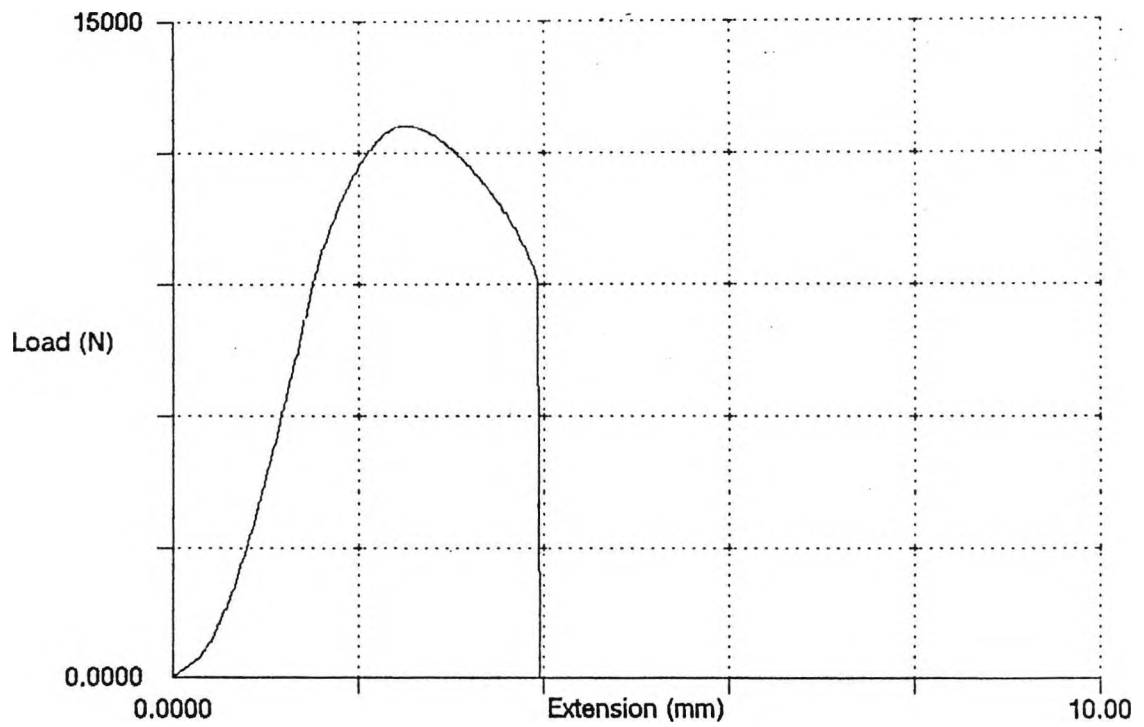
Figure 5.14: Stress/strain curve for the flanges ice-water quenched from 900°C after holding for 1 hour.
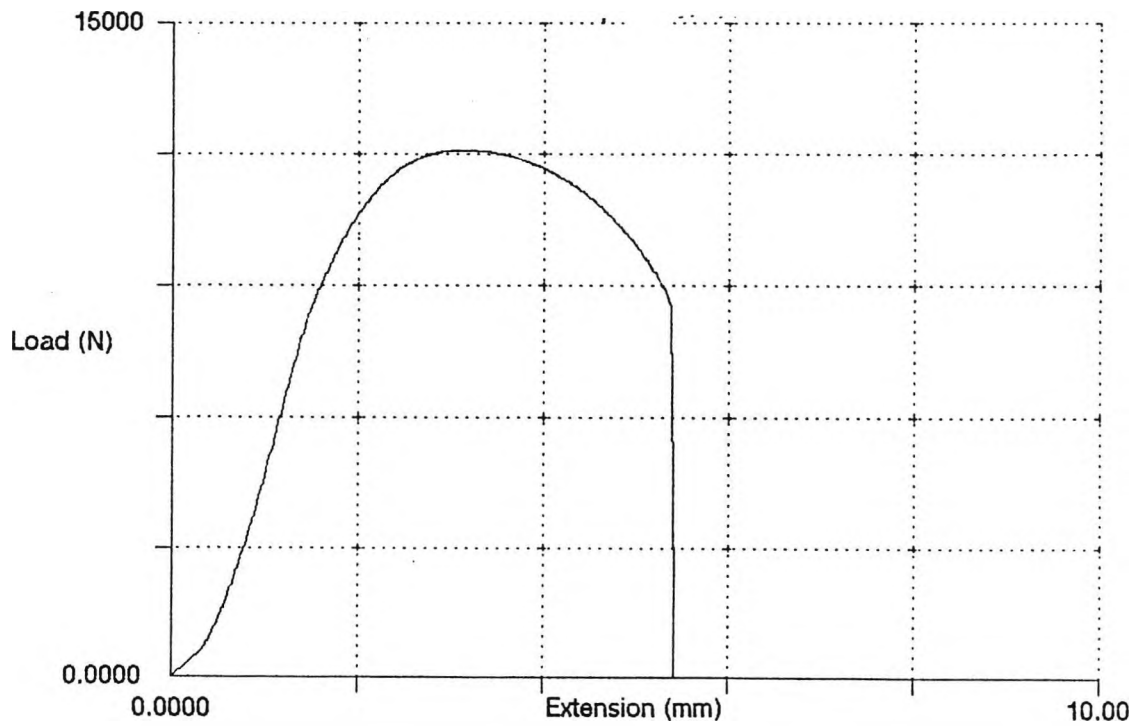
Figure 5.15: Stress/strain curve for the flange ice-water quenched and tempered at 300°C.

199
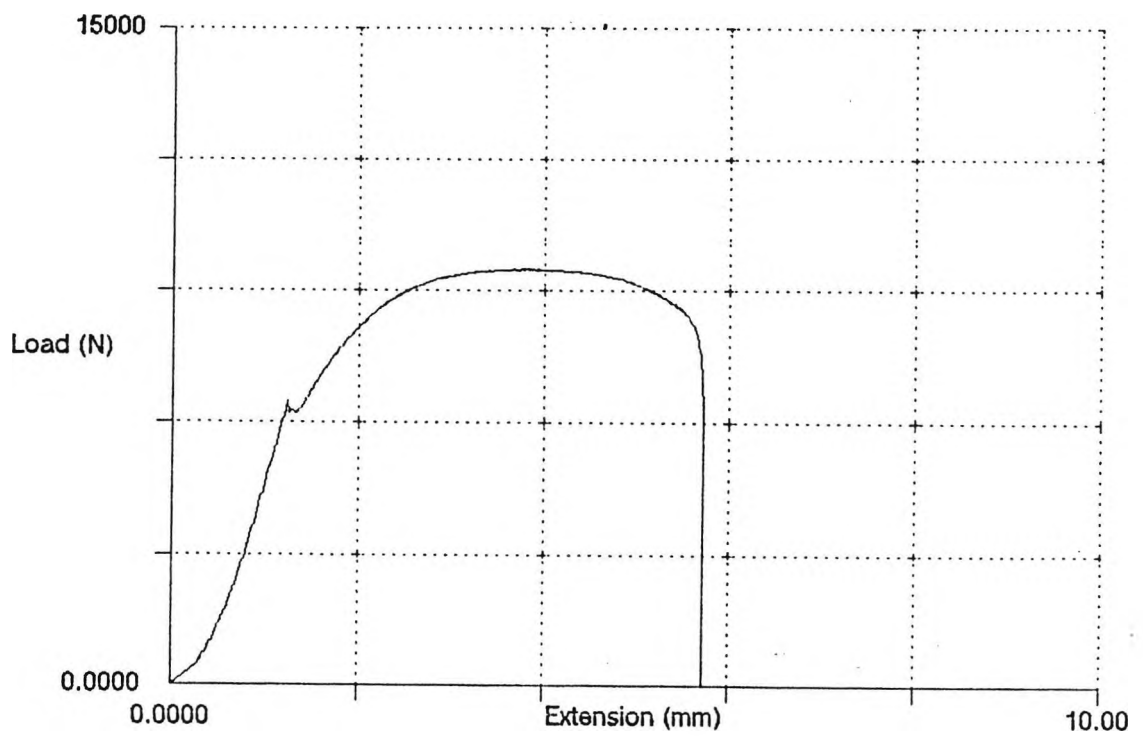
Figure 5.16: Stress/strain curve for the flange ice-water quenched and tempered at 600°C.
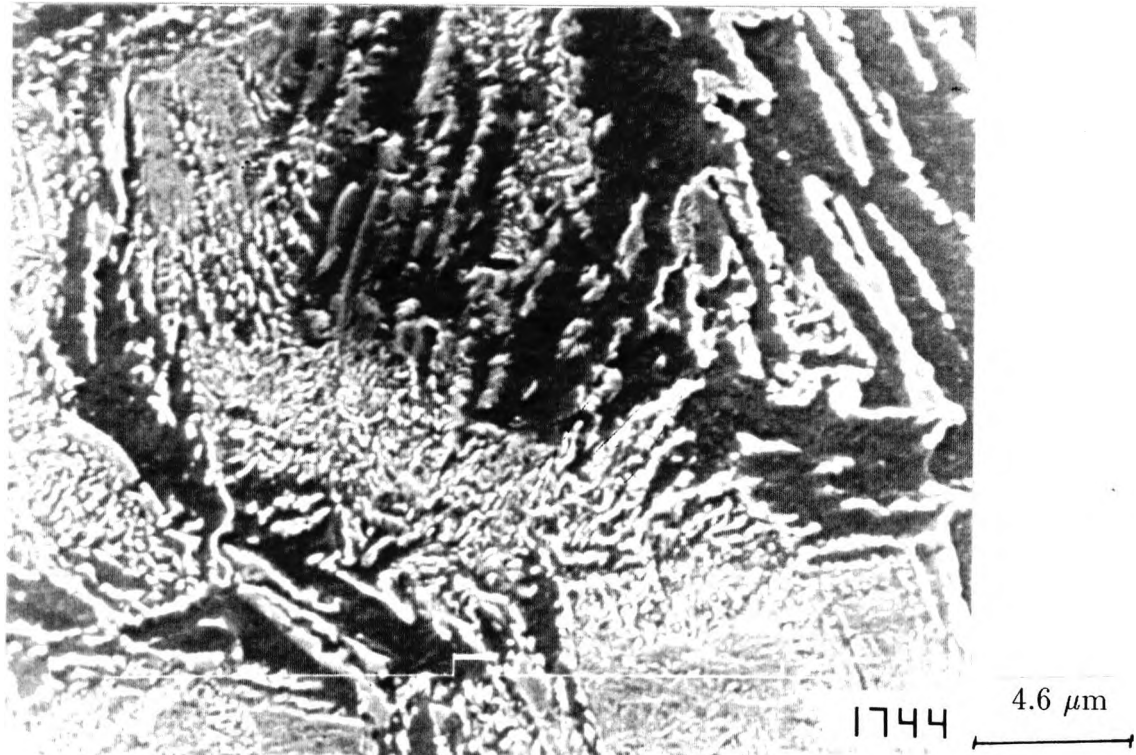
Figure 5.17: Microstructure of steel flanges ice-water quenched from 900°C after holding for 1 hour. (SEM)
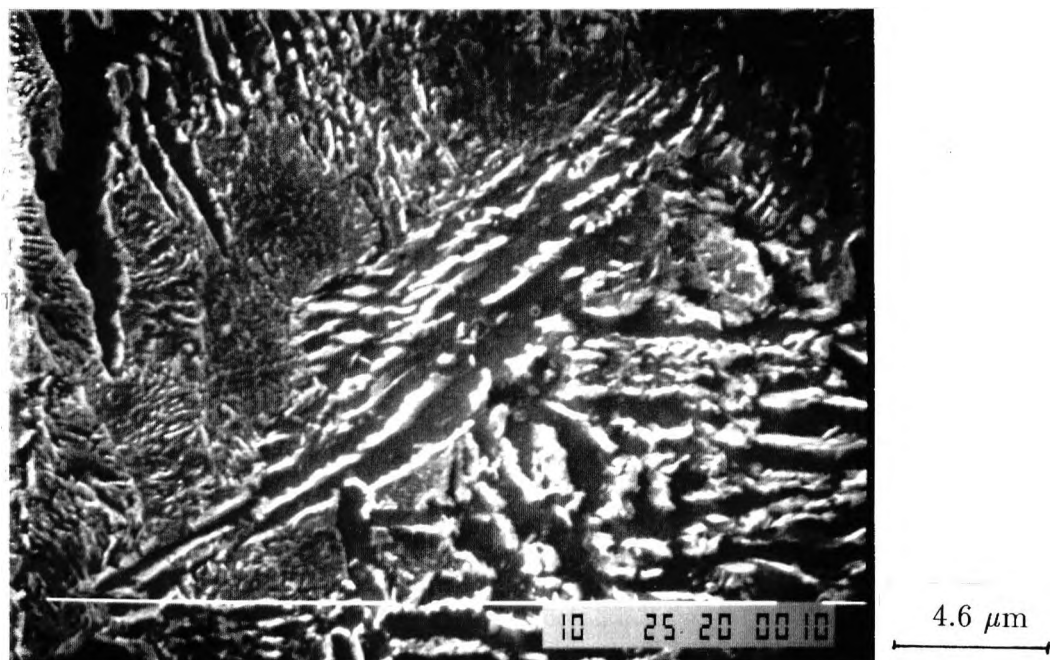
Figure 5.18: Microstructure of steel flanges ice-water quenched from 900°C and tempered at 300°C for 1 hour. (SEM)
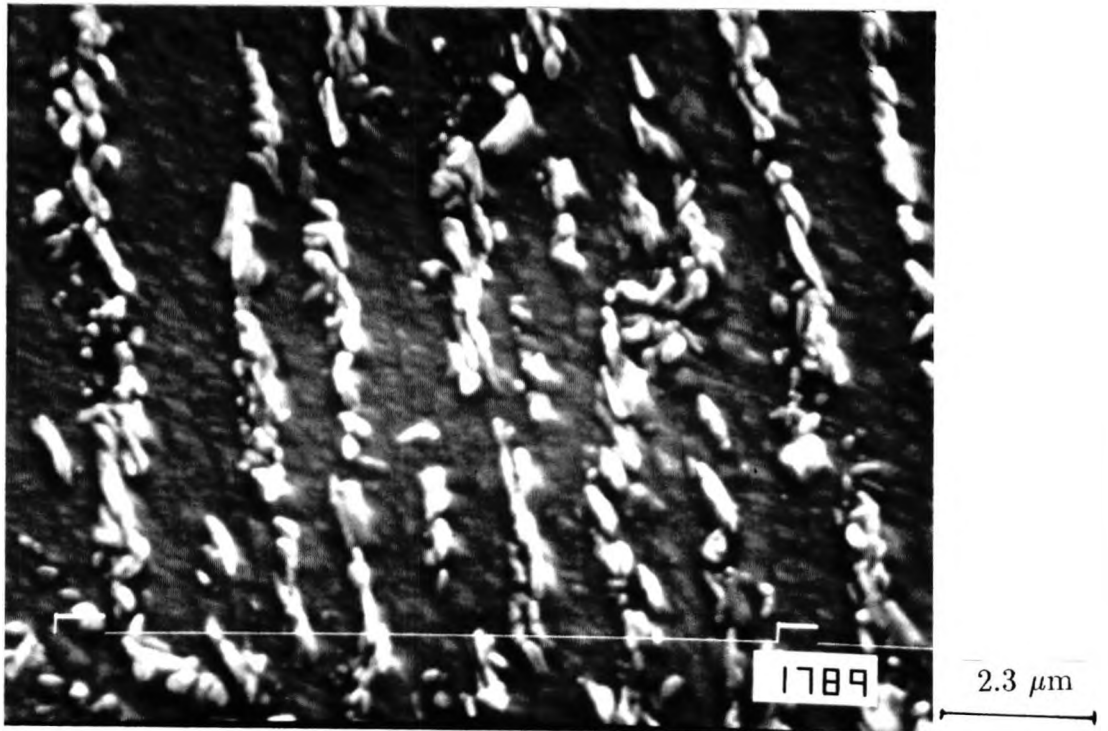
Figure 5.19: Microstructure of steel flanges ice-water quenched from 900°C and tempered at 600°C for 1 hour. (SEM)
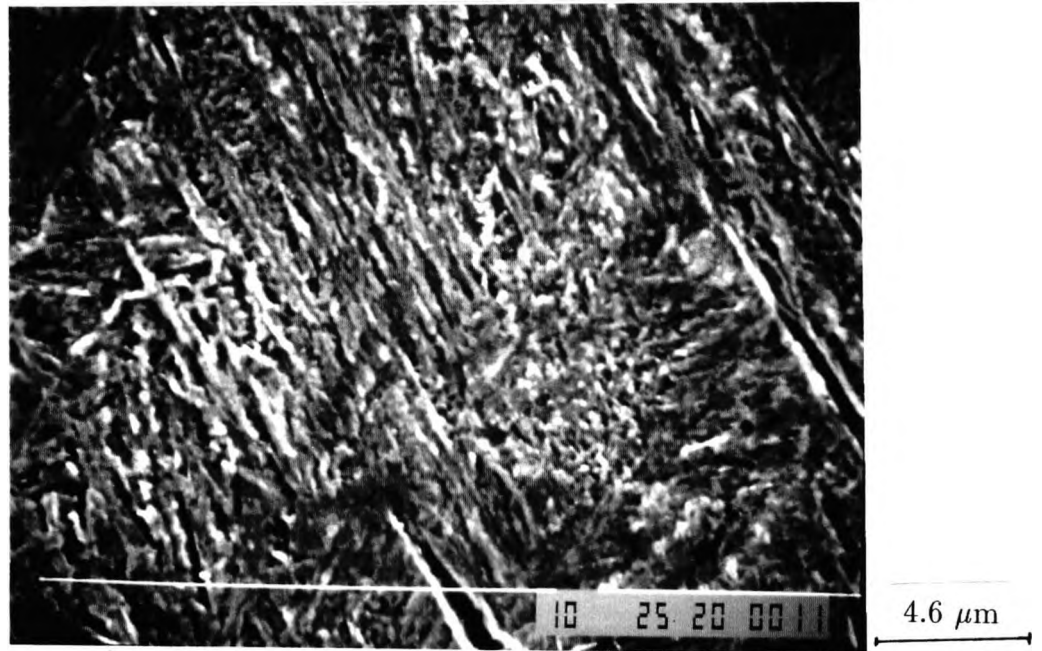
Figure 5.20: Microstructure of steel flanges ice-water quenched from 1250°C and tempered at 300°C. (SEM)
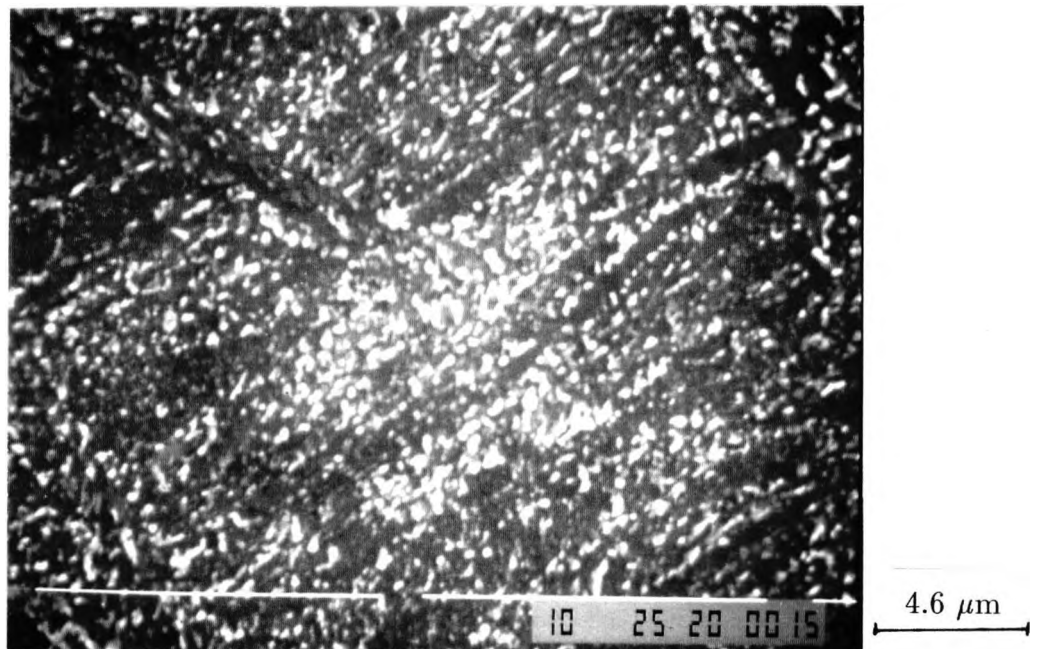
Figure 5.21: Microstructure of steel flanges ice-water quenched from 1250°C and tempered at 600°C. (SEM)

TEMPERING
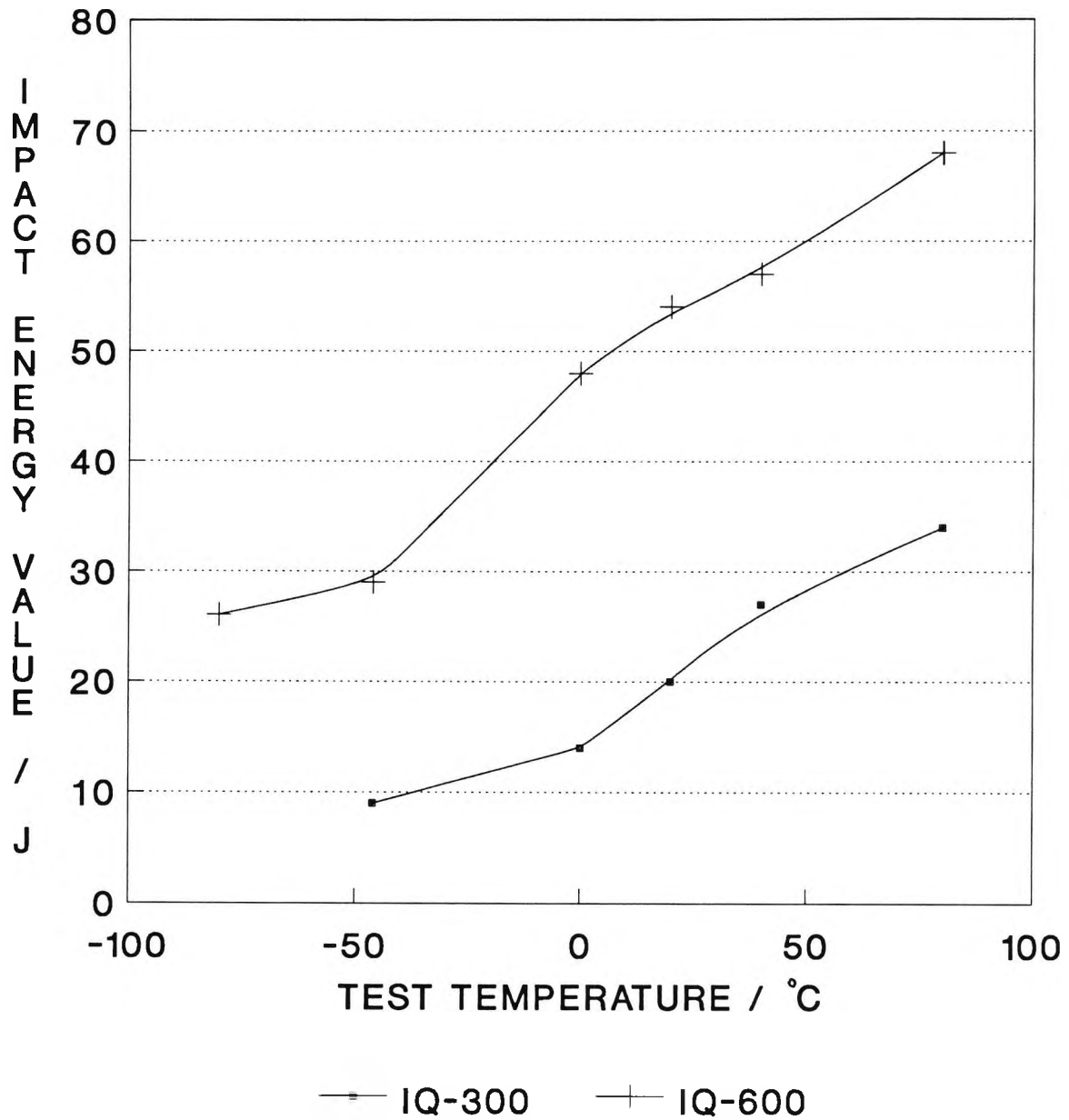
Fig 5.22 IMPACT TRANSITION CURVES
FOR SAMPLES ICE-WATER QUENCHED FROM
1250 °C AND TEMPERED.
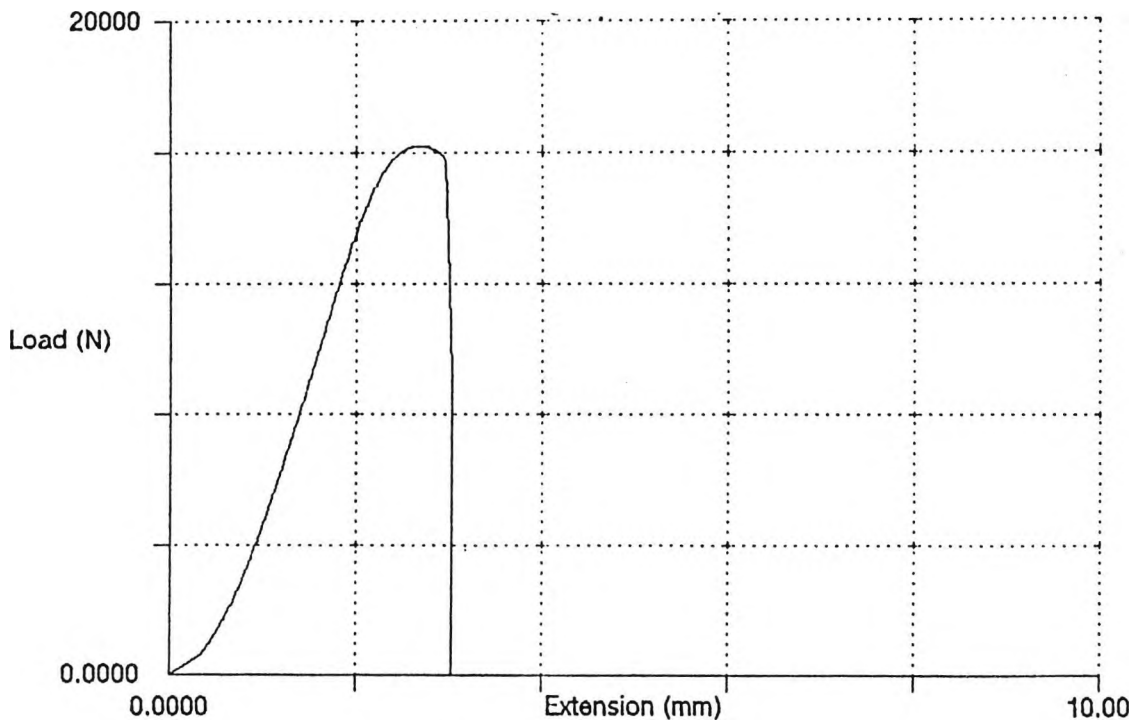
Figure 5.23: Stress/strain curve for the flange ice-water quenched from 1250°C and tempered at 300°C.
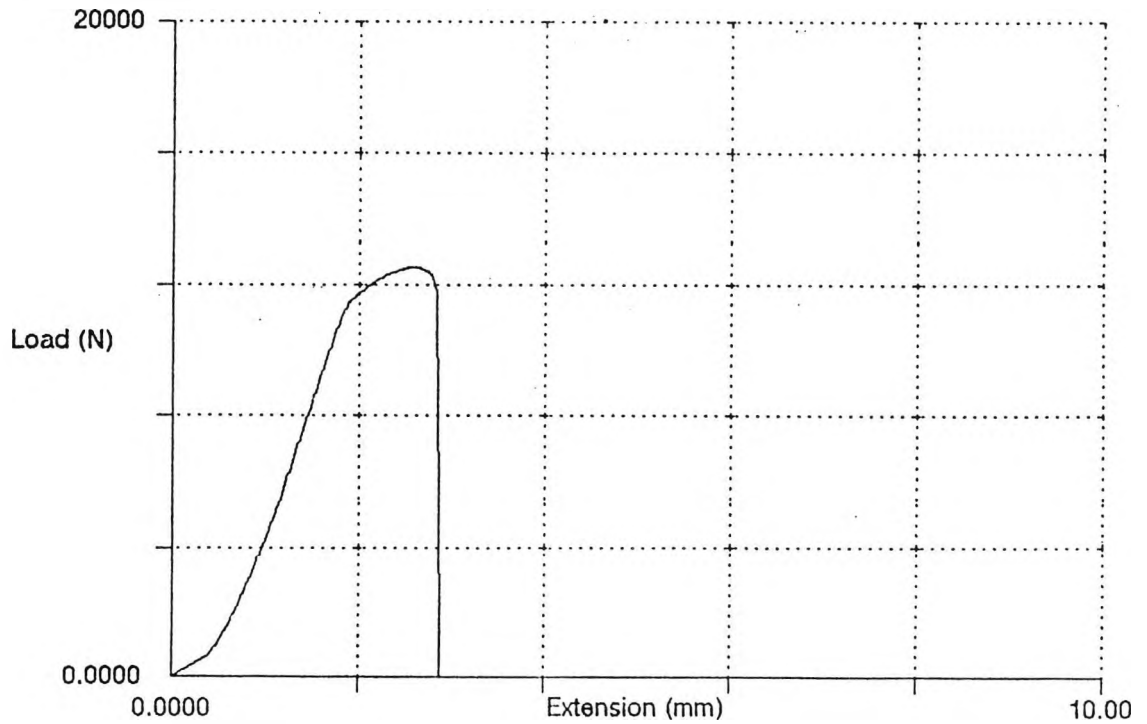
Figure 5.24: Stress/strain curve for the flange ice-water quenched from 1250°C and tempered at 600°C.

205
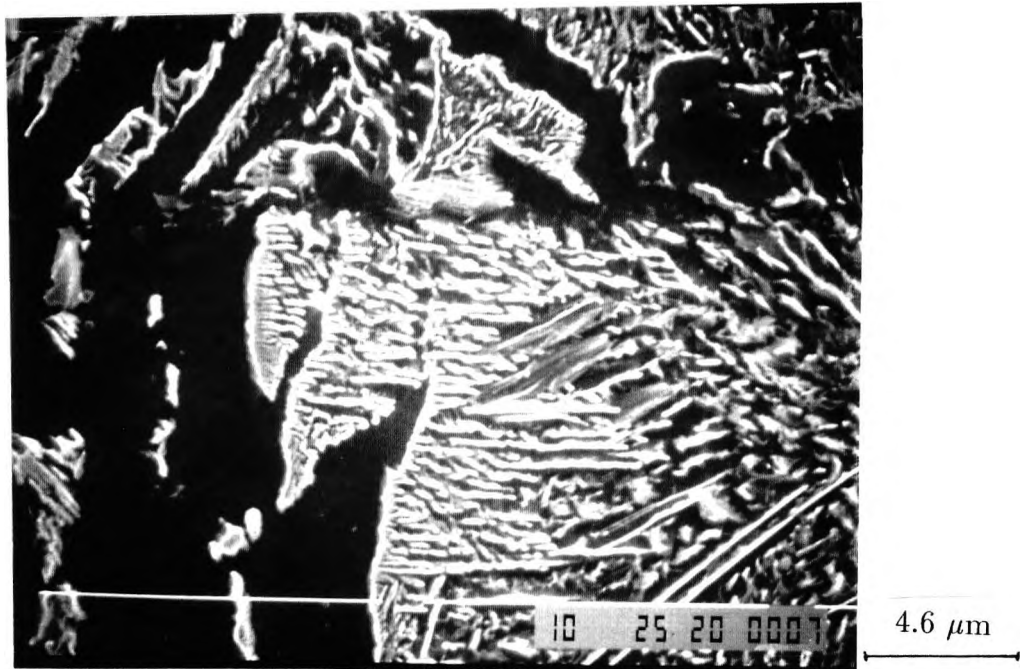
Figure 5.25: Microstructure of steel flanges oil quenched from 1250°C and tempered at 300°C.
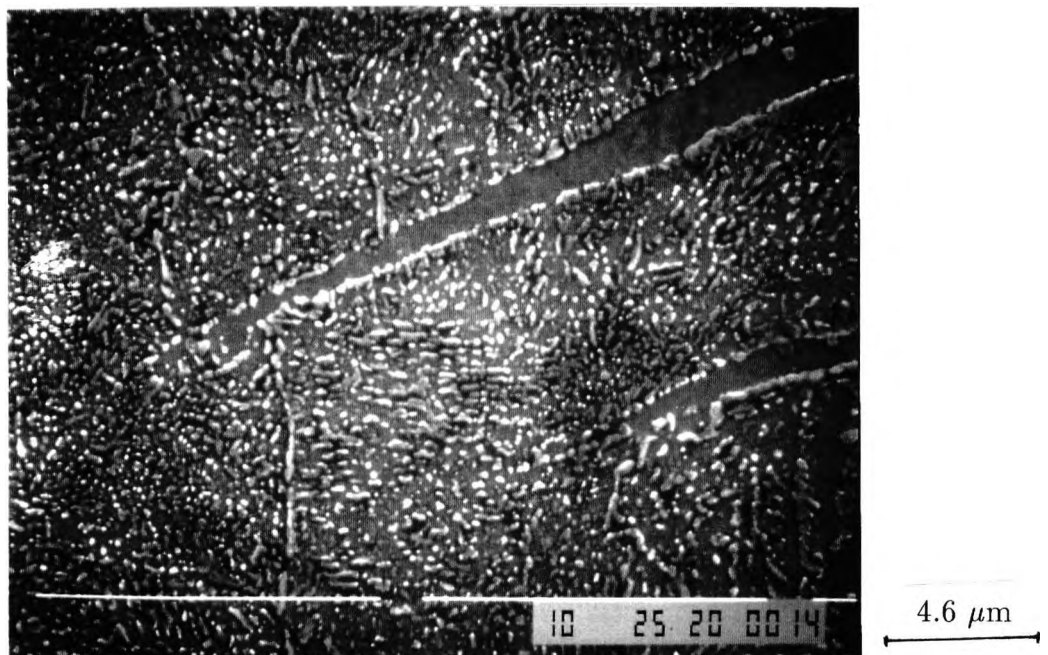
Figure 5.26: Microstructure of steel flanges oil-quenched from 1250°C and tempered at 600°C.

TEMPERING
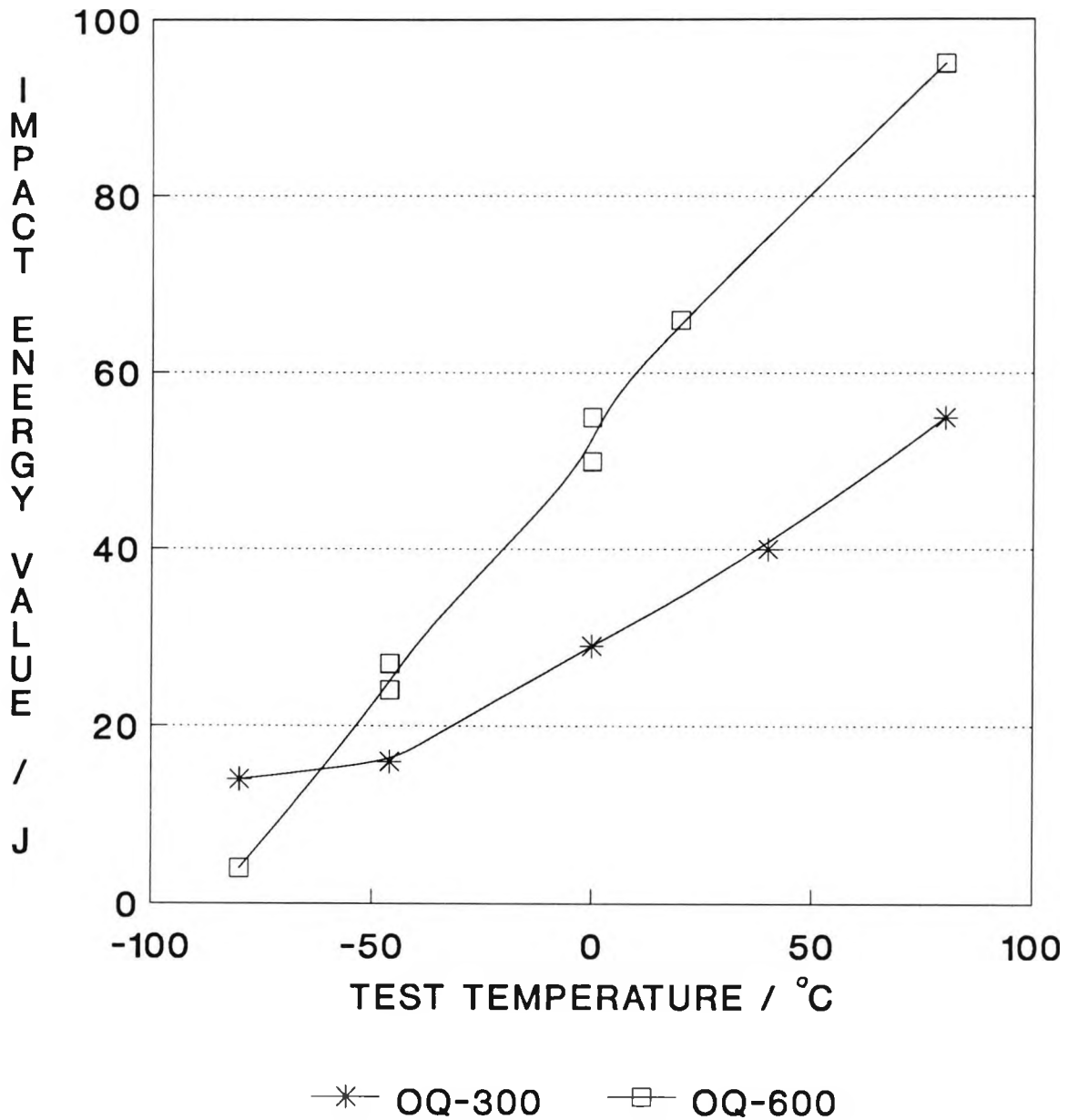
Fig 5.27 IMPACT TRANSITION CURVES FOR
SAMPLES OIL QUENCHED FROM 1250 °C AND
TEMPERED.
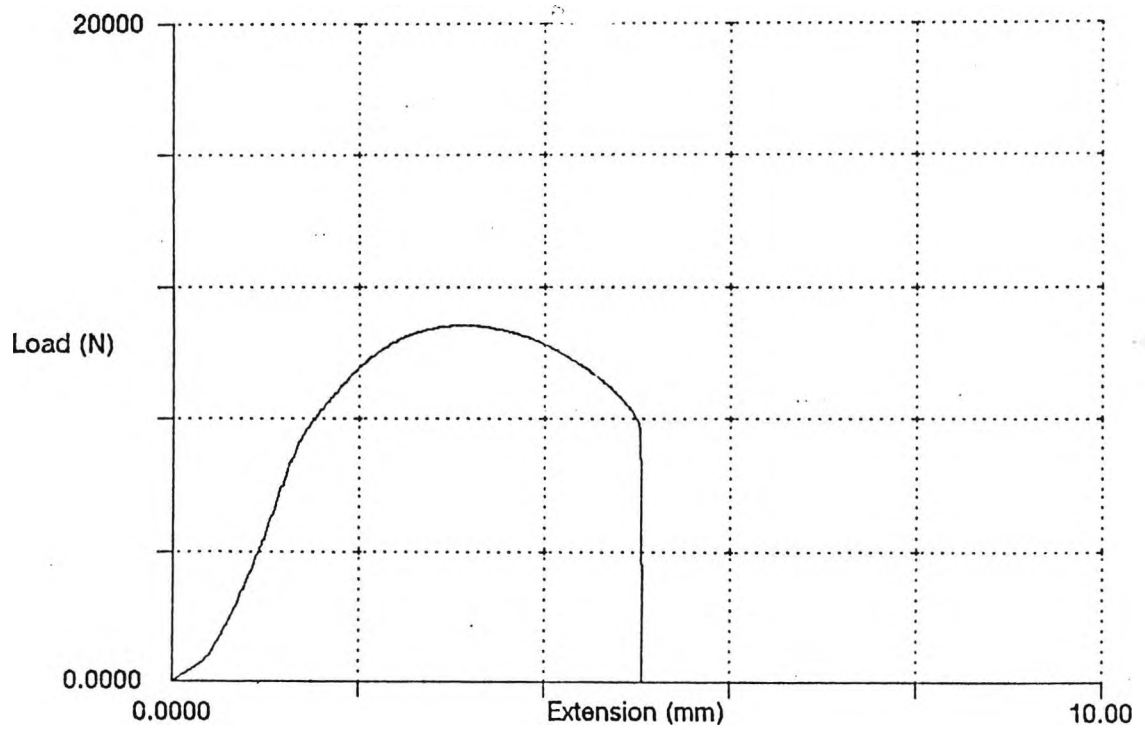
Figure 5.28: Stress/strain curve of the flange oil quenched from 1250°C and tempered at 300°C.
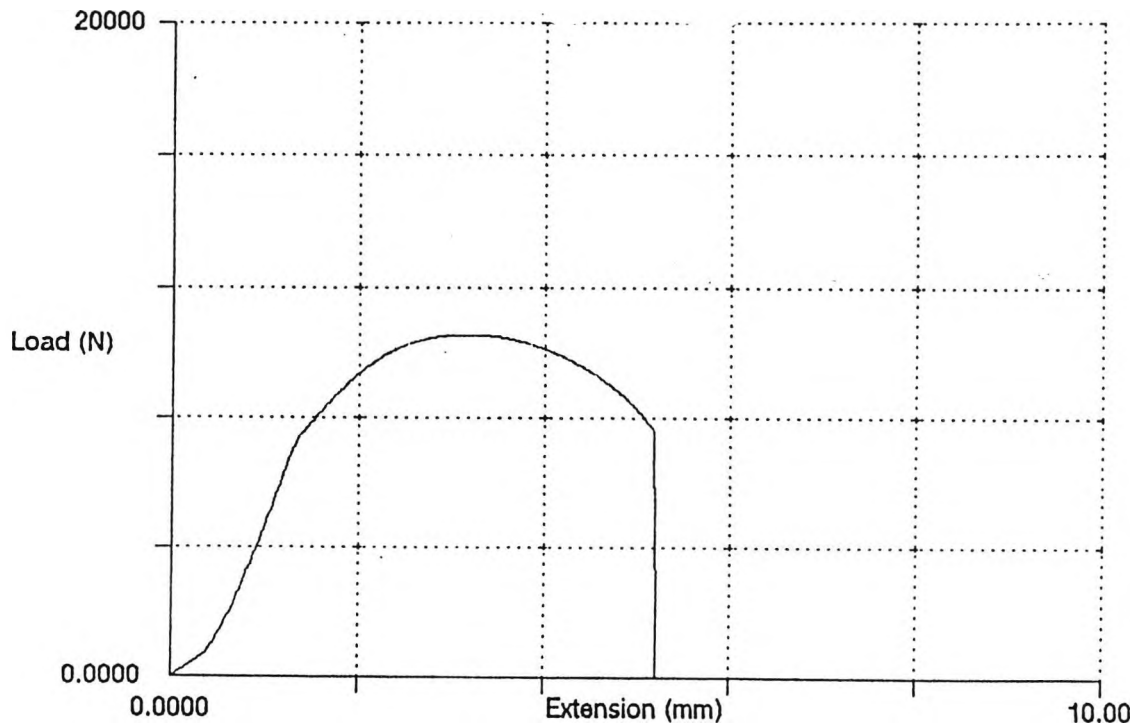
Figure 5.29: Stress/strain curve of the flange oil quenched from 1250°C and tempered at 600°C.

208
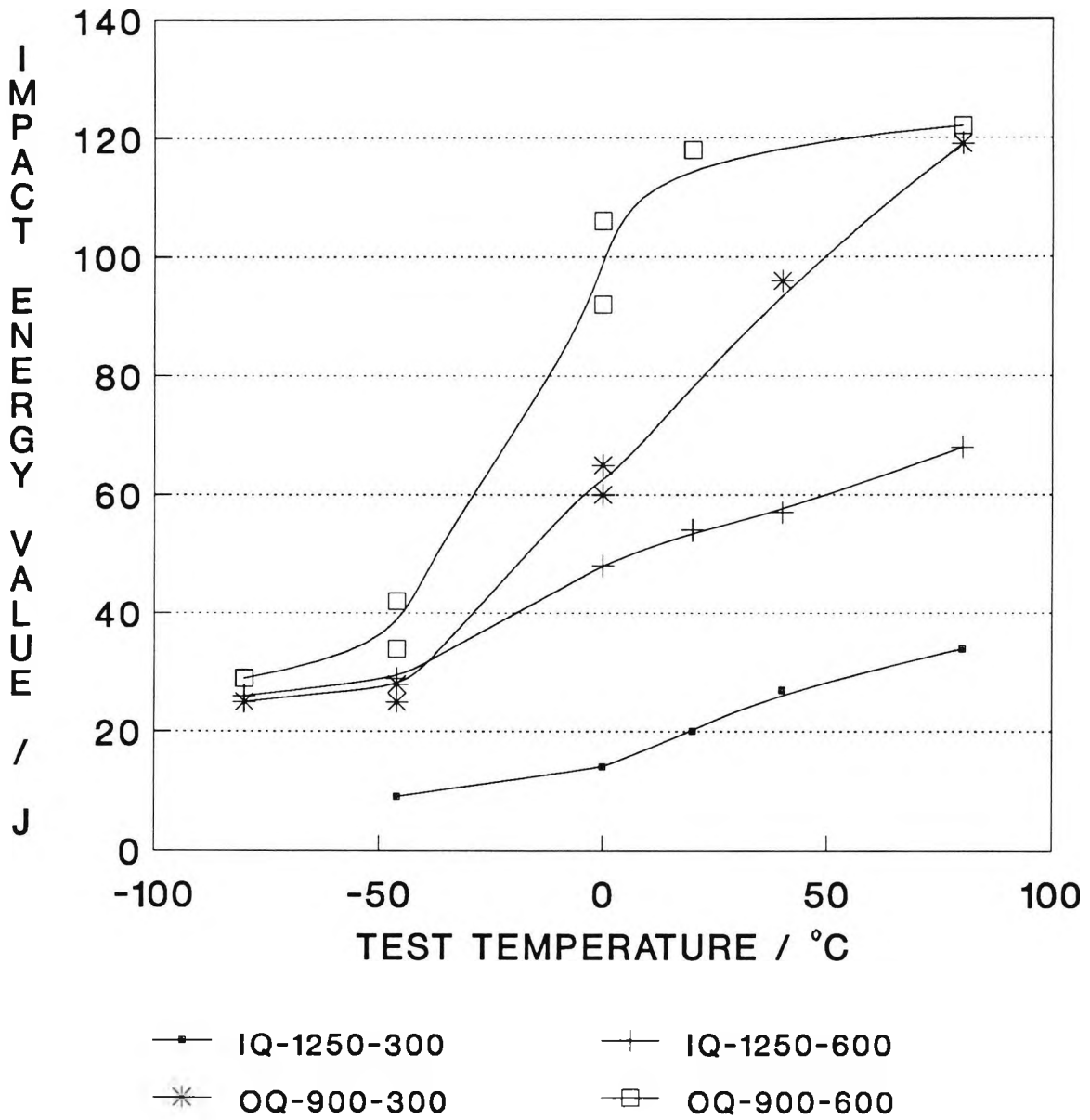
TEMPERING

Fig 5.30 Impact transition curves for
samples ice-water quenched from 1250
or 900 °C and tempered.
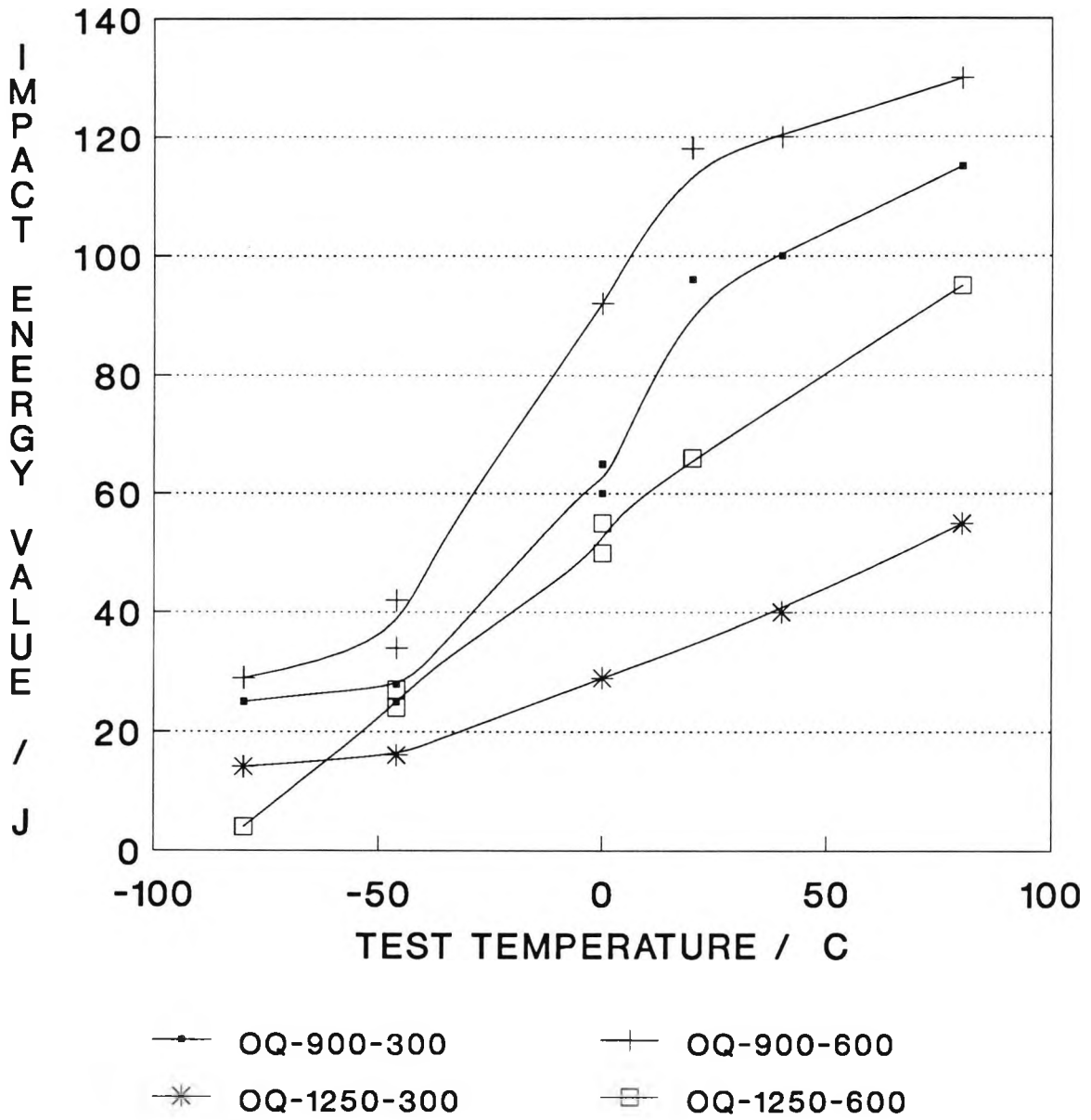
TEMPERING

Fig 5.31 Impact transition curves for
samples oil quenched from 1250 or
900 °C and tempered.
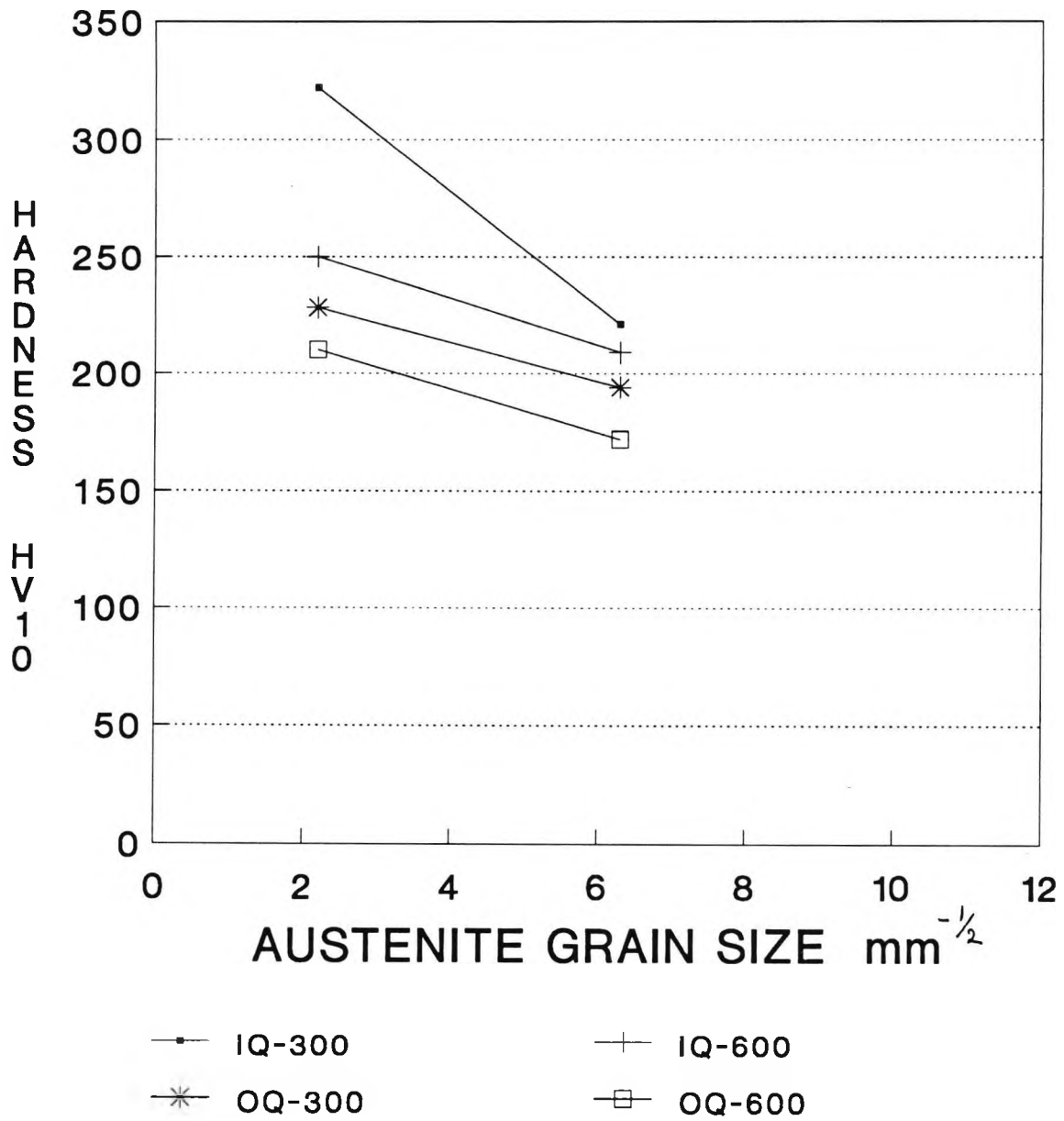
TEMPERING

FIG 5.32   VARIATION OF AUSTENITE GRAIN
SIZE WITH HARDNESS.

211

TEMPERING

FIG 5.33 VARIATION OF IMPACT ENERGY
WITH HARDNESS

TEMPERING
IQ AND OQ FROM 900 C
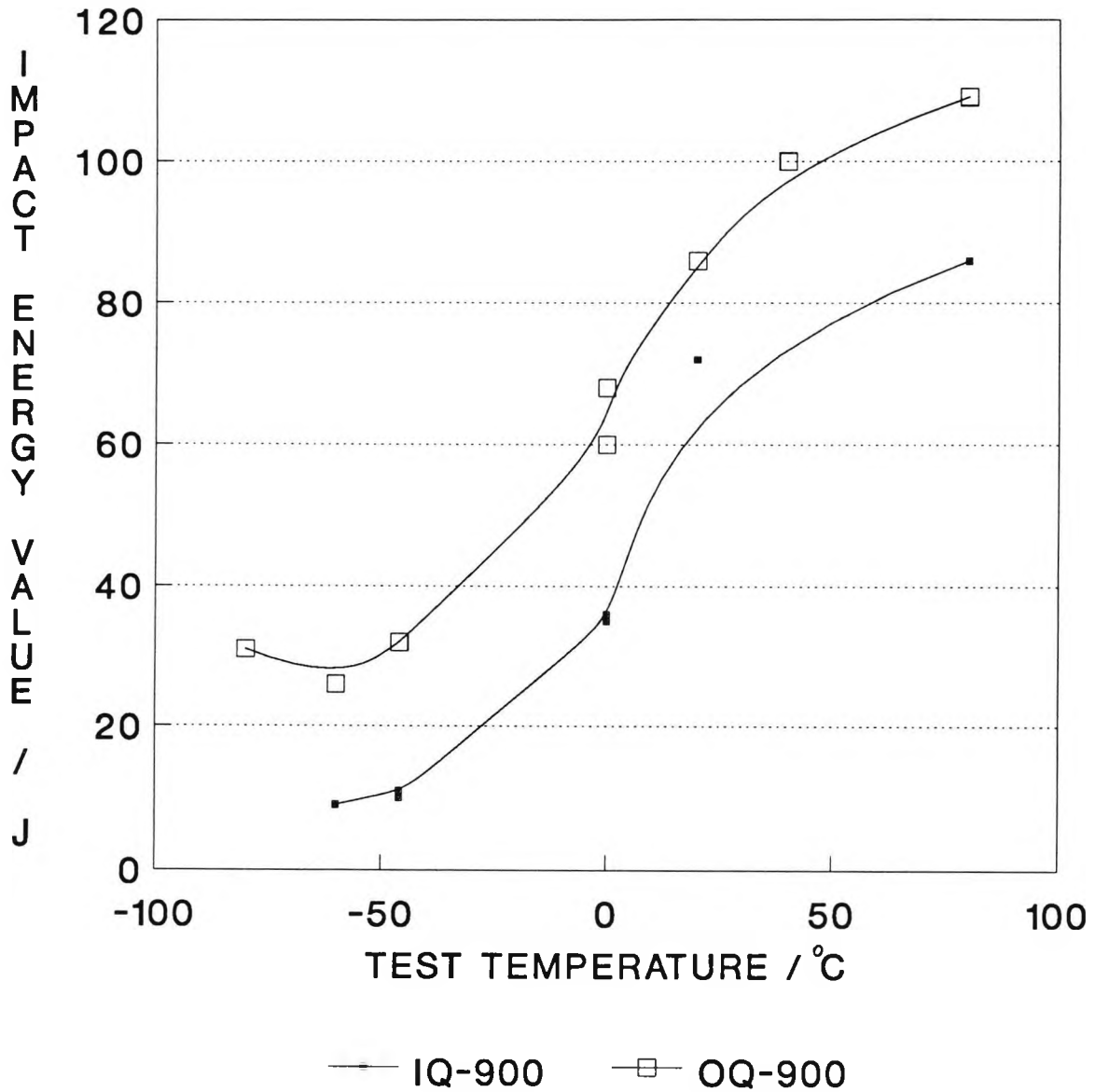
Fig 5.34 IMPACT TRANSITION CURVES
FOR SAMPLES ICE-WATER AND OIL QUENCHED
FROM 900 °C

213

20 μm

20 μm
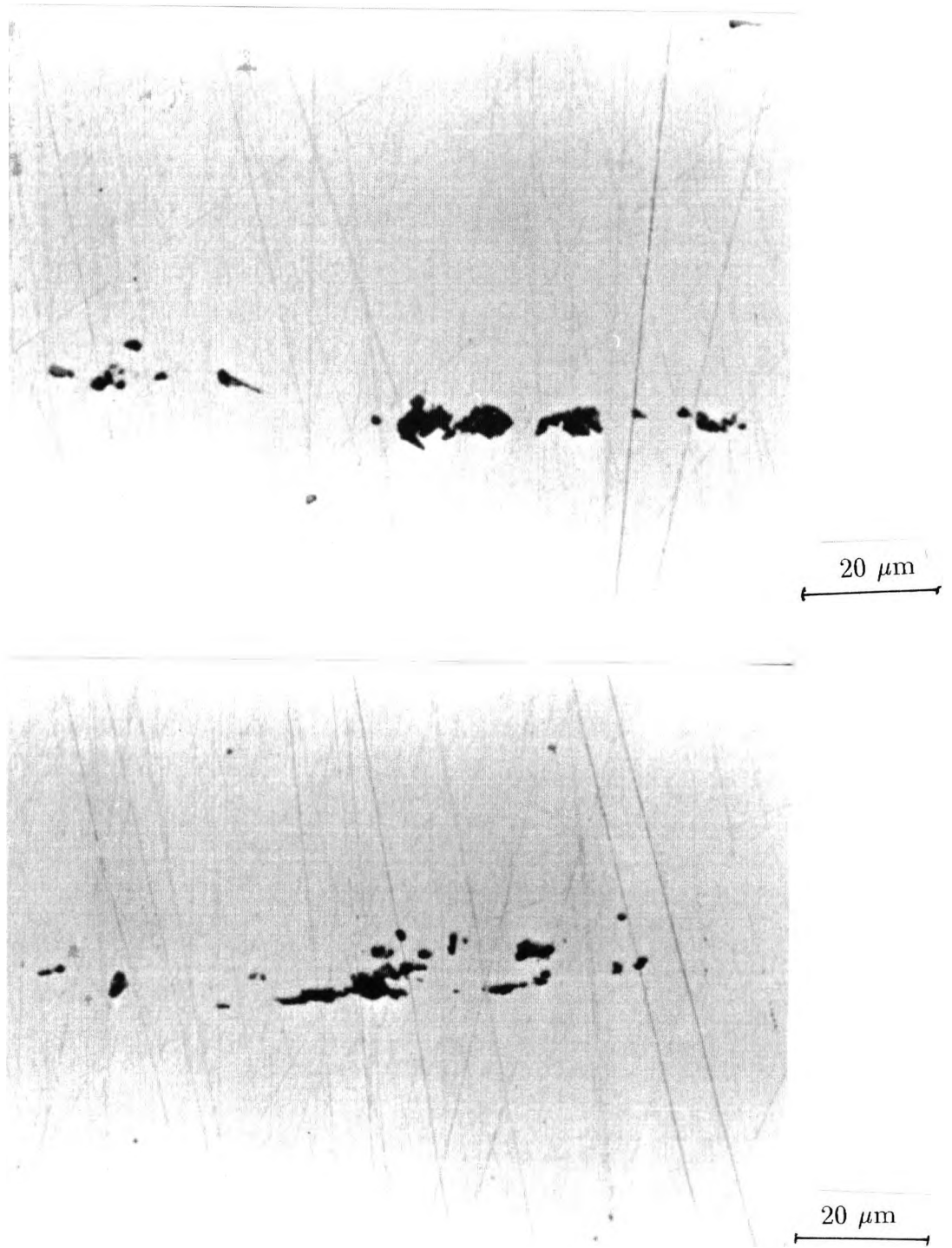
Figure 5.35: MnS inclusion photographs

214
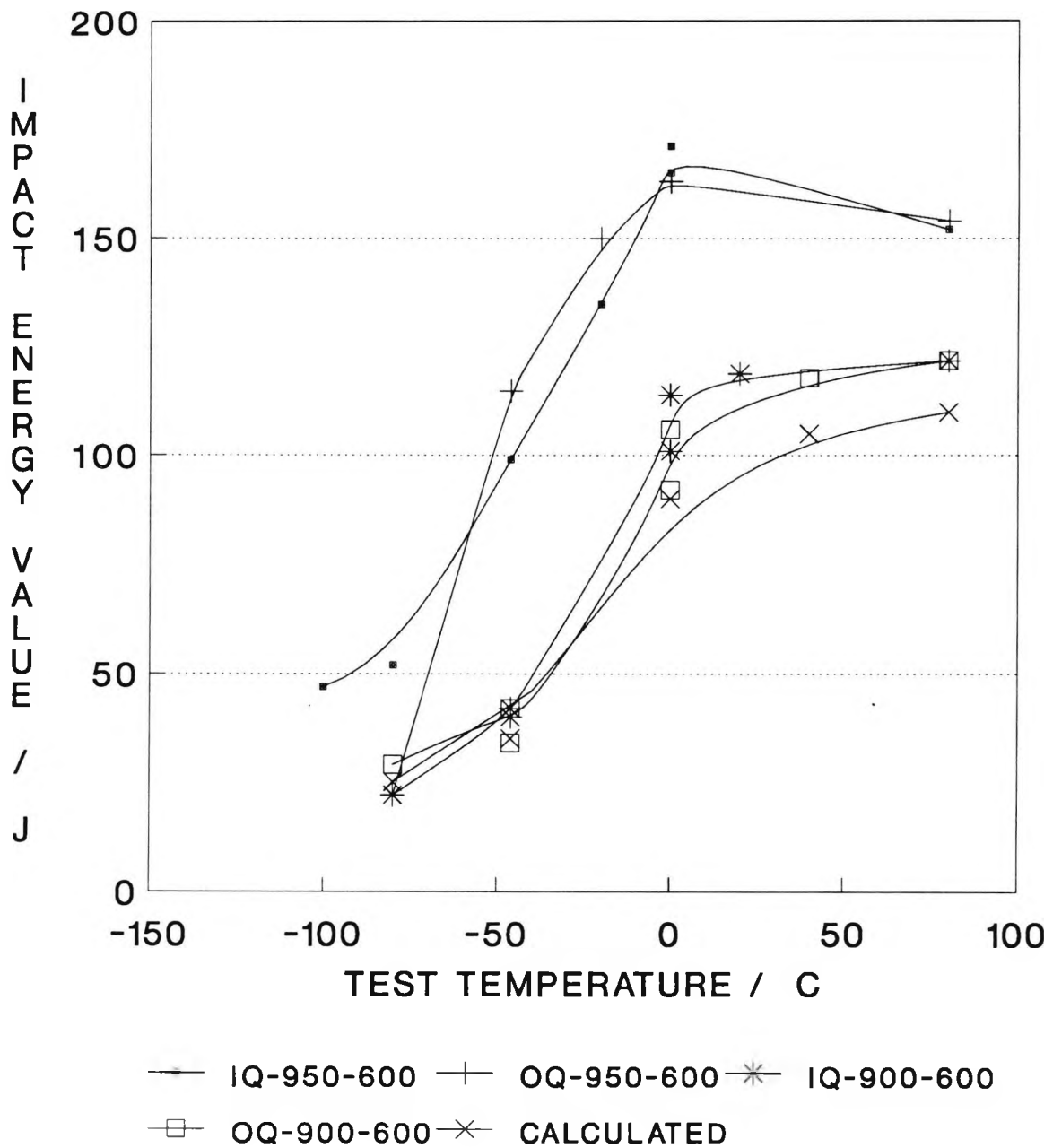
TEMPERING

Figure 5.36: Comparing impact transition curves for flanges ice-water or oil quenched from 950 or 900°C and tempered at 600°C with calculated curve.

TEMPERING
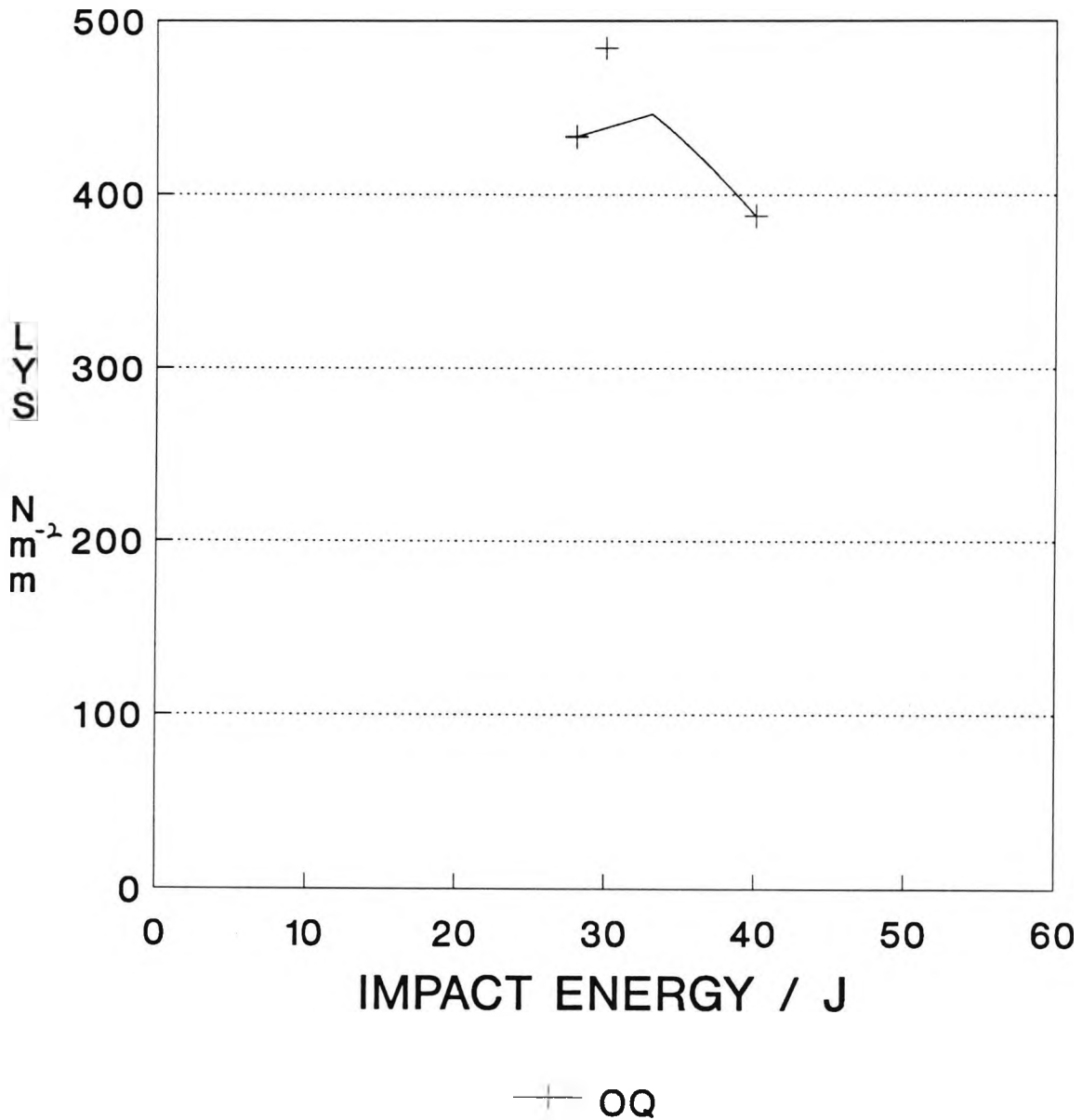
FIG 5.37 Variation of impact energy
at -46°C with changes in strength
on tempering for oil quenched steels

TEMPERING
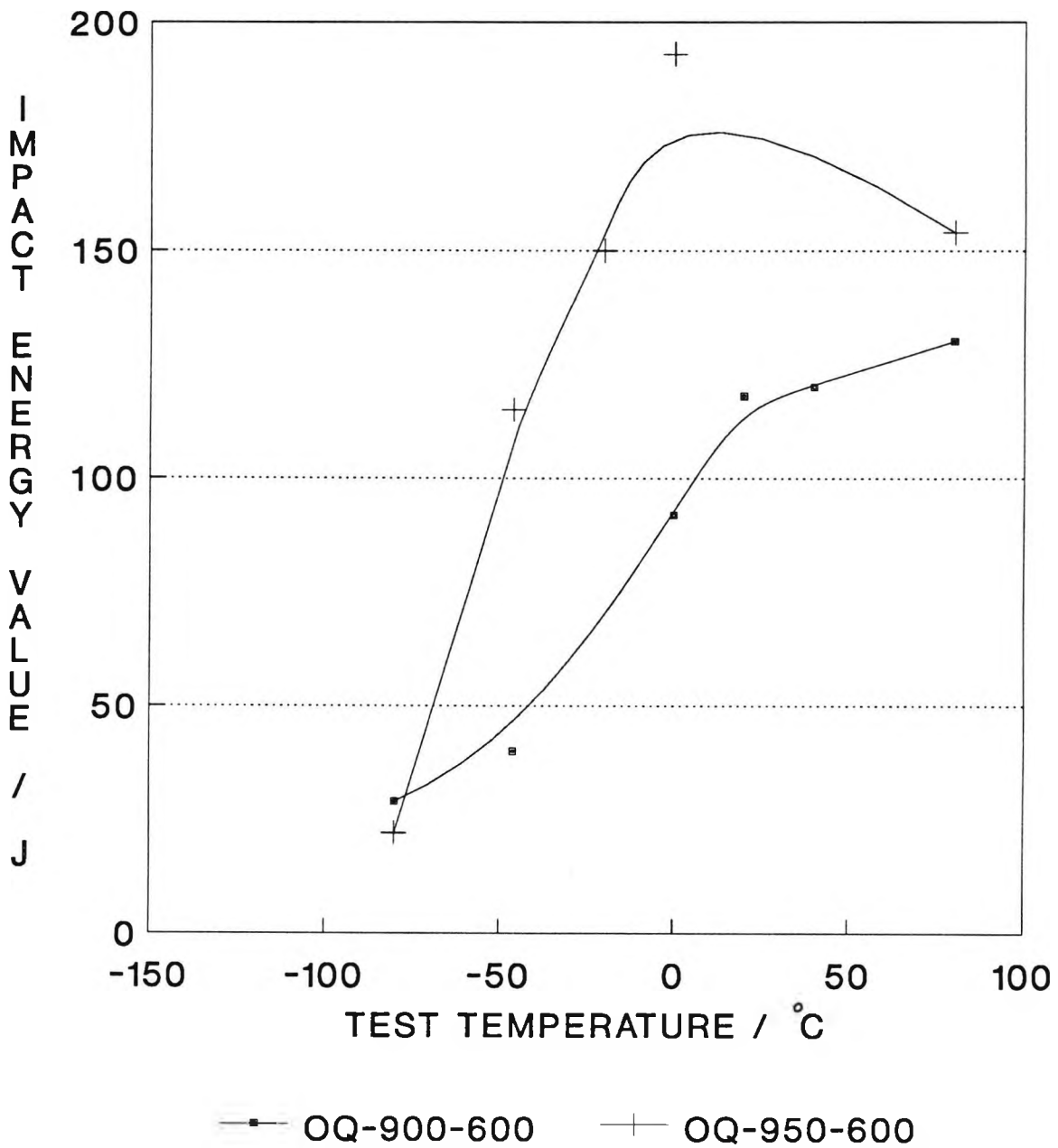
Figure 5.38: Impact transition curves for oil quenched flanges from 950 or 900°C and tempered at 600°C.
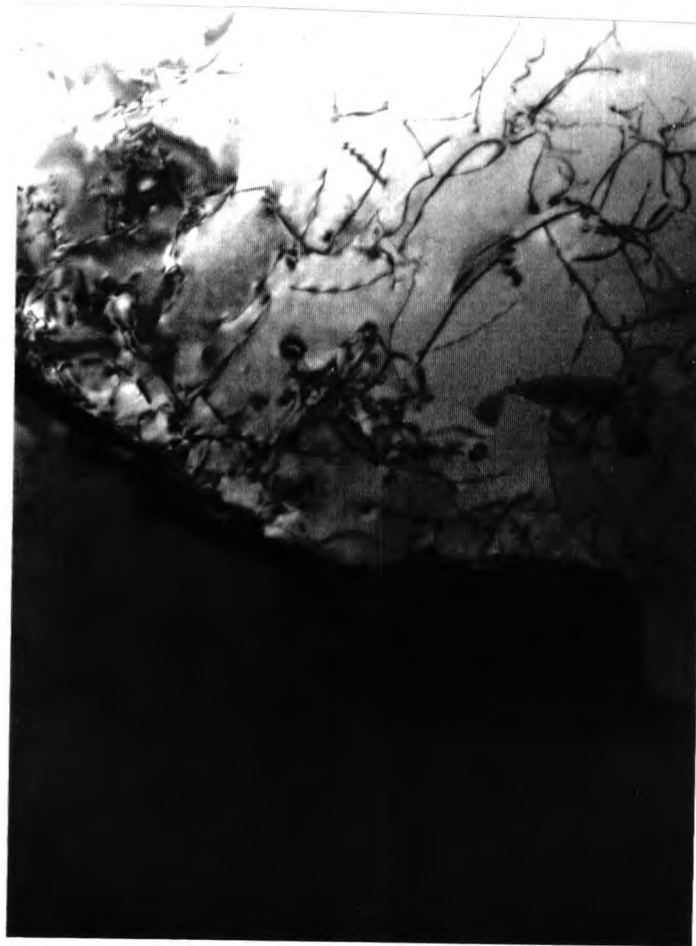
Figure 5.39: TEM microstructure of steel flanges ice-water quenched from 900°C and tempered at 300°C, showing the presence of dislocations in the ferrite. (MAG 38000X)

TEMPERING
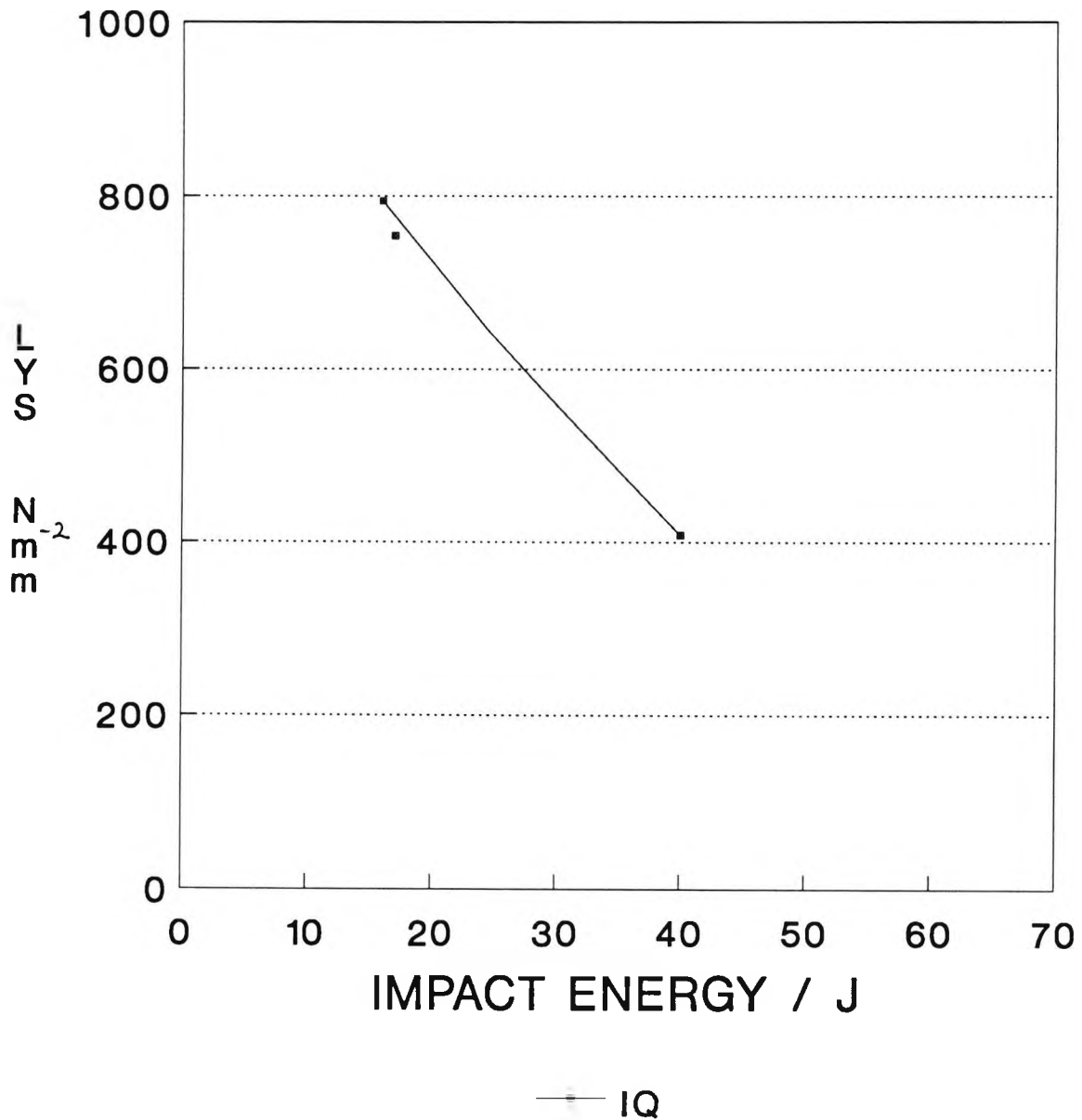
FIG 5.40 Variation of impact energy
at -46°C with changes in strength on
tempering for ice-water quenched steels.

TEMPERING
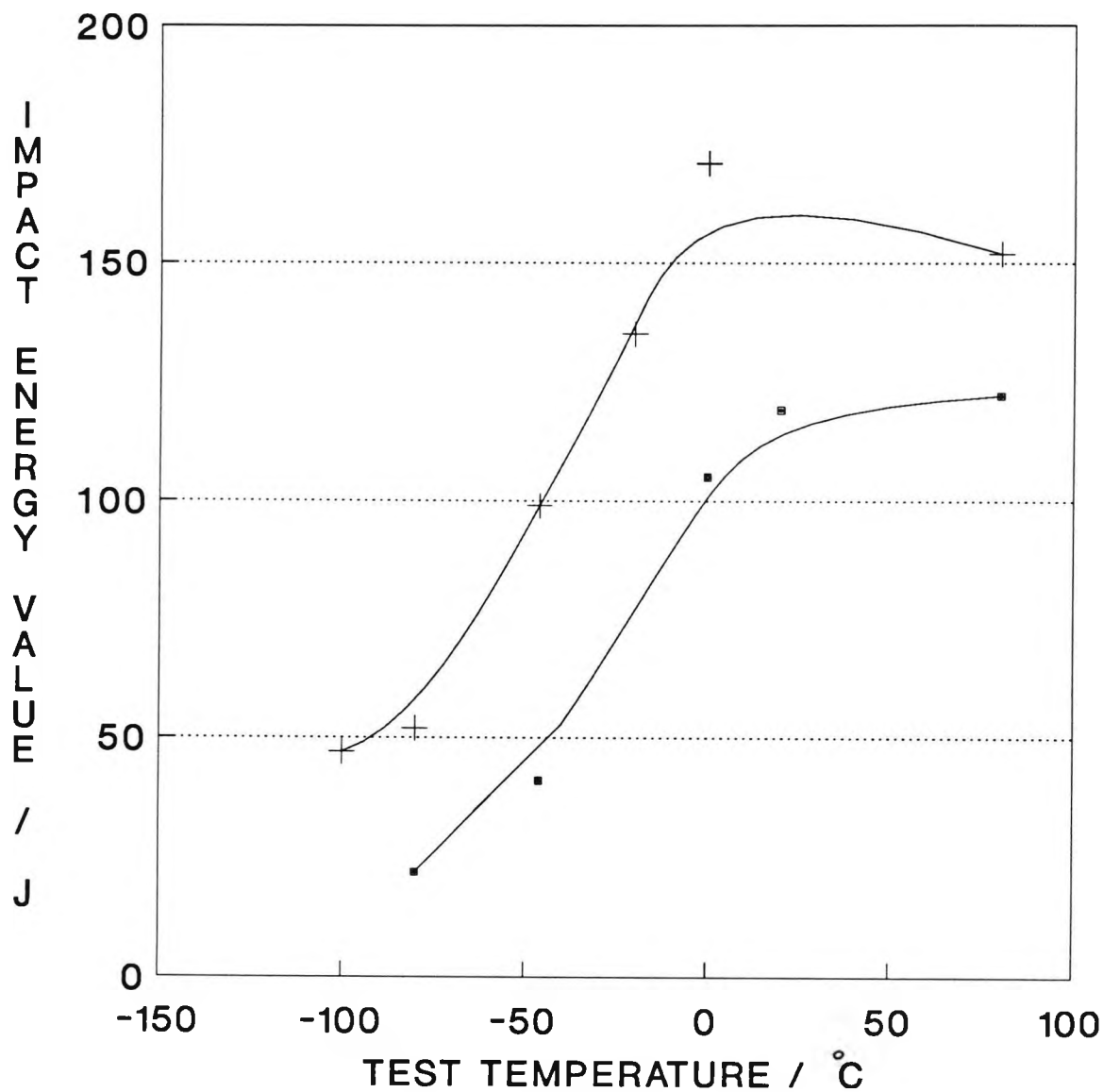
Figure 5.41: Impact transition curves for flanges ice-water quenched from 900 or 950°C and tempered at 600°C.
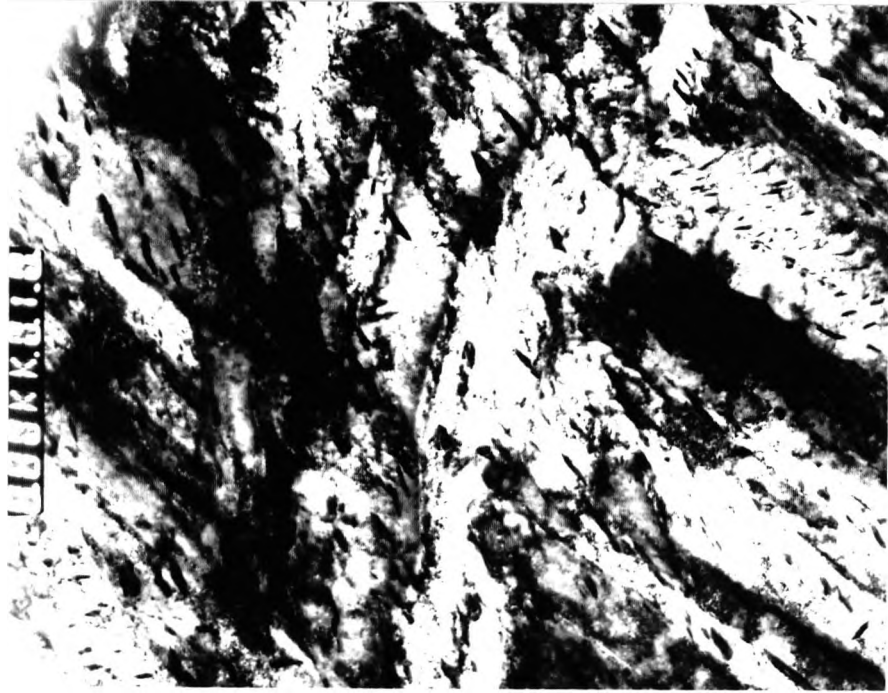
Figure 5.42: TEM microstructure of steel flange ice-water quenched from 1250°C and tempered at 300°C. (MAG 12000X)
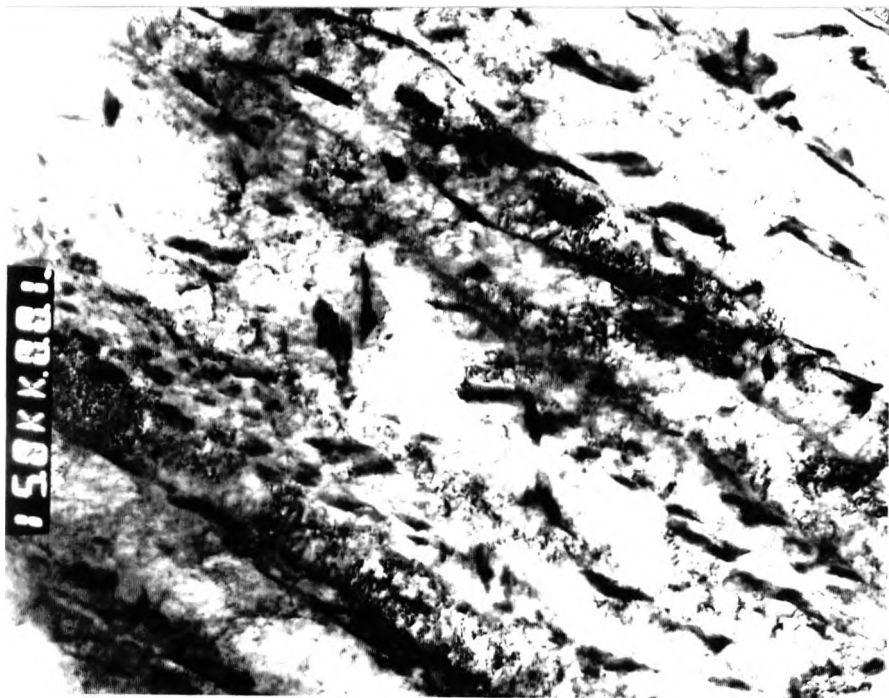
Figure 5.43: TEM microstructure of steel flange ice-water quenched from 1250°C and tempered at 300°C. (MAG 21000)

221
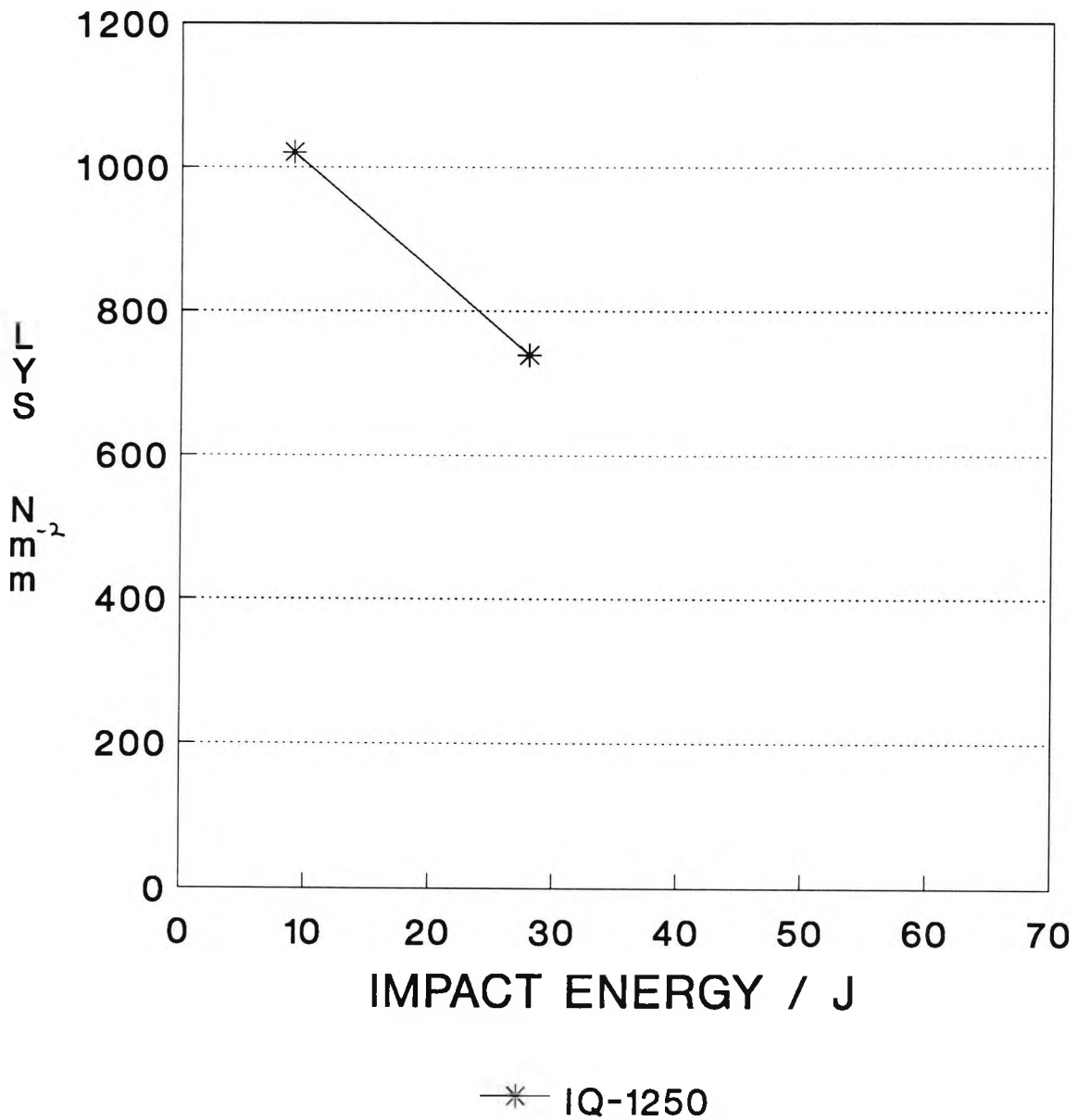
TEMPERING

Figure 5.44: Variation of impact energy at -46°C with changes in strength on tempering for flanges ice-water quenched from 1250°C.
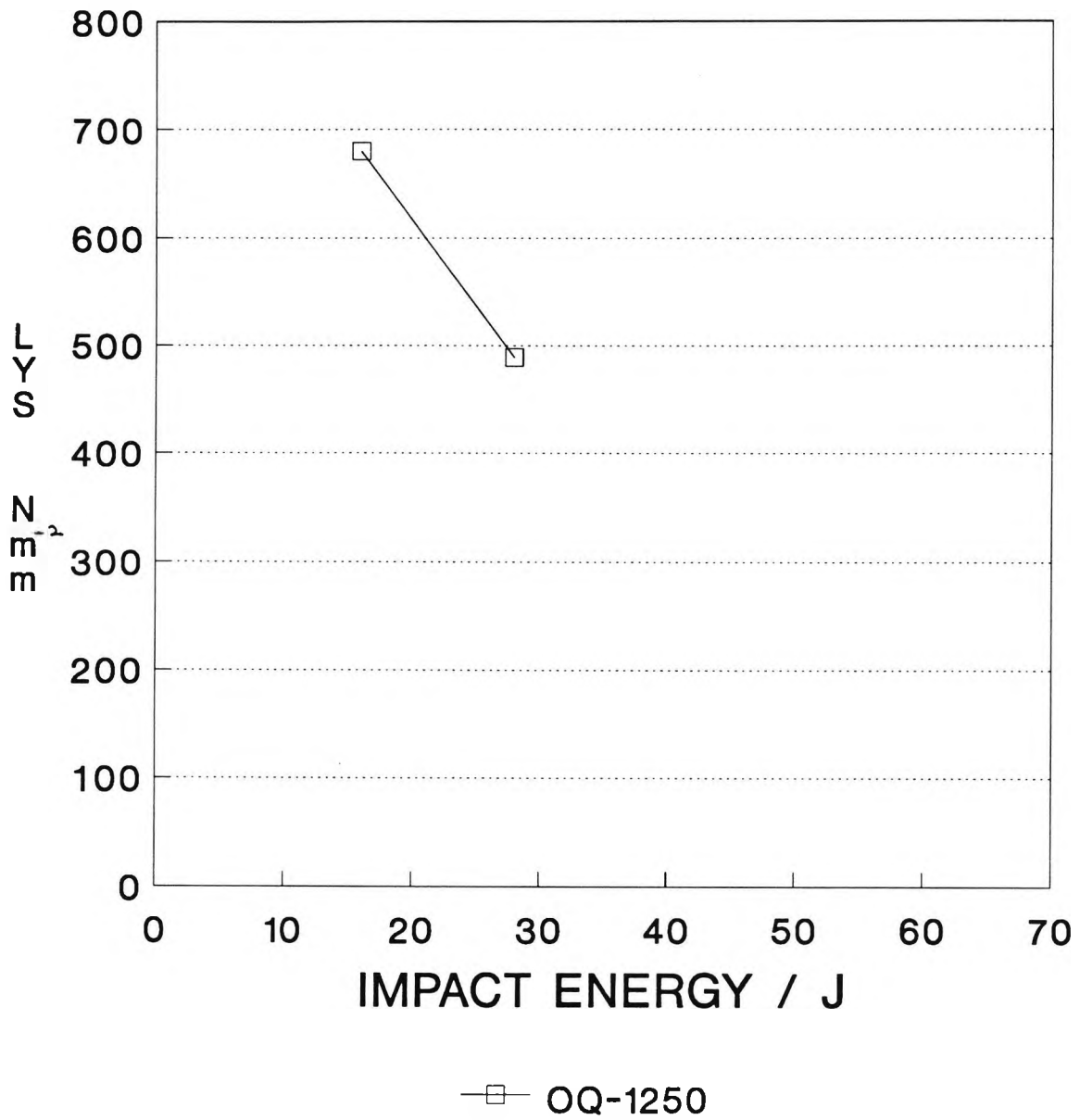
TEMPERING

Figure 5.45: Variation of impact energy at -46°C with changes in strength on tempering for flanges oil quenched from 1250°C.
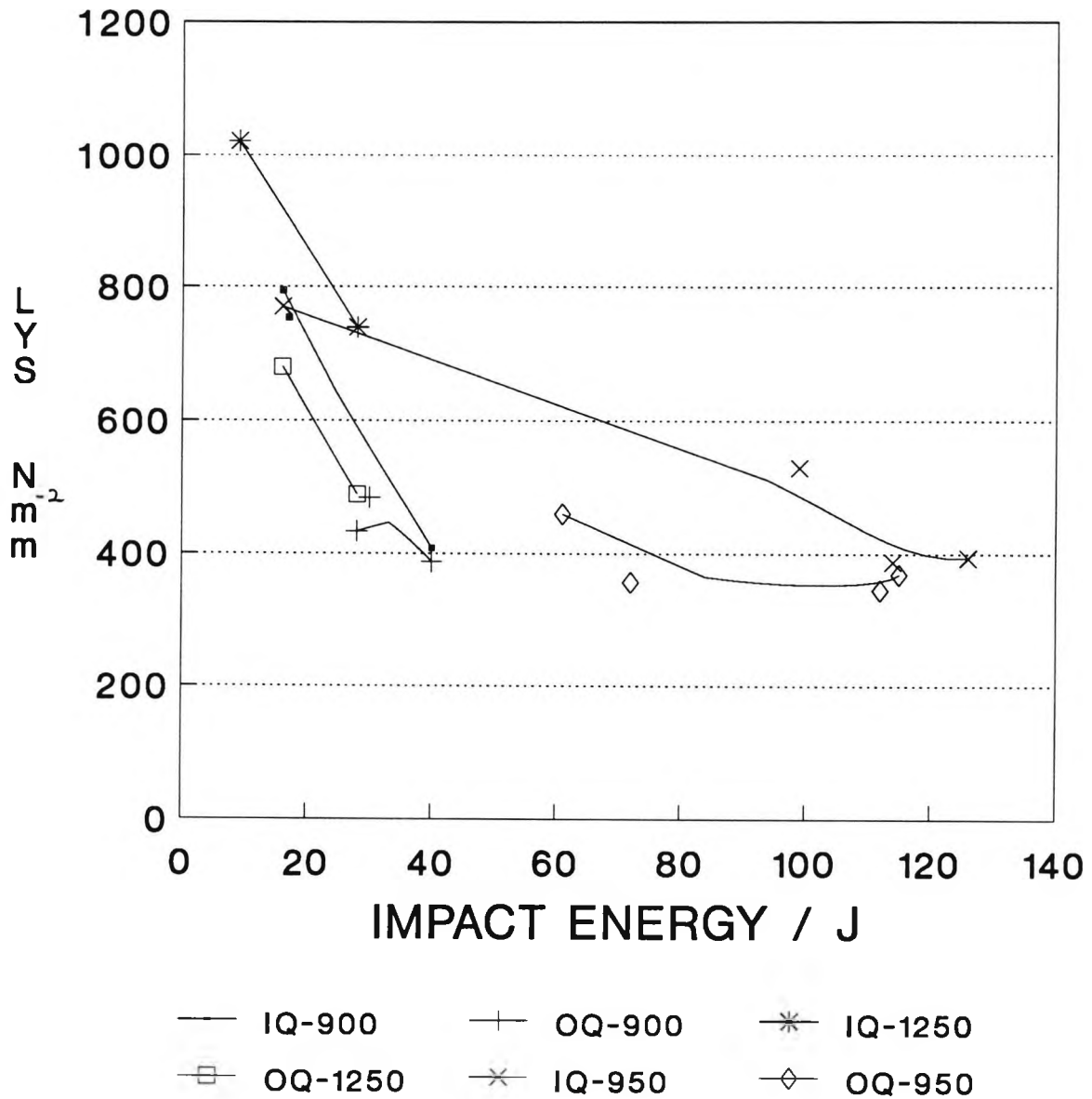
TEMPERING

FIG 5.46 Variation of impact energy
at -46°C with changes in strength
on tempering

Chapter 6

THE INFLUENCE OF NORMALISING AT 900 ^{0}C AND 1050 ^{0}C ON THE IMPACT AND STRENGTH OF V AND V FREE FLANGES

6.1   Introduction

The work to date has looked at quenched and tempered steels and tried to establish simple micro-structural techniques and evaluation of the micro-structures to assess the impact and tensile properties. Considerable work has been made in interpreting the structure/property relationships in normalised steels with ferrite/pearlite structures. In the case of flanges made to the ASTM A350 LF2 specification very simple measurements of pearlite volume fractions and ferrite grain size are enough to establish the impact value at the specification test temperatures of -46°C. The simpler the techniques the easier it is to quality control and one of the aims of the current reasearch programme has been to see how far this avenue can be taken, and where are its limitations. Previous examination[106,107] on flanges for low temperature service have noted that steels which contained Vanadium gave worse impact behaviour than would have been predicted from simple metallographic examinations. This was found to be particularly marked for quenched and tempered flanges made to the ASTM A350 LF2 specification but more recently[107] there has been evidence to indicate that this discrepancy may also apply to the normalised route [106]. Whereas for C-Mn-Al steels, impact behaviour can be predicted from measurements of the pearlite volume fraction and grain size[18] this may not be so for V containing steels. This probably arises because even when normalised some V may be able to precipitate during transformation in a very fine sub-microscopic form conferring precipitation hardening on the steel. This precipitation hardening will reduce impact energies and hence result in an over estimation of the predicted impact energies when only simple micro-structural techniques are used.

In order to examine this problem in more detail, two steels of otherwise

similar compositions one with V and having no Al addition and the other V free with Al have been chosen and their impact and tensile properties determined. Two conditions were investigated :

- Normalised, in which a large part of the V or Al will be precipitated in the form of the grain refining precipitates, VN and AlN. These precipitates are too coarse to influence strength.

- Austenitised at high temperature when most of the precipitates will have redissolved so that the Al and V will be largely in solution, the latter being able to precipitate on cooling in a fine sub-microscopic form, strengthening the steel.

6.2   Experimental

The composition of the flanges are given in table 6.1. The V free steel contained Al while the V containing steel had only residual Al present. The base composition of the steels were similar but it should be noted that the V containing steel had lower sulphur and phosphorous levels, both of which elements are known to influence impact behaviour. The flanges were of similar thickness and the same diameter. (400 mm dia and 42 mm and 35 mm thick for V containing and V free steels respectively). Blocks of 60 x 70 mm x flange thickness were cut from these flanges and these were heated to 900 and 1050 $^{\circ}$C, held for an hour at temperature and then air-cooled.

Table 6.1: Composition of steel examined Wt.%

TYPE	C	Mn	Si	P	S	Al	V	N
Al containing	0.22	1.24	0.25	0.025	0.020	0.015	—	0.011
V containing	0.21	1.21	0.22	0.012	0.011	0.008	0.10	0.012

Charpy V notch samples were taken in the radial direction in the flange face and tensiles were taken tangentially (see chapter 3, Fig. 3.3).

The tensiles having a 20 mm gauge length were tested on a Lloyds tensile machine using a cross-head speed of 5 mm per min. The charpy impact transition curves were established for the two steels for the two heat-treated conditions.

The micro-structural measurements, pearlite volume fraction, ferrite grain size and grain boundary carbide thickness were made. Pearlite volume fraction was assessed by point counting , a minimum of 700 counts being made, grain size was measured by the mean linear intercept technique a total of 1000 grains being counted. The grain boundary carbide thickness was determined by the method of Mintz et al[101] using a JEOL 100 Scanning Electron Microscope, the average thickness of 50 carbides being taken as the carbide thickness, with a stage tilt of 45° .

6.3 Results

The impact transition curves for the V and Al containing steels are shown in Figs. 6.1 and 6.2 respectively. The normalised heat-treatment gave the higher impact energies as would be expected. Surprisingly, the V containing steel showed better impact behaviour than the Al containing steel. This was very marked after normalising at 900 °C but was observed to a lesser degree

even after austenitising at 1050 $^{\circ}$C. The Al containing steel failed to meet the ASTM A350 LF2 specification at the higher austenitising temperature.

After normalising, the two steels have similar strengths, the V steel being only 5 MPa higher, Table 6.2. A very marked increase in strength was noticeable in the V steel after austenitising at 1050 $^{\circ}$C.(66 MPa increase over strength at 900 $^{\circ}$C). Hardness changes followed the same trends as the strength, Table 6.2. After austenitising the V steel at 1050 $^{\circ}$C, the hardness value exceeded that allowed by the specification (208 VPN) even though the flange would have met the impact requirement.

The micro-structural measurements are detailed in table 6.3. As expected the grain size after nomalising was fine and coarsened at 1050°C. The V steel had a finer grain size than the Al steel (1 to 1.5 mm$^{1/2}$ finer).

Pearlite volume fractions were very high in these steels in accord with the high C level. The volume fraction increased as the grain size coarsened at the higher austenitising temperature. This is probably a hardenability effect. Grain boundary carbide thickness was fine and similar for both steels. The higher austenitising temperature produced slightly coarser carbides, probably because there are fewer carbide nuclei present in this condition for the carbon in solution to precipitate out on.

6.4   Discussion

In order to discuss the present results, it is necessary to have some knowledge of the N in solution for the varrious conditions. This can be calculated from the solubility data derived by Irvine et al[36] and is given in table 6.4 for the two steels.

Surprisingly in the present exercise the impact properties of the V steel

have been found to be superior to those obtained in the Al containing steel. Whereas the V steel met the 20 J impact requirement at -46 °C at both austenitising temperatures, the Al containing steel only satisfied the specification after normalising.

6.4.1   Normalised steels

The microstructures produced from the normalising temperature of 900°C for the V and Al containing steels are shown in Figs 6.3 and 6.4 respectively. After normalising at 900 °C there was little difference in strength and hardness between the two steels. Table 6.2. The small increase in strength and hardness shown by the V steel can be well accounted for by the refinement in grain size (10.4 to 11.3 mm$^{-1/2}$, Table 6.2). Thus there is no evidence for the sub-microscopic VC interphase precipitation hardening in this steel.

If all the N combined with the V at the high temperature to form a "coarse" non-hardening grain refining precipitate, then there would be approximately 0.05% V available for precipitation at lower temperatures. (see Table 6.4 which gives the solubility data with expected Al, N and V contents).

The relatively slow cooling rate from the normalising temperature appears not to allow the formation of the fine vanadium carbides. Precipitation hardening can be avoided by either too slow cooling which coarsens precipitation or too fast cooling which suppresses precipitation. In the present instance it is likely to be the former[109].

The marked improvement in impact behaviour shown by the V steel over the Al containing steel (Table 6.2) cannot be explained by the extra grain refinement and this will be discussed in a later section.

6.4.2 Austenitised at 1050 ^{0}C

Microstructures produced from a normalising temperature of 1050°C for V and Al containing steels are shown in Figs 6.5 and 6.6, respectively. In contrast to normalising, austenitising at 1050 ^{0}C caused precipitation hardening in the V steel, as can be seen by its high hardness which exceeded the specification requirement, and high strength Table 6.2. The increased temperature causes most of the V and N to go back into solution Table 6.4 and this combined with the coarser γ grain size, lowers the transformation temperature so that a finer more concentrated precipitation of V takes place.

Not all the V goes back into solution at 1050 ^{0}C (Table 6.4) and there appears to be sufficient present to still give some grain refinement (9.2 mm $^{-1/2}$ Table 6.3) and this grain refinement is just enough for the steel to meet the impact requirement of 20 J at -46 ^{0}C (Table 6.2) even with its high degree of precipitation hardening.

6.4.3 Prediction of strength and impact behaviour

Previous work[101] has established empirical regression equations which relate micro-structural variables and composition to properties.

These are as follows:

Lower yield stress = 43.1% Mn + 83% Si + 15.4 d$^{-1/2}$ + 1540 N$_f$ + 105   in Mpa   (6.1)

where d = grain diameter mm and N$_f$ = free nitrogen content given in table 6.4 for the various conditions.

54 J ITT ^{0}C = 192 t$^{1/2}$ - 10.1 d$^{-1/2}$ + 0.5 δy - 23   (6.2)

27 J ITT ^{0}C = 173 t$^{1/2}$ - 8.3 d$^{-1/2}$ + 0.37 δy - 42   (6.3)

Where t = grain boundary carbide thickness in μm.

δy = the degree of hardening and is the difference between the actual LYS and that calculated from equation (6.1).

Using these equations and the experimental data in Table 6.3, the LYS, 54 J ITT and 27 J ITT can be predicted, Table 6.5.

It can be seen from this table, that the calculated LYS is always lower than the observed even when no precipitation hardening is present. this arises because of the very high pearlite contents present in the steels. The original equation was derived for steels with average pearlite content of 20%. The present steels have almost twice this volume fraction and 1% pearlite raises the LYS by 1 $MNm^{-2[110]}$. Thus the approximately 20 MNm^{-2} lower predicted yield stresses can be accounted for by the increased pearlite volume fraction. However the positive δy value for these non-precipitation hardening steels does enable the influence of pearlite on impact performance to be accounted for by equations (6.2) and (6.3).

Predicted impact behaviour is generally reasonable, Table 6.5, except for the normalised Al containing steel where there is a difference of 44 ^{0}C between observed and calculated 54 J ITTs.

For the Al containing steel raising the austenitising temperature from 900 to 1050 ^{0}C causes a 20 to 50 ^{0}C rise in ITTs while predictions show a similar average 35 ^{0}C rise in ITT Table 6.5. This change can be accounted for in the main by the coarsening of the grain size (10.4 to 7.6 $mm^{-1/2}$ but there is also a small contribution from the coarsening of the grain boundary carbides).

For the V containing steel raising the austenitising temperature from 900 to 1050 ^{0}C causes an approximately 65 ^{0}C rise in ITT and a similar rise is noted in the predicted changes. This change in impact behaviour is accounted for by a combination of the coarse grain size (2 $mm^{-1/2}$ coarser equivalent to

an approx. 20 $^\circ$C rise in ITT), and precipitation hardening (approx 50 $^\circ$C rise in ITT).

In addition to using equations 6.2 and 6.3 for calculating ITTs there is also another completely independent simpler method based on reading off the impact value on curves of grain size and pearlite volume fraction[18] Figs 6.7 and 6.8. These relationships were specifically obtained for flanges and were determined at two temperatures -46[18] and 0 $^\circ$C. The predicted values are given in Table 6.6. Of particular interest and importance is the fact that the technique successfully isolates the one instance when a flange would have failed the ASTM A350 LF2 specification. However, again for the normalised Al containing steel agreement between predicted and observed impact values is poor.

It is possible using these two independent methods of assessing impact behaviour to achieve the ultimate in structure/property relationships and draw a full impact transition curve. These are shown in Figs. 6.7 and 6.8, together with the observed curves for the V and Al containing steels respectively. Agreement is very good for the V steel Fig 6.9 and reasonable for the Al containing steel at 1050 $^\circ$C Fig 6.10. However at 900 $^\circ$C except at low impact values, i.e. less than 30 Joules, agreement is poor, Fig 6.10. Hence although the technique is good for the ASTM A350 LF2 specification, (20 joules at -46°C) for specifications requiring higher impact values, considerable deviations between predicted and observed values may arise.

6.4.4 Influence of shelf energies on impact predictions

As has been observed in an earlier chapter, chapter 4, one factor which may be influencing the structure/property relationship for the Al containing

233

steel is its very low shelf energy even when it is fully grain refined. Structure/property relationships have not been obtained for fine grained steels with these very high volume fractions of pearlite. The effect the shelf energy can have on the ITTs is illustrated in Fig. 6.11 which shows the observed curve for the V containing steel and that calculated assuming the steel has half the shelf energy. For simplicity brittle shelf has been taken as zero for both observed and calculated curves. The calculated curve can be seen to be similar to that obtained for the low shelf energy fine grained Al steel. It therefore appears that some revision of structure/ property relationships is required to take into account marked changes in shelf energy. Presumably it is the higher S level (i.e. the greater volume fraction of inclusions) combined with the high volume fraction of pearlite which gives the Al containing steel its very low shelf energy.

6.4.5 Role of V in influencing the predictability of impact behaviour

In the present excercise a V addition has been found not to influence predictions of impact behaviour based solely on grain size and pearlite volume fraction measurements. For the normalised steel this arises because there is no precipitation hardening. For the austenitised at 1050 $^{\circ}$C condition, this arises because at -46 $^{\circ}$C, the steel is being tested in the brittle shelf range even when there is no precipitation hardening Fig 6.9. Hence precipitation hardening is likely to have only a small influence.

Despite these results, there is some evidence from Al containing V steels that V additions may on occasions lead to problems [106]. V steels are capable of giving precipitation hardening on normalising, and it is possible that

234

the problem may be aggravated by Al. When Al is present it will combine preferentially with the N, so increasing the amount of V in solution available for precipitating. Certainly if normalising takes place at high temperature substantial precipitation hardening can take place. Such hardening can to a large extent be inferred from a high hardness value and the specification does not allow the hardness to exceed 208VPN.

Further work is, however, still required to establish the cooling rates (i.e. flange thickness), γ grain size, and V, N, Al levels which will give precipitation hardening on normalising, and so produce excessively high predicted impact values.

In quenched steels, tempering will always cause the VCN to be precipitated out in a fine form giving precipitation hardening. Certainly prediction of impact behaviour on Q and T flanges containing V has been found very difficult and a wide safety margin has been found to be necessary.

6.5 Conclusions

- 1) The present exercise has shown that the V containing steel examined had very good strength and impact properties and met the ASTM A350 LF2 impact requirement for the two heat treated conditions examined.

- 2) Normalising the V steel at 900 ^{0}C produced a fine grained steel with no evidence of precipitation hardening.

- 3) Austenitising at 1050 ^{0}C redissolved most of the V precipitates and gave marked precipitation hardening on cooling to room temperature. The hardening produced exceeded the specification requirement.

- 4) The V steel was found to have better impact properties than the

235

Al containing steel. A small part of this improvement probably derives from its lower S level, giving rise to higher energy ductile fractures.

- 5) The simple metallographic measurements of pearlite volume fraction and grain size were able to isolate the one instance when a steel did not meet the ASTM A350 LF2 impact requirement of 20 J at -46 ^{0}.

- 6) Further work is required to determine the conditions and compositions (i.e. heat treatment and combinations of V, Al and N) which leads to the metallographic technique giving erroneously high predicted impact values at -46 ^{0}C.

STEEL	HEAT TREAT	LYS MN mm^{-2}	UTS MN mm^{-2}	HARDNESS VPN	IMPACT ENERGY -46^{0}C J	54 J ITT^{0}C	27 J ITT^{0}C	SHELF ENERGY J
Al	900 ^{0}C	369.5	531	177	33	+5	-50	90
Al	1050 ^{0}C	329.5	530	192	6	+24	0	77
V	900 ^{0}C	374.5	528	180	64	-53	-78	160
V	1050 ^{0}C	440.5	587	218	23	+12	-17	90

TABLE 6.2 MECHANICAL PROPERTIES OF STEELS EXAMINED

STEEL	HEAT TREATMENT	γ GRAIN SIZE μm	FERRITE GRAIN SIZE $d^{-1/2}$ mm$^{-1/2}$	%PEARLITE VOLUME FRACTION	GRAIN BOUNDARY CARBIDE THICKNESS μm
Al	900^{0}C	16	10.4	32.0	0.165
Al	1050^{0}C	100	7.6	38.5	0.23
V	900^{0}C	17	11.2	35.0	0.160
V	1050^{0}C	82	9.2	39.0	0.190

TABLE 6.3 MICRO-STRUCTURAL DETAILS

237

STEEL	TEMP ^{0}C	wt.% Al in solution	wt.% N in solution
Al	1130	0.015	0.011
Al	1050	0.010	0.0085
Al	900	0.003	0.005
STEEL	TEMP ^{0}C	wt.% V in solution	wt.% N in solution
V	1110	0.10	0.012
V	1050	0.084	0.0075
V	900	0.062	0.0015

TABLE 6.4 SOLUBILITY DATA FOR TWO STEELS

$$\log [Al] [N] = (- 6770 / T) + 1.03^{[36]}$$

$$\log [V] [N] = (- 8830 / T) + 3.46^{[36]}$$

STEEL	HEAT TREATMENT ^{0}C	LYS MNm^{-2} PRED OBS	δy MNm^{-2}	54J ITT^{0}C PRED OBS	27 ITT^{0}C PRED OBS
Al	900	347.1 369.5	22.4	-39 +5	-50 -50
Al	1050	309.3 329.5	20.2	+2 +24	-15 0
V	900	350.2 374.5	24.3	-47 -53	-57 -78
V	1050	328.6 440.5	111.9	+24 +12	-2 -17

TABLE 6.5 PREDICTED AND OBSERVED LYS, 54J ITT and 27 ITTS[115]

STEEL	HEAT TREATMENT ^{0}C	IMPACT ENERGY AT -46^{0}C JOULES ACTUAL PREDICTED	IMPACT ENERGY AT 0^{0}C JOULES ACTUAL PREDICTED
Al	900	33 92	48 127
Al	1050	6 6	26 25
V	900	64 100	130 140
V	1050	23 20	35 42

TABLE 6.6 PREDICTED IMPACT VALUES OF FLANGES

AT -46^{0}C AND 0^{0}C

NORMALISING
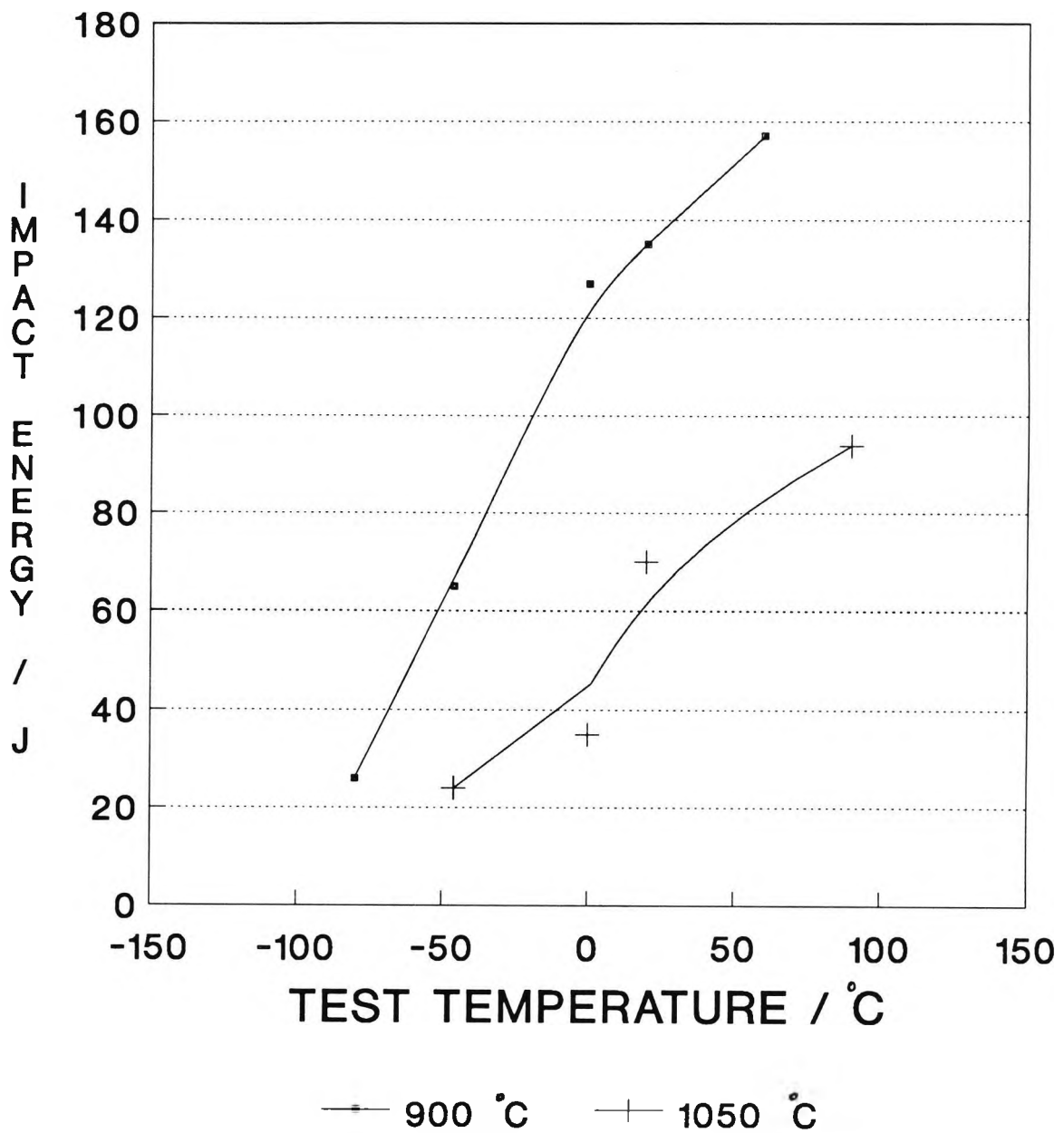
FIG 6.1 IMPACT TRANSITION CURVES
FOR V CONTAINING STEEL

NORMALISING
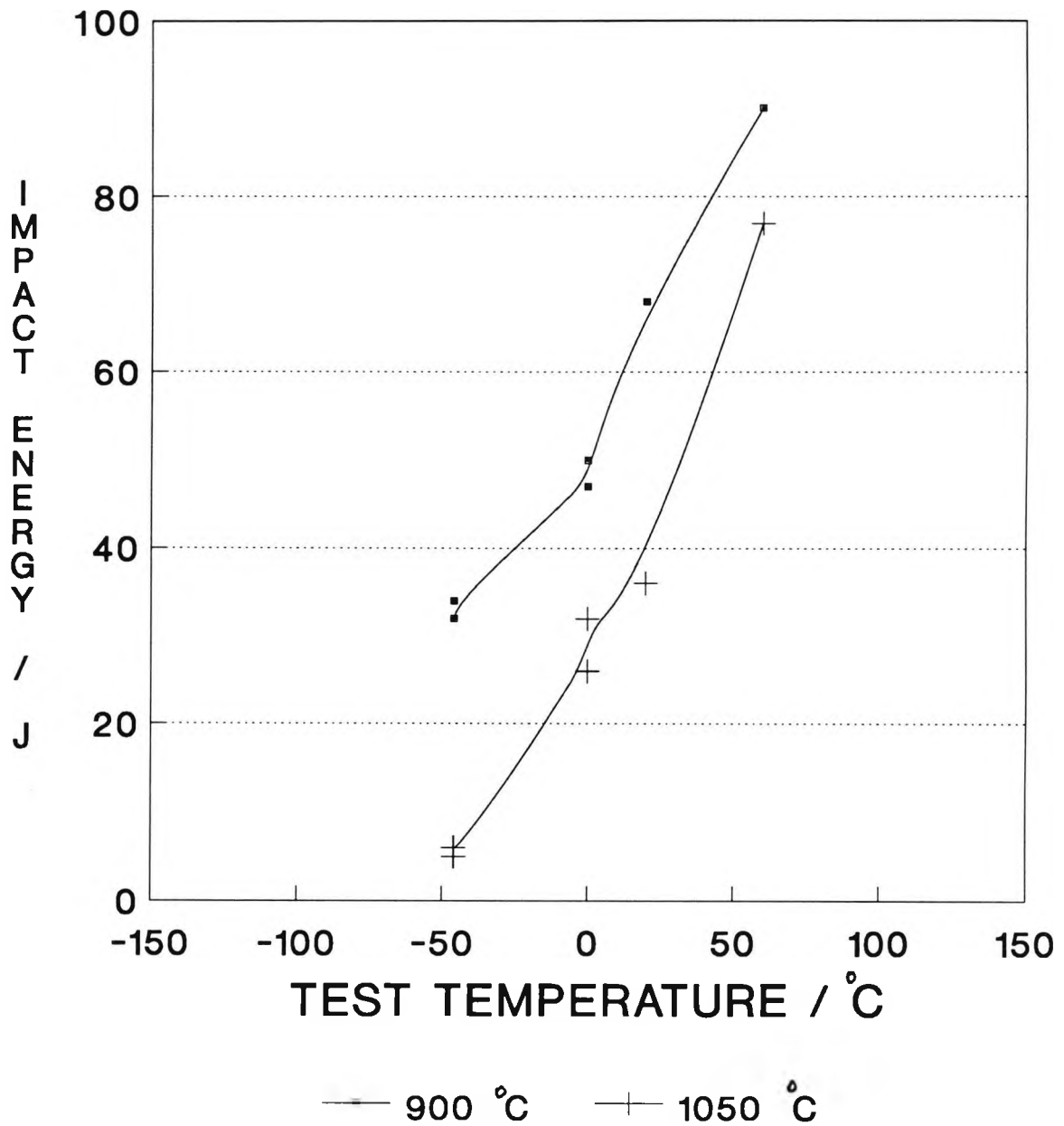
FIG 6.2 IMPACT TRANSITION CURVES FOR AI
CONTAINING STEEL

Figure 6.3: Microstructure of V containing steel obtained when normalised from 900°C after holding for 1 hour.
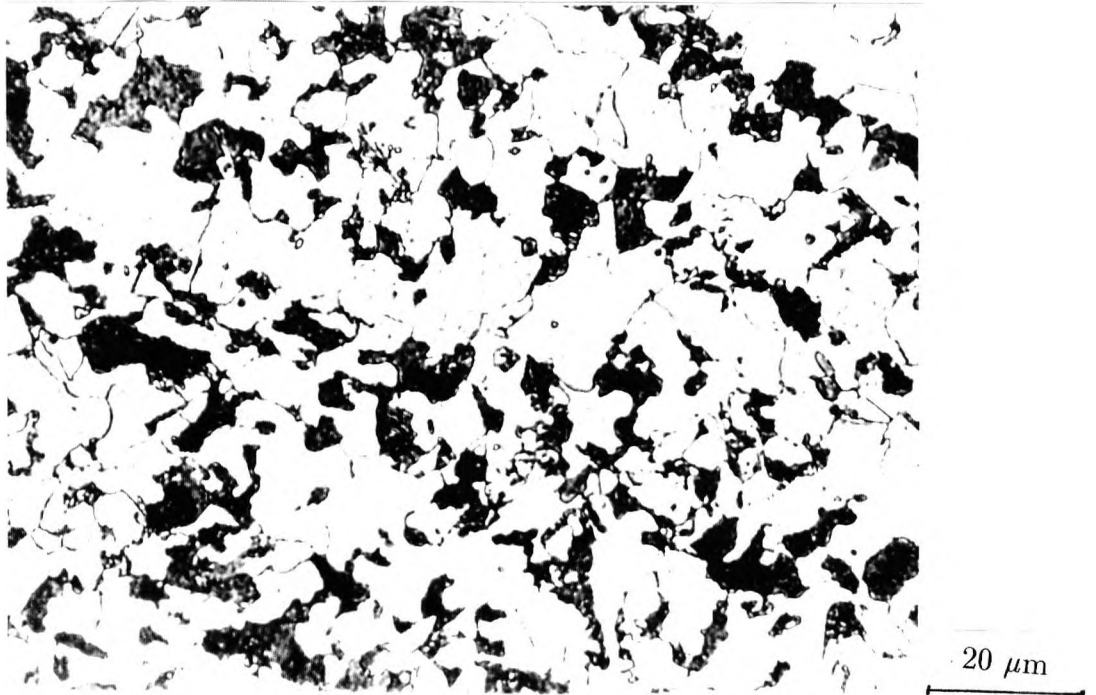
Figure 6.4: Microstructure of Al containing steel obtained when normalised from 900°C after holding for 1 hour.

242

Figure 6.5: Microstructure of V containing steel obtained when normalised from 1050°C after holding for 1 hour.
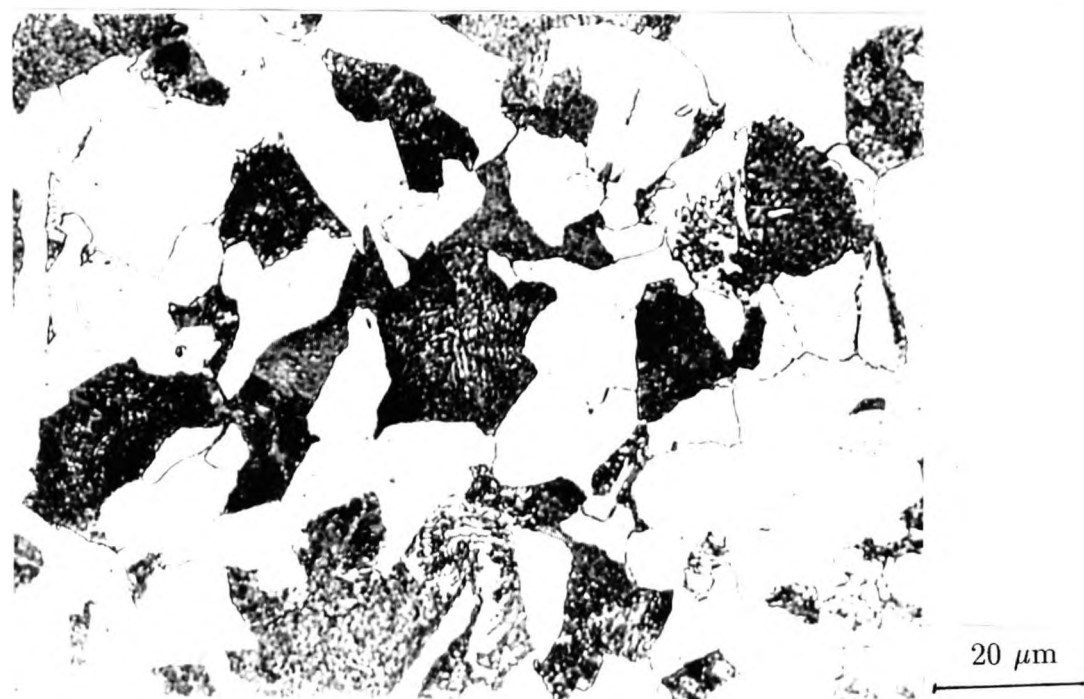
Figure 6.6: Microstructure of Al containing steel obtained when normalised from 1050°C after holding for 1 hour.
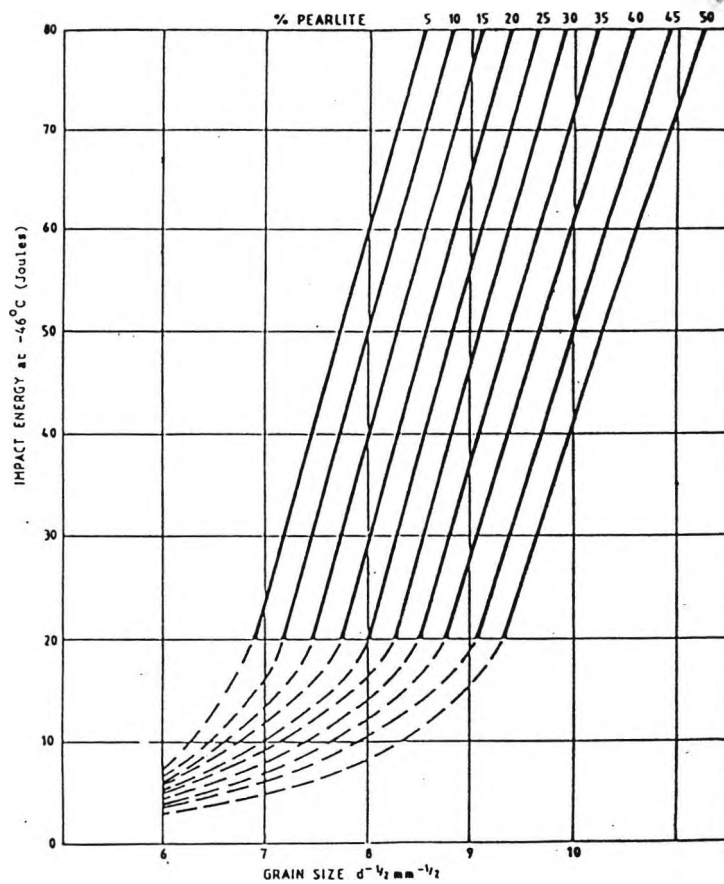
Figure 6.7: Combined influence of grain size and pearlite volume fraction on impact energies of normalised flanges at -46°C[18].
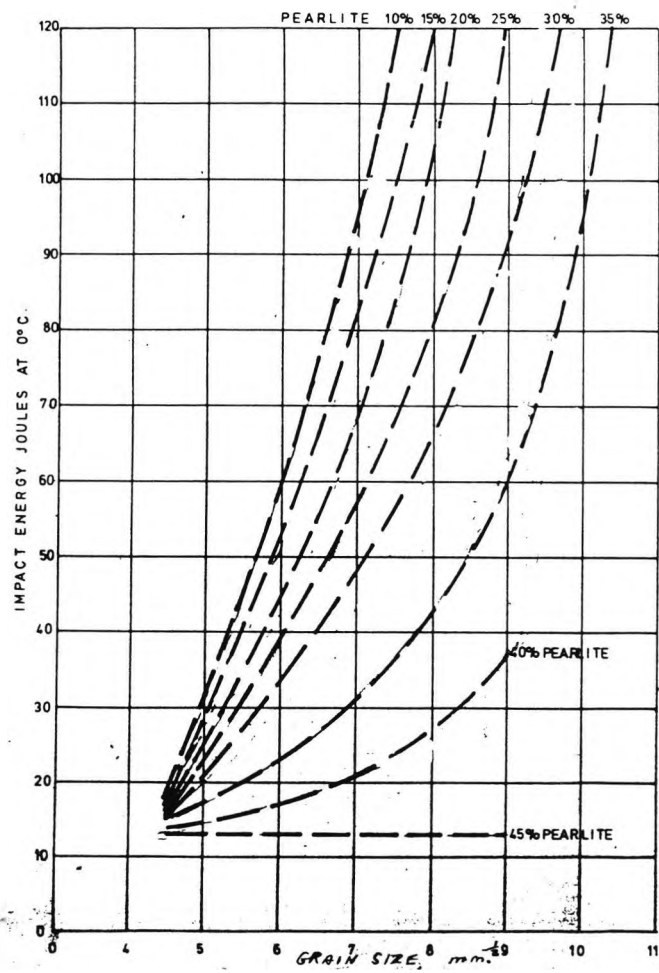
Figure 6.8: Impact energy at 0°C against grain size for various pearlite contents[18].

245
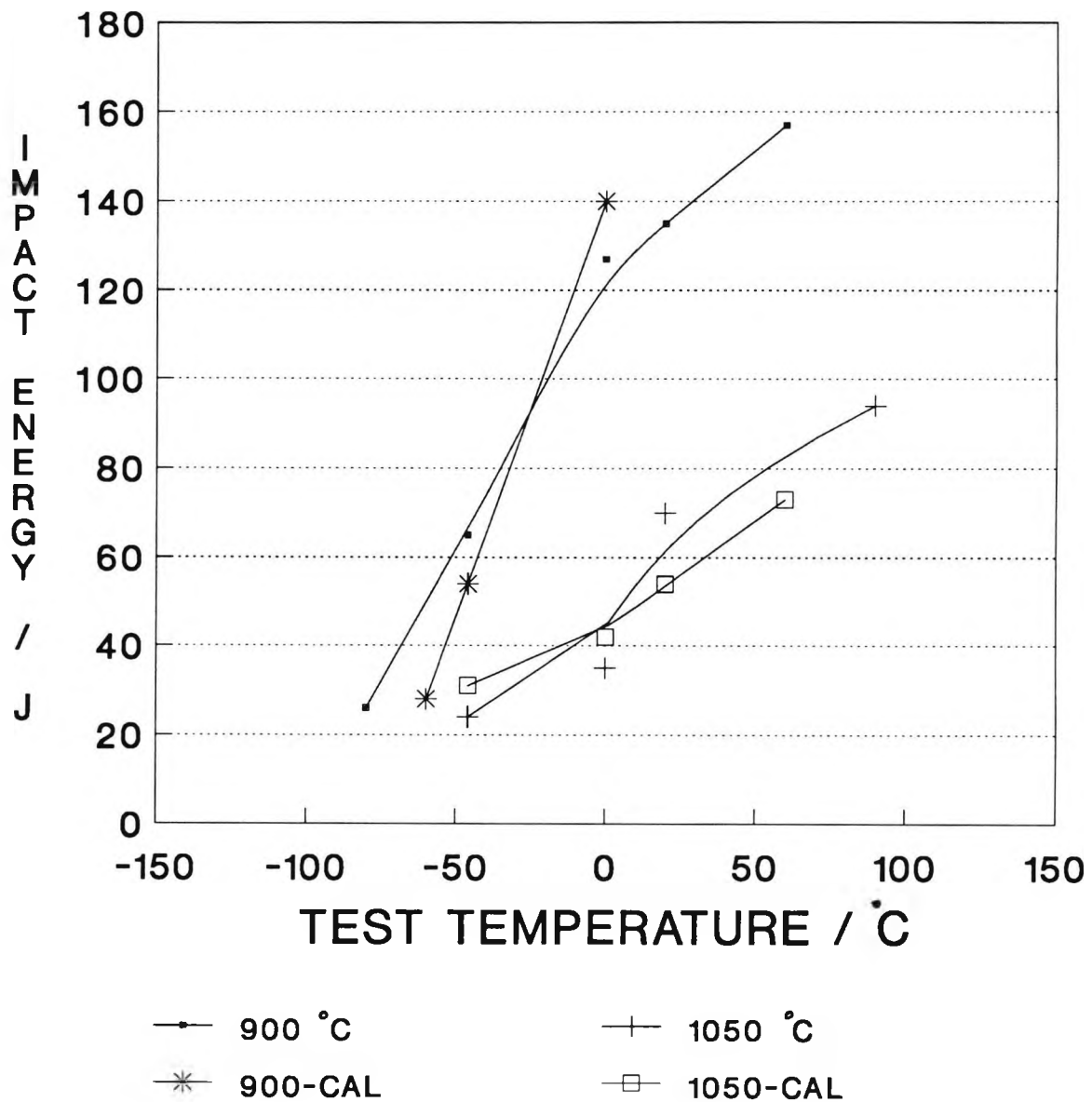
NORMALISING

FIG 6.9 OBSERVED AND CALCULATED IMPACT
TRANSITION CURVES FOR V CONTAINING
STEEL (CAL = CALCULATED)
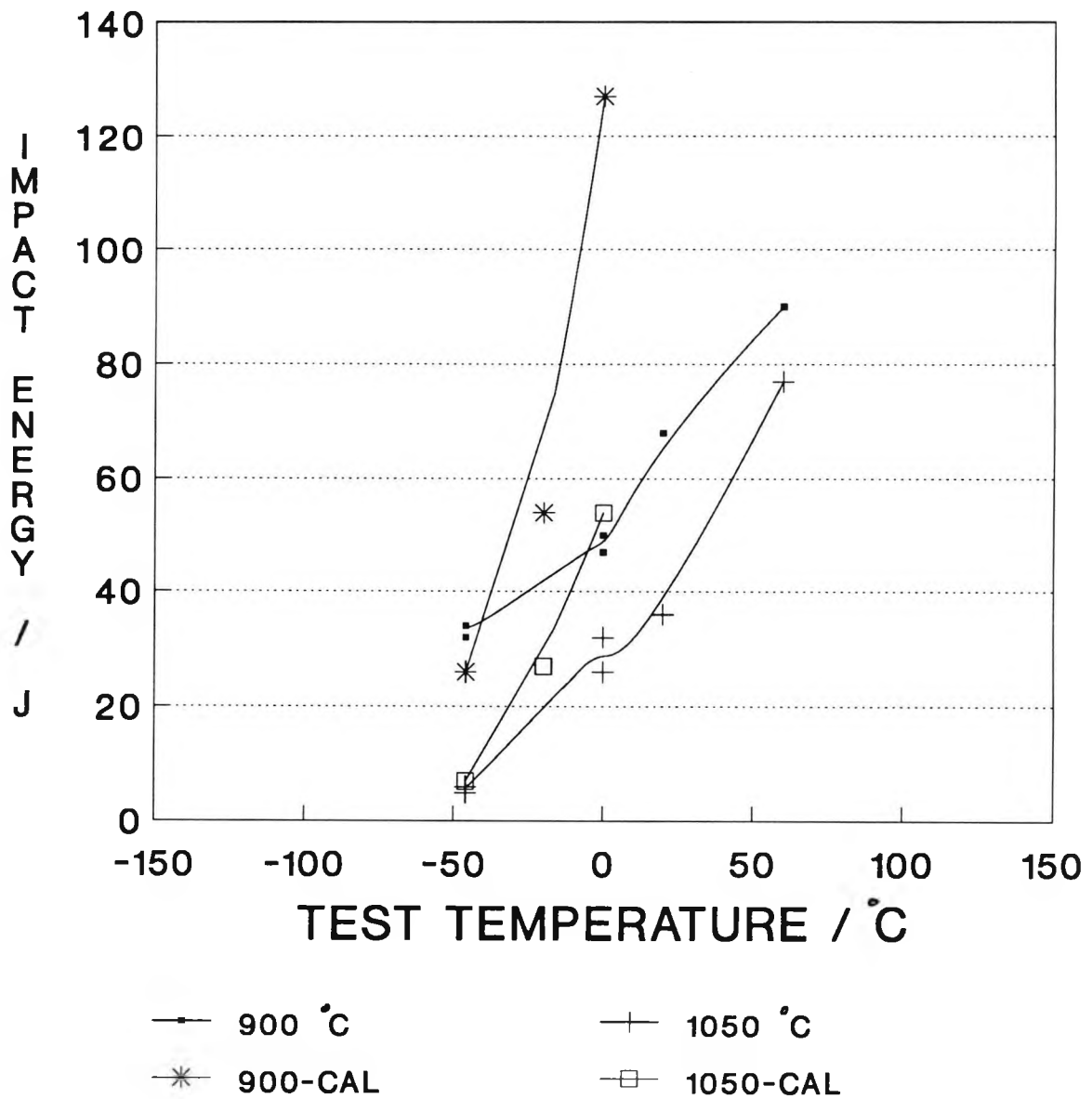
NORMALISING

FIG 6.10 OBSERVED AND CALCULATED IMPACT
TRANSITION CURVES FOR Al CONTAINING
STEEL (CAL ▪ CALCULATED)

NORMALISING
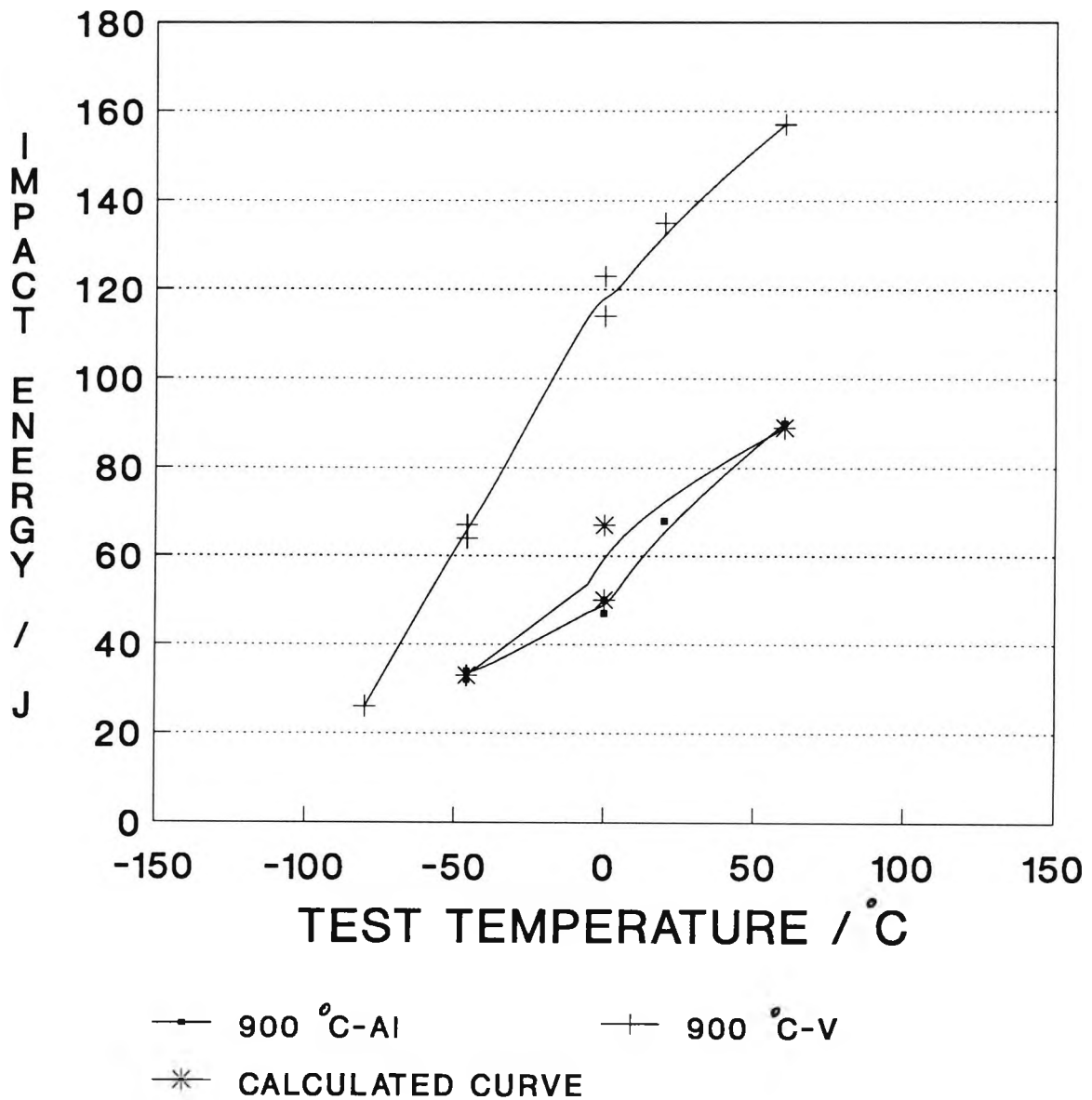
FIG 6.11 CALCULATED IMPACT TRANSITION
CURVE ON THE BASIS OF CHANGES IN THE
DUCTILE SHELF ENERGY

Chapter 7

FUTURE WORK

The work carried out in this thesis on quenched and tempered steels has
mostly been concentrated on the compositonal range of the ASTM A350 LF2
(Table 4.1), and the suggestions for future work on quenched and tempered
steels will concentrate on steels meeting this specification.

- Full charpy curves as well as tensile results are required to observe the
  effect of quenching and tempering on impact transition temperatures,
  charpy shelf energy, LYS and UTS for various compositions within the
  specification. This should result in a larger quantity of data, which can
  be employed to produce a more accurate regression equation. It has
  been difficult in the present work to obtain accurate analysis because
  of the diversity of the source of the flanges. Thus flanges have been
  supplied by different companies in which residual levels vary as well
  as processing conditions making comparisons difficult. For example in
  chapter 4 and 5 it was hoped that the data would be mutually support-
  ive. However, the small differences in composition produced markedly
  different impact behaviour. To avoid this problem in future it is sug-
  gested that the work should be carried out on plate steel made from

laboratory casts in which strict control of composition and processing conditions can be maintained.

- One of the aims of this work has been to use simple metallographic techniques to predict the impact behaviour of steels. In Q and T steels, the austenite grain size has been shown to be important but this cannot generally be determined on flanges in cold service. As prior austenite grain size has a large influence on impact properties, it is desirable to be able to measure this accurately on quenched and tempered flanges with an unknown history. A simple etching method has to be devised in order to fulfil this task.

- Facet size, length and continuity of carbides seem to influence the impact behaviour of quenched and tempered steels. More work is required to establish quantitatively the influence of carbides and facet size on impact performance by devising a more accurate method of measuring carbide length and spacing as well as the facet size.

- Another factor which seems to influence the mechanical properties of quenched and tempered steels, is the presence of dislocations. Further transmission work is therefore required.

- The influence of tempering at lower temperatures (200-600°C) has to be fully investigated. It has been suggested[55] that toughness may actually decrease if steels are tempered in the range of 260 to 370°C. This decrease in toughness is reffered to as temper embrittlement.

- One of the major findings in this work is that the shelf energy can have a large influence on the impact transition temperatures and this needs

250

to be explored more fully. It is important that the future work should be directed to including the effect of S level on the structure/property relationships.

- For ferrite/pearlite steels, the ferrite grain size dominates impact behaviour, whereas for Q and T steels it is the austenite grain size. It is important that a link be more clearly established between when the change over occurs, i.e. for a given composition, what is the critical cooling rate.

REFERENCES

1) Honeycombe, R. W. K Steels Microstructure and properties (1981).

2) Baker, T.J., Charles, J.A., The Effect of Second Phase Particles on the Mechanical Properties of Steel. London : The Iron and Steel Institute (1971).

3) Hall, E.O. (1951), Proc. Phys. Soc, Series 64, 747.

4) Petch, N.J. (1953), J. Iron Steel Inst, London 174, 25.

5) Griffith, A.A. Phil Trans. Roy. Soc., (1920) A221, p.163.

6) Orowan, E. (1948). Rep. Prog. Phys., 12,185.

7) Kolahi-aval, J., Mintz, B., Submitted to the Materials Science Technology, (1983).

8) Kolahi-Aval, J., (1988), PHD Thesis, City university, UK.

9) Cracknell, A., Petch, N.J. (1955), Acta Met, 3, 186.

10)Gensamer, M., Pearsall, E. B., Pellini, W.S., Low, J.R. (Jr.) (1942), Trans, ASM 35, 383.

11)Austin, C.R. (1943), Trans, ASM 31, 321.

12)Gladman, T., Pickering, F.B. (1983), in Yield, Flow and Fracture of poly-crystals; Baker, T.N. (Ed.). London: Elsever Applied Science Publishers, p. 141.

13)Morrison, W.B. (1976), in: Controlled processing of HSLA steel, Proc. of British Steel Corporaion conference, York. Sheffield: British Steel Corporation, paper 1.

14)Gladman, T., Holmes, B., Pickering, F.B. (1970), J. Iron Steel Institute, London 208 273.

15)Gladman, T., Pickering, F.B. (1963), in: Metallurgical Developments in Carbon Steel, Spec. Rep. No. 81. London: The Iron and Steel Institute,

p.10.

16) Preston, R.R. (1983), in: Yield, Flow and Fracture of Polycrystals: Baker, T.N. (Ed.). London: Applied Science Publishers, p.199.

17) Mirovics, I., Trans. Inst. Eng. Aust., (July 1986), 112.

18) Mintz, B., ASTM Journal of Testing and Evaluation, NOV 1988.

19) Hutchinson, M. (1963), Phill, Mag, 8, 121.

20) McCutcheon, D.B., Jamieson, R.M. (1973), Can. Met, Quar. 12, 105.

21) Gladman, T., Dulieu, D., McIvor, I.D. (1977), in: Microalloying '75: Korchynsky, M.(Ed.) New York: Union Carbide Corporation, 32.

22) Holmes, B., Dyson, D.J. (1970), J. Iron Steel Inst. London 208, 269.

23) Irvine, K.J. Strong, Tough Structural Steels. ISI publications, 104, 1967, p.1.

24) Ashby, M.F. (1966 a), in: Oxide Dispersion Strengthening, Warrendale, PA: AIME, p. 143.

25) Gladman, T., Holmes, B., McIvor, I.D. (1971), in: Effect of Second Phase Particles on the Mechanical Properties of Steel. London: The Iron and Steel Institute, p.68.

26) Cahn, R. W., Hassen, P., Kramer, E.J., Materials Science and technology. A Comprehensive Treatment Volume 7. Volume Editor Pickering, F.B., (1992)

27) Narita, K. (1975), Trans, Iron Steel Inst, J. 15, 145.

28) Wadsworth, J., Woodhead, J.H., Keown, S.R. (1976), Met. Sci, 10, 342.

29) Microalloying '75, Korchynsky, M. (E.d.). New York: Union Carbide Corporation, p.59.

30) Bramfitt, B.L., Marder, A.R. (1973), in: Processing and Properties Of Low Carbon Steel. Warrendale, PA: AIME, p. 191.

31) Pickering, F.B., Conf. on Hardenability Concepts in steels, Ed. Doori, Kirkaldy, (1978), AIME, Pennsylvannia, New york, p.32.

32) Mintz, B., Metals Tech., Feb, (1984), 11, p.52.

33) Cochrane, R.C. Conf. On Effect of Second Phase Particles on the Mechanical Properties of Steels , (1971), London ISI Conf. p. 101.

34) Pickering, F.B. (1977), in: Microalloying 75 : Korchynsky, M.(Ed.) New York: Union Carbide Corporation, p. 9.

35) Pickering, F.B. (1978 a), in: Hardenability Concepts with Application to Steel: Doane, D.V., Kirkaldy, J.S. (Eds). Warrendale, PA: AIME, P.179.

36) Irvine K.J., Pickering. F.B., Gladman, T. (1967), J. Iron Steel Inst. London 205, 161.

37) Mintz, B., Kolahi-aval, J., Saggese, M., (1988) The Institute of Metals.

38) Mintz, B., Davies, G., Morris, P., Morrison, W.B., The Metals Soc. London, 1976. Procs. 4th Int. Conf. on Texture of Materials, cambridge, (1975), pp.224-233.

39) McMahon, C.J., Cohen, M. (1963), Acta, Met. 13, 991.

40) Almond. E.A. (1969), in: Fracture, London: The Iron and Steel Institute, p.253.

41) Mintz, B., in "Strength of Metals and Alloys" 6th Int. Conf. Melbourne, (1982), (Ed. Gifkins, R.C.) vol.1, 217, (1982), Oxford, Pergamon.

42) Gladman, T. (1979), in: Inclusions, Monograph No 3: Pickering, F.B. (Ed.). London: The Institution of Metallurgists, p.157.

43) Mintz, B., Morrison, W.B., Jones, A., Met. Technol., (1979), 6, 252.

44) Bucher, J.H., Grozier, J.D., Enrietto, J.F. (1968). Fracture 6. 244.

45) Mintz, B. (1977), in: Low Carbon Steel for the Erghties, London: The Institution of Metallurgists, series 3, No. 6. p. I- 47.

46) Banks, T.M., Gladman, T. (1979), Met. Tech. 6 (3), 81.

47) Baker, T.J., Charles, J.A. (1971), in: Effect of Second Phase Particles on the Mechanical Properties of Steel. London: The Iron and Steel Institute, p.79.

48) Garrison, W.M. (1986), Met. Trans. A, 17 A. 669.

49) Baker, T.J. (1974), in: Inclusions and their Effects on Steel Properties, Rotherham: British Steel Corporation, paper 8.

50) Gladman, T., McIvor, I.D., Pickering, F.B.(1972). J.Iron steel Inst. London 210, 916.

51) Dollar, M., Bernstein, I.M., Thompson. A.W.(1988), Acta Met. 36, 311.

52) Karlsson, B., Linden. G. (1975), Mat, Sci, Eng, 17, 153.

53) Marder, A.R., Bramfitt, B.L. (1976), Met. Trans. 7A, 365.

54) Whittaker, D.(1979), Metallurgia 46(4), 275.

55) Krauss, G.(1980). Principles of Heat Treatment of Steels. Metals Park. OH: American Society for Metals.

56) Hyzak, J.M., Bernstein, I.M. (1976), Met, Trans. 74A, 1217.

57) Garbaz, B., Pickering, F.B. (1988), Mat. Sci. and Tech. 4,328.

58) Pickering, F.B., Garbarz, B. (1989), Mat. Sci. and Tech. 5,227.

59) Garbaz, B.(1990), in: Microalloyed Vanadium steels: Korchynsku., M., Gorczca, S., Blicharski, M(Eds.). Krakow: Assoc. of Polish Engineers and Strategic Minerals Corporation, p.193.

60) Alexander, D.J., Bernstein, I.M. (1982), Met. Trans. 13A, 1865.

61) Honeycombe, R.W.K., Pickering, F.B. (1972), Met. Trans. 3A.1099.

62) Irvine, K.J., Pickering, F.B. (1957), J.Iron Steel Inst. London 187,292.

63) Pickering, F.B. (1978 b), Physical Metallurgy and the Design of Steels. London: Applied Science Publishers Ltd.

64) Steven, W., Haynes, A. G. (1956), J. Iron Steel Inst. London 183,349.

65) Pickering, F.B. (1967), in: Transformations and Hardenability in Steels, Ann Arbor: Climax Molybdenum Company, p. 169.

66) Onel, K., Nutting, J. (1979), Met. Sci. 13(10),573.

67) Plaut, R.L. (1974), PHD thesis, Sheffield University, UK.

68) Bush, M.E., Kelly, P.M. (1971), Acta Met.19, 1363.

69) Whiteman, J.A. (1977), in: Low Carbon Steels for the Eighties. London: The Institution of Metallurgists, Series 3, No.6, p.I-1.

70) Irvine, K.J., Pickering, F.B. (1963), J, Iron Steel Institute, London 201, 518.

71) Ohtani, H., Terasaki, F., Kuitake, T. (1972), Trans. Iron Steel Institute, Jap. 12, 118.

72) Pickering, F.B. (1990), in: Proc, 31st Mech. Working and Steel Processing Conf, Warrendale, PA: AIME, 381.

73) Nomura, I. (1989), SAE Preprint. No. 890511.

74) Ochi, T., Takahashi. T., Takada, H. (1988), Paper presented To 30th Mechanical Working and Steel Processing Conference, Dearborn. Warrendale, PA: AIME.

75) Dolby, R.E. (1982), in: Advances in the Physical Metallurgy and Applications of Steels. London: The Metals Society, p.111.

76) Mills, A.R., Thewlis, G., Whiteman, J.A. (1987), Mat. Sci, Tech. 3(12), 1051.

77) Leslie, W.C. (1966), in: Strengthening Mechanisms. Syracuse University press, 43.

78) Pickering, F.B. (1989), in: High Nitrogen Steels '88: Foet. J. Hendry. A. (Eds.). London: The Institute of Metals, p.10.

256

79) Cohen, M. (1962), Trans. AIME 224,638.

80) Irvine, K.J., Pickering F.B., Garstone, J. (1960), J. Iron Steel Inst, London 196,66.

81) Kelly, P.M., Nutting. J. (1965), Spec, Rep. No.93. London: The Iron and Steel Institute,166.

82) Smith, D.W., Heheman, R.F. (1971), J. Iron Steel Inst. London 209, 476.

83) Winchell, P.G., Cohen, M. (1962), Trans, ASM 55,347.

84) Leslie, W.C., Sobers, R.J. (1967), Trans, ASM 60,459.

85) Grange, R.A. (1966), Trans, ASM 59,26.

86) Swarr, T., Krauss, G. (1976), Met, Trans. 7A, 41.

87) Roberts, M.J. (1970), Met, Trans. 1A,3287.

88) Naylor, J.P., Krahe, P.R. (1974),Met, Trans. 5A. 1699.

89) Naylor, J.P. Krahe, P.R. (1975), Met, Trans. 6A. 594.

90) Pickering, F.B. (1987), in: Tool Materials for Molds and Dies: Krauss, G., Nordberg, H.(Eds), Goldon: Colorado School of Mines Pub. Dept., P.3

. 91) Wadsworth, J.,Woodhead, J.H., Keown, S. R. (1976), Met. Tech. 4, 205.

92) Little, E.A., Harries, D.R., Pickering, F. B., Keown, S. R. (1977), Met. Tech. 4, 205.

93) Contractor, G.P., Schempp, E. G., Morgan, W. A. (1961), Trans. ASM 54, 208.

94) Nordberg, H. (1983), in: Tool for Die Casting. Stockholm: Uddeholme Swedish Institute for Metals Research, P.1.

95) Knott, J.F. (1974), in: Inclusion and their Effects on Steel Properties, Rotherham: British Steel Corporation, paper 8.

96) Dulieu, D., Gouch. A.J. (1974), in: Inclusion and their Effects On Steel

Properties. Rotherham: British Steel Corporation, paper 16.

97) British standards 131: part2, (1972), Charpy V-notch Impact Test on Metals.

98) British Standards 18: Part 2, (1971). Tensile Test of Metals, Steel.

99) British Standards 427: Part 1, Vickers Hardness Test.

100) Pickering, F.B., The basis of quantitative metallography. Inst. of metallurgists, Monograph.

101) Mintz, B., Morrison, W.B., Jones,A., Technol., 1979, 6, 252.

102) British Standards 1827, Reference Tables for thermocouples.

103) Flemington, D., B.S.C. Final years Project 1984, The City University, London.

104) Siriwardene, P.P.L.G., PhD Thesis, Cambidge University, (1955).

105) Deep, G., and Williams, W.M., Canadian Metal, Quart, 14, 1975, 85-96.

106) Mintz, B., and Kolahi-aval, J., An assessment of the micro-structural technique for predicting impact behaviour of flanges made to the ASTM A350 LF2 Specification. May 1989. Shell Report No. 1.

107) Mintz, B., A Comparison of the micro-structures produced at the surface (sliver position) and charpy impact position for normalised and quenched and tempered flanges made to the ASTM A350 LF2 specification. Santos Report No. 7. February 1985.

108) Irvine, K. J., Pickering, F. B., Gladman, T.,:J. Iron Steel Inst., 1967, 205, 161.

109) Cochrane, R. C., British Steel Private Communication.

110) Kolahi-aval, J., Mintz. B., Mat.Sci and Technol, 1989,5,pp 457-464.

111) Anand, L., Gurland, J., Metal Trans (a), 1976, 191, 74.

112) Materkowski, J. P., Krauss, G., Metal Trans Nov 1979, 1643.

113) Caron, R. N., Krauss, G., (1972), Metal. Trans. 3, 2381.